

University of Bath



PHD

The electrophoretic mobility of non-aqueous dispersions

Parkins, David Anthony

Award date:
1986

Awarding institution:
University of Bath

[Link to publication](#)

General rights

Copyright and moral rights for the publications made accessible in the public portal are retained by the authors and/or other copyright owners and it is a condition of accessing publications that users recognise and abide by the legal requirements associated with these rights.

- Users may download and print one copy of any publication from the public portal for the purpose of private study or research.
- You may not further distribute the material or use it for any profit-making activity or commercial gain
- You may freely distribute the URL identifying the publication in the public portal ?

Take down policy

If you believe that this document breaches copyright please contact us providing details, and we will remove access to the work immediately and investigate your claim.

Download date: 13. May. 2019

THE ELECTROPHORETIC MOBILITY OF NON-AQUEOUS DISPERSIONS

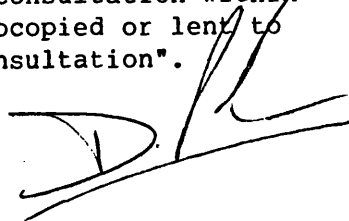
submitted by David Anthony Parkins
for the degree of Ph.D
of the University of Bath

1986

COPYRIGHT

*Attention is drawn to the fact that copyright of this thesis rests with its author. This copy of the thesis has been supplied on condition that anyone who consults it is understood to recognise its copyright rests with its author and that no quotation from the thesis and no information derived from it may be published without the prior written consent of the author".

"This thesis may be made available for consultation within the University Library and may be photocopied or lent to other libraries for the purposes of consultation".

A handwritten signature in black ink, appearing to be 'D.A. Parkins', written over the end of the second paragraph.

UMI Number: U499963

All rights reserved

INFORMATION TO ALL USERS

The quality of this reproduction is dependent upon the quality of the copy submitted.

In the unlikely event that the author did not send a complete manuscript and there are missing pages, these will be noted. Also, if material had to be removed, a note will indicate the deletion.



UMI U499963

Published by ProQuest LLC 2013. Copyright in the Dissertation held by the Author.
Microform Edition © ProQuest LLC.

All rights reserved. This work is protected against
unauthorized copying under Title 17, United States Code.



ProQuest LLC
789 East Eisenhower Parkway
P.O. Box 1346
Ann Arbor, MI 48106-1346

BOOK 763

UNIVERSITY OF BATH LIBRARY		
23	15 JUL 1987	
PHD		

To my parents.

(1)

Acknowledgements

The author would like to express his thanks to Mr B.J. Meakin (School of Pharmacy and Pharmacology, University of Bath) and Dr G.W. Hallworth (Glaxo Group Research) for their help and guidance in supervising this thesis.

The work contained in this thesis was carried out at the School of Pharmacy and Pharmacology, University of Bath and was funded through a Science Engineering Research Council CASE award in association with Glaxo Group Research.

The author would like to thank all the staff and postgraduates of the School of Pharmacy and Pharmacology for their help and support. Similar thanks are extended to the members of the Inhalation Technology Department, Glaxo Group Research, Ware.

The author would like in particular to acknowledge the following contributions:

Dr R.T. Lipczynski (Department of Electrical Engineering, University of Bath) and Mr R Hartley (Glaxo Group Research) for their technical contributions.

Dr B.Vincent (Department of Physical Chemistry, University of Bristol) for making available the General Radio conductivity bridge and with Dr D.Skuse for supplying the polymer coated silica spheres.

Dr D. Wyatt (Glaxo Group Research) for his advice and interest.

(2)

SUMMARY

The physical behaviour of many aqueous pharmaceutical suspensions can be explained in terms of the DLVO theory. Its applicability to dispersions in non-polar media such as the metered dose inhalation aerosol (MDI) formulated as a suspension is however unclear.

A test of the theory requires the determination of the electrophoretic mobility of the dispersed particle. Such measurements are not possible by conventional microelectrophoresis because of the difficulties of charge leakage, electrohydrodynamic, charge acquisition and space charge effects.

To overcome these problems a technique using a differential heterodyne velocimeter in conjunction with a narrow gap electrode assembly has been developed. Field strengths of $\sim 10^4 \text{ kV m}^{-1}$ at reversal rates of 2-5 Hz can be applied to non-polar dispersions held within the electrode gap. A low humidity housing permits control of the suspension moisture content, an important factor in charge generation in non-polar media.

The technique has been validated using model systems comprising silica spheres of up to $5 \mu\text{m}$ diameter, dispersed in a low permittivity model propellant blend of Arcton 113 and n-hexane. True electrophoresis has been demonstrated through the field independence of the determined electrophoretic mobility and compliance with the criteria of Van der Minne and Hermanie (86, 87). Electrophoretic mobilities were typically $1 - 5 \times 10^{-9} \text{ m}^2 \text{ s}^{-1} \text{ V}^{-1}$ and independent of particle size, over the range studied.

(3)

The influence of Aerosol OT and oleic acid concentration, on the electrophoretic mobility of both silica spheres and the bronchodilator drug salmefamol, dispersed in model propellant blend was studied. Both additives produced negatively charged drug particles, demonstrating reversal of charge from the positive electrostatically charged dry powder.

As such "surfactants" are conventionally included in MDI suspensions, the technique developed should prove invaluable to the study of drug/surfactant interactions which occur in low permittivity media.

THE ELECTROPHORETIC MOBILITY OF NON-AQUEOUS DISPERSIONSCONTENTS

1	INTRODUCTION, BACKGROUND AND SCOPE OF WORK.	
1.1	The physical stability of pharmaceutical suspensions.	1
1.2	Formulation of the metered dose inhalation aerosol product.	4
1.3	The non-aqueous dispersion.	14
1.4	The scope and objective of this study.	15
1.5	A note on units.	16
2	THE COLLOID CHEMISTRY OF NON-AQUEOUS DISPERSIONS	
2.1	The electric double layer.	17
2.2	The origin of surface charge in dispersions of non-polar media.	24
2.2.1	Basic mechanisms of surface charge generation.	24
2.2.2	The effect of surfactants and water on surface charge.	25
2.3	Electrostatic repulsion.	30
2.4	Attractive forces.	31
2.5	Colloid stability arising solely from electrostatic repulsion.	33
2.6	Steric stabilisation of non-aqueous dispersions.	37
2.7	Methods of stability determination.	40
3	DETERMINATION OF PARTICLE CHARGE IN NON-AQUEOUS DISPERSIONS	
3.1	Electrokinetic phenomena.	42
3.2	Electrophoretic mobility and zeta potential.	44
3.3	Non-aqueous electrophoresis.	49

(5)

3.3.1	Space charge effects and dielectrophoresis.	50
3.3.2	Electrohydrodynamics.	51
3.4	Microelectrophoresis.	52
4	LASER-DOPPLER SPECTROSCOPY	
4.1	Introduction.	58
4.1.1	Glossary of terms.	58
4.1.2	Laser-Doppler spectroscopy.	59
4.1.3	The use of laser-Doppler spectroscopy in colloid science.	60 60
4.2	Basic principles of laser-Doppler velocimetry.	61
4.2.1	Properties of laser light.	61
4.2.2	The Doppler shift.	64
4.2.3	Heterodyne detection.	66
4.2.4	Local oscillator heterodyne design of velocimeter.	68
4.2.5	The fringe model of laser-Doppler velocimetry.	70
4.2.6	Differential heterodyne design of velocimeter.	72
4.3	Design criteria for construction of a laser-Doppler velocimeter.	75 75
4.3.1	Selection of velocimeter design and optical components.	75 75
4.3.2	Selection of laser.	77
4.3.3	Photodetection.	78
4.3.4	Signal processing.	80
4.3.5	Electrophoresis cell design.	84
4.3.6	Electrode drive.	86
5	DEVELOPMENT AND DESCRIPTION OF LASER-DOPPLER VELOCIMETER	
5.1	Introduction.	89

(6)

5.2	The optical bench.	89
5.3	Laser and optical components.	93
5.3.1	Summary of optical components.	93
5.3.2	Construction and alignment.	93
5.4	Electrodes and electrophoresis cell.	96
5.5	Electrode supply.	98
5.6	Photodetection.	99
5.6.1	Photodetection development.	99
5.6.2	Photomultiplier assembly.	101
5.7	Signal processing.	103
5.7.1	Amplification.	103
5.7.2	Filtering.	103
5.7.3	Electrical noise.	106
5.7.4	Signal analysis.	106
5.8	Low humidity housing.	106
6	MATERIALS AND GENERAL METHODS	
6.1	Materials and instrumentation.	109
6.1.1	General materials.	109
6.1.2	Drug materials.	111
6.1.3	Equipment.	112
6.1.4	Model particles.	116
6.1.5	Temperature measurements.	117
6.1.6	Glassware.	121
6.1.7	pH measurements.	122
6.2	Characterisation of drug materials.	122
6.2.1	Particle size of micronised powder.	122
6.2.2	Densities of drug materials.	124

(7)

6.2.3	Electrostatic charges associated with micronised drug materials.	126
6.3	Physico-chemical properties of the propellant model and other liquids.	128
6.3.1	The propellant model.	128
6.3.2	Purification of Aerosol OT.	130
6.3.3	Purity of oleic acid.	131
6.3.4	Density determination of propellant model and its solutions.	131
6.3.5	Determination of liquid viscosities.	136
6.3.6	The control and assay of moisture.	137
6.3.7	Refractive indices of solutions used in study.	145
6.3.8	Determination of relative permittivities.	146
6.3.9	Estimation of solution conductivities.	148
6.3.10	Evidence for the formation of oleic acid dimers in 113/n-hexane/oleic acid solutions.	151
7	VALIDATION OF THE LASER-DOPPLER VELOCIMETER	
7.1	Introduction.	154
7.2	Preparation of erythrocyte dispersions.	155
7.3	Preparation of the electrodes.	156
7.4	Electrode voltage supply.	158
7.5	Experimental technique.	158
7.6	Estimation of operator error in frequency determination.	161
7.7	Variation in frequency shift with probe volume position.	163
7.8	Variation in frequency shift with field reversal rate.	165
7.9	Determination of electrophoretic mobility.	165

(8)

8	ELECTROPHORESIS IN NON-AQUEOUS SYSTEMS: THE ROLE OF PARTICLE SIZE	
8.1	Development of experimental method.	171
8.1.1	Visual observations.	171
8.1.2	Experimental procedures used.	173
8.2	Investigations using dispersions of Polymer B coated silica spheres.	176
8.2.1	Verification of electrophoresis.	176
8.2.2	The influence of particle size on electrophoretic mobility.	188
8.2.3	Dispersions in 113/n-hexane.	194
8.3	Investigations using Polymer A coated silica dispersions.	196
8.4	Investigations using Hypersil ODS.	196
8.4.1	Dispersions without a surfactant.	196
8.4.2	The influence of moisture and Aerosol OT upon the determined electrophoretic mobility.	198
9	THE INFLUENCE OF SURFACTANT CONCENTRATION ON OBSERVED ELECTROPHORETIC MOBILITY	
9.1	Studies conducted with Aerosol OT.	210
9.1.1	Dispersions of Hypersil ODS in model propellant.	210
9.1.2	Dispersions of salmefamol in model propellant.	221
9.1.3	Dispersions of Betamethasone Valerate in model propell- ant.	228
9.2	Studies conducted with oleic acid in model propellant.	228
9.2.1	Dispersions of Hypersil ODS in model propellant.	230
9.2.2	Dispersions of salmefamol in model propellant.	238
10	PHYSICAL INTERACTIONS OF DRUG AND SURFACTANT MATERIALS	

10.1	Analytical techniques.	241
10.1.1	A quantitative assay for Aerosol OT.	241
10.1.2	A quantitative assay for Aerosol OT in the presence of salmefamol.	246
10.1.3	A quantitative assay for oleic acid.	250
10.1.4	A quantitative assay for salmefamol.	252
10.2	Adsorption studies.	259
10.2.1	Adsorption of Aerosol OT on to Hypersil ODS from 113/n-hexane.	259
10.2.2	Adsorption of Aerosol OT on to salmefamol from 113/n-hexane.	263
10.2.3	Adsorption of oleic acid on to Hypersil ODS from 113/n-hexane.	265
10.2.4	Adsorption of oleic acid on to salmefamol from 113/n-hexane.	267
10.3	The solubility of salmefamol in 113/n-hexane.	270
10.4	Deposition of salmefamol on to the electrode surface.	272
11	DISCUSSION AND CONCLUSIONS	
11.1	Application of laser-Doppler velocimetry to the study of electrokinetic behaviour in non-polar media.	275
11.1.1	Laser-Doppler velocimetry.	275
11.1.2	Laser-Doppler velocimeter design.	277
11.1.3	Validation of laser-Doppler velocimeter design.	278
11.2	The control of non-electrophoretic motion.	281
11.3	Model dispersions.	282
11.4	Studies with model particles.	284

(10)

11.4.1	Spectral quality.	285
11.4.2	Demonstration of true electrophoresis.	286
11.4.3	The role of particle size.	290
11.4.4	Definition of the diffuse layer.	291
11.4.5	Calculation of zeta potential.	292
11.4.6	The influence of moisture content.	295
11.4.7	The effect of Aerosol OT upon electrophoretic mobility.	296
11.4.8	The effect of oleic acid upon electrophoretic mobility.	300
11.5	Studies with drug dispersions.	303
11.5.1	Salmefamol.	303
11.5.2	Betamethasone valerate.	305
11.5.3	Comparison of salmefamol dispersions with model particle studies.	306
11.6	Conclusions and further work.	308
REFERENCES		R1
APPENDIX 1 : STATISTICAL METHODS		A1-1

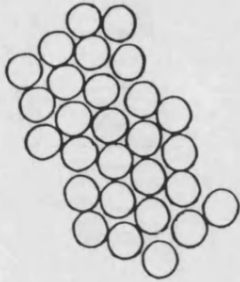
CHAPTER 1INTRODUCTION, BACKGROUND AND SCOPE OF WORK1.1 The physical stability of pharmaceutical suspensions

To produce a solid in liquid dispersion it is usually necessary to break up the clumps of particles which are often present in the starting material. In some cases reduction in size of individual particles may occur. The resultant increase in effective surface area will, in principle, lead to an increase in the surface free energy of the system. However, in practice this tendency is reduced by the particles undergoing aggregation, either by flocculation to form easily reversible loosely bound structures (flocs), or coagulation to produce closely packed relatively irreversible structures (agglomerates). The latter may produce dense solid cakes of material on sedimentation, giving irreversible separation of the two phases (Figure 1.1).

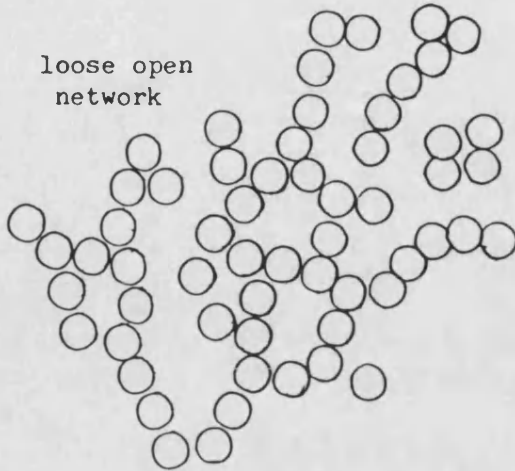
In the colloid chemistry sense, a dispersion is stable if it consists of free particles and resists flocculation or coagulation. The degree of 'resistance' is used as a measure of stability. Pharmaceutically speaking, a dispersion is considered physically stable if it is free from drug loss due to cake formation (caking), or deposition, and can in practice be uniformly dispersed prior to its use, thereby permitting uniform dosage. In this thesis the term 'stable', will be used in the colloid chemistry sense, when applied to the physical stability of a dispersion.

For lyophobic colloids of particle size ranging up to $1\ \mu\text{m}$ (1) the DLVO theory (see section 2.5) sets out to predict the behaviour of such dispersions from an understanding of the attractive and

closely packed



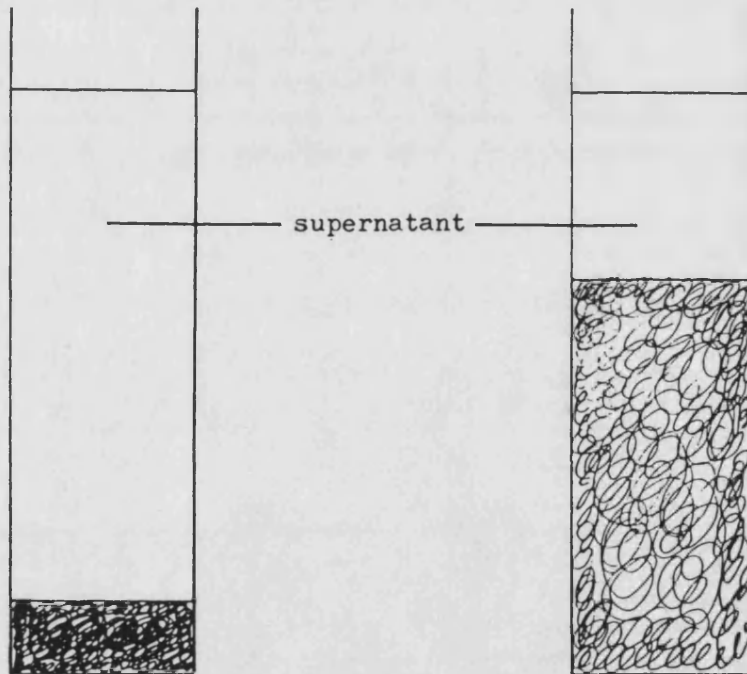
loose open network



A. Microscopic appearance of particles

Difficult to reverse on shaking.

Easily reversed on shaking.



Coagulated system

Flocculated system

Figure 1.1 Characteristics of a Dispersion Which Undergoes Flocculation or Coagulation

repulsive forces between adjacent particles. However, the applicability of the DLVO theory in understanding the behaviour of pharmaceutical dispersions has been questioned, since the theory was not developed for application to the coarse dispersion typical of most pharmaceutical products (2). Measurements of zeta potential (see section 2.1) have been used in experimental tests of DLVO theory.

For pharmaceutical systems the early work of Haines and Martin (3-5), who studied sulfamerazine and bismuth subnitrate dispersions, showed that controlled flocculation using electrolyte ions could lead to a reduction in the caking of aqueous pharmaceutical dispersions. Concomitant microelectrophoresis shows that flocculation corresponds to a fall in the zeta potential of the dispersed particles, to a numerical value below 10 to 45 mV (4, 6), depending on the system studied. Subsequently measurement of zeta potential has been widely used to evaluate the charge characteristics of dispersed drug particles (7-10). Amongst the many studies (e.g. 4, 7, 10) which have related zeta potential to the degree of flocculation, the work of Matthews and Rhodes (6, 11) is noteworthy. They considered the effect of a series of electrolytes on griseofulvin, sulfamerazine and hydrocortisone dispersed in aqueous solutions of ammonium and sodium dioxyethylated dodecyl sulphate. It was concluded that for particles in the 3 to 4 μm diameter range, flocculation was essentially similar in character to the lyophobic colloidal behaviour considered by the DLVO theory. Computer models have been published which can be used to test whether observed zeta potentials and corresponding dispersion stability fit the colloidal behaviour predicted by the DLVO theory (12).

Controlled flocculation is considered to result from a deepening of the secondary minimum (7), following the addition of an electrolyte (see section 2.5). A more appropriate term might be controlled aggregation, since flocculation can also be caused by the adsorption of polymers and polyelectrolytes (7, 10, 13, 14). If the depth of the primary minimum (see section 2.5) is restricted by an adsorbed layer, control of flocculation may be obtained. Similarly, flocculation may be caused by the bridging of particles by adsorbed polymers and polyelectrolytes. Dispersions stabilised by such mechanisms may be resistant to the effects of electrolyte addition (13), and may not show the relationship between zeta potential and stability described by Haines and Martin (7, 10).

1.2 Formulation of the metered dose inhalation aerosol product

The term "aerosol", in a colloid chemistry sense, describes a suspension of small particles, either solid or liquid, of radius less than 50 μm , dispersed in either air or gas (15). However, in the commercial and manufacturing world the term has long been synonymous with the aerosol product. Such products have been distinguished by the term 'aerosol package', defined as a "pressurised sealed container with liquefied or compressed gases, so that the product is self dispensing" (16). The term as used in this thesis is not merely confined to the scientific colloidal definition.

The technology of aerosol products has been the subject of several major treatise (15, 17-19). Pressurised metered aerosols for inhalation are designed to deliver drugs in to the lower respiratory tract. Frequently it is found that delivery offers the important advantages of rapid onset of action, more prolonged action and

reduced systemic side effects, when compared with oral administration (20). The ratio of effective dose administered by this route to the more conventional oral route may be as high as 1:200 (21). Table 1.1 summarises those drugs which are currently available in the UK as metered dose aerosol formulations for inhalation use (22, 23).

An aerosol product for inhalation may be either formulated as a suspension or solution. Suspensions are preferred where they are technically feasible, as they give superior chemical stability and lower oropharyngeal deposition (24). Typical formulations consist of a 0.15 to 5.0% w/v dispersion of a microfine drug in a liquefied, low boiling point propellant blend. A dispersing agent may be added, typically at a concentration of 0.2 to 2.0% w/w or lower (24). The drug dispersion is generally sealed in to an aluminium can fitted with a metering valve. The whole package fits into an actuator (Figure 1.2). When actuated, a metered volume of the mixture is released through an atomising jet in the actuator. The propellant rapidly boils off or 'flashes', leaving, after the evaporation of the propellant from the spray droplets, a cloud of dry solid particles (25). This cloud of drug particles is then inhaled by the patient.

Two regions of the lung are commonly distinguished in considering airway deposition from oral aerosol therapy, namely, the trachea-bronchial region (trachea and bronchial tree to terminal bronchioles) and the pulmonary region (respiratory bronchioles to alveolar sacs) (26). Whilst the site of action of many inhaled drugs is unclear, it can be appreciated that for a local action the drug must penetrate and be deposited in the lower regions of the respiratory tract. Clearly for the relief of bronchospasm, bronchodilator drugs must be

Drug	Action	Notes
Salbutamol Terbutaline SULPHATE Fenoterol Hydrobromide Pirbuterol ACETATE Reproterol Hydrochloride	Bronchodilation by selective beta 2 adrenoceptor stimulation	Drugs of choice in the treatment of mild to moder- ate asthma
Adrenaline Acid Tartrate Isoprenaline Sulphate Orciprenaline Sulphate	Bronchodilation by adrenoceptor stimulation	Less selective than beta 2 adrenoceptor stimulants
Ipratropium Sulphate	Bronchodilation by anticholin- ergic action	Traditionally regarded as effective in relieving bron- choconstriction associated with chronic bronch- itis
Beclomethasone Dipropionate Betamethasone Valerate Budesonide	Corticosteroid	Treatment of moderate to severe asthma, maximum penetra- tion facilitated by inhalation of beta 2 adreno- ceptor stimulant
Sodium Cromoglycate	Stabilisation of mast cell mem- branes	Prophylaxis of asthma

Table 1.1 Principle Drugs Available as Metered Dose
Inhalation Aerosol Formulations in the UK

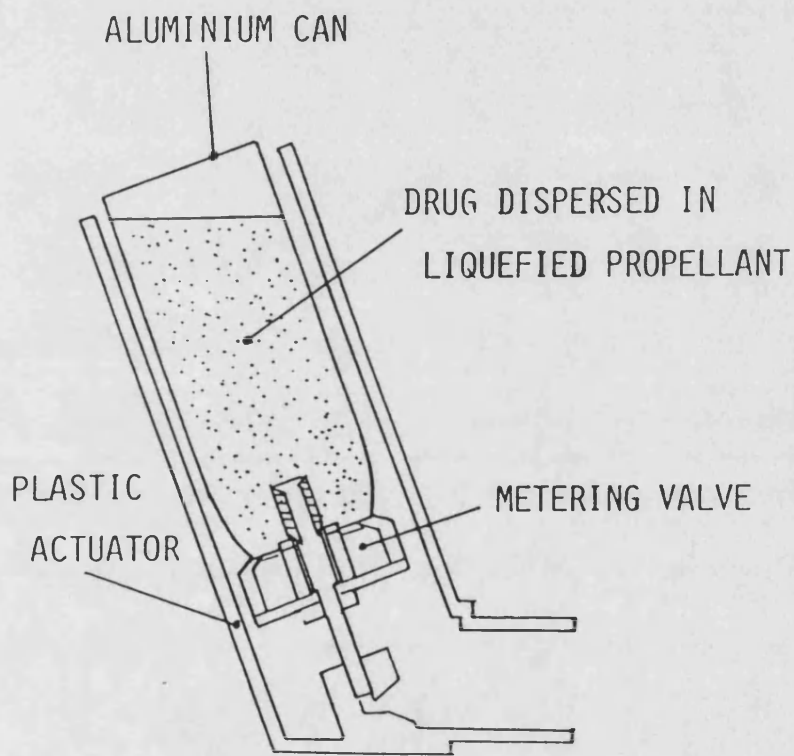


Figure 1.2 The Pharmaceutical Metered Dose
Inhalation Aerosol

targetted towards the respiratory bronchioles. Particle size is thus of great importance.

For many inhalation aerosols the important size range is considered to comprise aerodynamic diameters from 0.5 to 10 μm , peak pulmonary deposition being obtained for particles around 2 μm (20, 27). The aerodynamic diameter of a particle is equivalent to the diameter of a sphere of unit density which would exhibit the same sedimentation rate as the particle in a particular orientation.

Particles are deposited in the lung by three main mechanisms, inertial impaction, sedimentation and diffusion, the latter being only of importance to submicron particles. These mechanisms are influenced by particle aerodynamic diameter (impaction and sedimentation), particle velocity (impaction) and residence time in the lung (sedimentation and diffusion). Additionally particle hygroscopicity and electrical charge may influence deposition (27, 28).

The recognition of the importance of drug particle size in dictating lung deposition performance is evidenced by a move to tighten Pharmacopoeial standards for aerosols in America. The United States Pharmacopeia (USP) XXI states "For inhalation therapy, the particle size of the delivered medication must be carefully controlled and the average size should be under 10 μm ". Monographs for some individual products e.g. Ergotamine Tartrate Inhalation do contain specific limits for the particle size of the delivered drug. Assessment is by microscopic examination of a slide on to which a single actuation has been fired. The majority of particles must be below 5 μm with no more than ten being greater than 10 μm in 25 fields of view (magnification X450). Agglomerates are not included in this specification, which

applies to individual particles only. The USP is now moving to a general standard for inhalation therapy products, requiring the majority of drug particles to be less than $5\ \mu\text{m}$ as determined by microscopy or "an appropriate method" (29).

Particle size limits for aerosol products are also set out in the appropriate monographs of the Pharmaceutical Codex XI which refers back to the British Pharmaceutical Codex, 1973. This has a requirement that the majority of particles are below $5\ \mu\text{m}$ and none greater than $20\ \mu\text{m}$. Such microscopic methods do have the serious disadvantage in that non-drug particles, arising from excipients, will also be assessed.

Such compendial standards do not reflect the performance of the products in the patient, since it is the aerodynamic diameter which is of importance in dictating deposition. Clearly the product must be assessed in a more realistic manner. At present the most reliable method is to fire the inhaler into a suitable chamber and then draw the aerosol cloud through a cascade impactor. Such methods show that acceptable products give a log-normal size distribution with a mean mass aerodynamic (MMAD) size of about $3\text{-}4\ \mu\text{m}$ and a geometric standard deviation of about 1.5 to $2.0\ \mu\text{m}$ (21, 30-32). A more realistic measurement is achieved by firing the inhaler into a throat device and measuring the fine particle penetrative fraction (33, 34).

The only acceptable propellants for international use in metered dose inhalers are propellant 11 (trichlorofluoromethane), propellant 12 (dichlorodifluoromethane) and propellant 114 (dichlorotetrafluoroethane) (18). It has been shown that the propellant blend can affect the amount of drug delivered to the patient (35). A blend with a high

vapour pressure may produce a reduction in the particle size of the delivered drug by breaking up any aggregates which might be present (36). Conversely, a blend with too low a boiling point will not have all boiled off before reaching the patient, consequently droplets of drug suspension of increased size are delivered instead of individual drug particles.

Ideally the drug should be insoluble in the propellant blend used, otherwise particle growth due to Ostwald ripening may occur (37). This will modify deposition characteristics and may block valves. Partially soluble materials may be deposited on the expansion orifices of the actuator (15). The density of the propellant blend may differ from that of the dispersed drug; for instance isoprenaline hydrochloride has a density of $1.16 \times 10^3 \text{ kgm}^{-3}$ (38), whilst a typical propellant blend (39) has a density of the order of $1.38 \times 10^3 \text{ kgm}^{-3}$ (40). Such differences will often lead to 'creaming' of the drug on standing (41); this must be reversed by shaking the product before it is used.

Using antibiotic and steroid formulations, Zahrzewski et al (42) have demonstrated that the first few months of storage are critical in terms of potential agglomeration. After this period, further storage has little effect. If aggregation is not reversed by shaking, the effective drug particle size is increased and so is liable to block the valve. Even if this does not occur the drug particles may be too large for penetration into the desired region of the lung. Both will cause a marked decrease in the therapeutic efficacy of the product. Solid cakes, formed often as a consequence of creaming, are not easily reversed and so will also decrease the available drug.

Consequently a dispersing agent, or "surfactant", may be included in a formulation to reduce agglomeration and caking effects. Such an additive must be non-toxic, biodegradable and miscible with respiratory fluids, so as not to cause respiratory irritation. A dispersant must also not diminish the drug's bioavailability, induce its chemical degradation or promote chemical or physical interaction with components of the can. The dispersant must also not solubilise the drug in the propellant blend. For all these reasons the concentration of the dispersant is minimised, although the inclusion of surfactant has been shown to reduce the particle size of the delivered drug (36). However, inclusion of sufficient non-volatile surfactant may retard the 'flashing' of the propellant which would cause an increase in the particle size of the delivered aerosol cloud (43). Dispersants must themselves be soluble in the propellant mixture and should be liquids. Those which are solid at room temperature have been found to be unsuitable due to blockage of the valve and actuator orifices (44). One patent claims the most suitable dispersants are surfactants which are non-ionic, with HLB values of less than 10 and ideally between 1 and 5 (44).

The presence of a surfactant may also play an important role as a valve lubricant in some products, so improving its reproducibility of metered delivery by easing the mechanical action of the valve (28).

Surfactants currently in use, in commercial pharmaceutical inhalation aerosols include oleic acid (HLB = 1), lecithin and various sorbitan esters e.g. sorbitan mono-oleate (Span 80, HLB = 4.3) and sorbitan trioleate (Span 85, HLB = 1.8) (45-47).

Traces of moisture have a marked effect on non-aqueous suspension

stability (see section 2.2). Unfortunately some studies on the role of surfactants in aerosol formulations do not report control of the moisture content (48). The studies of Kanig and Cohn (38, 49) underline the importance of moisture; they report that Arlacel 83 (sorbitan sesquioleate, HLB = 3.7 (47)) and Emcol 14 (a polyglyceride ester of a fatty acid) are both effective at stabilising dispersions of prednisolone with moisture levels below 500 ppm. For dispersions of isoprenaline, Arlacel 83 was effective for moisture contents below 50-100 ppm and Emcol 14 for those less than around 250-500 ppm. Neither dispersion was properly stabilised by Tergitol NP14 (a nonylphenyl polyethylene glycol ether, HLB=14 (50)) at moisture levels down to 50 ppm. Dispersions of talc were found resistant to aggregation at moisture levels of up to 5000 ppm, for both Arlacel 83 and Emcol 14. This observation supports the postulate that the more water soluble the dispersed solid, the more susceptible its dispersions will be to moisture effects. The origin of the moisture in the dispersion, whether introduced with the drug or from the propellant produced no significant differences.

An early patent (44) sets an upper limit of 300 ppm water in the dispersion for obtaining a suitably stable formulation. The studies of Kanig and Cohn would suggest that in some cases this value is too high (38, 49). In contrast, a patent covering the aerosol formulation of sodium cromoglycate, a water soluble, hygroscopic drug, states that the product should contain preferably less than 0.2% ^w/_w (2000 ppm) of water (51).

In a similar way to moisture, it is conceivable that polar extractives from rubber and plastic valve components which include plasticizers,

accelerators and activators (52), may also have a marked effect upon the aggregation characteristics of the dispersion.

Aggregation of aerosol dispersions, may be controlled by the addition of an inert, finely divided powder rather than by use of a surfactant (53). This approach has a very restricted potential for the pharmaceutical inhalation aerosol because of the problems of finding a toxicologically acceptable compound for inhalation use.

The components used in the aerosol package can influence the performance of the final product. Clearly the metering valve plays an important role in ensuring uniform and reproducible dosage to the patient. Dose control is effected via a metering chamber which samples a fixed volume of dispersion, typically 25 to 100 μ l. To ensure reproducibility of dosing, it is essential that the drug dispersion is homogeneous when sampled by the valve.

The volume of the metering chamber chosen obviously depends upon the dispersion concentration and dose required. However, there is some evidence that the product of size of metering valve used and the suspension concentration used to provide a given nominal dose affects the amount of drug delivered to the patient (43).

The material of the can can have a marked effect upon the degree of drug deposition on to the inner wall. Internally lacquered aluminium containers have been reported to cause less wall deposition than unlacquered containers. Both show considerably less deposition than corresponding glass containers (54). Deposition of the drug on to the wall in the headspace has been noted, with particles 'creeping' above the liquid/vapour interface (44).

The actual amount of drug which is deposited in the lungs depends on a large number of other variables including actuator design (54), technique in using the inhaler (56, 57) and respiratory function of the patient (20). Studies have shown that around 10 - 16% of the dose delivered by the inhaler is actually deposited in the lungs (58). Almost half the dose may be deposited in the mouth (59) and after being swallowed lead to local side effects (60).

1.3 The non-aqueous dispersion

Strictly, non-aqueous dispersions are those in which the liquid phase is other than water. The majority of these liquids are non-polar similar to hydrocarbons, although there are exceptions such as methanol (61). Consideration here is limited to non-aqueous dispersions which have a non-polar liquid phase.

The relative permittivity (ϵ_r) of a material is a measure of its polarity, a large value corresponding to a polar material. Typical non-polar liquids like benzene, hexane and p-xylene have values at 20°C of 2.28, 1.89 and 2.27 respectively, whilst water has a value of 80.10 (62). Since propellants 11, 12 and 114 have relative permittivities of 2.28 (29°C), 2.13 (29°C) and 2.17 (31°C) respectively (63), dispersions of drugs in liquefied aerosol propellants can be considered as non-polar, non-aqueous dispersions.

Non-polar dispersions are traditionally of importance in the paint (64) and oil industries (65). More recently their role as liquid toner systems in electrophotography has become an important application (66). Such dispersions also find a role in electrophoretic display devices (67) and in the fabrication of electronic

components by electrodeposition (68). The majority of the literature therefore tends to be concerned with the commercially important dispersions of carbon black and titanium dioxide.

1.4 The scope and objective of this study

It can be seen that the nature of inhalation aerosols differs considerably from most other pharmaceutical dispersions, which are generally aqueous. Experimental observations on the latter, indicate that the DLVO theory is broadly applicable in understanding the physical nature of such dispersions in terms of flocculation, sedimentation and caking behaviour. It is generally agreed that controlled flocculation of charged particles based on DLVO principles, can be used to provide formulations having suitable redispersion characteristics.

The role of particle charge in connection with the stability of non-polar dispersions is not well understood. It may or may not be significant in the caking, agglomeration and/or can wall deposition effects which have been observed in inhalation aerosols. This lack of understanding has continued for several decades because of the experimental difficulties in reliably assessing particle charge in non-polar dispersions. Literature data on drug-propellant particle charges is non-existent. The carbon black and titanium dioxide data is frequently unreliable, due to the use of inappropriate experimental methodology.

Fundamental investigations into the factors pertinent to the formulation of inhalation aerosols must examine the role of surface potential. Thus, the primary objective in this study was to set out to develop a theoretically and practically sound method for the

determination of such potentials, based on electrophoretic measurements in non-polar dispersions, which model inhalation aerosols. Consequent upon this the effect of surfactants on measured potentials could be investigated.

1.5 A note on units

The SI (Système International d'Unités) system of units are used throughout this text. Thus some formulae may appear to differ from those commonly quoted in the literature. Wherever D_c (the dielectric constant) appears in older formulae it has now been replaced with the parameter $4\pi\epsilon_0\epsilon_r$, where ϵ_0 is the permittivity of a vacuum and ϵ_r is the relative permittivity (69).

Thus the traditional Smoluchowski equation for electrophoretic mobility (U_E) given as equation 1.1,

$$U = \frac{\zeta D_c}{4\pi\eta} \quad - 1.1$$

(where ζ is the zeta potential and η the viscosity of the medium) now becomes equation 1.2,

$$U_E = \frac{(4\pi\epsilon_0\epsilon_r)\zeta}{4\pi\eta} = \frac{\epsilon\zeta}{\eta} \quad - 1.2$$

where ϵ is the permittivity of the medium as given by equation 1.3.

$$\epsilon = \epsilon_0\epsilon_r \quad - 1.3.$$

The relative permittivity (ϵ_r) has the same numerical value as the dielectric constant but is used to avoid confusion with older texts.

Hamaker constants, traditionally expressed in ergs have been converted to Joules where $1 \text{ erg} = 1 \times 10^{-7} \text{ J}$ (62).

CHAPTER 2THE COLLOID CHEMISTRY OF NON-AQUEOUS DISPERSIONS2.1 The electric double layer

The electric double layer model has been developed from the original work of Helmholtz (70), Gouy (71), Chapman (72) and Stern (73). It deals with the distribution of counter and co-ions at a charged surface immersed in a liquid and the electric potentials that will occur in this region. The electric double layer can be divided into two parts, an inner region which may include adsorbed ions and an outer diffuse region.

A solid body in contact with a liquid will often acquire a nett surface charge. In the liquid, free ions of opposite charge (counter ions) will be attracted towards the surface, whilst those of similar charge (co-ions) will be repelled. In consequence, a nett accumulation of counter ions will occur around the surface. The counter ions do not all accumulate at the surface, since electrical attractive forces are balanced by the tendency of counter ions to move into the bulk of the liquid through random thermal motion. The resulting equilibrium is termed the diffuse layer (Figure 2.1).

The approximate decay in potential from the surface through the diffuse layer is given by equation 2.1.

$$\psi = \psi_d (\exp - \kappa x) \quad - 2.1$$

ψ is the potential at a given point a distance x from the Stern layer being equal to ψ_d . The value κ is derived from equation 2.2:

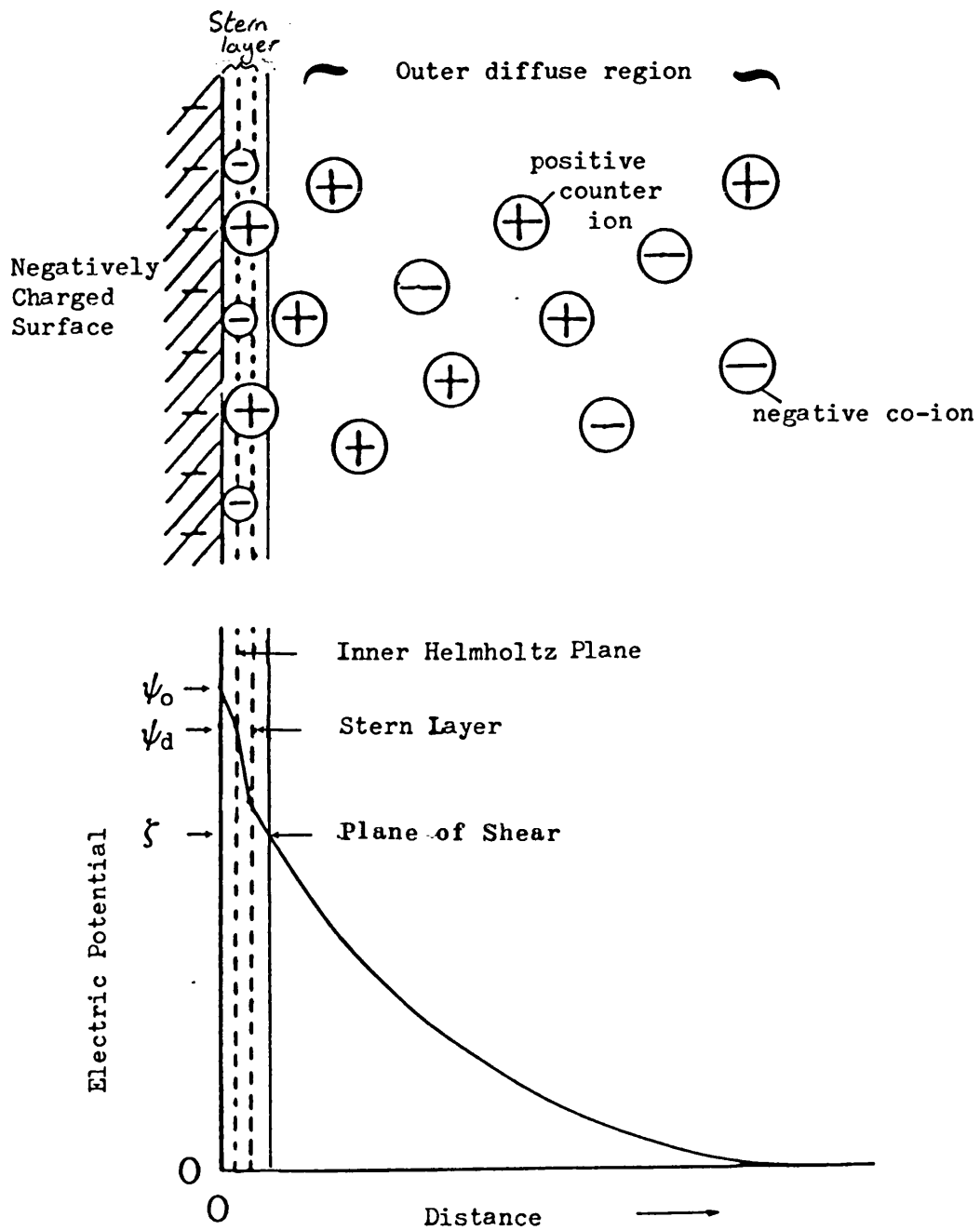


Figure 2.1 Schematic Representation of the Distribution of Ions and Corresponding Electric Potential Across the Double Layer (Specific adsorption occurs in this case).

$$\kappa^2 = \frac{e_0^2 n_i z_i^2}{\epsilon kT} \quad - 2.2$$

where n_i is the number of free ions per m^3 , e_0 the elementary charge (1.6×10^{-19} C), z_i the valency of the free ions, ϵ the permittivity of the liquid (Fm^{-1}), and k the Boltzmann constant ($1.38 \times 10^{-23} JK^{-1}$). κ is the Debye-Hückel function and is a measure of the diffuse layer thickness; the distance over which ψ falls to a value equal to $\psi_d/2.718$ is equal to $1/\kappa$.

These equations are derived from the basic Poisson and Boltzmann equations (69) and make several important assumptions.

1. The charged surface is assumed to be flat, of infinite extent and uniformly charged.
2. The ions in the diffuse layer are point charges, distributed according to Boltzmann's equations.
3. The liquid influences the diffuse layer only through its permittivity, which is constant throughout.
4. The Debye-Hückel approximation that $z_i e_0 \psi_d/kT < 1$ is made, which is only valid for values of $\psi_d < 25$ mV.

In a non-polar system the diffuse layer thickness is greater than in aqueous systems despite lower values of liquid permittivity. This is because concentrations of ions in such systems are low and ill defined. However, even in the absence of dispersants or polar impurities, carefully purified hydrocarbons contain some stable excess charge carriers; these may arise from any kind of irradiation e.g. γ -rays (74).

Since ion concentrations are low, estimation of the diffuse layer thickness using equation 2.2 is difficult. Methods for obtaining an estimate of the diffuse layer thickness are usually based on the conductance of the liquid phase of the dispersion.

The approach of Kitahara (75) is to use Walden's law to estimate the number of ions present. Walden's law states that for a dispersed material in a given liquid, the product of the dispersant's equivalent conductance at infinite dilution (Λ_0) in that liquid and the liquid's viscosity (η), is constant for all solutions of that dispersant (equation 2.3).

$$\Lambda_0 (\text{aqueous}) \eta (\text{aqueous}) = \Lambda_0 (\text{non-aqueous}) \eta (\text{non-aqueous}). \quad - 2.3$$

If Λ_0 (aqueous), η (aqueous) and η (non-aqueous) are known, or can be determined an estimate of Λ_0 (non-aqueous) can be made. The specific conductivity (σ) of a non-aqueous dispersant supernatant containing that dispersant can then be measured, and equation 2.4 used to obtain an estimate of n_1 .

$$\sigma = \frac{n_1 e_0 \Lambda_0}{F} \quad - 2.4$$

F is the Faraday constant ($9.64 \times 10^4 \text{ C mol}^{-1}$). Kitahara (75) has estimated diffuse layer thicknesses for a particle dispersed cyclohexane to range from 1 - 95 μm , for varying concentrations of Aerosol OT.

An alternative approach to the estimation of the diffuse layer thickness can be made using equation 2.5 (76).

$$1/k = (\epsilon D_1 / \sigma)^{\frac{1}{2}} \quad - 2.5$$

However, calculation of D_1 using the standard Einstein equation (76)

requires a knowledge of the radius of the ion (r_i) (equation 2.6).

$$D_i = \frac{kT}{6\pi\eta r_i} \quad - 2.6$$

Since this is not always known, an estimate is made; a value of 1 nm being typical.

For a spherical particle of radius a , κa is a good measure of the sphericity of the diffuse layer surrounding that particle; if $\kappa a > 10$ the flat diffuse layer model is valid. In non-polar systems where values of $\kappa a < 0.1$ are typical, particles can be treated as point charges (Figure 2.2). The distribution of charge through the diffuse layer, after making the Debye-Hückel approximation, is described by equation 2.7.

$$\psi = \psi_0 \frac{a}{r} \exp [\kappa(a - r)] \quad - 2.7$$

ψ is the potential of the diffuse layer at radial distance r .

The charge on the particle (Q) is described by equation 2.8.

$$Q = 4\pi\epsilon a (1 + \kappa a) \psi_0 \quad - 2.8$$

In the limiting case where $\kappa = 0$ equation 2.7 and 2.8 become equations 2.9 and 2.10 respectively.

$$\psi = \frac{\psi_0 a}{r} \quad - 2.9$$

$$Q = 4\pi\epsilon a \psi_0 \quad - 2.10$$

Combining equations 2.9 and 2.10 gives equation 2.11.

$$\psi = \frac{Q}{4\pi\epsilon r} \quad - 2.11$$

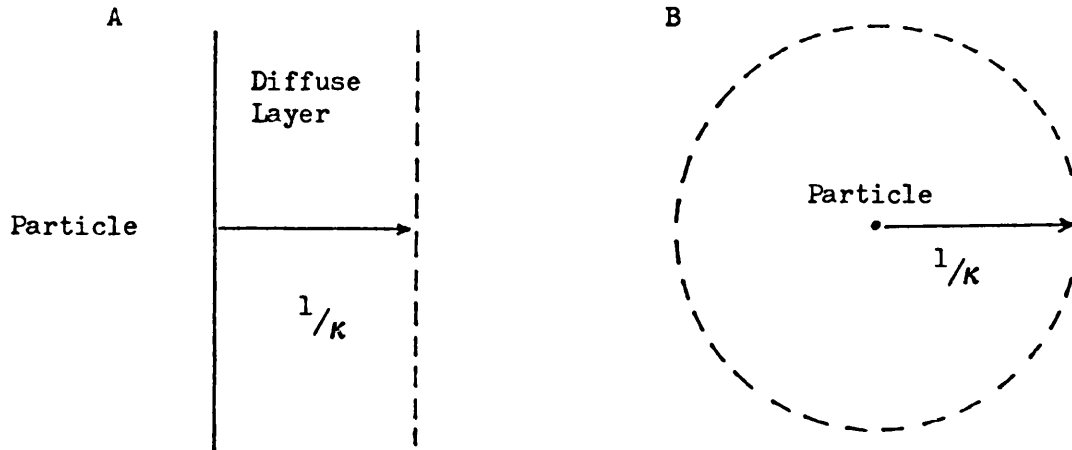


Figure 2.2 Schematic Representation of the Diffuse Layer in Limiting Cases

- Where:
- A) $\kappa a > 10$: The particle surface approximates to a flat diffuse layer
 - B) $\kappa a < 0.1$: The particle approximates to a single point charge

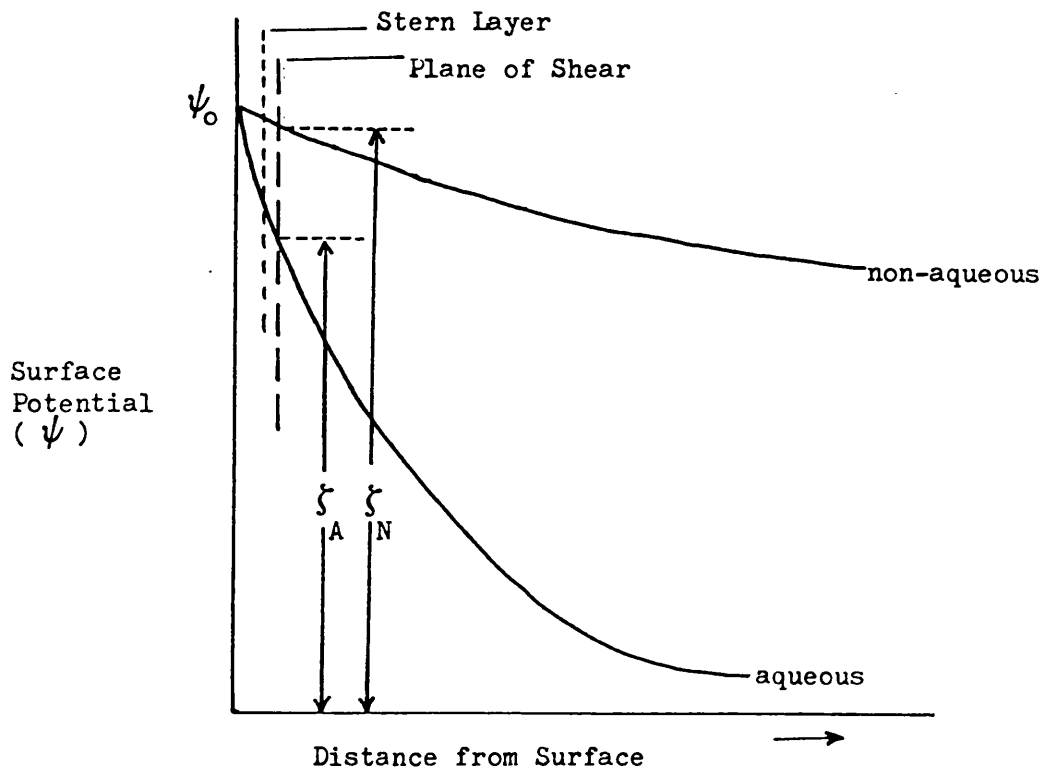


Figure 2.3 Double Layer Potentials in Non-aqueous and Aqueous Media

- ζ_A = Measured aqueous zeta potential
- ζ_N = Measured non-aqueous zeta potential
- ψ_0 = Surface potential

This demonstrates the screening effect of the counter ions, since equation 2.11 (where $\kappa = 0$) is that which describes the potential decay as described by simple Coulombic law.

Since ions have finite size the inner boundary of the diffuse layer will be limited. In aqueous systems, without specific adsorption, an ion can only approach to within its hydrated radius; this limiting distance is termed the Stern plane. Specifically adsorbed ions can be located between the particle surface and the Stern plane, at the inner Helmholtz layer.

Charge measurements which utilise electrokinetic phenomena record the electric potential at the plane of shear, which in aqueous systems will be at least the diameter of a hydrated ion away from the particle surface. This shear plane potential is termed the zeta potential (ζ) and in aqueous systems can be considerably different from the surface potential and the potential at the stern plane (ψ_d). In a non-polar system the electric potential decay with distance is much smaller (figure 2.3), so in the absence of specifically adsorbed ions, the measured zeta potential can be closely related to the surface potential ψ_0 .

Doubts have been expressed over the validity of the basic double layer model in non-polar dispersions (75, 77, 78). In a typical non-polar dispersion a particle of radius 100 nm with a zeta potential of 50 mV, requires just 8 elementary charges to be distributed upon its surface. The double layer model requires that the surface charge is uniformly spread over the particle surface; at such low charge coverages it seems unlikely that such an approximation is itself valid. In conducting aqueous media both positive and negative ionic species are present in

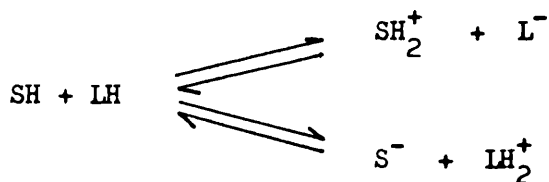
high concentrations in the diffuse layer. Novotny (79), considers that since the diffuse layer in non-aqueous media contains essentially ions of one species, the diffuse layers in the two media are dissimilar. A re-examination of the importance of relaxation and retardation effects (see section 3.2) in non-aqueous media might therefore be required.

2.2 The origin of surface charge in dispersions of non-polar media

The existence of surface charge on particles in suspension can easily be established from the results of electrokinetic experiments. The mechanism of charge production is very dependent upon the nature of the particle, the non-polar media, the presence of any surfactant and the water content of the system.

2.2.1 BASIC MECHANISMS OF SURFACE CHARGE GENERATION

Surface charge generation in non-polar media can, in the main, be considered to be due to either proton or electron transfer. In the absence of any dispersant (e.g. surfactant), the general mechanism of charge generation is through dissociation of surface groups, with either a proton being accepted or donated (75). Consider a particle surface (SH) in contact with a liquid (LH), transfer of a proton will result in a surface charge.



The question of whether the surface accepts a proton and becomes positive or vice versa will depend upon the relative acidity (in the Brønsted sense) of the surface to the liquid. Titanium dioxide

is positive in heptanol yet negative in the more basic nitrobenzene (80).

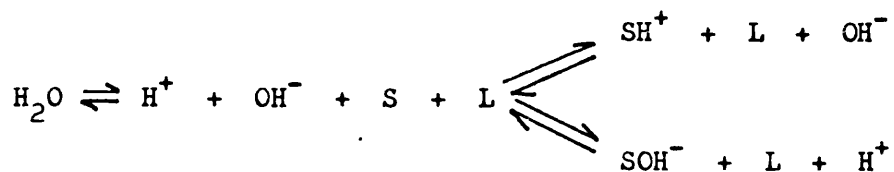
When two dissimilar metals are brought into contact a potential difference can be developed, due to a difference in their electron affinity. Hunter (69) has considered, that with the exception of metal sols, such a mechanism is unlikely to be of importance at solid-liquid interfaces. However, work by Labib and Williams (81-83) indicates that this mechanism may be of importance. The 'electron donicity' (or Lewis basicity) is a measure of a material's tendency to donate electrons in a Lewis acid-base reaction. Labib and Williams measured the enthalpy of reaction of a large number of solids and liquids with a reference Lewis acid (SbCl_5 in 1, 2 dichloroethane), the magnitude of the enthalpy change was used to rank materials according to their 'electron donicity'. When a solid was placed in contact with a liquid of lower 'electron donicity' the former behaved as a Lewis base and a positive surface charge resulted. Since this was observed with a wide range of chemically different liquids and solids of different bonding type, it suggests electron involvement in the charge transfer step.

A third method of generating charge in non-aqueous dispersions involves the triboelectric phenomena of charging by friction in an insulating medium. It is unlikely that this is an important mechanism in the pharmaceutical systems considered in this thesis. However, evidence of charging of oxides dispersed using an ultrasonic field has been reported (84).

2.2.2 THE EFFECT OF SURFACTANTS AND WATER ON SURFACE CHARGE

In practice non-aqueous dispersions are rarely free from trace water,

which can dissociate weakly. The resultant ions can be adsorbed preferentially to produce a surface charge, the relative acidity of the solid dictates the sign of that charge.



A more basic surface will result in a positive charge and vice versa.

Lyklema (78) suggests that since water is poorly soluble in non-polar media, there will be a tendency for the undissociated water to adsorb on to the particle surface and so render it more basic. This is supported by the findings of Romo (85) who demonstrated that anhydrous alumina particles dispersed in anhydrous alcohols became positively charged with the addition of water, the zeta potential passing through a maximum with increasing water content. A similar observation has been made by Micale et al (80) for rutile dispersed in heptanol. The subsequent decrease in surface charge is thought to arise from a change in double layer structure, due to the presence of a region of higher permittivity adjacent to the particle surface.

Following the work of Van der Minne and Hermanie (86, 87), the addition of ionic surfactants to non-aqueous dispersions was known to induce surface potentials. The proposed mechanism is essentially that seen in aqueous systems.

Surfactant molecules in non-aqueous solutions may show a small degree of dissociation, resulting in the preferential adsorption of one of the ions. The relative affinity of the ions for the particle surface results from either the acid/base interaction already considered or from the relative hydrophilic/lipophilic properties of the ions.

A different mechanism has been proposed for molecules capable of proton transfer, after work carried out with C_{14} tagged basic polymeric surfactants (88, 89). Unionised molecules adsorb on to the particle surface at points where proton transfer from an acidic to a basic site may occur, possibly in a region of higher permittivity than the bulk liquid. Desorption will then occur leaving a nett surface charge.

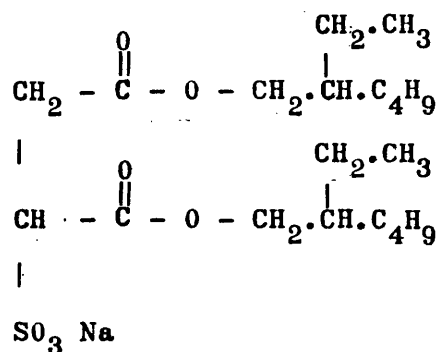
As with the aqueous dispersion, the relationship between sign and magnitude of zeta potential and surfactant concentration is of importance. In some cases reversal of the charge sign has been observed with increasing surfactant concentration (87, 90). This relationship between zeta potential and surfactant concentration can be largely classified into three main types, after Kitahara (75, 91). Type A behaviour is characterised by an increase in zeta potential with increasing surfactant concentration until a maximum is reached, after which a gradual decline takes place. The initial increase in zeta potential is thought to be due to preferential adsorption of ions, producing an increasing surface charge. However, when this reaches a certain magnitude, adsorption of oppositely charged ions occurs; resulting in a fall in the zeta potential. Type B behaviour is characterised by a gradual decline in zeta potential with increasing concentration; this is generally considered to represent post maximum Type A behaviour. Systems exhibiting Type C behaviour show no variation in zeta potential with changing surfactant concentration.

Van der Minne and Hermanie (86, 87) who studied carbon black in benzene with tetraisoamylammonium picrate suggested that the subsequent fall in potential seen was due to the adsorption of ion association

products. The maximum observed in Type A cases has also been analysed in terms of the discreteness of surface charge. A decrease in effective surface charge occurs as individual surface charges interact with each other as the surface charge density increases (92).

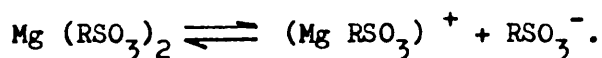
A large proportion of the work which considers the role of surfactants in non-polar dispersions has been carried out using metal sulphosuccinates, in particular sodium 1,2 - bis (2 - ethyl hexyl oxycarbonyl) - 1 - ethane sulphonate (trade name Aerosol OT), whose formula is shown

below.



Aerosol OT can be designated as NaRSO_3 for convenience. Sulphosuccinates of divalent and trivalent metal ions can also be obtained e.g. $\text{Ca}(\text{RSO}_3)_2$, $\text{Mg}(\text{RSO}_3)_2$, $\text{Al}(\text{RSO}_3)_3$. Titanium dioxide dispersions in cyclohexane with $\text{Ca}(\text{RSO}_3)_2$, $\text{Ba}(\text{RSO}_3)_2$ and $\text{Al}(\text{RSO}_3)_3$ have been reported as showing a type A relationship between zeta potential and surfactant concentration (75). The same has been reported for carbon black dispersed in benzene with Aerosol OT (93). Carbon black however shows a type B relationship when dispersed in benzene with $\text{Mg}(\text{RSO}_3)_2$, $\text{Ca}(\text{RSO}_3)_2$ or $\text{Ba}(\text{RSO}_3)_2$ (94). Carbon black and alumina dispersed in xylene both showed no variation in zeta potential with Aerosol OT concentration. These type C systems maintained appreciable zeta potentials, over - 125mV in the case of carbon black and around + 40mV for the alumina (95).

The sign of the surface charge can vary from surface to surface and with the nature of the cation. Carbon black exhibits a negative charge in hydrocarbon solutions of Aerosol OT through preferential adsorption of the organic anion RSO_3^- ; divalent alkaline earth salts (Ca, Ba, Mg) produce a positive charge. Parreira (94) proposed that for such divalent salts dissociation only occurs to the first stage e.g.



Polar groups upon the surface of the carbon black then produce induced dipoles in the resultant cation and adsorption occurs.

Trace water further complicates any complete understanding of the system. Vigorously dried rutile in xylene-Aerosol OT solutions is initially negatively charged. When left to pick up water charge reversal occurs, the water adsorbed on to the rutile surface preferentially adsorbing the free sodium ion (95). With increasing water concentration the zeta potential has been reported to pass through a maximum at around 30 to 80 ppm water, for both negatively charged carbon black in benzene and positively charged copper phthalocyanines in n-heptane (93, 96). The subsequent reduction in surface charge is probably due to the effect of the adsorbed surface water upon the diffuse double layer.

From his extensive review of the literature Kitahara (75) concludes that non-ionic surfactants do not produce a surface charge. Although such charges have been reported, they may be ascribed to poor experimental methodology. Garner (97) reports that carbon black is negatively charged when dispersed in toluene with oleic acid. Since a negative charge is also noted for dispersions in toluene alone and there is no control of water content, the role of oleic acid in the generation of surface charge cannot be ascertained. Fowkes (88) also

reports a negative charge for carbon black dispersed in oil with oleic acid, again no control of water content is reported. Whilst non-ionic surfactants in themselves do not seem to charge surfaces, their adsorption on to already charged surfaces is known to lead to a reduction in zeta potential. This is due to a steric effect, whereby the adsorbed surfactant molecules cause the plane of shear of the particle to be moved away from the surface and so cause a decrease in the observed electrokinetically-derived zeta potential (98).

2.3 Electrostatic repulsion

As two particles of like charge approach one another interpenetration of their diffuse layers will occur, giving rise to repulsion. There are two mechanistic models for this interaction.

1. Constant surface potential model. The surface potential is assumed to remain constant as the particles approach; a reduction in surface charge density must therefore occur, necessitating rapid desorption of the charging species.
2. Constant surface charge model. In this case surface charge density remains constant, necessitating an increase in surface potential as the particles approach.

Which of these mechanisms more closely represents the situation in non-aqueous media has not been established. However, since solvation energies of ions are high, their desorption might be slow, possibly suggesting the second model.

The limiting equation for the constant potential mechanism (equation 2.12) is where $H = 0$. (H is the distance between the interacting

particle surfaces and is given by $H = R - 2a$, where R is the distance between particle centres).

$$V_R = \frac{Q^2}{4 \pi \epsilon R} \quad - 2.12$$

substituting Q (equation 2.10).

$$V_R = \frac{4 \pi \epsilon a^2 \psi_0^2}{R} \quad - 2.13$$

Although this equation takes no account of diffuse layer distortion, it is considered satisfactory for potentials of up to about 75 mV (99).

The variation in potential with distance $\frac{d\psi}{dx}$ gives the field strength (E) (equation 2.14).

$$E = \frac{-d\psi}{dx} \quad - 2.14$$

The low field strengths found with extended diffuse layers mean that the repulsive force exerted on a particle is smaller, but of longer range, than with the thinner diffuse layers found in aqueous systems.

2.4 Attractive forces

Between adjacent atoms induced dipoles can lead to attractive forces. Such London - van der Waals forces are weak and decay rapidly with distance. Hamaker (100, 101) considered these forces to be additive, so the interaction energy between two collections of atoms is both significant and of long range.

The attraction energy (V_A) for equal spheres of medium 1 dispersed in medium 2 can be approximated for close approach of the particles ($H \ll a$) by equation 2.15.

$$V_A \approx - A_{12} a/12H. \quad - 2.15$$

A_{12} is the mixed Hamaker constant and can be approximated from the Hamaker constants for each material using equation 2.16.

$$A_{12} \approx \left[(A_{11})^{\frac{1}{2}} - (A_{22})^{\frac{1}{2}} \right]^2 \quad - 2.16$$

A_{11} and A_{22} being the Hamaker constants for the particle material and the liquid medium respectively.

Schenkel and Kitchener (102) make corrections to equation 2.15 to allow for retardation (see section 3.2) which, due to finite propagation times of electromagnetic waves, is significant at larger separations. For separations greater than about $2\lambda_l$, λ_l is the wavelength of the intrinsic oscillations of the atoms (typically of the order of 10^{-7} m), V_A can be approximated from equation 2.17.

$$V_A \approx - \frac{2.45 A_{12} a \lambda_l}{120 \pi H^2} \quad - 2.17$$

At intermediate distances, no simple formula is available, equation 2.18 gives an approximation of V_A when $H \gg a/6$.

$$V_A \approx \frac{A_{12} a}{\pi} \left[- \frac{2.45 \lambda_l}{120H^2} - \frac{\lambda_l^2}{1045H^3} + \frac{\lambda_l^3}{5.62 \times 10^4 H^4} \right] \quad - 2.18$$

Hamaker constants can be estimated from optical data, lattice parameters, surface interface parameters and from stability experiments. Values for non-aqueous systems can, in many cases, be approximated to aqueous system values since often $A_{11} \gg A_{22}$; A_{12} is therefore relatively insensitive to A_{22} . A value of 1×10^{-18} J has been found experimentally for carbon black in Aerosol OT/n heptane solutions (103).

Similar equations to those derived by Schenkel and Kitchener have been

obtained by Lifshits (78), where materials were characterised by their relative permittivities.

The curves described by equations 2.15, 2.16 and 2.17 are not affected by media, so are applicable to non-aqueous systems without alteration.

2.5 Colloid stability arising solely from electrostatic repulsion

Since V_A and V_R are scalar quantities they can be added to obtain the total energy of interaction (V_T).

$$V_T = V_A + V_R \quad - 2.19$$

The DLVO (Derjaguin, Landau, Verwey, Overbeek) theory assumes that dispersion stability is related to the total interaction energy (98).

Construction of the total potential energy curve for two approaching particles, usually shows the energy curve to pass through a maximum (V_{max}) at a certain separation distance (Figure 2.4); for two particles to come together they must overcome this repulsive barrier. The particles will have thermal energy kT and if $V_{max} \gg kT$ few particles will overcome V_{max} , so the particles remain dispersed and agglomeration will not occur. A value of $15kT$ is generally considered sufficient to provide stability against agglomeration (98). In aqueous systems a secondary minimum might develop where particles are weakly attracted together, this appears to be of little importance in non-aqueous systems. Figure 2.5 shows that unlike aqueous systems, the shape of the potential energy curve for non-aqueous dispersions is relatively independent of A_{12} . Consequently if the interaction of particles in non-aqueous systems is only determined by double layer repulsion and van der Waals' attraction, a precise knowledge of

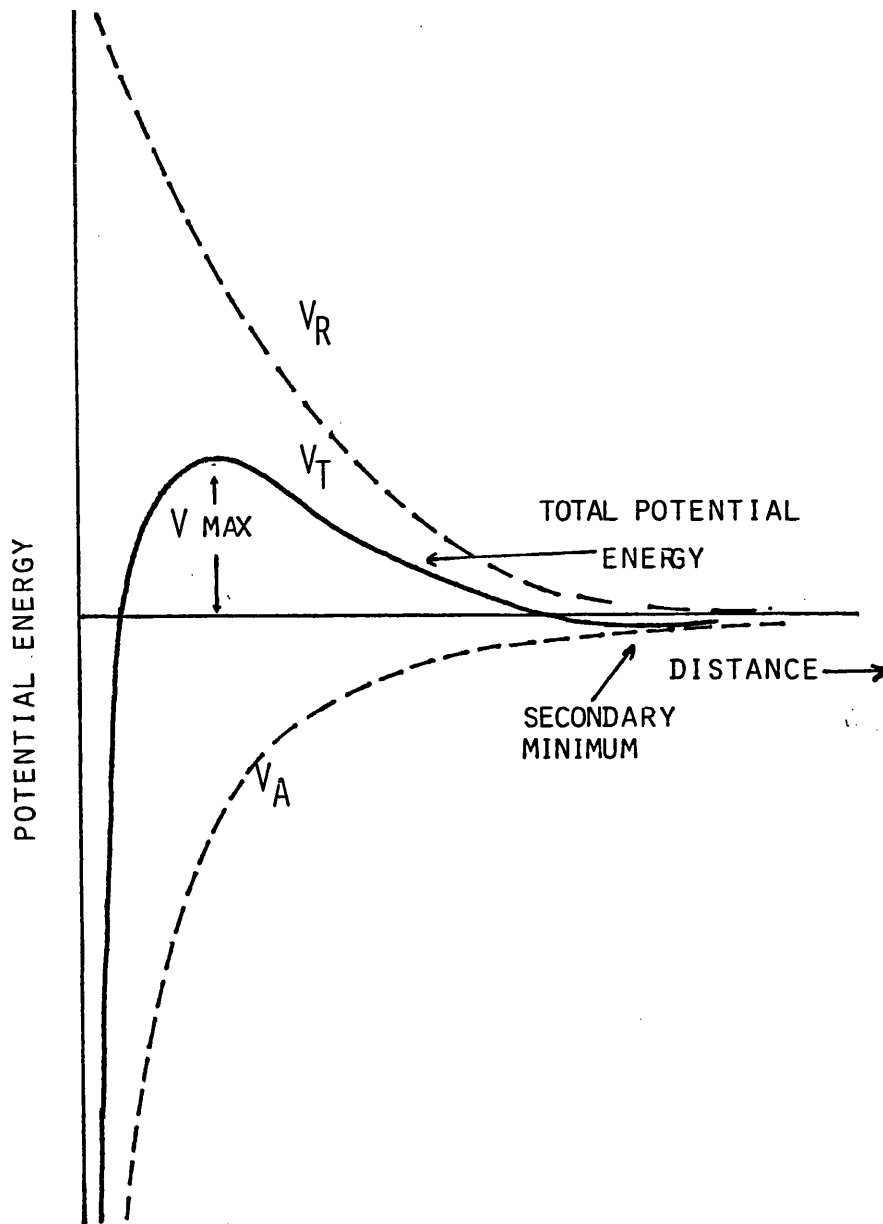


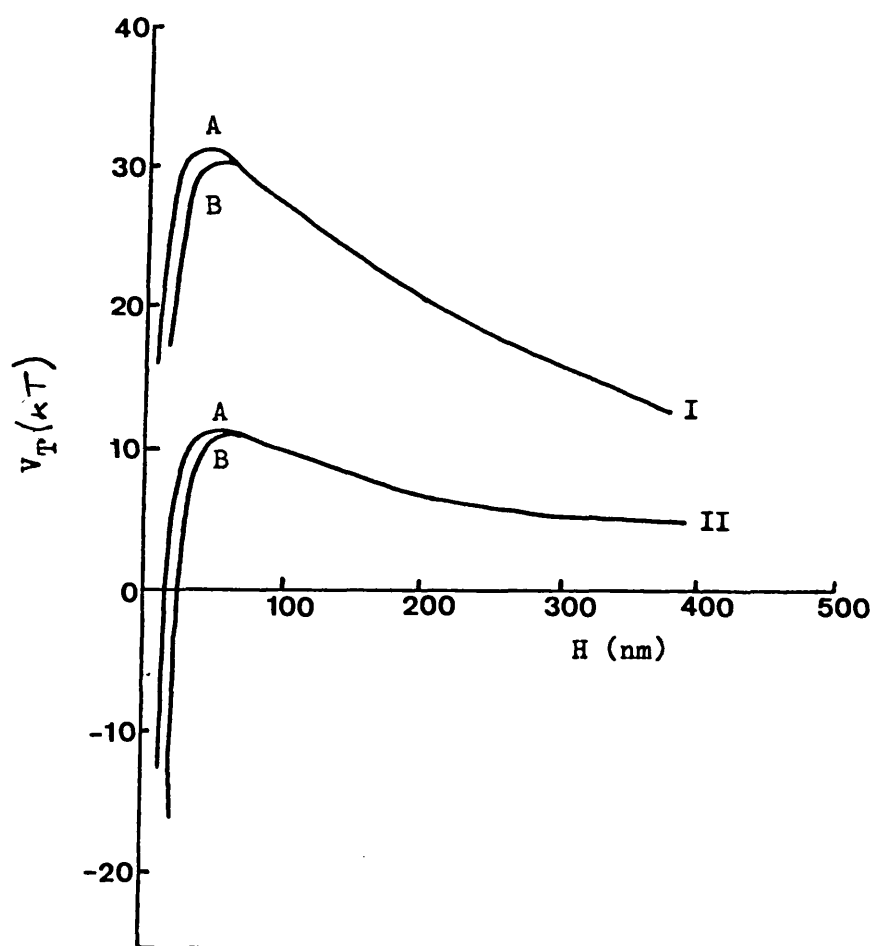
Figure 2.4 Potential Energy Curves for the Interaction of Two Particles

V_R = Electrostatic Repulsion

V_A = van der Waals Attraction

V_T = Total Interaction Energy

Figure 2.5 Total Interaction Potential Energy (V_T)
Between Two Spherical Particles in Non-
aqueous Media (after reference 78),
 $a = 100 \text{ nm}$, $\epsilon_r = 2$.



Hamaker constants (A_{12}) : $A = 1.5 \times 10^{-20} \text{ J}$

$B = 2.0 \times 10^{-19} \text{ J}$

Zeta potentials : $I = 75 \text{ mV}$

$II = 45 \text{ mV}$

A_{12} is not necessary to construct the interaction profile.

Since V_A is proportional to particle size (equations 2.15, 2.17 and 2.18) and V_R is proportional to the square of the particle size (equation 2.13), the larger the particle the more likely it is that it can be electrostatically stabilised. Koelmans and Overbeek (104) showed that large particles ($\sim 1 \mu\text{m}$) can be electrostatically stabilised whilst for smaller ($\sim 10 \text{nm}$) particles such stabilisation is unlikely.

Many workers have attempted to relate the surface potential and therefore calculated V_{max} , to the physical stability of the dispersion. The correlation between calculated V_{max} and the dispersion stability in non-aqueous media is however unclear. This could be due to problems in determining surface potentials (see chapter 3), problems in defining a stable dispersion (see section 2.7) or to the inapplicability of the DLVO theory to such systems.

Micale (80) found a zeta potential of 30 mV ($V_{\text{max}} \sim 10 \text{kT}$) sufficient to stabilise rutile dispersions in heptanol, whilst other workers (85, 95) have reported the critical V_{max} to be around 5 - 7 kT. In contrast copper phthalocyanines in heptane - Aerosol OT could not be stabilised because the resultant zeta potentials (up to 27 mV) were inadequate (96). Osmond and Waite (105) concluded that zeta potentials of between 50 mV and 100 mV were insufficient to produce stability. These conclusions are in agreement with more recent work with carbon black dispersed in dodecane/polyisobutene succinamide, where zeta potentials of over 100 mV were required to provide stability (106).

2.6 Steric stabilisation of non-aqueous dispersions

Water in oil emulsions will flocculate rapidly, despite the fact that the energy barrier (V_{max}) is theoretically large enough to retard flocculation. This observation led Albers and Overbeek (107) to show theoretically that as total potential energy curves overlap, there is a decrease in the energy barrier to flocculation. Feat and Levine (108) similarly concluded that for a concentrated dispersion, with overlapping double layers, the double layer effects alone would lead to attraction between adjacent particles. Thus it would seem that electrostatic stabilisation alone is unlikely to provide a stable dispersion in many practical non-aqueous dispersions, where overlapping double layers will occur.

Romo (109) observed that titanium dioxide dispersed in butylamine with a zeta potential of + 12.7 mV was unstable, but in a linseed oil - xylene system stability was observed despite a lower zeta potential. This effect he concluded was due to steric stabilisation. Steric stabilisers, long chain fatty glycerides in the case of linseed oil, prevent the approach of two particles to a distance where attractive forces will produce flocculation or coagulation. Steric action requires the adsorption of a stabiliser, often a polymer, on to the particle surface.

When two particles with adsorbed polymer layers approach to a distance of less than double the adsorbed layer thickness, interaction between the two layers will occur. The resultant Gibbs free energy change ΔG is given by equation 2.20.

$$\Delta G = \Delta H - T \Delta S \quad - 2.20$$

ΔH is the enthalpy change and ΔS the entropy change at temperature T;

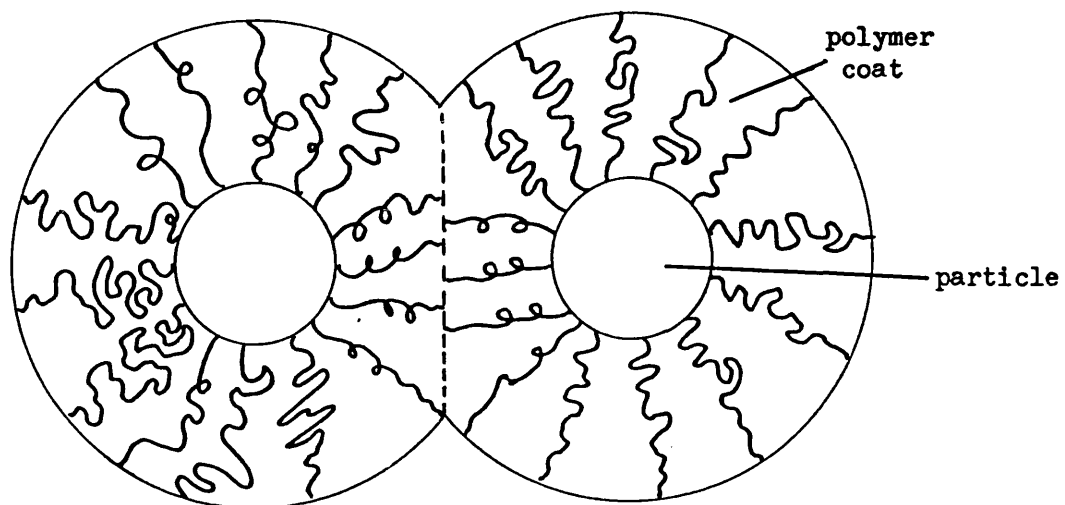
for repulsion to occur upon interaction ΔG must be positive.

Many theories for the mechanism of steric stabilisation have been proposed (110), broadly they can be divided into two types.

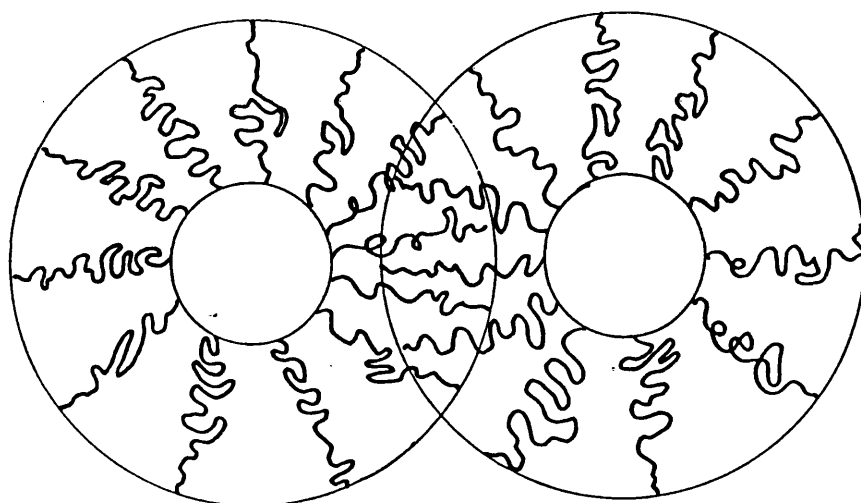
- A. Entropic mechanism. It is assumed that the two layers which interact are impenetrable, therefore compression will occur. An adsorbed polymer in the compressed state can occupy fewer configurations than in the uncompressed state (Figure 2.6A), consequently a reduction in configurational entropy occurs. This reduction in entropy increases ΔG , producing a nett repulsion between the particles.

- B. Osmotic mechanism. In contrast it is assumed that the adsorbed layers of the two particles can overlap (Figure 2.6B), with no desorption occurring. The polymer molecules are in contact with molecules of the dispersion medium, overlapping of adsorbed layers leads to a reduction in this contact, producing an increase in enthalpy of mixing. An increase in segment concentration in the overlapping region also leads to a reduction in configurational entropy. Thus the total free energy change, due to overlap of the layers, is a function of both an enthalpic and entropic change.

The structure of the adsorbed layer is of great importance and has been extensively reviewed (61, 111 - 113). The thickness of the layer, anchoring, configuration and orientation of the polymer all having a marked effect upon stability.



A. Adsorbed layers impenetrable



B. Adsorbed layers overlap

Figure 2.6 Schematic Representation of the Interaction
Between two Polymer Coated Particles on
Approaching Each Other.

2.7 Methods of stability determination

Methods available for stability determination of suspensions can be divided into two main groups; kinetic and static measurements (114).

Kinetic measurements allow comparison of experimentally determined flocculation rate with theory. The initial stages of flocculation for a monodisperse system, if governed only by diffusion is described by the Smoluchowski equation for flocculation (equation 2.21):

$$\frac{1}{N} = \frac{1}{N_0} + k't \quad - 2.21$$

where N_0 is the number of particles per unit volume at time zero, N is the number at time t and k' is the rate constant for rapid flocculation.

N can be determined by direct counting or by indirect^{counting} methods. Direct counting methods whilst accurate, do have the disadvantage of being time consuming, so tend not to be used. Indirect methods involving resistance changes (e.g. Coulter counter) or light obscuration (e.g. Hiac) are more rapid, albeit less accurate, and require sampling. Methods based upon the turbidity of the dispersion tend to be limited to dilute dispersions, where particle size is significantly smaller than the wavelength of the light used. Such methods do however have the advantage of being non-invasive.

A more qualitative assessment of dispersion stability can be obtained by measuring such parameters as turbidity of the supernatant, electrical conductivity of the dispersion, viscosity of the dispersion, sedimentation volume and sedimentation rate. The use of such static methods give a measure of stability which is arbitrary in nature.

Of note is the development of laser methods of dynamic stability assessment which have begun to be reported in the last few years (115, 116). Such methods offer rapid and dynamic information on the flocculated state and are reasonably non-invasive.

CHAPTER 3DETERMINATION OF PARTICLE CHARGE IN NON-AQUEOUS DISPERSIONS3.1 Electrokinetic Phenomena

If an external electric field is applied tangentially to a charged surface in contact with a liquid, relative motion of the two phases will occur. Conversely, if relative motion is created by an external force an electric field will be generated. These electrokinetic phenomena provide the basis for particle charge determination; four distinct effects can be described.

1. Electrophoresis; movement of a charged surface relative to a stationary liquid by an applied electric field.
2. Electroosmosis; movement of a liquid relative to a stationary charged surface by an applied electric field.
3. Streaming potential; creation of an electric field by the flow of liquid relative to a stationary charged surface.
4. Sedimentation potential; creation of an electric field by the movement of charged particles relative to a stationary liquid.

It is theoretically possible to use any of the electrokinetic phenomena to evaluate zeta potentials in non-aqueous dispersions. Experimental methods using electrophoresis (86), electroosmosis (117), streaming potential (117) and sedimentation potential (118) have all been reported.

Kitahara (119) compared the zeta potentials, of barium sulphate in

hydrocarbon solutions of Aerosol OT, obtained by particle electrophoresis, electroosmosis and streaming potential. Those obtained by particle electrophoresis were found to be larger than by the other two methods. This difference was correlated with an overlapping of the diffuse layers in the latter two methods, since neither use dilute dispersions. Further work has as yet been unable to resolve this observation (120). Recently Horn (115) reported no difference in electrophoretic mobility between a concentrated (5%) and a dilute dispersion of β -copper phthalocyanine in a toluene based printing medium. Insufficient experimental details, however, make comment upon these results difficult. It is possible that since the observations were in the presence of 15% binder, the diffuse layer was not extended sufficiently to allow appreciable overlap.

Whilst consideration in this thesis is limited to methods suitable for studying dilute dispersions, there are other techniques suitable for the study of concentrated dispersions. These techniques include moving boundary electrophoresis (97), electrophoretic deposition weight determination (121), sedimentation potential method utilising a centrifugal field (118), and electrical and optical transients. The last technique is described by Novotny and co-workers (79, 122 - 125) and may have application to dilute dispersions. Interestingly a new technique for assessing particle charge mobility, based on ultrasound, has been recently developed (126). It is claimed that the measured 'acoustophoretic' mobility can be directly related to electrophoretic mobility. As yet no detailed assessment of the technique is available so comment upon the technique's applicability is not possible.

3.2 Electrophoretic mobility and zeta potential

A charged particle suspended in a liquid experiencing an external electric field (E) will, on equilibration, move with a uniform velocity in a direction parallel to the field. This electrophoretic velocity (V_E) is dependent upon the magnitude of the applied field; for this reason it is more common to consider electrophoretic behaviour in terms of electrophoretic mobilities (U_E), equation 3.1.

$$U_E = \frac{V_E}{E} \quad - 3.1$$

The SI units of electrophoretic mobility are $m^2 s^{-1} V^{-1}$, but are frequently expressed in terms of the potential gradient, as $\mu m s^{-1} / V cm^{-1}$.

To establish the relationship between electrophoretic mobility and zeta potential, the following assumptions are made.

1. Interaction between adjacent particles is negligible.
2. When a particle moves there is an associated stationary layer of liquid close to the particle surface. The particle and associated liquid is considered to act as a sphere.
3. The conductivity of the particle is zero.
4. The permittivity of the particle is constant throughout.
5. The mobile part of the electric double layer is described by Gouy and Chapman theory (see chapter 2).
6. The permittivity and viscosity of the liquid are constant,

regardless of position relative to the particle.

7. Only one species of positive and one species of negative ion are considered present.
8. Brownian motion of the particle is considered negligible.

In 1924 Von Smoluchowski derived equation 3.2 for the electroosmotic flow of a liquid adjacent to a flat charged surface, under the influence of an applied electric field (127).

$$U_o = - \frac{\epsilon \zeta}{\eta} \quad - 3.2$$

U_o is the electroosmotic flow of the liquid.

The electrophoretic motion of a large particle with a thin double layer (large κa) can be considered as the reverse situation, with the liquid stationary and the particle moving in the opposite direction to any electroosmotic flow (equation 3.3).

$$U_E = \frac{\epsilon \zeta}{\eta} \quad - 3.3$$

This equation is the Smoluchowski equation for electrophoresis.

An equation for electrophoretic motion can be derived by balancing the electric and frictional forces upon the particle (equation 3.4).

$$U_E = \frac{V_E}{E} = \frac{Q}{6\pi\eta a} \quad - 3.4$$

Combining equations 2.8 and 3.4, and assuming that $\zeta = \psi_o$ gives equation 3.5.

$$U_E = \frac{2\epsilon\zeta(1+\kappa a)}{3\eta} \quad - 3.5$$

In the limiting case of small κa , $(1 + \kappa a) \rightarrow 1$ and equation 3.5 becomes identical to that proposed by Hückel in 1924 (128), namely equation 3.6.

$$U_E = \frac{2 \epsilon \zeta}{3 \eta} \quad - 3.6$$

There is an obvious and significant difference in the equations of Hückel and Smoluchowski. This arises in part from electrophoretic retardation, which is a phenomenon caused by the effect of the applied field on the double layer ions. Smoluchowski assumed this was the dominant force and that the particle motion was equal and opposite to the ion motion; Hückel made proper allowance for electrophoretic retardation. However, his equation is only valid for small values of κa , where electrophoretic retardation is relatively unimportant and the main retarding force is the frictional resistance of the medium.

The reason for the apparent discrepancy was identified in 1931 by Henry (129), as being due to the differences in the accounting of the behaviour of the applied field in the region close to the particle. Hückel had disregarded any deformation of the field due to the particle. Smoluchowski had taken this into account, having assumed the field to be uniform and parallel with the particle surface when close to it. Henry proposed a general equation relating zeta potential and electrophoretic mobility (equation 3.7).

$$U_E = \frac{2 \epsilon \zeta}{3 \eta} f(\kappa a) \quad - 3.7$$

At low values of κa (< 0.1), $f(\kappa a) = 1$ and the equation takes the form described by Hückel. Conversely for large values of κa (> 100), $f(\kappa a) = 1.5$ and the equation becomes that of Smoluchowski. The

variation of $f(\kappa a)$ with κa is shown in Figure 3.1. It can clearly be seen that if the particle is non-spherical or conducting then values of $f(\kappa a)$ can differ greatly. This general equation takes into account the deformation of the applied field by the particle and the effect of retardation.

Movement of counter ions under the influence of the applied field will lead to distortion of the double layer. This creates an electric field which acts on the particle in a direction opposite to the external field; it is termed the relaxation effect. A reduction in velocity may occur if this relaxation effect is significant. Relaxation effects are considered negligible for small (< 0.1) and large (> 100) values of κa . For values between 0.1 and 100, relaxation effects can be severe, unless the zeta potential is below 25 mV, where relaxation effects are only of the order of a few per cent (130). Wiersema et al (131) have proposed a set of equations taking into account both retardation and relaxation effects. Analytical solutions of these equations is not possible but numerical solutions have been obtained. From this work Haichisu (132) makes the surprising observation that for a particle with $\kappa a = 5$ at 25°C , the electrophoretic mobility will never exceed $4.8 \times 10^{-7} \text{ m}^2 \text{ s}^{-1} \text{ V}^{-1}$ regardless of the magnitude of the zeta potential. It follows that the validity of using electrophoresis to calculate zeta potentials in dispersions where κa is between 0.1 and 100 must seriously be questioned.

A finite time is required to restore the symmetry of the diffuse layer following particle movement. This relaxation time (T_R) can be calculated using equation 3.8 where σ is the specific conductivity of the liquid.

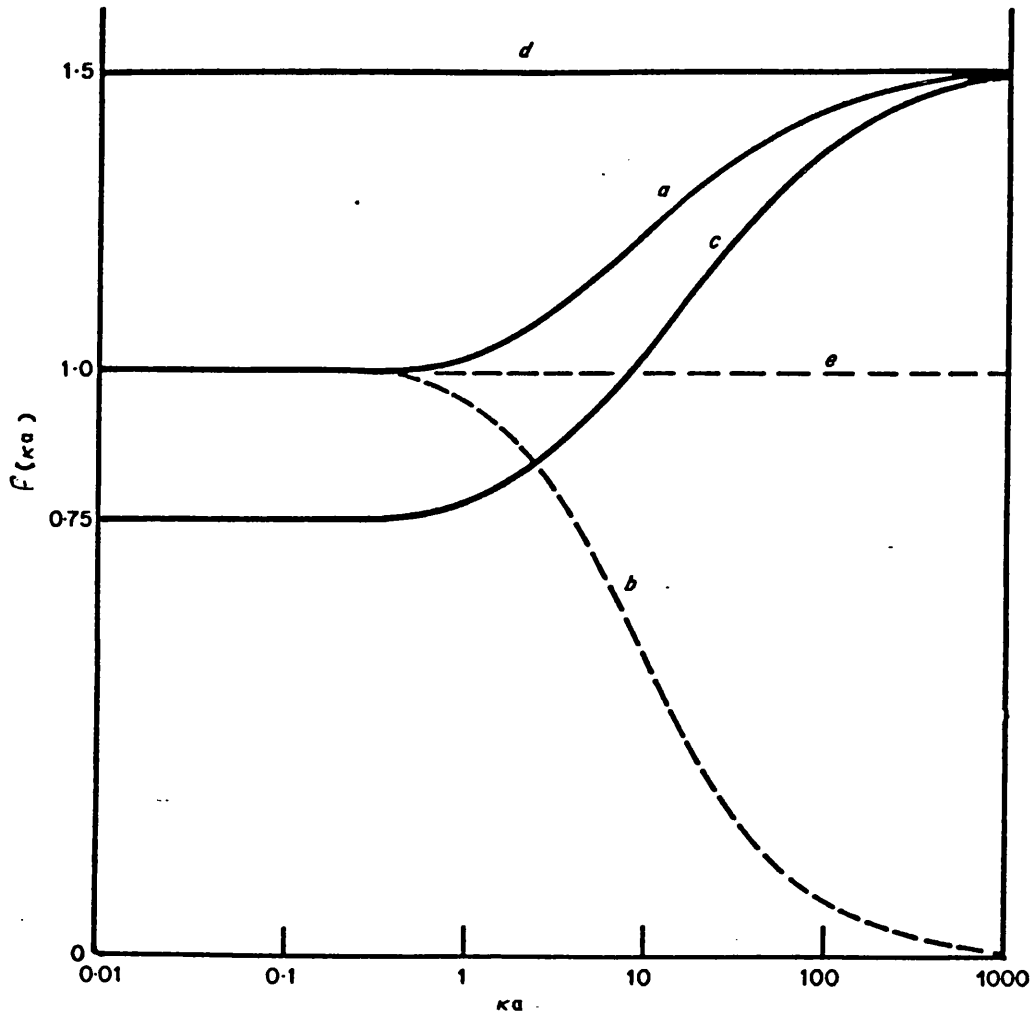


Figure 3.1 Henry's Function ($f(Ka)$) for Particles of Varying Size, Shape, Orientation and Conductivity.

- a. Non-conducting sphere.
- b. Conducting sphere.
- c. Non-conducting cylinder perpendicular to field.
- d. Non-conducting cylinder parallel to field.
- e. Particle of any shape with same conductivity as dispersing media.

$$T_R = \frac{\epsilon}{\sigma} \quad - 3.8$$

If a particle moves a distance greater than the diffuse layer thickness in less than time T_R , the diffuse layer will become decoupled and direct calculation of particle charge rather than zeta potential is possible. A critical velocity (V_c) above which decoupling will occur is given by Stotz (76) (equation 3.9).

$$V_c = \frac{1}{\kappa T_R} \quad - 3.9$$

This equation is only valid for values of $\kappa a < 1$ and typical values calculated by Stotz show that V_c can easily be exceeded in electrophoretic studies of non-aqueous systems. V_c need only be around $7.8 \mu\text{m s}^{-1}$ for a diffuse layer thickness ($1/\kappa$) of $20 \mu\text{m}$, such thicknesses are typical for many low conductivity dispersions (75).

3.3 Non-aqueous electrophoresis

In principle electrophoresis in non-aqueous dispersions differs little from that of aqueous systems, except that low electrophoretic mobilities will be expected due to the lower permittivity of the liquid phase (equation 3.7). Consequently higher electric fields must be used to obtain a given electrophoretic velocity. Electrophoretic mobilities for non-aqueous dispersions are of the order of $10^{-9} \text{m}^2 \text{s}^{-1} \text{V}^{-1}$ (95, 115, 123).

Van der Minne and Hermanie (86, 87), through their studies of carbon black dispersed in benzene, were the first to make significant steps towards the determination of electrophoretic mobilities in non-polar, non-aqueous dispersions. In doing so they published three criteria

for the observation of true electrophoresis:

1. The motion of the particle should be rectilinear between electrodes and uniform.
2. The velocity should be independent of the position of the particle in the electric field.
3. The velocity should be proportional to the field strength and should reverse on reversal of the field.

Conformity to these criteria, if observed, should ensure that the applied field is uniform and that turbulence in the liquid is absent. Non-uniformity of the field and turbulence present the major problems of non-aqueous electrophoresis.

3.3.1 SPACE CHARGE EFFECTS AND DIELECTROPHORESIS

When an electric field is applied across a uniformly dispersed colloid, the field is uniform at time zero. As separation of opposite charges occurs, a nett charge distribution is created. This may lead to a non-uniform, time variant electric field within the dispersion. This situation is referred to as 'space charge limited'.

This effect is particularly problematical with suspensions having a conductivity of less than $10^{-10} \text{ S m}^{-1}$ (133) and can only be avoided by using very low dispersion concentrations. For greater conductivities space charge effects are less important, since uniformity is less perturbed; such dispersions are typical of those with a surfactant present in solution.

Non-uniformity of the applied field makes calculation of electro-

phoretic mobility difficult, due to uncertainty in the size of the applied field experienced by the particle. Additionally non-uniform fields can lead to dielectrophoresis.

Dielectrophoresis is a motion set up due to a field induced polarization of the particle, as it experiences a variation of applied field over the particle. A detailed description of the effect is given by Parreira (134), it suffices here to observe that 'dielectrophoretic' mobility is proportional to the difference in permittivity between the liquid and particle. It is also necessary to have a divergent electric field such as that produced by space charge effects.

It is apparent that most of the early reports of non-aqueous electrophoresis reported dielectrophoresis rather than electrophoresis, although Gemant (135) avoided the problem by examining polystyrene dispersed in a hydrocarbon mixture, such that the permittivities of solid and liquid were identical.

3.3.2 ELECTROHYDRODYNAMICS

Ions moving in a liquid under an external applied field will drag molecules with them, resulting in turbulence usually in the form of vortices. This phenomena of electrohydrodynamics can easily be recognised in dispersions; particles will follow the fluid flow, resulting in movement in all directions, often opposite to that expected from their polarity. Particles may therefore be seen moving in opposite directions under the same field. Electrohydrodynamic effects do not occur at low voltages, the voltage at which onset of turbulence is seen depends upon many factors including charge injection, space charge effects, conduction mechanism and

properties of the medium. Typical critical voltages for hydrocarbons are between 200 and 300 volts (136).

It should be stressed that the effect is dependent upon the applied voltage rather than the applied field. As a consequence, where large applied fields are required, closely spaced electrodes should be used to minimise the applied voltage. Many equations are available for calculation of the electrohydrodynamic threshold voltage (V_T); for unipolar conduction equation 3.10 is given by Novotny (133).

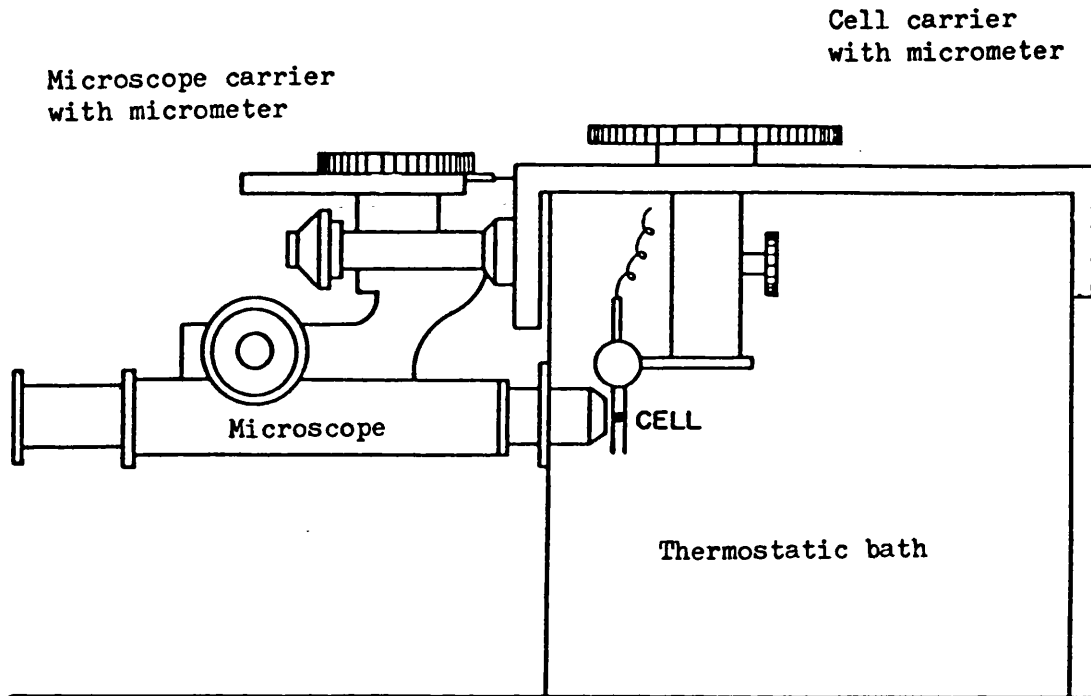
$$V_T = 30\eta / (\rho\epsilon)^{\frac{1}{2}} \quad - 3.10$$

Where η is the viscosity, ρ the density and ϵ the permittivity of the liquid.

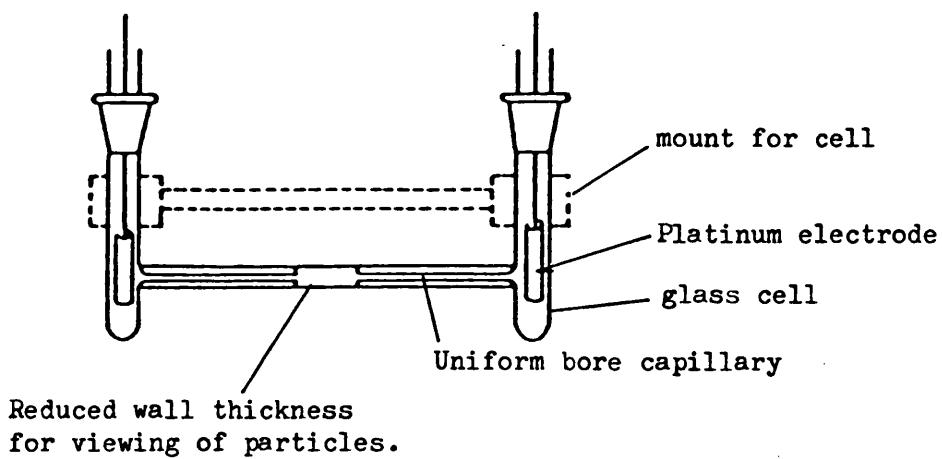
Where care is not taken to avoid electrohydrodynamic turbulence the measurement of non-aqueous electrophoretic mobilities is not possible (137).

3.4 Microelectrophoresis

Microelectrophoresis, often referred to as particle electrophoresis, has traditionally been the technique of choice for the determination of electrophoretic mobilities of particles which are visible under the light microscope. A classical type of microelectrophoresis apparatus is shown in Figure 3.2. A closed transparent chamber (usually glass), is either mounted between or contains within, two reversible non-gassing electrodes. This cell is mounted, in the case shown horizontally, and is maintained at a constant temperature usually by a thermostatic bath; a microscope arrangement permits viewing of the suspended particles. The electrophoretic velocity



A. Microelectrophoresis apparatus after Bangham et al (138).



B. Typical capillary cell suitable for aqueous investigations.

Figure 3.2 Typical Microelectrophoresis Experimental Apparatus and Capillary Cell

of each particle is determined after application of a voltage across the electrodes. This is done by recording the time required for the particle to move a known distance towards the electrode of reverse polarity to the particle charge. A knowledge of cell geometry and the applied voltage allows calculation of the electrophoretic mobility. In practice after each determination the electrode polarities are reversed and the time recorded for particle movement in the opposite direction. Many such measurements need to be made to obtain a reasonable estimate of electrophoretic mobility.

Observation of particle motion is complicated by the electroosmotic flow of liquid along the cell wall. In a closed cell this must return down its central axis. Since this flow is additive to the particle velocity a variation in the observed particle velocity across the cell will be seen (Figure 3.3). The true electrophoretic velocity is only observed at the stationary level, where electroosmotic and return flows are balanced. Equations are available to calculate the position of this stationary level in the two main types of cell; cylindrical and flat cells (139). Coating the cell walls with a layer of a material such as agarose or methylcellulose renders this electroosmotic effect negligible, by removing the charged surface away from the liquid (139).

Detection of particle motion by techniques such as laser-Doppler spectroscopy avoid the limitations in the geometry of the cell imposed by microscopic methods. Electroosmotic interference can be obviated by moving the electrodes away from the cell walls. Uzgiris (140) describes such a cell (see chapter 4) which additionally makes the cleaning and dismantling of the cell easier.

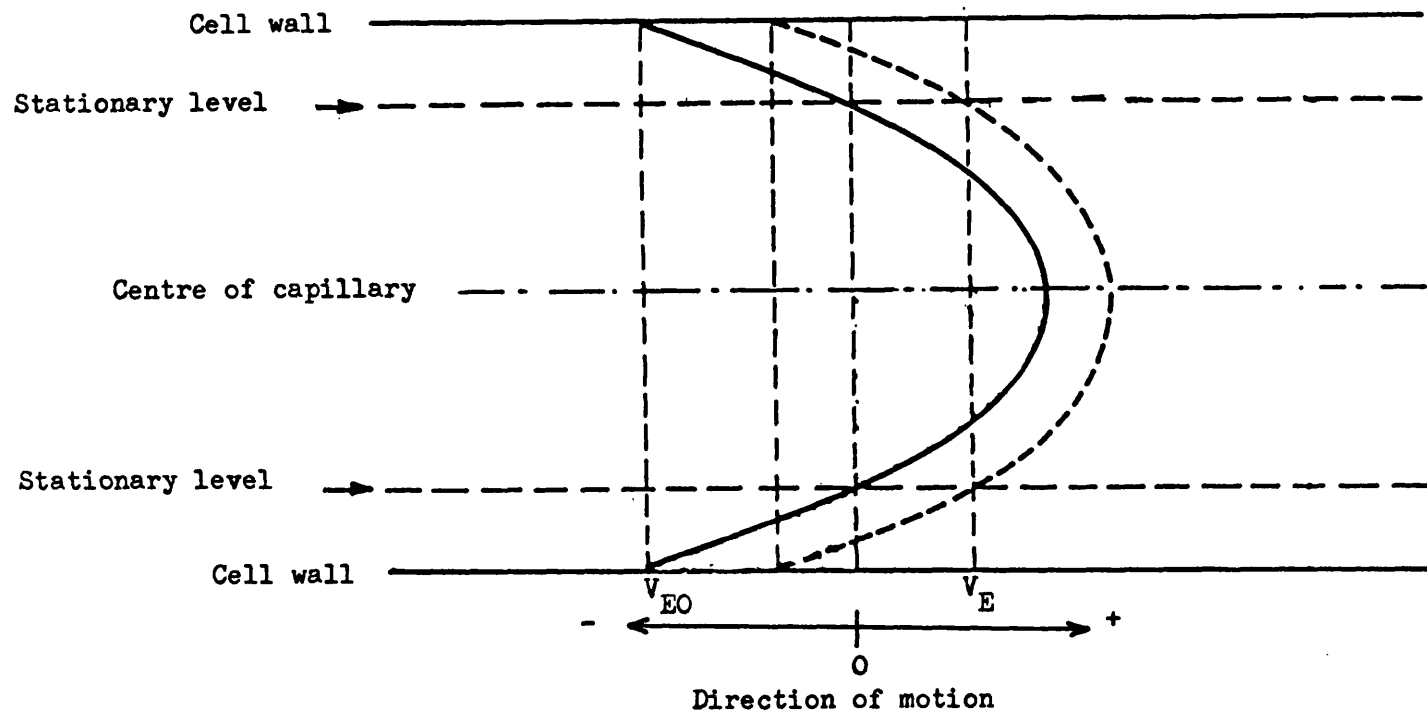


Figure 3.3 Velocity Profile in a Capillary Cell: Full Line shows liquid motion due to Electroosmosis (Electroosmotic velocity = V_{EO}), Broken line shows Observed Particle Velocity. Electrophoretic Velocity (V_E) only being observed at the Stationary Level.

The construction of a cell suitable for non-aqueous electrophoresis is of prime importance. Current leakage through glass walls (conductivity $\sim 10^{-12} \text{ S m}^{-1}$) can be a problem despite its lower electrical conductivity than most dispersions (typically $10^{-10} \text{ S m}^{-1}$) (86). This problem is particularly bad where the cell is located in a water bath and is not always avoided by using a cell constructed from quartz (conductivity $\sim 10^{-15} \text{ S m}^{-1}$) (141).

Non-aqueous electrophoresis was first demonstrated using a thin walled quartz capillary enclosed in an evacuated jacket. Quartz was selected because its surface is more homogenous than glass. The outer surface of the capillary was treated with silicones to eliminate any surface conductivity. The complexity of the cell and the use of cement in its construction is disadvantageous, consequently this cell has not been widely used. The majority of reported work has been done using a rectangular flat cell of the type described by Parreira (142). Construction is mostly in quartz, although polycarbonate has been used successfully (93) providing the liquid phase does not behave as a solvent towards the plastic. Observations are usually made at the stationary level in the same manner as the aqueous technique. Where particle mobility is low and large applied fields are to be avoided, measurements may be made at other levels and extrapolated to the stationary level values (143).

Narrow gap electrode arrangements with pulsed electric fields have been used for non-aqueous electrophoresis (76, 144). Although the use of laser light scattering in making non-aqueous electrophoretic measurements has been described (115), its use in conjunction with pulsed fields has yet to be reported.

Video techniques have been recently used in conjunction with pulsed fields to produce a method for characterising non-aqueous dispersions (90).

It is claimed that the commercially available Pen Kem 3000 instrument can produce high quality microelectrophoresis measurements in non-aqueous systems. It seems unlikely that this should be the case since the apparatus, which operates on a Doppler type principle, uses a traditionally designed cell. Its claims in respect of non-polar dispersions were heavily criticised at a recent symposium (145).

CHAPTER 4LASER-DOPPLER SPECTROSCOPY4.1 Introduction

4.1.1 GLOSSARY OF TERMS

THE DOPPLER SHIFT. In any wave propagation, frequency changes can occur due to the relative movement of source, receiver, propagating medium and intervening reflector or scatterer. These changes or 'shifts' in frequency are termed Doppler shifts after the Austrian physicist who first considered the phenomena in 1842. The effect was originally shown to apply to sound waves and is commonly connected with the apparent change in frequency of a train whistle as it passes through a station. The phenomena can however occur with wave propagations of any wavelength.

LASER. A laser can be thought of as a bright, monochromatic, coherent, unidirectional light source. Its name is derived from its principle of operation, namely, Light Amplification by Stimulated Emission of Radiation.

LASER-DOPPLER VELOCIMETRY. This is a technique which utilises the Doppler shift of scattered laser light to derive velocity information about the scatterer. The term velocimetry is used here in preference to anemometry, since the latter suggests a restriction to air or gas flow.

LASER-DOPPLER SPECTROSCOPY. A method of determining electrophoretic velocities using laser-Doppler velocimetry; other names for this technique in current use include Electrophoretic Light Scattering and Laser-Doppler Electrophoresis.

PHOTODETECTOR. An opto-electronic device which detects light and converts an optical signal in to a corresponding electrical signal.

INTERFERENCE FRINGES. From the wave nature of light, if two light beams of sufficiently well defined frequency and consistent phase are superimposed, light and dark bands will occur. These alternating bands are termed interference fringes.

HETERODYNING. The principle of heterodyning, often used in radio circuits, is that if two signals of unequal frequency are mixed in an appropriate manner, a beat frequency will be produced. This heterodyne beat is equal in frequency to the frequency difference of the two signals.

4.1.2 LASER-DOPPLER SPECTROSCOPY

Photon correlation spectroscopy* is now a widely accepted research tool in colloid science. Information on particle size is contained in light which has been scattered from suspended particles; modulation of the light having occurred due to their translational Brownian motion. Collection and analysis of the scattered light permits extraction of the size information.

Laser-Doppler spectroscopy also derives its information from the translational motion of suspended particles. It differs from photon correlation spectroscopy in that the translational motion of the particle is due to electrophoresis. The method eliminates

(* The use of the term photon correlation spectroscopy is strictly incorrect since it is a specific signal analysis technique (see section 4.3.4). Its use here is in the colloid chemistry sense, referring to the complete experimental technique.)

the tedious and often subjective nature of manual microelectrophoresis. Measuring times are shorter, enabling sufficient data to be collected in 2 - 3 minutes. Systems containing components of differing electrophoretic mobilities can be examined, with each component being resolved and measured simultaneously. The technique can be used with the traditional cylindrical electrophoresis cell. However the small probe volume and the required ability to pulse power supplies allows for a radically different cell design.

4.1.3 THE USE OF LASER-DOPPLER SPECTROSCOPY IN COLLOID SCIENCE

Laser-Doppler Velocimetry (LDV) was first used for fluid flow measurements by Yeh and Cummins in 1964 (146), development of Laser-Doppler Spectroscopy (LDS) is attributed to Flygare (1970) (147), with the first published results being obtained with bovine serum albumin (148). Validation of the technique for investigating dispersions came in 1972 when Uzgiris measured the electrophoretic mobility of erythrocytes in saline (149). LDS is now widely used in medical fields as an investigative and diagnostic tool. For example a difference in the electrophoretic mobility of white blood cells has been noted in patients suffering from acute lymphocytic leukemia (150).

Despite this, little use of the technique has been made in investigating non-biological dispersions. Of those reported the majority restrict investigation to model systems comprising mono-sized, spherical latices. The technique has been used to characterise individual batches of such material (151). Investigations, using LDS, into the effect of pH and buffer type upon their electrophoretic mobility has also been made (152). Similarly the effects

of salt (153) and surfactant (154) concentrations have also been investigated. The observed dependence in the electrophoretic mobility of clay suspensions with varying surfactant concentrations, demonstrates the potential of LDS for investigating non-model dispersions (155). Mixed dispersions can also be successfully investigated the hetero-coagulation of rutile and latex particles at the iso-electric point has been clearly observed using LDS (156). The technique has also been reported as useful in the investigation of micro-emulsions (157).

The application of LDS to non-aqueous dispersions has been suggested as feasible, although little use of the technique has been made (124). A laser-Doppler velocimeter has been used to investigate liquid movement in electrically stressed dielectric liquids (158). The technique has also been applied to moving boundary electrophoresis and more recently to dilute non-aqueous dispersions (115).

4.2 Basic principles of laser-Doppler velocimetry

4.2.1 PROPERTIES OF LASER LIGHT

A laser may operate in many different modes, each producing a different beam pattern. Only that known as TEM_{00} is of practical use in LDV. In TEM_{00} the beam is spatially coherent and possesses a long coherence length. Spatial coherence occurs when different parts of the beam at a uniform distance from the source are in phase with each other. A beam which is radiated without discontinuities is said to be temporally coherent. Laser beams are not in practice temporally coherent but they do exhibit a long coherence length, this being the distance between discontinuities. TEM_{00} yields a beam with a Gaussian light intensity distribution which is truncated

at some point by the laser bore or some limiting aperture in the optical train. The beam radius is normally defined as the distance from the peak intensity to a point where it has fallen to a value of 0.135 of its peak value (Figure 4.1).

At the front mirror of the laser the beam has a perfect plane wavefront, however the beam acquires curvature and begins to spread with increasing distance from the laser. When such a beam is focussed by a lens (Figure 4.2) a beam waist will be produced. This waist region may not occur at the focal length (f_1) of the lens. Dickson (159) followed the work of Kogelnik (160) and considered the special case where the lens is positioned directly in front of the laser ($d = 0$). For any laser a term f_f can be derived (equation 4.1).

$$f_f = \frac{\pi r_o^2}{\lambda} \quad - 4.1$$

Where r_o is the radius of the beam and λ its wavelength. When $f_f \gg f_1$ the beam waist is effectively located at f_1 . However as f_f becomes smaller to the order of $5 f_1$ or below, the effective focal length (d_{min}) becomes significantly shorter than f_1 . For the location of d_{min} and the radius of the beam waist r_{min} , equations 4.2 and 4.3 respectively are used.

$$d_{min} = f_1 \left[1 + \left[\frac{f_1}{f_f} \right]^2 \right]^{-1} \quad - 4.2$$

$$r_{min} = r_o \left[1 + \left[\frac{f_1}{f_f} \right]^2 \right]^{-\frac{1}{2}} \quad - 4.3$$

where $r_f = \lambda / \pi r_o$.

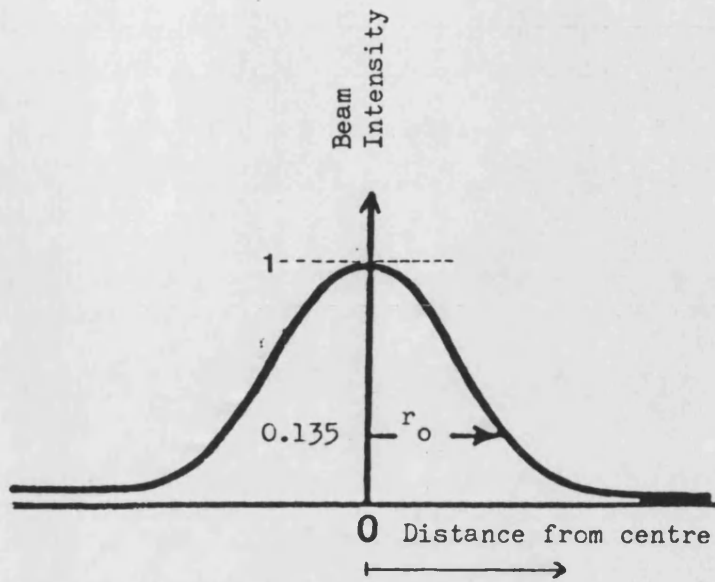


Figure 4.1 Light Intensity Distribution of a Beam Produced from a Laser Operating in TEM₀₀

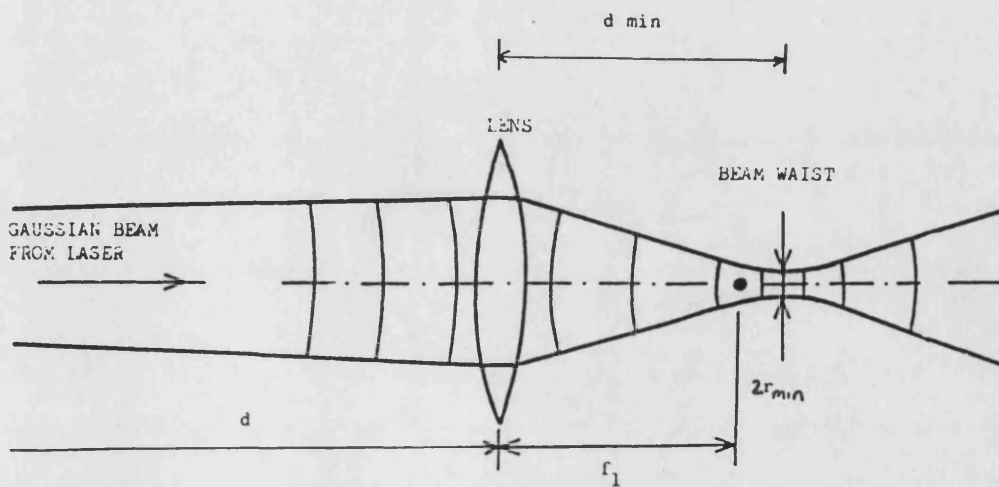


Figure 4.2 Effect of Focussing A Gaussian Light Beam with a Lens

These effects can be significant for combinations of narrow beams and long focal length lenses. Incorrect focussing of the beam may lead to a variation in fringe spacing across the probe volume (section 4.2.5). In many applications such effects are often small and have been completely ignored.

4.2.2 THE DOPPLER SHIFT

LDV utilises the shorter wavelengths of visible light to determine the velocity of a moving body. No relative movement of source and receiver occurs, frequency shifts are produced by the movement of a body which scatters light from source to receiver.

The basic geometry of a laser-Doppler velocimeter is shown in Figure 4.3. The incident and scattered light is characterised by the vectors K_i and K_s respectively. The size of the scattering vector K , where $K = K_i - K_s$, is given by equation 4.4.

$$K = \frac{4 \pi n}{\lambda_i} \sin \left[\frac{\theta}{2} \right] \quad - 4.4$$

Where n is the refractive index of the medium and λ_i the wavelength of the incident light in the medium. θ is the scattering angle in degrees. The scattered light at the detector will be shifted in frequency (Δf) and is related to the velocity of the body by equation 4.5.

$$\Delta f = \frac{2 v n}{\lambda_o} \cdot \sin \frac{\theta}{2} \cdot \cos \beta \quad - 4.5$$

v is the velocity of the scattering body and λ_o is the wavelength of the incident light in vacuo. β is the angle from normal of the particles' motion relative to the incident vector. In LDS the applied field is so arranged that $\beta = 0$; $\cos \beta$ therefore equals one and the term disappears from the equation. Since λ_o and n are

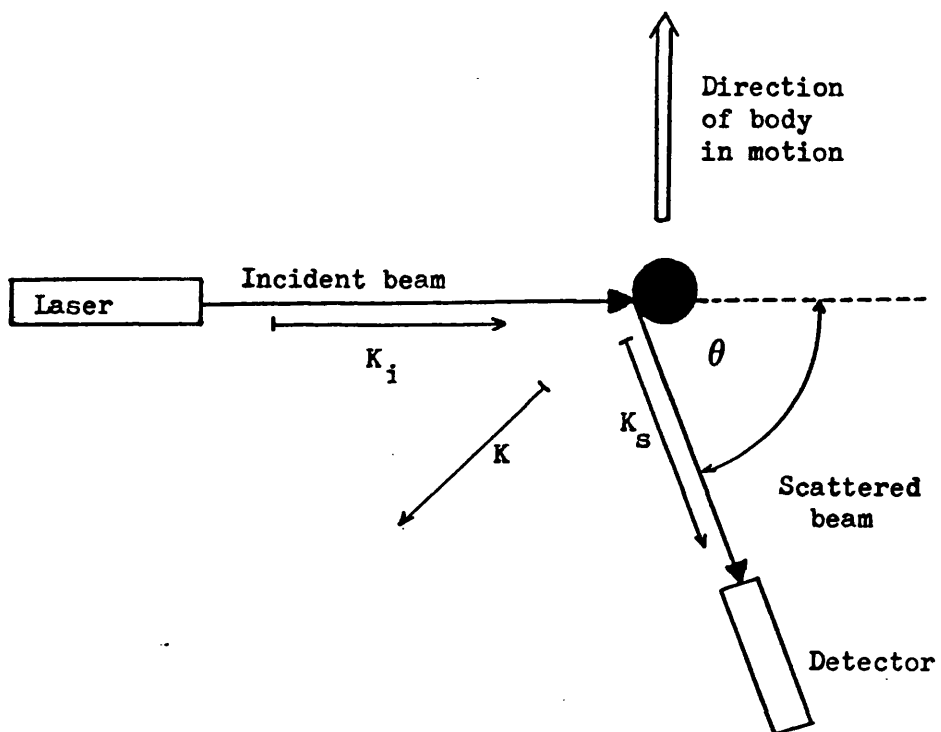


Figure 4.3 Basic Geometry of a Laser-Doppler Velocimeter.

constant for a given arrangement, and θ and β are defined, the only variable left is the velocity of the body. Therefore the frequency shift is proportional to the velocity and can be used to determine the velocity, provided the values of the other constants are known.

4.2.3 HETERODYNE DETECTION

Since the particle velocities to be examined are small compared with the velocity of light, the corresponding Doppler shifts are small. For example a particle with velocity of $135 \mu\text{ms}^{-1}$ will produce a frequency shift of 110 Hz, using a He-Ne ($\lambda_0 = 632.8 \text{ nm}$) laser and a scattering angle of 30° . The frequency of the incident light is $4.7 \times 10^{14} \text{ Hz}$, so the shift represents a change of less than 5 in 10^{12} . Resolution of such small shifts is not possible by direct measurement, the technique of heterodyning must therefore be used. In LDV the scattered (shifted) light is mixed with some of the incident (unshifted) light to produce a beat with a frequency equal to the Doppler shift. Consequently, measurement of the beat frequency will enable calculation of the velocity of the scatterer.

In practice a photodetector is used to measure the resultant beat frequency. Output of a photodetector is proportional to the square of the total light field at the photocathode. The power spectrum obtained is a Lorentzian frequency distribution centred on Δf , with a width at half height equal to DK^2/π (Figure 4.8); D is the diffusion coefficient of the scattering body and K is the scattering vector (equation 4.4).

The implication is that even in a system free from signal degradation from other sources, the Doppler signal obtained will never be sharp

but will be broadened by diffusion. In practice further broadening from other sources occurs, including those associated with the limits of spectral analyser resolution, non-uniform flow and vibration. The quality (Q_s) of a signal is defined by its shift to width ratio (equation 4.6).

$$Q_s = \frac{\Delta f}{DK^2/\pi} \quad - 4.6$$

Since K is proportional to $\sin \theta/2$ (equation 4.4), the quality of the signal deteriorates as the scattering angle increases. Thus a smaller angle gives a better signal quality. Small angles, typically less than 10° , can be difficult to define accurately; resultant Doppler shifts are low (equation 4.5), therefore mechanical noise can be problematical. This analysis omits other sources of signal broadening and whilst giving a good approximation for small particles, the conclusion with regards to small scattering angles is not so pertinent for larger particles, where diffusion effects are less. Uzgiris (161) concluded that for particles around $10 \mu\text{m}$ in diameter, the optimum angle increased with particle size. This conclusion is in contrast to the heuristic approach of Durst (162) given by equation 4.7.

$$\theta_{\text{optimum}} \approx \frac{\lambda_i}{16 a} \quad - 4.7$$

a is the particle radius. Therefore, the general inference is that when selecting a scattering angle it is necessary to balance the size of the shift with the quality of the obtained spectrum. In practice, large angles may be preferred so that large shifts may be obtained for a given particle velocity. Another practical problem is that as the angle is increased there may be a decrease in the

intensity of light scattered by the particle; leading to possible detection problems.

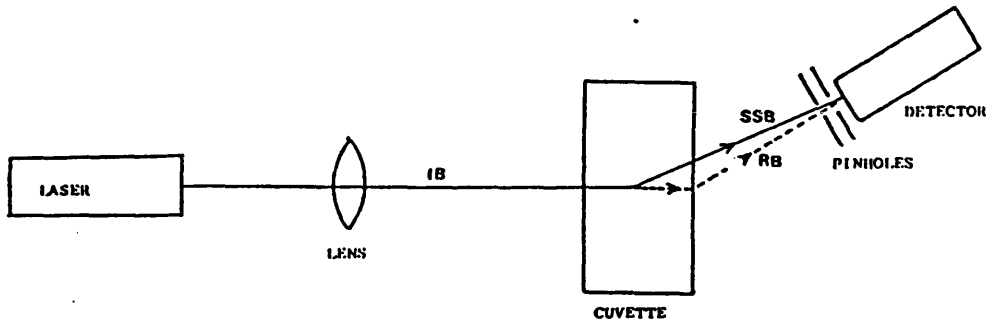
4.2.4 LOCAL OSCILLATOR HETERODYNE DESIGN OF VELOCIMETER

The single beam, local oscillator heterodyne** design for LDV is in its simplest form, the easiest to construct. It is for this reason that the majority of the reported work has been carried out using this arrangement (Figure 4.4A).

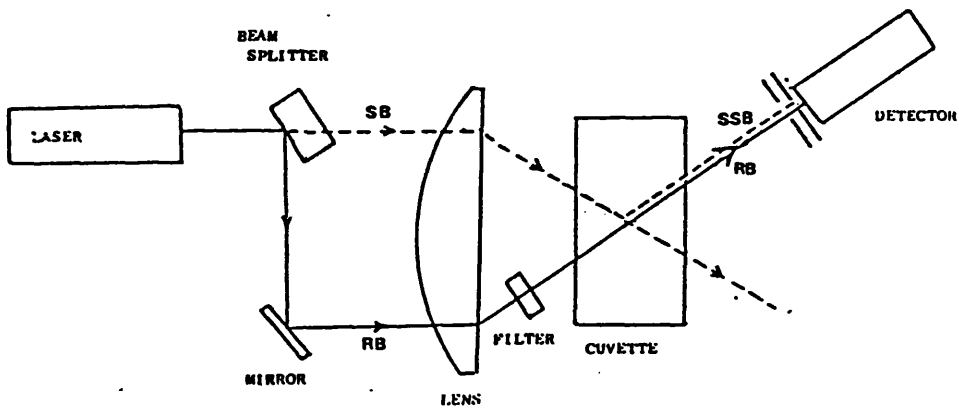
In this design the incident laser beam (I.B.) strikes the particle in motion and is scattered through an angle (θ) to fall upon the detector. The reference (unshifted light) is obtained from the light not scattered by the particle, which on striking the glass cell wall is then scattered in to the detector (RB). The shifted and unshifted light mix to produce the resultant heterodyne signal. Since this design relies on scattered light for the unshifted light, its use is restricted to small scattering angles. To overcome this problem the laser beam is split with one beam forming the reference unshifted light, this may be steered around the cell so that it coincides and therefore heterodynes with the scattered light at or near the detector.

An alternative method is shown in Figure 4.4B; here the reference beam passes through the scattering volume and mixes with the scattered light from the signal beam (SSB) before passing into the detector (165, 166). To obtain a good signal to noise ratio the reference

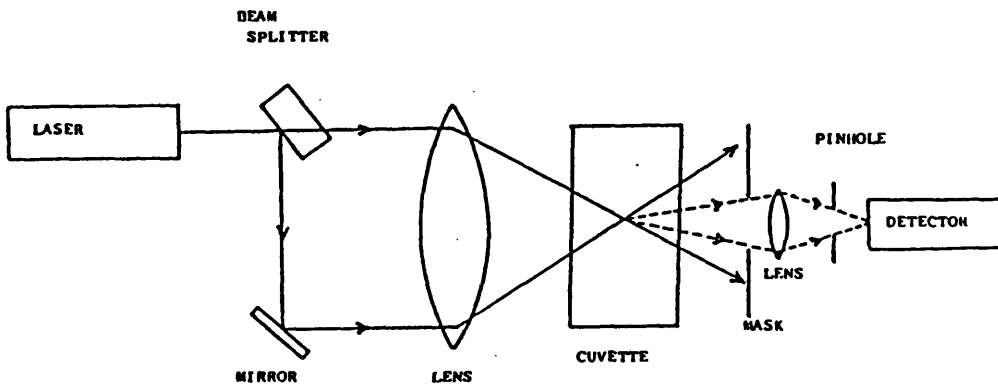
(** 'Local oscillator heterodyne' is the term used by Wang and Synder (163). Another common description is that of Drain (164) who refers to it as 'coherent' in design.)



A. Basic single beam local oscillator heterodyne design after Goff and Luner (156)



B. Wide angle local oscillator heterodyne design after Uzgiris (161)



C. Differential heterodyne design after Wang and Snyder (163)

Figure 4.4 Basic Designs of Laser Velocimeters

(SB - Signal Beam, SSB - Scattered Signal Beam,
RB - Reference Beam)

beam should be attenuated using either a neutral density filter or some other method. A ratio of reference beam to scattered light intensity of 10:1 is suitable for most systems. An increase in this ratio may prove advantageous when using photodiode detectors.

It has been assumed that the detector surface is small when compared to the wavelength of light. This in practice is not the case and variations in the phase of the beat signal will occur. Should these variations be large, contributions from different parts of the detector will not be additive and a resultant decrease in output may occur. To avoid this problem it is necessary to restrict the angle of view so as to minimise these variations (164). This restriction is termed the coherence limitation.

4.2.5 THE FRINGE MODEL OF LASER-DOPPLER VELOCIMETRY

The fringe model was first proposed by Rudd (167) and it provides a more easily visualised model of LDV operation. When two coherent light beams with plane wavefronts (as found at the waist of a focussed Gaussian beam) intersect a series of interference fringes will be set up (Figure 4.5).

The fringe spacing $\lambda_i^{(d_f)}$ given by equation 4.8.

$$d_f = \frac{\lambda_i}{2 \sin \Psi_s/2} \quad - 4.8$$

A particle moving normal through the fringes will scatter light, the intensity depending upon whether the particle is in a light or dark fringe. The frequency $f^{(f)}$ of intensity fluctuations to an external observer is given by equation 4.9 (where Ψ_s = intersection angle).

$$f = \frac{v}{d_f} = \frac{2 v \sin \Psi_s/2}{\lambda_i} \quad - 4.9$$

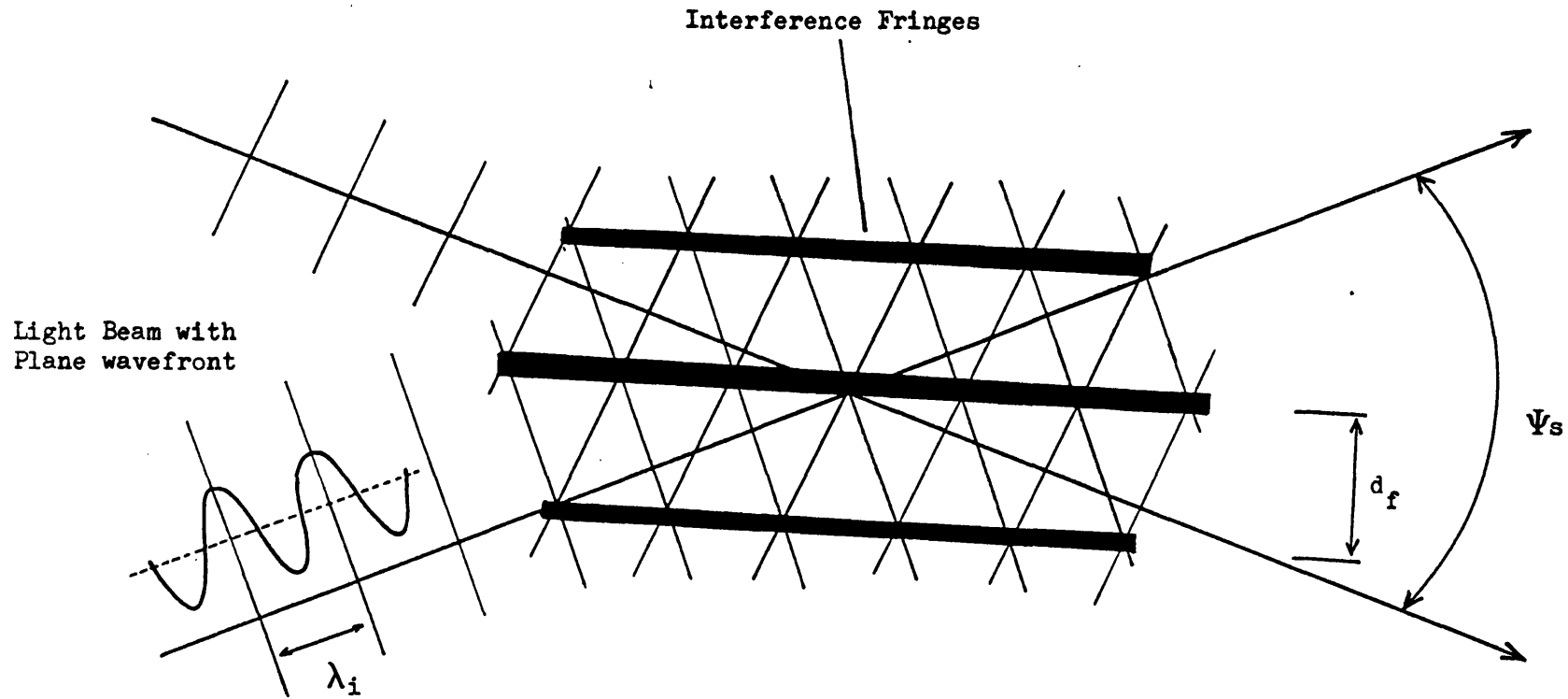


Figure 4.5 Interference Fringes Set Up by the Intersection of Two Beams with Plane Wavefronts.

Where v is the velocity of the particle. This is exactly equal to the Doppler equation (equation 4.5), taken that $\Psi_s = \theta$ (since $\lambda_i = \lambda_o/n$).

The region of intersection of the two beams is often referred to as the probe or scattering volume. Using 0.135 of the peak intensity to define the boundaries, the probe volume is ellipsoid in shape with semi-axes r_o , $r_o/\sin(\Psi_s/2)$ and $r_o/\cos(\Psi_s/2)$. The smaller the crossing angle the more elongated becomes the probe volume. The effect of improper beam intersection can easily be visualised; if spherical rather than plane wavefronts intersect i.e. not at the beam waist (Figure 4.2), the resultant fringes will become distorted and no longer parallel. As a consequence particles moving with the same velocity but through different parts of the probe volume will produce different frequencies.

4.2.6 DIFFERENTIAL HETERODYNE DESIGN OF VELOCIMETER

The operation of the differential heterodyne, also termed non-coherent (164), design of velocimeter is based upon the fringe model. A typical design is shown in Figure 4.4C. The laser beam is split into two equal paths and steered into the scattering volume. Scattered light is collected by a lens and focussed on to the detector; masks ensure that only the scattering volume is viewed. Unlike in the local oscillator heterodyne design, the frequency is independent of the direction of reception; increasing the detector aperture will not result in broadening of the spectrum. The coherence limitation does not apply; permitting larger receiving apertures to be used, stronger signals are therefore obtained from the particles in motion.

The passage of a series of single particles through the probe volume can be visualised as a series of 'bursts' of frequency (Figure 4.6A). The resultant signal will have a DC (Direct Current) and an AC (Alternating Current) component, after the modulated light has been converted to an electrical signal by a photodetector (see section 4.3.3). In practice several particles may pass through the fringes simultaneously and this effect must be considered. Since the particles are randomly distributed throughout the scattering volume, their phases must also be random, leading to considerable cancellation. The root mean square (RMS) of the beat signal can be shown to be proportional to the square root of the number of particles present (164). The DC signals, which in terms of signal analysis constitute noise, are directly additive. An increase in particle number therefore leads to a decrease in the signal to noise ratio (Figure 4.6B). This would suggest that as the number of particles increases, the signal to noise ratio would approach zero (assuming no reduction in mean collected light intensity). However this is not the case since a residual signal is always observed. This residual signal is produced by optical beating of light scattered from the moving particles i.e. true Doppler beating (168). For optimum operation between 1 and 10 particles should be present in the scattering volume at any given time.

When the particle becomes large relative to the fringe spacing a degradation in the signal should be observed. Large particles will span both light and dark fringes simultaneously hence reducing the modulation of the signal. The optimum range of particle diameter to fringe spacing ratios is up to 3 with the optimum value being 0.586 (164). However this situation is not clear cut since Preece and Luckman (169) have successfully investigated macrophages ($15 \mu\text{m}$ in

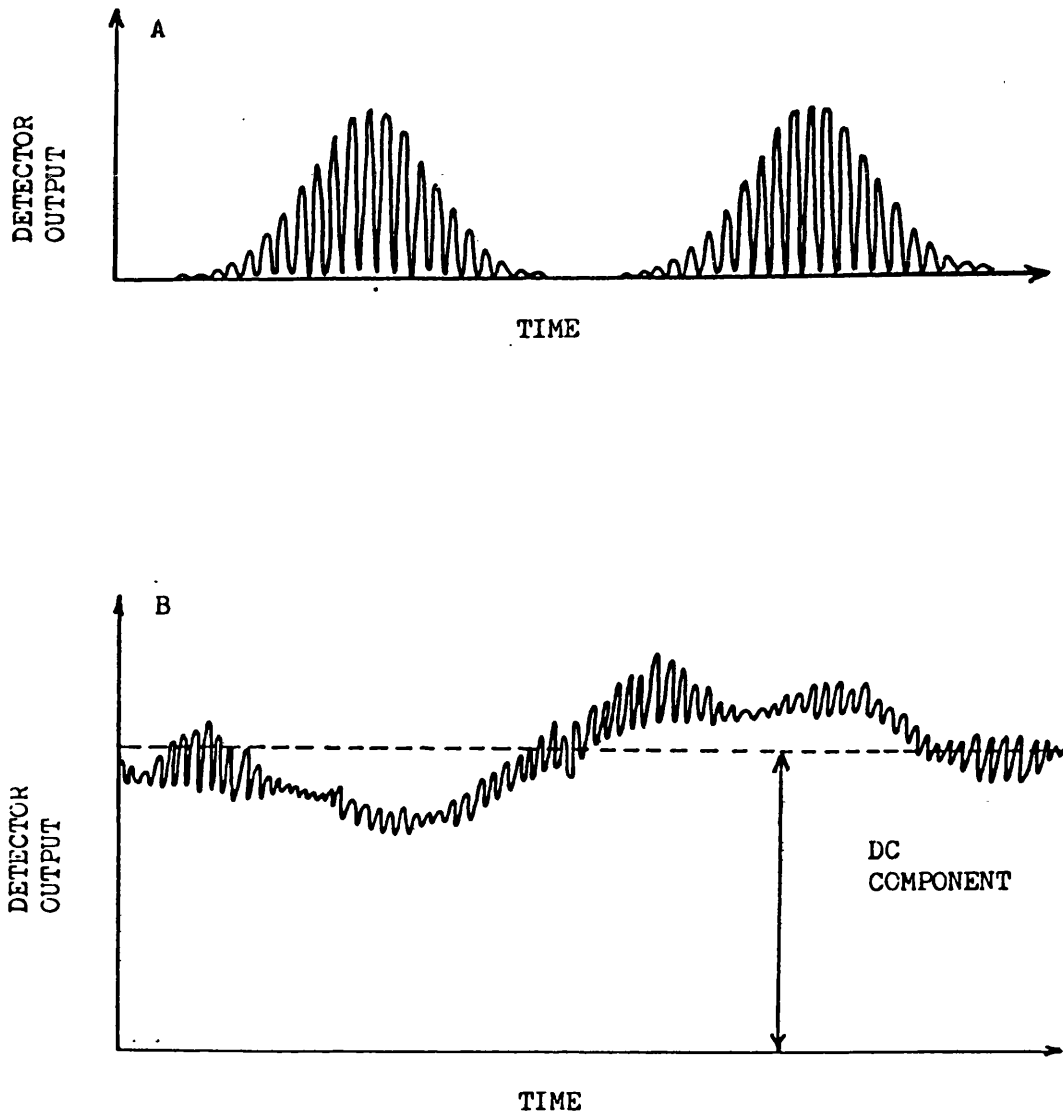


Figure 4.6 Fringe Crossing Signals from A) Single Particle and B) Multiple Particle Crossings of the Probe Volume

diameter) using a fringe spacing of $0.5 \mu\text{m}$. The situation may be further complicated if the system under examination has a wide particle size distribution. Signals of high and low signal to noise ratios will be obtained; in practice only the former will be processed.

It can therefore be seen that whilst the fringe model provides a useful insight into the operation of differential heterodyne velocimeters, it is as yet incomplete.

4.3 Design criteria for construction of a laser-Doppler velocimeter

4.3.1 SELECTION OF VELOCIMETER DESIGN AND OPTICAL COMPONENTS

The relative advantages between local oscillator heterodyne and differential heterodyne designs of velocimeter are summarised in Table 4.1.

The low electrophoretic mobilities seen in non-aqueous dispersions, suggest a combination of large applied electric fields and large scattering angles is necessary to produce sufficient frequency shifts. However it is desirable to keep applied fields to a minimum when investigating non-aqueous dispersions, to avoid electrohydrodynamic effects etc (section 3.3); consequently large scattering angles must be used. To minimise the effects of interparticulate interactions, due to extended diffuse layers, dilute dispersions must be examined. These two factors lead to the selection of a differential heterodyne design; increased optical complexity possibly being balanced out by a greater ease in detector alignment.

Optical components have two distinct functions, steering and focussing of the laser beam and imaging of the scattered light on to the

Design	Local Oscillator Heterodyne	Differential Heterodyne
Mode of Operation	Doppler beating	Particle tracking
Ease of construction and complexity of optics	Simple construction and optics	Complex optics requiring careful alignment
Range of operating angles	Without a reference beam, restricted to small angles	Wide range
Particle concentration required for operation	High	Low
Detector Alignment	Critical due to coherence condition	Large receiving apertures, alignment not critical

Table 4.1 Summary of Major Factors Involved in Velocimeter Design Selection

detector. Lenses and beam splitter arrangements are used to focus the beam so that a plane wavefront beam waist is produced at the required point. These optical components must be of the highest quality. Spherical aberration of any lenses must be kept to a minimum. The surface tolerances of beam splitters and mirrors must be small, since irregularities will reduce the beams' coherence. Lenses and pinholes are used to focus and define the probe volume which is allowed to fall on to the detector. The tolerances of these components are greater than those used for steering and focussing (see section 5.3). Some detector optics provide a reflex viewing arrangement allowing the operator to view the image which is falling on to the detector.

All components must be mounted on to a rigid mechanical arrangement so that vibration of optical components is minimised. In practice many are mounted on to optical benches which are then placed upon suitable vibration free surfaces.

4.3.2 SELECTION OF LASER

The properties of laser light have been discussed in section 4.2.1. Selection of the laser depends upon two relevant parameters; wavelength and power.

The monochromatic property of laser light is not essential for velocimeter operation. What is required is a greater precision in the light wavelength than the desired velocity resolution. Precision to within a few per cent of the desired wavelength can be obtained using a conventional thermal light source combined with a filter (170). The selected wavelength should exhibit minimal absorption by the particles, to reduce the possibility of thermophoresis and

possible photochemical damage. Increased photodetector efficiency favours the selection of a shorter wavelength. Since signal quality is proportional to wavelength (equations 4.4 - 4.6), a slight advantage may be gained in using longer wavelengths, when diffusion broadening is problematical. The majority of laser-Doppler velocimeters incorporate a He-Ne laser (primary wavelength 632.8 nm). Krypton (wavelength 647.1 nm) (171) and Argon (operated at 488.0 nm) (172) lasers have also been successfully used.

Laser power required is very dependent upon the particle system under investigation. It has been calculated theoretically that typically 5×10^{-6} W are required for every m s^{-1} of velocity measured (173). In practice this value is found to be far too low. An increase in the scattering coefficient (Mie theory) of the sample, the number of fringes viewed and the photodetector efficiency will all lead to a reduction in the required laser power (174). Lasers ranging from 3 mW (152) to 15 mW (175) have been successfully used.

The popularity of He-Ne lasers is attributable to their low cost and easy availability in a wide power range.

4.3.3 PHOTODETECTION

The intensity of fluctuations of light scattered from a moving object contains the velocity information which is of interest. It is the function of the photodetector to convert this optical signal into a corresponding electrical signal. All photodetectors produce three types of noise, all of which may contribute to the final signal to noise ratio.

1. Shot noise; inherent noise due to the random nature of photon arrival.

2. Dark noise; noise due to electron emission by thermal excitation.
3. Johnson noise; noise produced by the thermal movement of conducting electrons in resistors.

Photodetectors are of two types; photodiodes and photomultipliers.

The response time of some photodiodes is too slow to make them suitable for many applications. PIN and avalanche photodiodes however do possess sufficiently fast response times. A PIN photodiode consists of heavily doped n and p semiconductor layers sandwiched between a layer of pure (intrinsic) semiconductor (164).

This construction produces a photodiode with response times of less than a nanosecond. Since the photodiode has no inbuilt amplification, broadband low noise amplification must be provided. To avoid the predominance of Johnson noise large load resistances should be used. The resultant high RC value (Resistance x capacitance) of the circuit may decrease the frequency response.

Avalanche photodiodes do have some internal gain due to the internal multiplication of photogenerated electrons; signal gains in excess of 100 can be achieved. Silicon based photodiodes have their peak sensitivity in the red and near infra-red regions, ideal for the detection of He-Ne laser light.

The low cost of the photodiode and associated power supplies make their use attractive. Their small size makes them ideal in situations where the photodetector needs to be close to the scattering volume. The need for high gain low noise broadband amplification is their chief disadvantage.

Photomultipliers are considerably more complex and bulky in construction than photodiodes (Figure 4.7). A photon strikes a photocathode and an electron is emitted. The electron is focussed on to a series of electrodes (the dynode chain), where amplification occurs by secondary emission. The output is taken from the anode at the end of the dynode chain. Because all the elements are sealed into an evacuated glass tube, photomultipliers are more fragile than photodiodes. The output of photomultipliers has been raised above the level of Johnson noise, through the low noise amplification of the dynode chain. Frequency responses of up to 100 MHz can be achieved. Spectral response in the red region is poor. However, the S20 cathode photomultiplier is the most suitable for use with He-Ne laser light.

Despite the high cost of photomultipliers and their associated power supplies, they are at present the photodetector of choice for LDS, although the use of photodiodes has been reported (176).

4.3.4 SIGNAL PROCESSING

The output power spectrum, from the photodetector has the form shown in Figure 4.8. In addition to the expected frequencies, a low frequency component is present. This is due to the transit of particles through the light beam ^{at points other than the probe volume} and is termed the "pedestal signal". Removal of the pedestal signal is the first step in signal processing. This can be achieved simply by passing the photodetector output through a high pass filter. Selection of the frequency cut-off is critical to ensure that only the pedestal signal is removed. Light shifting techniques increase only the Doppler signal and not the pedestal signal, such techniques may be useful for their separation in

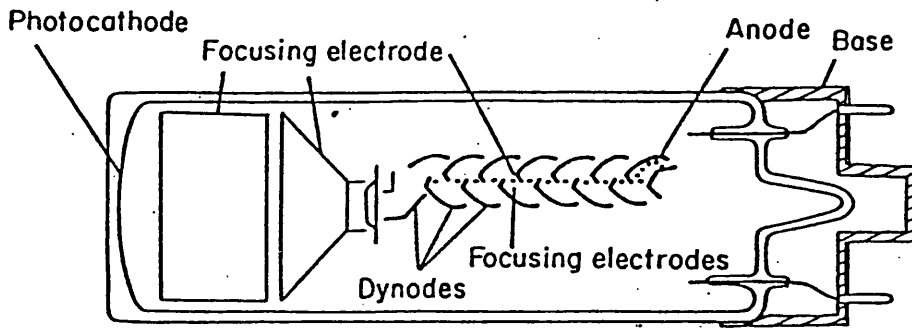


Figure 4.7 The Basic Construction of a Photomultiplier

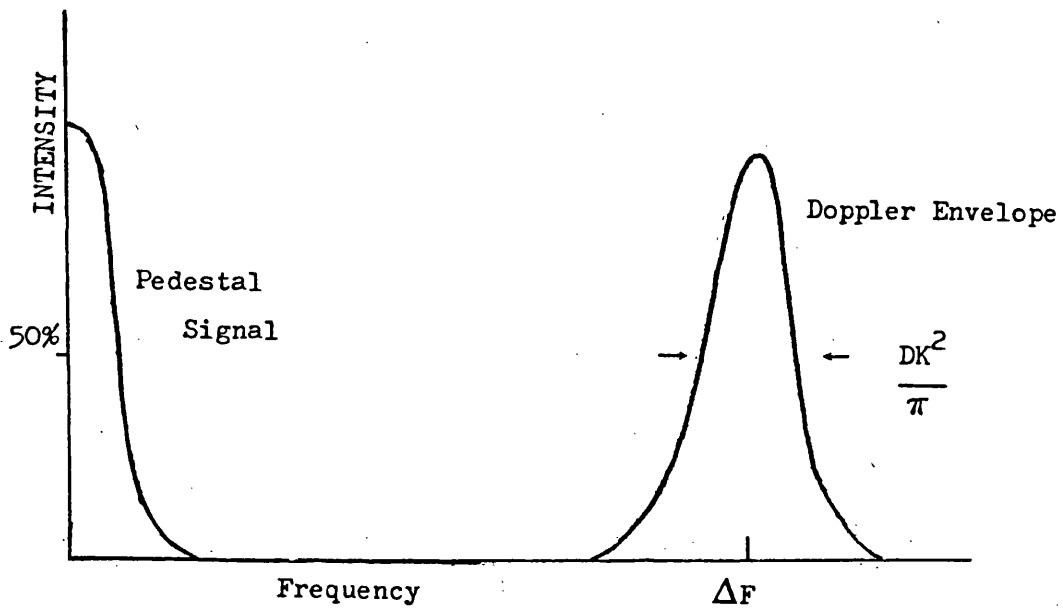


Figure 4.8 A Power Spectrum from a Photodetector
Showing a Pedestal Signal

application where small frequency shifts are expected.

The choice of processing technique will be influenced by the character of the signal. The signal may contain contributions from more than one particle at any given time, the depth of modulation being dependent on the size and position of each particle. Periodic absences of particles in the probe volume will result in an intermittent signal; some processing techniques require continual signals. Signals will usually contain noise, its source generally being electronic or mechanical. Ideally a signal should possess a high signal to noise ratio, this is not always possible and so will exclude some processing methods.

Many techniques can be applied to the analysis of LDV signals; including frequency analysis, photon correlation, counting and optical methods. The methods of choice in LDS are frequency analysis and photon correlation with approximately equal popularity.

FREQUENCY ANALYSIS

Frequency analysis could simply be accomplished by the use of a large number of filters of narrow bandwidth covering the frequency range of interest. The output of each filter is measured and plotted against its centre frequency. Whilst accurate, this method is expensive.

A tunable filter can be used whose centre frequency is swept across the range of interest. Such methods can require long data acquisition periods for good resolution, but are good for high frequency applications. Frequency tracking analysers also use a tunable filter, the filter is kept on the signal frequency by a voltage controlled oscillator (VCO). A change in signal frequency results in a change

in the VCO output which keeps the filter centred on the signal. Frequency tracking is not suitable for signals that are not continual, even though some machines now employ a dropout compensation mechanism.

The Fourier Transform establishes a mathematical relationship between every time domain function (signal) and a specific frequency domain function (spectra). Refinements of the Fourier Transform provide the basis of the operation of Fast Fourier Transform (FFT) spectrum analysers (177). The signal is sampled at discrete time intervals, these samples are digitised and the corresponding frequency spectrum is computed using the Fast Fourier Transform. Nearly instantaneous frequency spectra can be produced so FFT analysers are often referred to as 'real time***' analysers. They are however unsuitable for applications where the signal comes in short bursts.

PHOTON CORRELATION

Photon correlation spectroscopy is based upon the principle of converting the signal to a pulse train, each pulse corresponds to the arrival of a photon at the photodetector. The period of intensity variations is obtained by measuring the autocorrelation function $G(\tau)$ over time delay $\tau = r_t T_i$ (equation 4.10).

$$G(\tau) = \sum_{r_t=0}^{r_t=\infty} n_i(t) n_i(t - r_t T_i) \cdot [r_t = 0, 1, 2, 3 \dots] \quad 4.10$$

(*** No analyser is truly 'real time' since a finite time is required for the processing of data. However not a single datum is lost since incoming data is stored until needed for analysis).

Where $n_i(t)$ is the number of photons arriving in an interval of duration T_i starting at time t . The autocorrelation function is obtained using a shifting register counting arrangement, where for practical purposes r_t has to be limited. To increase speed and reduce cost, the technique of "clipping" is used. Before autocorrelation the signal is reduced to a 1 or 0 depending on whether the count is above a preset discrimination level. The autocorrelation function becomes

$$G(\tau) = n_k(t) n_k(t - r_t T_i) \quad - 4.11$$

where $n_k(t)$ is 1 or 0 depending on whether $n_i(t)$ was less or greater than the clipping level. The velocity of the particle is calculated from the autocorrelation period (τ_m) (equation 4.12).

$$\text{MEAN VELOCITY} = \frac{\lambda_i}{2 \tau_m \sin \theta} \quad - 4.12$$

Photon correlation is of particular use ^{with} λ low light intensities; should the levels be too high there will be overlapping of the pulses and the technique is unusable. The setting of the clipping level can also prove difficult. Photon correlation does not provide a frequency spectrum, this can only be obtained by using a Fourier Transform on the autocorrelation (140).

4.3.5 ELECTROPHORESIS CELL DESIGN

Laser-Doppler velocimetry can be applied directly to classical electrophoresis cells and electrode arrangements (147, 165, 178, 179). Since only small volumes and short measuring times are needed a radically different design is also possible. Such a design consists of a narrow gap electrode assembly which can be located into a standard cuvette (see section 5.4). The design permits quick sample changes, the narrow electrode gap allows for the application of large

electric fields from low voltage supplies. Good resistance to convective turbulence and the virtual elimination of electro-osmotic effects are additional advantages to this design.

The application of a voltage across a liquid may result in sufficient heating to cause development of convective turbulence. This will result in a broadening and destruction of the resultant spectra. Assuming the electrodes act as isothermal boundaries and the heat differential across the boundaries is parabolic. The maximum temperature rise (ΔT) experienced is given by equation 4.13 (140) where V is the applied voltage, ρ_r is the resistivity of the fluid and K_t the thermal conductivity.

$$\Delta T = \frac{0.2 V^2}{8 \rho_r K_t} \quad - 4.13$$

Temperature rises in excess of 2°C will cause sufficient heterogeneity in mobility to cause excess broadening of the obtained spectra. The resistance to turbulence of narrow gap electrode arrangements means that for a typical system, gaps of 5 mm, 3 mm and 1 mm can experience temperature rises of 1°C , 4°C and 5°C respectively, without exhibiting convective instability (161). Additionally since the heat rise is localised, heat is quickly dissipated to the surrounding bulk of the liquid.

Electroosmosis which complicates measurements in traditionally designed cells is negligible in the narrow gap arrangement. The only reported electroosmotic effects have occurred very close to the cuvette walls at distances of up to 100 μm (76, 140).

The principle disadvantage of the narrow gap arrangement is that the effects of electrode surface reactions, current induced gradients and

polarisation effects can be marked. For this reason careful selection of the electrode material must be made. Bright platinum electrodes may be used for non-aqueous systems but are unsuitable for aqueous systems, because of marked evolution of gas which will result in spectral degradation. Blacking of the electrodes using chloroplatinic acid will reduce this effect, so that electrodes are suitable for use in low ionic strength aqueous systems. However treatment of the electrode surfaces with bovine serum albumin is still necessary to avoid surface reactions. Silver-Silver chloride electrodes are unsuitable since they are prone to emit colloidal particles into the gap at high field strengths. A combination Platinum-Silver chloride electrode is available which can be used in aqueous systems (140).

4.3.6 ELECTRODE DRIVE

Unlike conventional microelectrophoresis apparatus, basic velocimeter designs do not produce directional information. Thus the pulsing or oscillation of the applied electric field in a square wave manner is possible. Such an approach avoids the problems of electrode polarisation and concentration gradients whilst investigating aqueous dispersions. In non-aqueous dispersions electrohydrodynamic and space charge effects may be avoided (section 3.3).

Van der Minne and Hermanie (86) observed that when performing electrophoresis on non-aqueous dispersions with conductivities of less than $5 \times 10^{-10} \text{ S m}^{-1}$ a 'running in time', up to 100s for a conductivity of $10^{-11} \text{ S m}^{-1}$, was necessary. This time was required for the particles to gain full electrophoretic velocity. The effect was thought to be due to the time that it took for the electrophoresis cell to charge

up, rather in the same way as a capacitor. Switching within this 'running in time' will result in little or no particle motion. This effect was reported from work using a conventional cylindrical cell. Narrow gap electrode arrangements do not appear to suffer from this problem. Application of the electric field in pulses of between 7 and 70 ms duration to polystyrene dispersed in media with conductivities as low as $1 \times 10^{-11} \text{ S m}^{-1}$ was free from this problem (76). Similar results have been reported for phthalocyanine dispersions in benzene with pulse durations of between 5 and 20 ms (144).

Consideration of the reponse of the suspended particle must also be made. The concept of a Reynolds number (R_e) is often applied to fluid flow through pipes, it can be equally applied to particles moving through a liquid. The Reynolds number can be calculated using equation 4.14.

$$R_e = \frac{v \cdot d \cdot \rho}{\eta} \quad - 4.14$$

Where v is the particle velocity and d the particle diameter; ρ and η are the density and viscosity of the fluid. A low Reynolds number i.e. less than 1, indicates that inertial forces are negligible in comparison to viscous forces. For a $5 \mu\text{m}$ particle suspended in hexane ($\eta = 2.98 \times 10^{-4} \text{ kg m}^{-1} \text{ s}^{-1}$, $\rho = 660 \text{ kg m}^{-3}$) (62) with an electrophoretic velocity of $100 \mu\text{ms}^{-1}$, the appropriate Reynolds number would be of the order of 10^{-3} . Such a low value indicates that inertial forces are negligible in comparison to viscous forces. Under this situation the particle response can be estimated from the approach of Uzgiris (140).

Due to its momentum a particle with electrophoretic velocity will continue in the same direction after the applied field has been removed, however its velocity will decay. A characteristic time (T_t) for the velocity to decay to $0.368 v$ is given by equation 4.15,

$$T_t = \frac{m}{6 \pi \eta a} \quad - 4.15$$

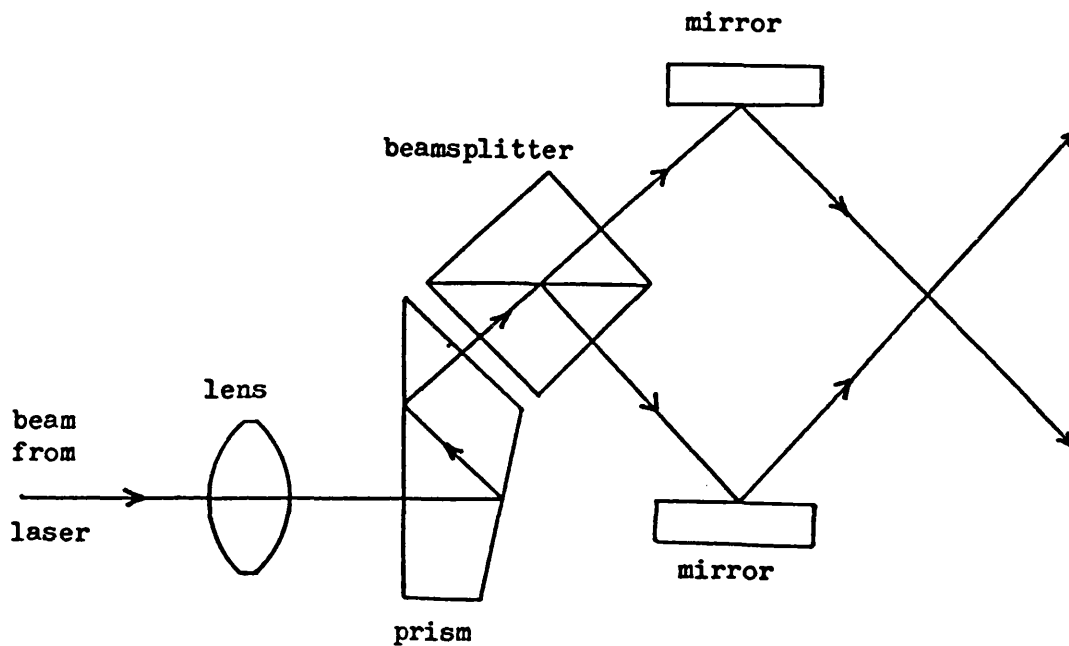
a is the particle radius, m the particle mass ($\rho \frac{4}{3} \pi a^3$). For the non-aqueous system considered above $T_t \approx 3 \mu s$ which represents a continued momental distance of $\approx 10^{-4} \mu m$. It can be seen that for practical purposes the particle response to switching the field can be considered instantaneous, so allowing the use of spectral analysers without time delays or gating arrangements. If the field is in the form of a square wave the obtained power spectrum can, in some instances be complicated by harmonic structures, making its interpretation more difficult. Additionally spectral resolution is dependent upon the observation time; reduction in observation time due to an increase in switching frequency will lead to a decrease in spectral resolution (140).

CHAPTER 5DEVELOPMENT AND DESCRIPTION OF LASER DOPPLER VELOCIMETER5.1 Introduction

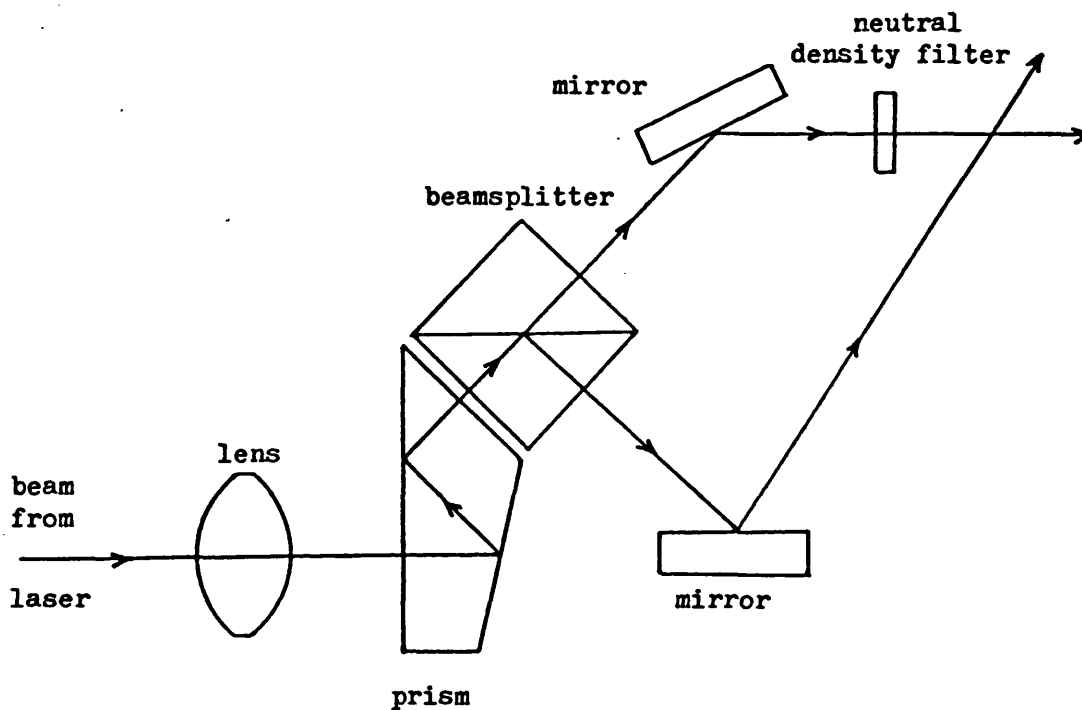
The apparatus is essentially based on the differential heterodyne design of velocimeter (section 4.2.6) to permit the investigation of dilute suspensions. The optical arrangement is derived from that described by Preece and Luckman (169). This design whilst being more difficult to align than integrated optical units, has the advantage of flexibility. The same optical components can produce either a differential heterodyne design (Figure 5.1A), or with the addition of a filter and slight rearrangement of the mount, a local oscillator heterodyne design (Figure 5.1B) of velocimeter. In the event all investigations were carried out solely using the differential heterodyne arrangement. A block representation of the apparatus is shown (Figure 5.2) along with a photograph of the completed apparatus (Figure 5.3).

5.2 The optical bench

To maintain optical alignment all components were pin mounted on a 2 metre aluminium optical bench (Ealing Beck 22-6928) using sliding carriers. Leveling crossfeet (Ealing Beck 22-7108) were attached and fitted with rubber feet. A vibration free base for the bench was essential for noise free electrophoretic motion. This was achieved by placing the bench on a polished slate slab (193 cm x 30.5 cm x 2.5 cm) which rested upon four partially inflated inner tubes (size 3.00 - 10), so completely damping background vibration.

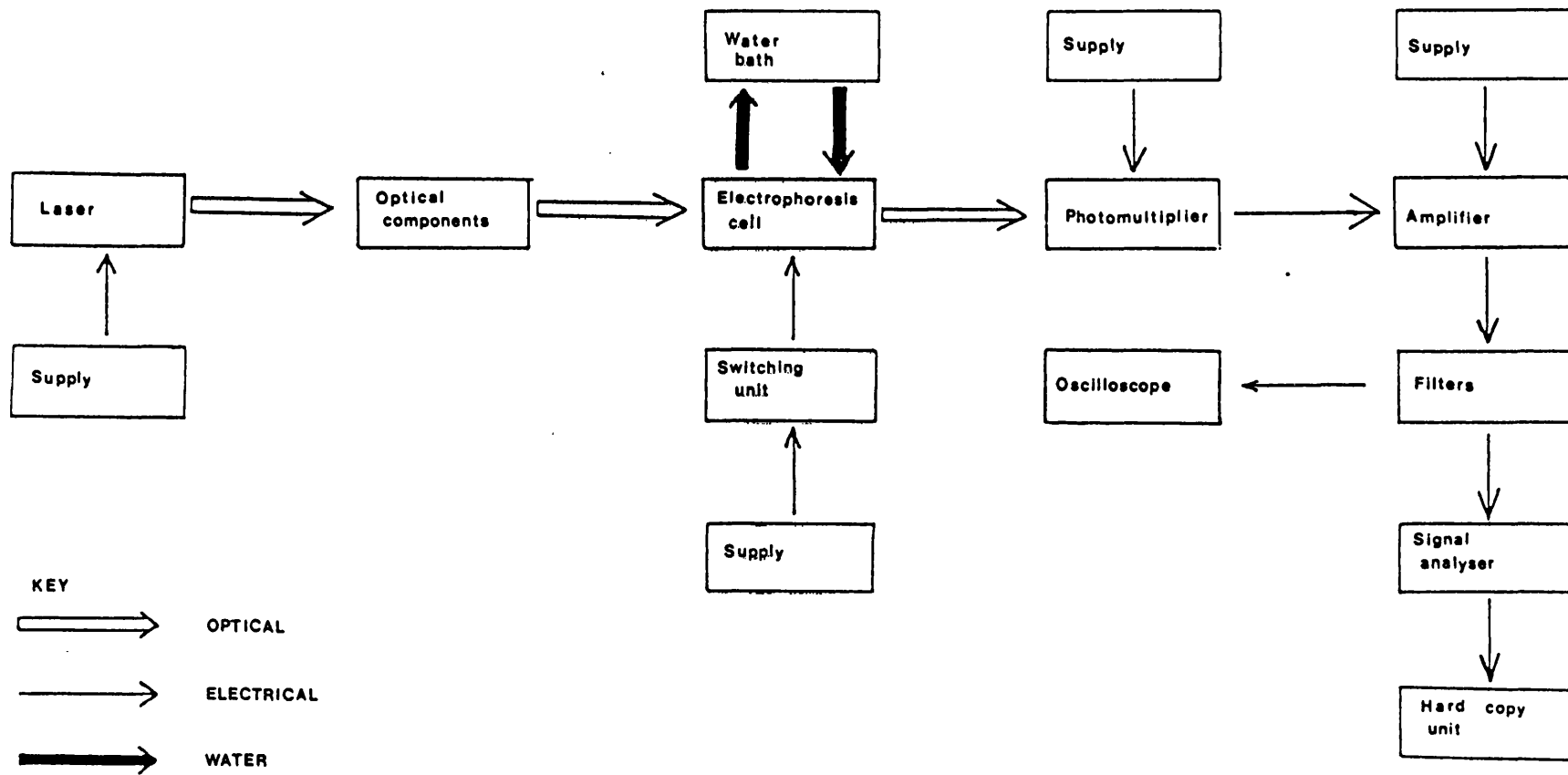


A. Optical arrangement for differential heterodyne velocimetry.



B. Optical arrangement for local oscillator heterodyne velocimetry.

Figure 5.1 Optical Component Arrangements for Laser-Doppler Velocimetry.



91

Figure 5.2 Block Representation of Apparatus

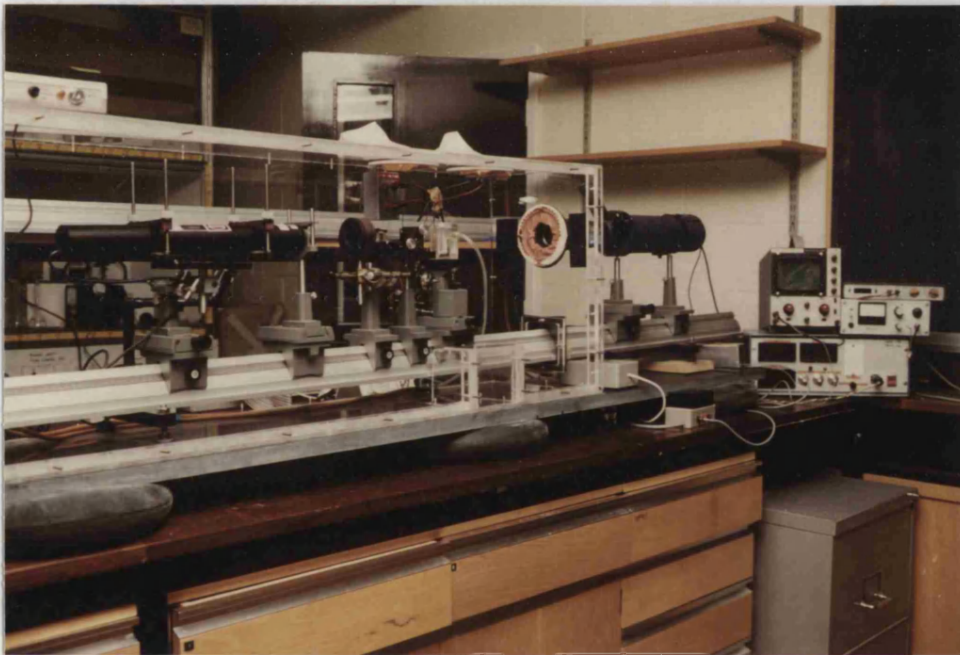


Figure 5.3 The completed apparatus (with exception of signal analyser)

5.3 Laser and optical components

5.3.1 SUMMARY OF OPTICAL COMPONENTS

3225-PC He-Ne laser, plane polarised, 5.4 mW, Hughes Corporation.

Laser power supply EL103, Barr and Stroud Ltd.

Neutral density filter,	Ealing Beck	35-3701.
Laser alignment mount,	" "	22-1739.
Transverse slide carriers,	" "	22-4873.
500 mm Biconvex research quality lens,	" "	23-9095.
Sliding grip lens holder,	" "	22-8106.
Transverse and vertical slide carrier,	" "	22-4899.
Steering mirrors,	" "	23-5853.
45° Prism,	" "	24-3824.
20 mm beamsplitter cube,	" "	24-3931
Filter holder,	" "	34-8847
Slide carriers,	" "	22-4634.

5.3.2 CONSTRUCTION AND ALIGNMENT

The He-Ne laser, wavelength 632.8 nm, was selected primarily on the basis of availability and cost. Operated in $T_{em_{00}}$ a beam of diameter 0.83 mm was produced at the front mirror. The laser was attenuated to a nominal 4.3 mW with a neutral density filter (Figure 5.4) in order to comply with the Bureau of Radiological Health (BRH) standards for class 3A lasers. This allowed the instrument to be used within a conventional laboratory environment. A series of refraction spots was produced by the neutral density filter, these were removed using a mask positioned before the prism. This arrangement prevented any injury to the eye within the blink response but damage from direct viewing of the primary beam was possible. For this reason ALL ALIGN-

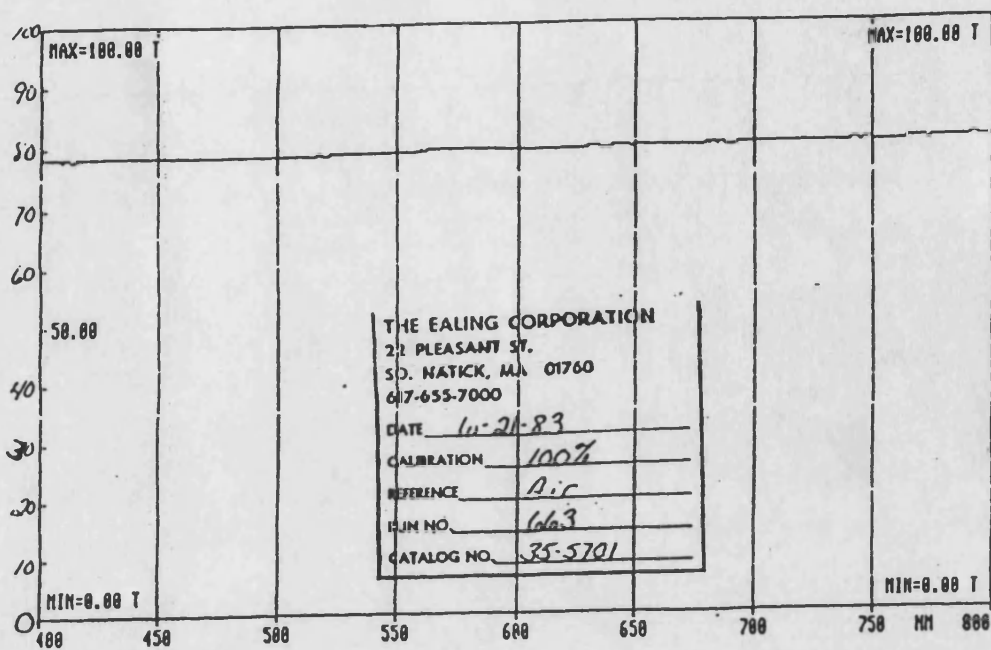


Figure 5.4 Spectral Response of Neutral Density Filter
Used to Derate Laser Output

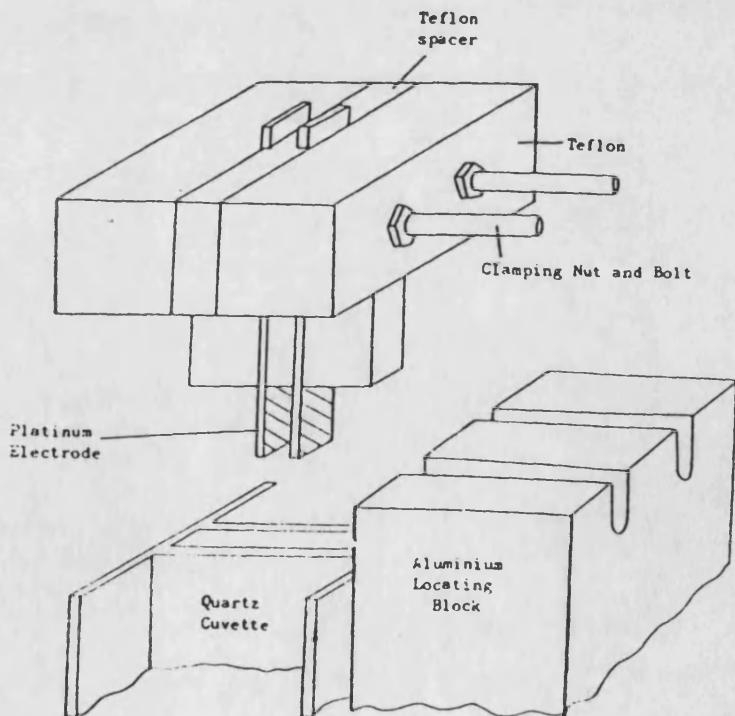


Figure 5.5 Narrow Gap Electrode Assembly
Electrophoresis Cell after Uzgiris (140)

MENT PROCEDURES WERE PERFORMED WITH THE BEAM ATTENUATED using crossed polaroids. The key operated power supply incorporated a 3.5s ignition delay to comply with BRH regulations. The laser was aligned with the plane of polarisation vertical, using an alignment mount and transverse slide carrier. Target cards were used to ensure that the beam was horizontal and parallel to the optical bench.

A 500 mm focal length biconvex research quality lens was positioned directly in front of the laser using a sliding grip holder and transverse slide carrier.

Since $f_f = 0.855$ m (equation 4.1) and $f_l = 0.5$ m, the effective focal length of the lens (d_{\min}) will be significantly less than 0.5 m.

Using equation 4.2 the calculated value for d_{\min} was 0.373 m and the radius of the beam at that point was 0.419 mm. The positioning of the laser and lens relative to the other optical components varied with the intersection angle being used.

The finalised optical arrangement used is that shown in Figure 5.1A with all the components securely mounted on to a black aluminium base. The beam was split by the prism and beamsplitter and then steered by the mirrors to intersect at varying crossing angles. When this intersection occurred on the central line of the bench the pathlengths were equal. Alignment of the beams was ensured by using pin-mounted target cards. A ground glass screen placed at the point of beam intersection was viewed using the RF313 assembly (see section 5.6.2). The use of additional extension tubes (typically 60 mm) provided an enlarged view, so facilitating maximum beam overlap.

The mirrors were flat to $\sim 0.2\lambda_0$, this was slightly greater than the

recommendation of Durst (173) who advocates a tolerance of $0.125\lambda_0$. However such mirrors were recommended by the manufacturer for laser applications and so were considered satisfactory. No tolerance for the beamsplitter cube was quoted, however it was similarly recommended for laser applications.

Measurement of the distance between the beams normal to the optical bench at a known distance from the intersection point, allowed calculation of the intersection angle (equation 5.1);

$$\tan \alpha a = \frac{(\text{separation of beams}) / 2}{\text{distance along bench}} \quad - 5.1$$

where $\alpha a = \theta/2$ in air. Since the refractive index of the cell windows and the liquid within differed from that of air, the intersection angle differed in the liquid. Assuming the cell windows were parallel and positioned normal to the axis of the optical bench, the angle in the liquid was independent of the refractive index of the cell material and could have been calculated using equation 5.2.

$$\sin \alpha_1 = \frac{n_a}{n_1} \sin \alpha a \quad - 5.2$$

Where $\alpha_1 = \theta/2$ in the liquid and n_a and n_1 were the refractive indices of air and liquid respectively. Since the refractive index of air is 1.00 (180) equation 5.2 approximated to equation 5.3.

$$\sin \alpha_1 = \frac{\sin \alpha a}{n_1} \quad - 5.3$$

The precise angles used are reported in the individual experimental chapters, all were however around 20° in liquid.

5.4 Electrodes and electrophoresis cell

The electrophoresis cell (Figure 5.5) used in this work was based upon

that described by Uzgiris (140). Although there were no literature reports of its use with non-aqueous systems, the narrow gap arrangement which allowed high field strengths together with ease in dismantling, made it a logical selection.

Two electrodes 0.26 mm x 2 mm x 50 mm were cut from a sheet of bright platinum. Sandwiched between these electrodes was a Teflon spacer nominally 1 mm thick, the electrodes extended 2 mm beyond the end of the spacer. They were mounted in a quartz spectrophotometer cuvette with the aid of two Teflon blocks, which fitted in to the top of the cell and held the sandwich together. The whole arrangement was clamped together using a pair of nuts and screws rather than cement, which might have leached into the systems under examination.

Teflon has a specific resistance of $10^{19} \Omega \text{ cm}$ (181) therefore the inter-electrode resistance through the Teflon spacer calculated from the spacer dimensions was of the order of $10^{19} \Omega$. A typical low conductivity dispersion has a resistivity of around $10^{14} \Omega \text{ cm}$ (104) offering a resistance between the exposed electrodes immersed in such a dispersion of $2.5 \times 10^{14} \Omega$. The estimated ratio of $4 \times 10^4 : 1$ between these resistances meant that Teflon was a suitable insulator, since electrical conductance through it would be negligible. Teflon was also compatible with chlorofluorocarbons, showing no tendency to swell and distort the electrode gap.

The electrode gap was measured using a Vernier microscope No 13 (Thornton Heath) with both front and back edges being measured at 100 μm intervals. The gap was invariably found to be slightly greater than the spacer, typically 1.1 mm for a 1 mm spacer. This effect has also been noted by Goff (176) who had cemented the electrodes to a spacer.

Care was taken when cleaning the assembly to remove any dispersion which had penetrated between the electrode and spacer. The electrodes were considered aligned when the variation in the measured gap did not at any point exceed $\pm 4.5\%$ of the mean measured gap. The figure of 4.5% was taken as satisfactory after the work of Uzgiris (140). Alignment of the electrodes was checked prior to each experiment and care was taken during use to avoid distortion of the electrode spacing.

The electrophoresis cell housing the electrodes was a fused silica Starna type 52 spectrophotometer cuvette, with internal dimensions 3 mm x 10 mm x 44 mm, constructed in Spectrasil quartz. Temperature control was obtained by locating the cell in a perspex water jacket through which water was pumped using a Grant water bath circulator. For temperatures below ambient an additional cooling unit (Neslab) was used. For details on precision of temperature control see sections 7.5 and 8.1.2.

To ensure reproducible location of the electrodes (Figure 5.5), a grooved aluminium block was fixed to the top of the thermostatic jacket, into which the protruding screws of the electrode assembly could be located. The whole assembly was mounted on to a vertical and transverse slide carrier fitted with two dial micrometers (Baty CL - 1).

5.5 Electrode supply

Two voltage sources were used for the non-aqueous studies; the majority of the work was carried out using a custom-built power supply (Mains Interport Supplies). Operation in either constant voltage or constant current modes was possible, however the low currents experienced limited its use to that of a voltage source capable of supplying between

28 and 670 V. For voltages below 30 V a Farnell laboratory power supply was used.

The output of the relevant power supply was connected to a relay box which generated the voltage waveform shown in Figure 5.6. T is the voltage application time and was variable from 80 to 400 ms. A deadtime (D) of 10 ms was incorporated to avoid accidentally shorting the power supply. Thus field reversal cycles of between 1.2 and 5.5 Hz could be made, the exact frequency being determined by an oscilloscope.

An additional current limiting safety device was incorporated in to the relay circuitry, the cut out current could be set for currents up to 20 mA. The unit was set so that it would cut the supply in response to a small increase in circuit current. Mercury relays were used to avoid contact bounce and were used to 300 V. It was important that the relay box was kept horizontal for correct relay operation. The output of the relays were connected to the free ends of the platinum strips protruding from the electrode assembly.

5.6 Photodetection

5.6.1 PHOTODETECTION DEVELOPMENT

Photodetectors are sensitive to a range of wavelengths; to ensure only laser light was detected, a narrow band interference filter was placed between collection optics and detector. Figure 5.7 shows the spectral response of the filter used. Transmission of only 51% at 632.8 nm led to a reduction in the light intensity reaching the detector. However, the advantages in allowing operation of the apparatus under normal laboratory lighting conditions far outweighed this drawback.

100

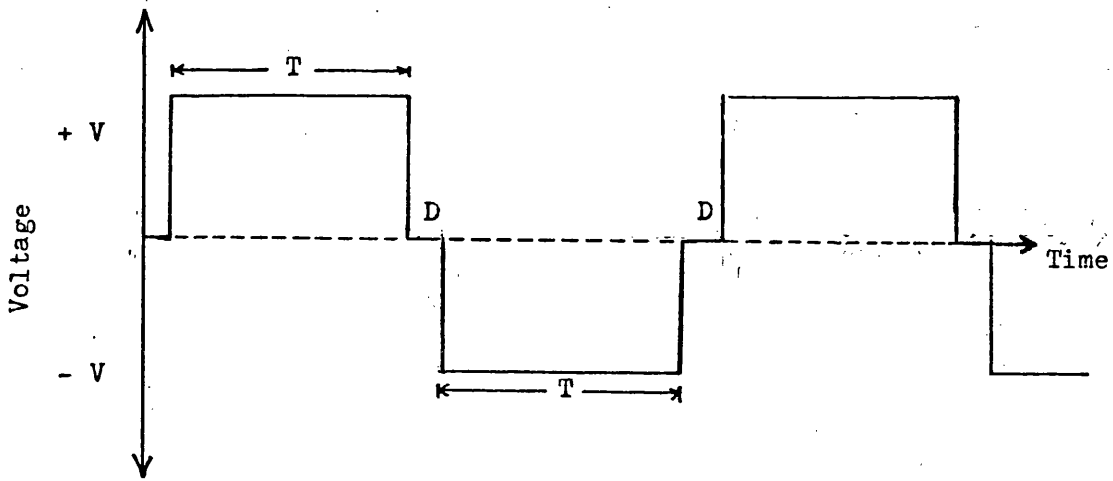


Figure 5.6 Voltage Waveform Produced by Relay Unit

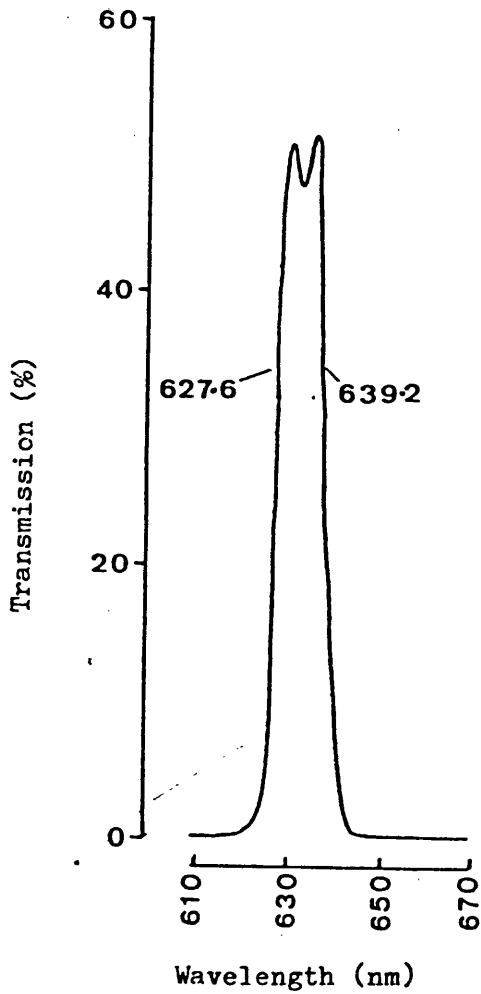


Figure 5.7 Spectral Response of
Interference Filter
Fitted into RF313
Assembly

The use of photodiode detectors was investigated since their application in LDV had been reported elsewhere (173). High gain amplification was however required; the experimental circuit used is shown in Figure 5.8. A FET 355 amplifier with an input impedance of $10^{12} \Omega$ was required because of the high junction resistance of the reverse biased photodiode. Two photodiodes were assessed, a BP X 65 high speed photodiode and a large area photodiode (Radiospares 303-674). In both cases the desired combination of high gain with low noise was not obtained. For this reason, attention was concentrated on the use of a photomultiplier. Initial studies using a 9558Q-AM-S20 photomultiplier tube showed the requirement for accurate detector alignment, consequently a Malvern RF313 assembly was used.

5.6.2 PHOTOMULTIPLIER ASSEMBLY

The Malvern RF313 photomultiplier assembly was fitted with a reflex viewer, allowing focussing of the scattering volume with a Hoya 80-205 mm zoom lens and 25 mm extension tube. A pinhole viewer allowed definition of the portion of the image which passed through the $200 \mu\text{m}$ pinhole, located in front of the photomultiplier. Between the pinhole and photomultiplier was an interference filter (Figure 5.7). The photomultiplier tube was a Thorn EMI 9863 KB/100 with an S20 photocathode. A PM2 photomultiplier power supply provided the optimum - 1.7 kV for tube operation.

The RF313 possessed comparator and discrimination circuits providing an output suitable for analysis by photon correlation. These circuits required an additional $\pm 15 \text{ V}$ power supply (Farnell 15-15-200P). The anode was directly monitored via a conhex plug marked 'ANODE', use of

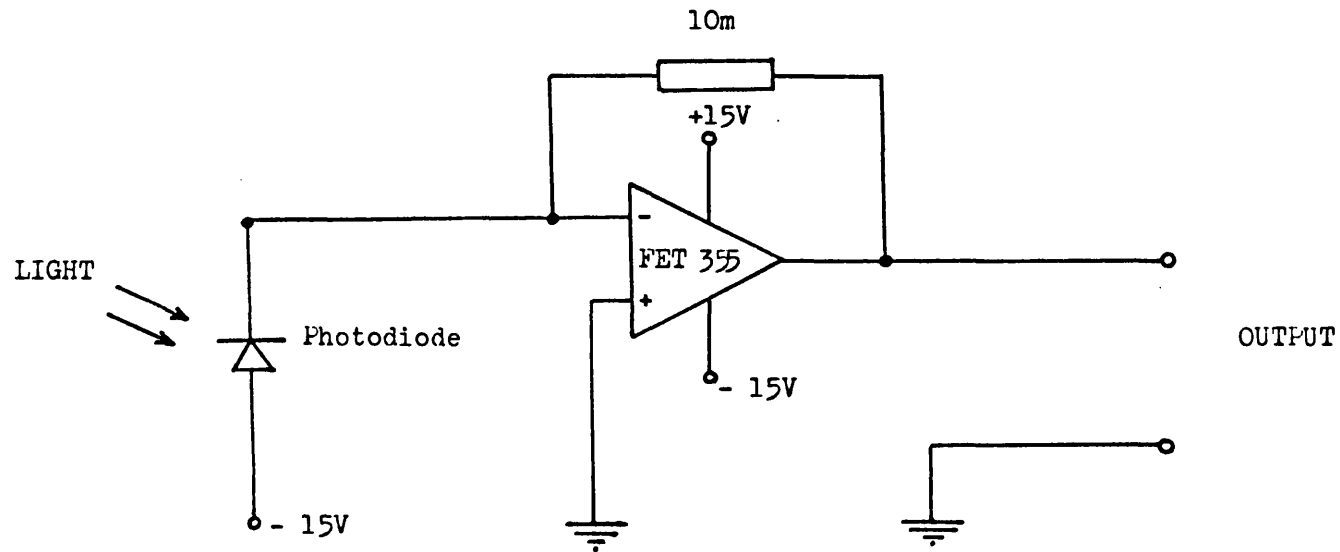


Figure 5.8 General Circuit for the Assessment of Photodiodes
(Resistor values in ohms)

this did not require the additional supply.

5.7 Signal Processing

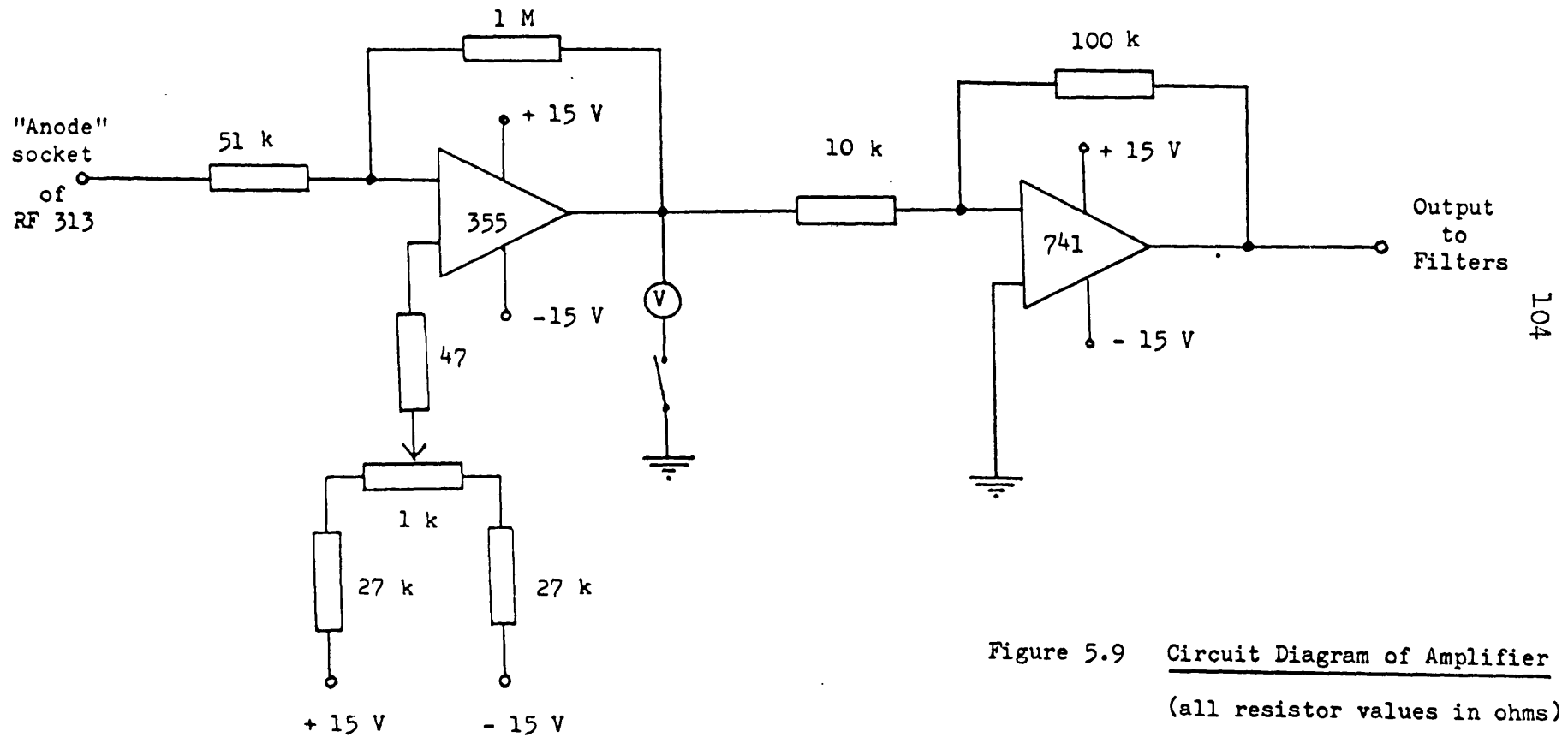
Fast Fourier transform signal analysis was selected as the method of signal processing on the basis of flexibility, 'real time' presentation of data and availability of apparatus. The signal was taken directly from the anode monitor of the RF313 and before analysis it was amplified and filtered.

5.7.1 AMPLIFICATION

The circuit used is shown in Figure 5.9 and involves 2 stages of amplification using an operational amplifier in inverting amplifier configurations. Stages 1 and 2 provided gains of X20 and X10 respectively. Stage 1 allowed the DC component of the signal to be offset, so as to ensure the AC signal component would not be clipped on stage 2 amplification. The offset was monitored using a moving coil meter (Radiospares audio balance meter) to ensure the DC output of stage 1 was close to zero.

5.7.2 FILTERING

The amplified photomultiplier signal was then passed through high and low pass filters. The high pass filter set at 0.5Hz removed the pedestal signal (section 4.3.4) and the low pass filter set at 100Hz removed high frequency noise. The circuit used was based on that described by Brown (182) and is shown in Figure 5.10. The response of the amplifier and filter pair was checked by feeding different frequency signals of constant amplitude from a testwave generator (Type TWG 300, Feedback Ltd.) through the amplifier and filter circuitry. The filter output was connected to an oscilloscope (Tele-equipment) and the signal



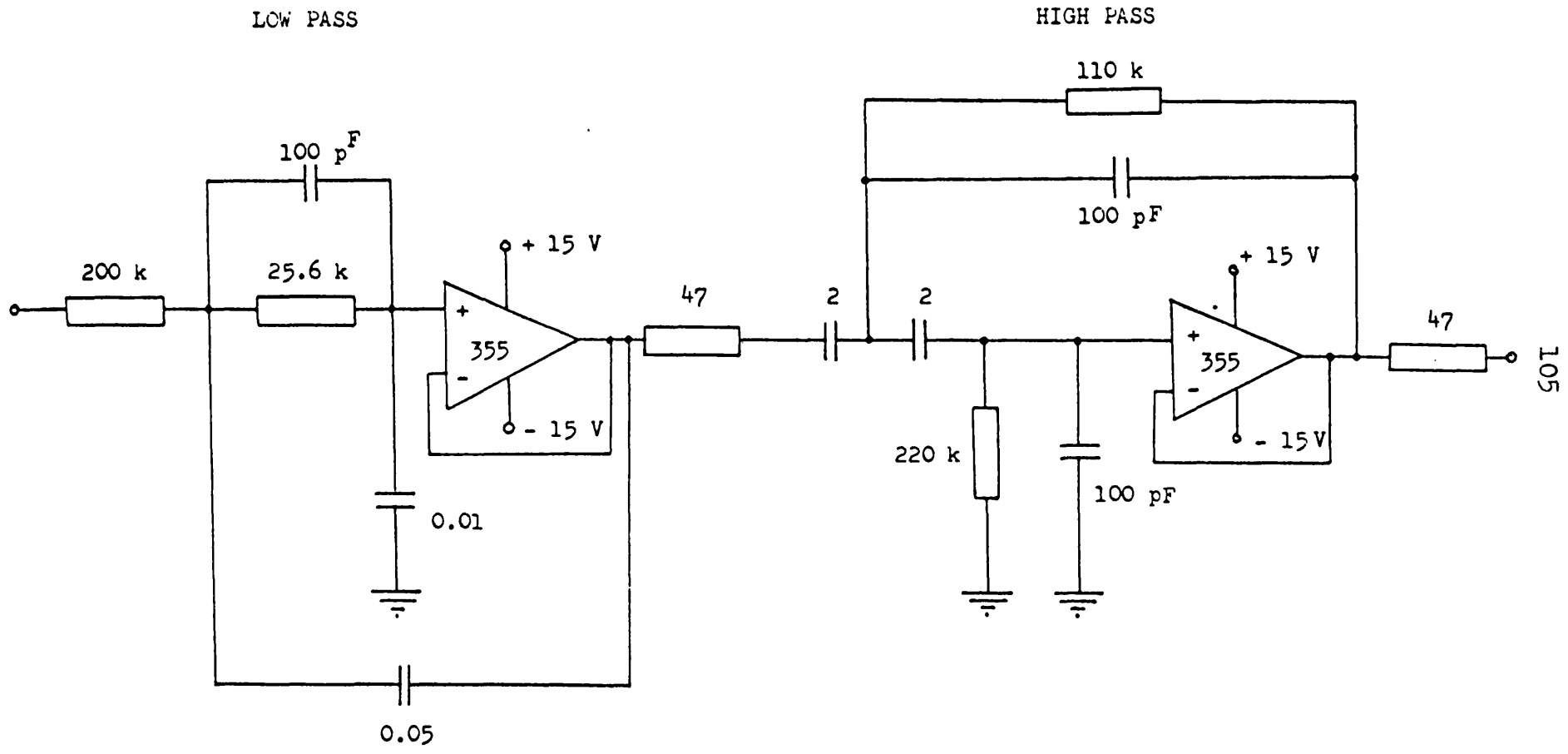


Figure 5.10 Circuit Diagram of High and Low Pass Filters, After Reference 182.

(Resistor values in ohms, capacitor values in micro farads unless indicated otherwise)

amplitude (peak to peak value) recorded. The response curve is shown in Figure 5.11 and demonstrates the required response, without any unwanted harmonics.

5.7.3 ELECTRICAL NOISE

To reduce mains noise all circuitry was mounted in an earthed aluminium box, with all input and output cables screened. The amplifier and filter circuitry was connected through screened cables to a ± 15 V encapsulated power supply (Radiospares 561-124). Care was also taken to avoid earth loops which can occur when several earthed pieces of equipment are interconnected.

5.7.4 SIGNAL ANALYSIS

The filter output was analysed by Fast Fourier transforms using a Nicolet 100A mini-analyser (Nicolet Scientific Corporation), this produced 'real time' power spectrums. For most experiments average spectra using the 0-200Hz range were collected by summing 4, 16, 64 or 256 consecutive spectra, a moving cursor facility being used to estimate the frequency shift. A hard copy unit (Nicolet Scientific Corporation model 132A) was used to produce permanent records of the spectra when required. It was also found useful to connect an oscilloscope in parallel to the analyser to allow viewing of the unprocessed signal.

5.8 Low humidity housing

To allow experiments to be conducted in low humidity conditions the apparatus, with the exception of the photomultiplier detector and processing equipment, was housed in a gloved Perspex box. The front panel was removable to facilitate optical alignment. The RF313

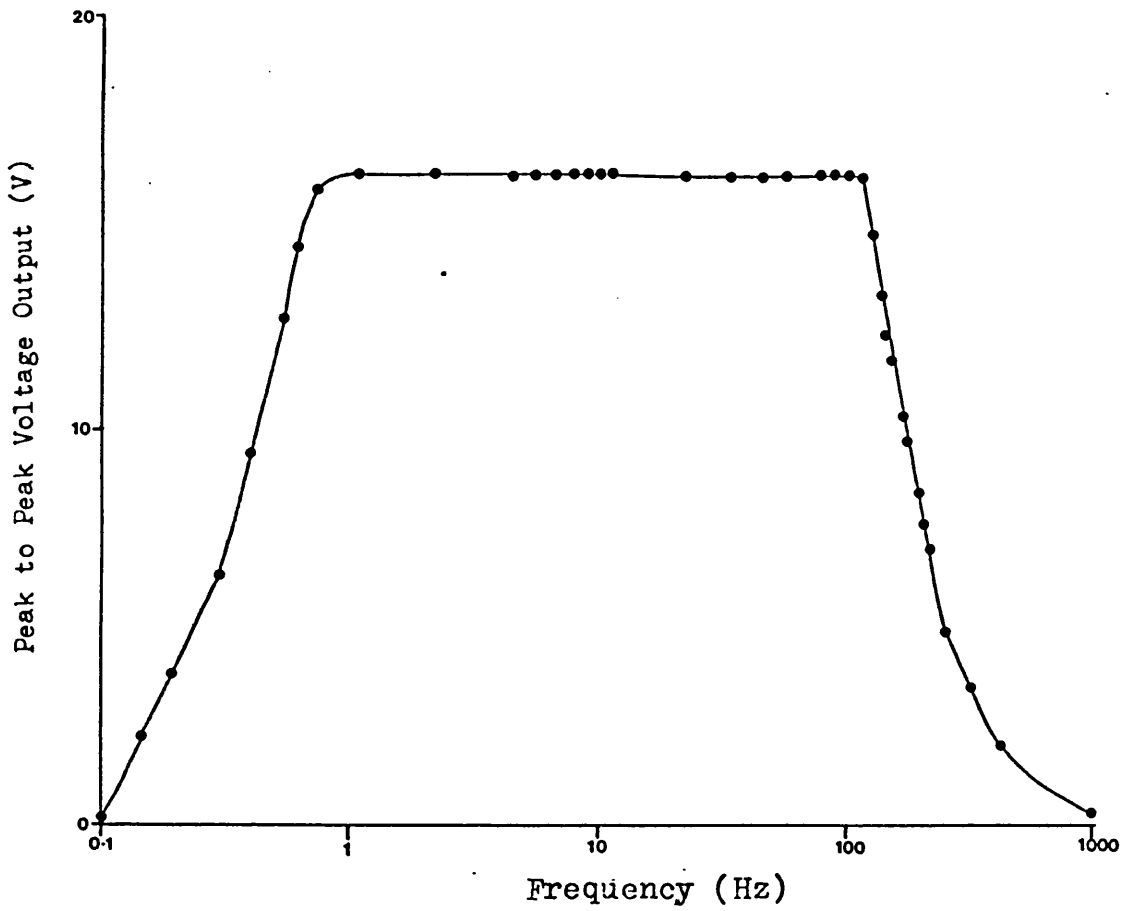


Figure 5.11 Response Curve of Low and High Pass Filters
Connected in Series

assembly was attached using a flexible rubber sleeve which allowed the movement required for focussing. Ports with PVC gaskets were used for the optical bench, nitrogen flushing tube, laser, water jacket and electrode connections. These ports were further sealed with waterproof tape. A small hatch allowed sample entry without removal of the complete front panel, which was held using wing nuts and sealed with tape.

Phosphorus pentoxide was placed inside the cabinet and with just the hatch partially unsealed, the cabinet was flushed with dry nitrogen for several minutes. After this, the cabinet was totally sealed using tape and left overnight. The relative humidity was monitored using a Hair hygrometer (Griffin Scientific) which was regenerated monthly. Experiments were conducted when relative humidities of less than 8% were attained inside the cabinet.

CHAPTER 6MATERIALS AND GENERAL METHODS6.1 Materials and instrumentation

6.1.1 GENERAL MATERIALS

Aquamicron reagents:	Mitshubishi Corporation.
Aerosol OT 100%:	A gift from Cyanamid of Great Britain Ltd.
Arcton 113:	5 litre samples, supplied as a gift from Imperial Chemical Industries.
Benzene:	Analar grade, BDH Chemicals.
Bovine serum albumin:	98-99%, Sigma Chemicals.
Calcium chloride:	GPR grade, BDH Chemicals.
Carbon disulphide:	Spectrosol grade, BDH Chemicals.
Chloroform:	Analar grade, BDH Chemicals.
Chloroplatinic acid:	GPR grade, Fisons Scientific Equipment.
Copper sulphate:	Analar grade, BDH Chemicals.
Cyclohexane:	Aristar grade, BDH Chemicals.
Elaidic acid:	Biochemical grade, BDH Chemicals.
Glass Treet:	Phase Separations Ltd.
Glucose BP:	Evans Medical.
Helium:	Air Products.
n-Hexane:	Analar grade, BDH Chemicals.
Hydrochloric acid:	Analar grade, BDH Chemicals.
Hypersil ODS:	3 μm and 5 μm , Shandon Southern Instruments.
Light liquid paraffin BP:	Evans Medical.
Membrane Filters:	0.47 μm PTFE (SM11806) and 0.01 μm cellulose nitrate (SM11318), Sartorius Instruments.

Methanol:	HPLC grade, BDH Chemicals.
Molecular sieve:	Grade 5A, Fisons Scientific Equipment.
Monobromonaphthalene:	GPR grade, Fisons Scientific Equipment.
Myristic acid:	Specially pure grade, Lot 14282, Milton Roy Company.
Nitrogen:	Air Products.
p-Nitrosodimethylaniline:	Gold label, Aldrich Chemical Co. Ltd.
Oleic acid:	99% pure, Lot 30152, Larodan Fine Chemicals.
Petroleum ether 100/120:	GPR grade, BDH Chemicals.
Phosphorous pentoxide:	GPR grade, BDH Chemicals.
Platinum wire:	0.46 mm gauge, Fisons Scientific Equipment.
Potassium chloride:	Analar grade, BDH Chemicals.
Potassium dihydrogen phosphate:	Analar grade, Fisons Scientific Equipment.
Potassium ferricyanide:	Analar grade, BDH Chemicals.
Potassium Hydrogen phthalalate:	Analar grade, BDH Chemicals.
Priolene 6952:	Commercial grade oleic acid, Unichema Chemicals.
Sodium acetate:	Analar grade, BDH Chemicals.
Sodium bicarbonate:	Analar grade, BDH Chemicals.
Sodium chloride:	Analar grade, BDH Chemicals.
Sodium dichromate:	GPR grade, Fisons Scientific Equipment.
Sodium dihydrogen phosphate:	Analar grade, BDH Chemicals.
Sodium tetraborate:	Analar grade, BDH Chemicals.
Sucrose:	Aristar grade, BDH Chemicals.
Sulphuric acid:	Analar grade, BDH Chemicals.

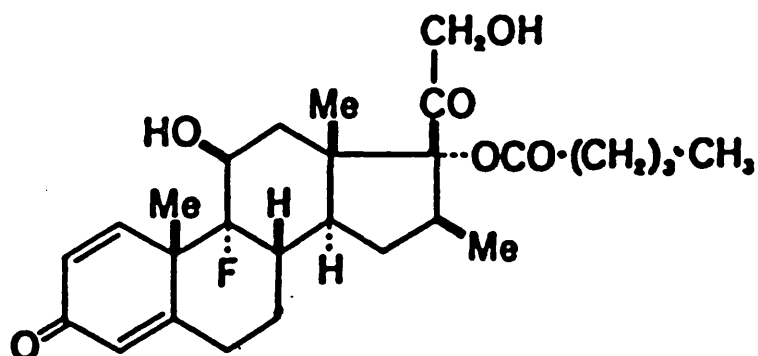
Tetra-n-butylammonium:	GPR grade, BDH Chemicals.
hydroxide:	
Toluene:	Analar grade, BDH Chemicals.
Water:	Distilled and double distilled collected from all glass stills.
Zinc (powdered):	Analar grade, Fisons Scientific Equipment.

6.1.2 DRUG MATERIALS

One steroidal drug and one model bronchodilator were selected as being representative compounds for this work; both materials were supplied by Glaxo Group Research.

Betamethasone - 17 - valerate

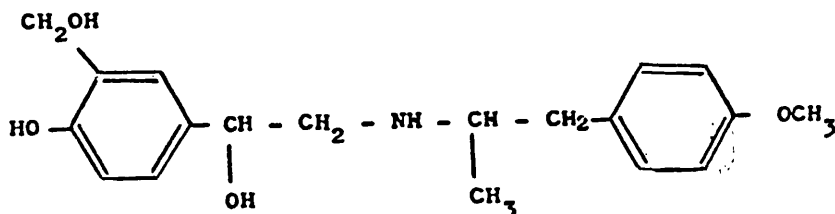
Betamethasone - 17 - valerate is a corticosteroid which is formulated as an aerosol for the prophylactic treatment of asthma. It is a white crystalline powder having the following structure:



Two samples of material meeting B.P. specifications were used, one a micronised powder, the other unmicronised; both originated from batch 931A. The specific surface area of the micronised powder had been determined, by gas adsorption, to be $5.01 \times 10^3 \text{ m}^2 \text{ kg}^{-1}$.

Salmefamol

Salmefamol (AH 3923) is a model bronchodilator, similar in action to salbutamol. It is a creamy white crystalline powder having the following structure:



Both micronised (batch 003/1) and unmicronised (batch 1622) samples were used. The specific surface area of the micronised powder was determined by Coulter Electronics Ltd, using a Micromeritics MIC 2200/2205 high speed surface area analyser, to be $2.7 \times 10^3 \text{ m}^2 \text{ kg}^{-1}$.

6.1.3 EQUIPMENT

Temperature measurements.

Digital thermometer type 3002 with NiCr/NiAl thermocouple

BS4937, Co Mark Electronics.

Glass/mercury thermometer, range -5 to 50°C, graduated in 0.1°C intervals.

Resistance thermometer bridge type 5840, Tinsley and Co Ltd.

NPL certified platinum resistance thermometer, ref 120076, Tinsley and Co Ltd.

Particle size analysis.

Malvern 2200 particle size analyser.

Jeol 35-C scanning electron microscope.

Density determinations.

Micromeritics helium/air pycnometer, model 1302.

Glass pycnometer with caps.

Electrostatic charges on powders.

Keithley Instruments solid state electrometer, model 6100, with Faraday Well.

Custom built vibrating hopper, lined with high density polyethylene.

Purification of Aerosol OT.

Buchi Rotavapor R110.

Infra-Red Spectroscopy.

Perkin Elmer 377 Infra-red grating spectrophotometer.

Perkin Elmer variable pathlength NaCl cell.

Moisture determinations.

Mitsubishi moisture meter CA-02.

Custom built Perspex glove box.

Atmosbag, Aldrich Chemical Company.

Refractive index determinations.

Abbé refractometer, model 586269, Bellingham and Stanley Ltd.

Pearl lamp light source.

Relative permittivities.

Wayne Kerr, B642, autobalance universal bridge.

Wayne Kerr, permittivity cell D121, and tubes.

Solution conductivities.

General Radio 615A capacitance bridge.

General Radio 1232A tuned amplifier and nullpoint detector.

Telequipment laboratory oscilloscope.

Radiospares 610-635 function generator.

Aluminium bob conductivity cell.

Viscosities.

Size 1 BS188 suspended level viscometer, Poulton, Selfe and Lee.

Viscometer thermostatically controlled bath, Laboratory Thermal

Equipment with Haake EK12 bath cooler; temperature control

$\pm 0.03^{\circ}\text{C}$ at 10°C , $\pm 0.01^{\circ}\text{C}$ at 20°C .

High Pressure Liquid Chromatography.

Constametric I pump, Laboratory Data Control.

Rheodyne valve fitted with $100\ \mu\text{l}$ loop.

Pye Unicam LC-UV adjustable wavelength detector.

115

15 cm stainless steel column, internal diameter 0.5 cm,
packed with 5 μ m Hypersil ODS.

Techne DB3 Driblock and SC-3 sample concentrator.

Gas Chromatography.

Heward Packard, level 2, 5880A, Gas chromatography apparatus.

CP Sil 5 - CB, 25m capillary column, Chrompack UK Ltd.

UV Spectroscopy.

Pye Unicam SP1800 UV Spectrophotometer with AR25 linear
recorder.

10 mm pathlength quartz spectrophotometer cells, Starna UK Ltd.

pH Measurements.

Philips PW 9421 Digital pH meter,

range pH 1 - 14 in 0.001 steps.

Combined glass-

Pye Ingold 401 Silver-Silver chloride electrode.

General Apparatus.

Edwards High Vacuum pump, model E550.

Hair Hygrometer, Griffin Scientific.

Haake EK12 Bath cooler.

Neslab 'U COOL' Bath cooler.

Grant SU6 thermostatic control unit and circulator.

Grant SS30 Shaking water bath.

Gilson Pipetman 200 automatic pipette.

Watson Barnett laboratory microscope.

Mettler ME5 ultrasonic cleaning bath.

Townsend and Mercer thermostatic vacuum oven.

Griffin-Grundy laboratory oven.

Hansen AT-1020 multimeter.

Griffin Scientific Haemocytometer.

Gillete medical lances.

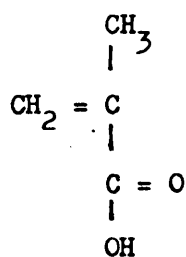
Farnell variable laboratory power supply.

MSE Bench centrifuge.

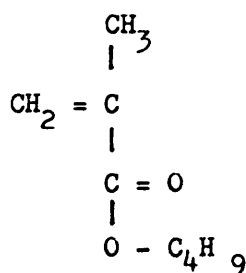
6.1.4 MODEL PARTICLES

Polymer coated monodisperse silica spheres were supplied by Dr B. Vincent and Dr D. Skuse (Department of Physical Chemistry, University of Bristol); their manufacture has been described elsewhere (183). The spheres were nominally 82 nm, 240 nm and 700 nm in diameter and were coated with one of two different polymer types.

Type A polymer was the product of the co-polymerisation of approximately 8% methacrylic acid with approximately 92% n - butyl methacrylate.

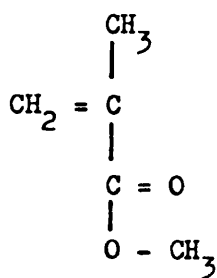


methacrylic acid

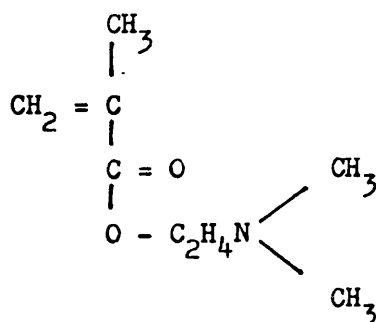


n - butyl methacrylate

Type B polymer was the product of the co-polymerisation of approximately 70% methylmethacrylate with 30% dimethyl amino-ethyl methacrylate.



methyl methacrylate



dimethyl amino ethylmethacrylate

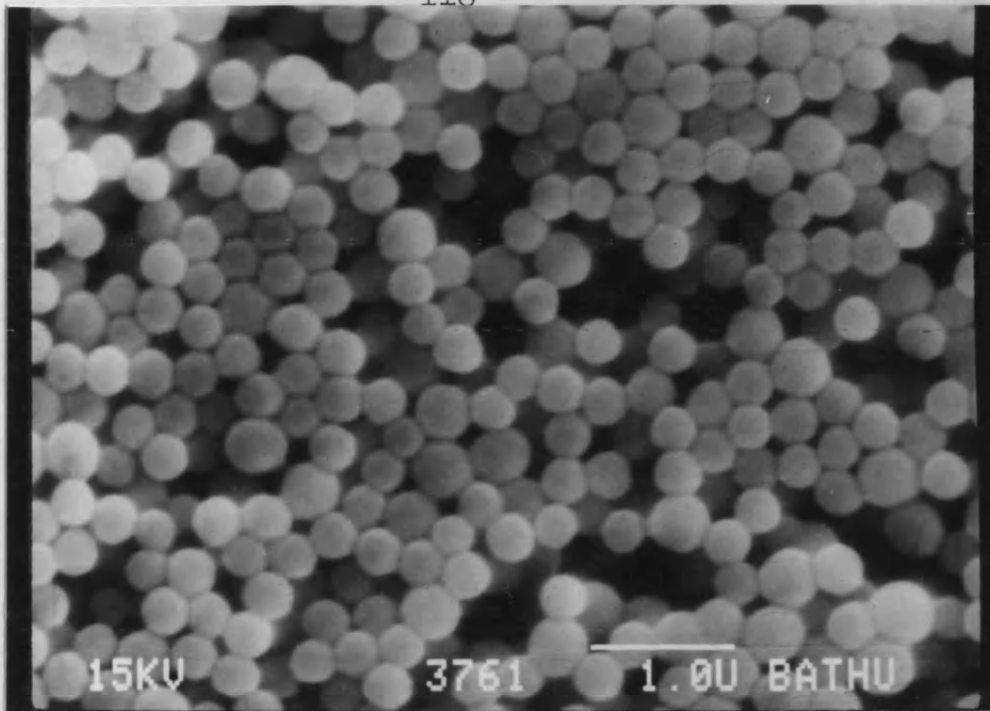
All were received as dispersions in toluene.

For larger model particles, Hypersil ODS HPLC packing material was used. Hypersil ODS consists of porous silica spheres whose surface Si-OH groups have been capped with non-polar C18 groups using octadecylsilane. Samples with nominal particle sizes of $3\ \mu\text{m}$ (batch S/1326) and $5\ \mu\text{m}$ (batch S/1336) were used.

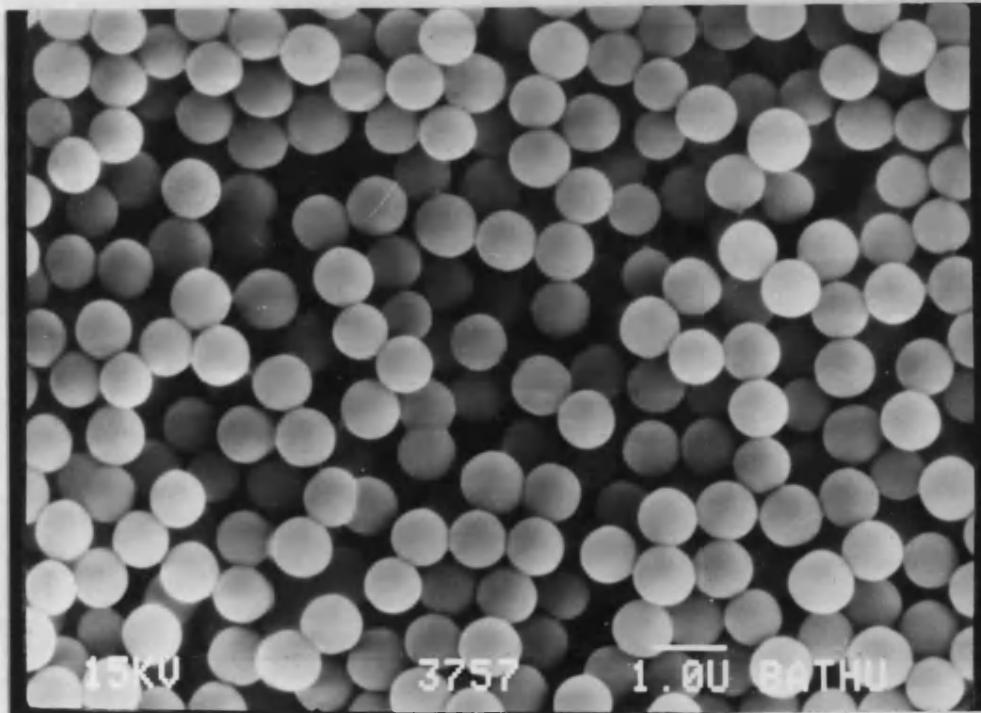
Figures 6.1 and 6.2 show scanning electron micrographs of the 240 nm and 700 nm B polymer coated spheres and the $3\ \mu\text{m}$ and $5\ \mu\text{m}$ Hypersil ODS spheres respectively. Histograms of particle size by number from electron micrographs are shown in Figure 6.3, being based on 200 particles counted from four fields of view. It was observed that the particle size of the nominal 240 nm model spheres was closer to 300 nm.

6.1.5 TEMPERATURE MEASUREMENTS

Where possible a glass/mercury thermometer was used to measure all temperatures. This was itself checked against an NPL certified resistance thermometer over a range of temperatures between 10°C and 26°C . The recorded glass/mercury thermometer temperature showed deviations of less than 0.05°C from that of the resistance thermometer for all temperatures checked. Temperature deviations were in both

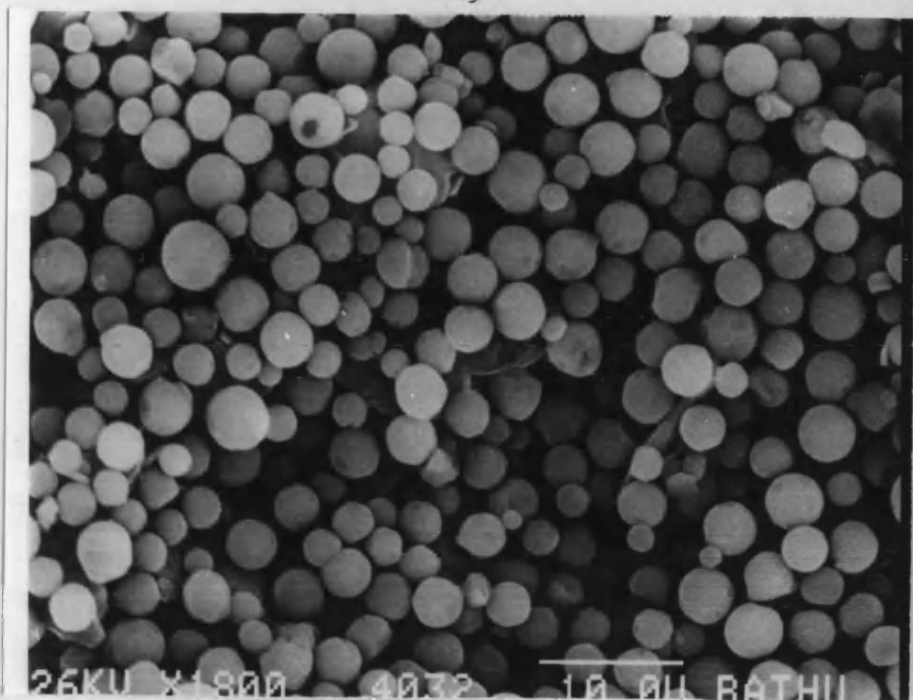
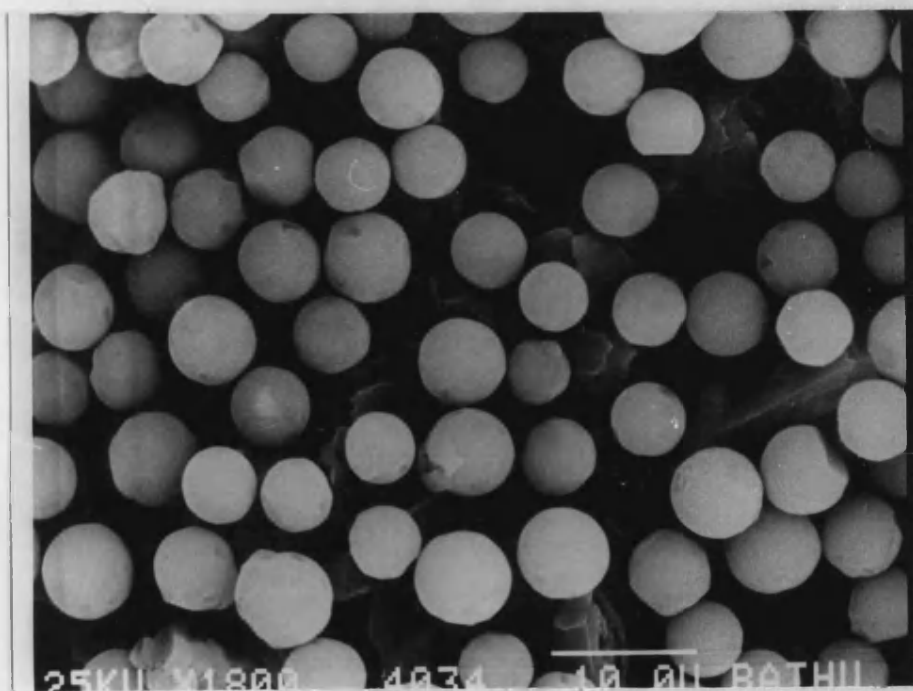


A. '240 nm' B polymer coated silica spheres. $\overline{1.0\mu\text{m}}$



B. 700 nm B polymer coated silica spheres. $\overline{1.0\mu\text{m}}$

Figure 6.1 Scanning Electron Micrographs of B polymer coated Model Particles Dispersed in Toluene

A. 3 μm Hypersil ODS $10\mu\text{m}$ B. 5 μm Hypersil ODS $10\mu\text{m}$ Figure 6.2 Scanning Electron Micrographs of Hypersil ODSModel Particles

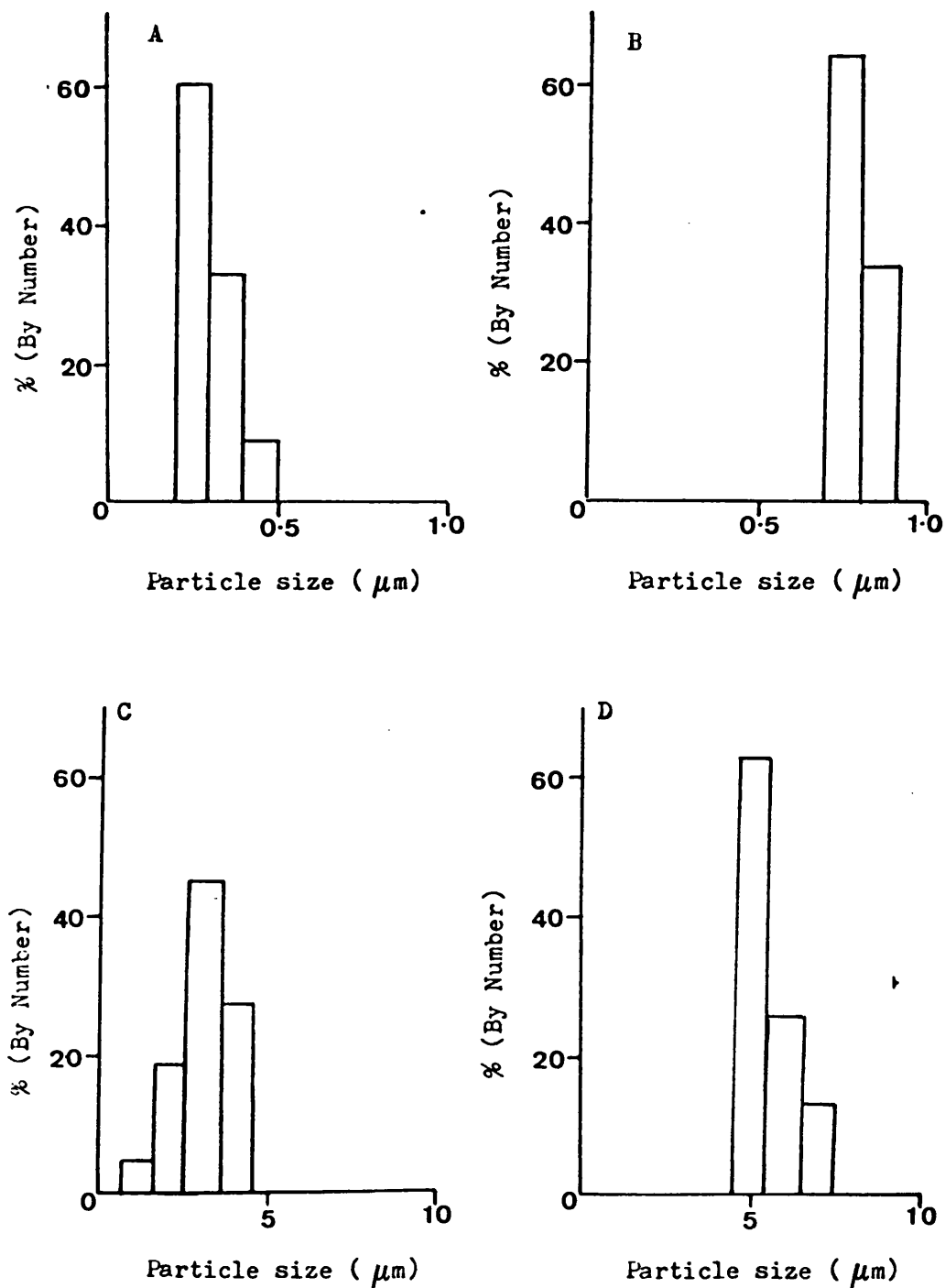


Figure 6.3 Particle Size Distributions By Number of Model

Particles as Determined by Scanning Electron Microscope

A : '240' nm B Polymer coated silica spheres

B : 700 nm B Polymer coated silica spheres

C : Hypersil ODS nominal size 3 μm

D : Hypersil ODS nominal size 5 μm

directions and were so small they were considered to be insignificant.

The small volume of the electrophoresis cell made it necessary to use a digital thermometer, sensitive to 0.1°C , with a NiCr/NiAl probe to measure dispersion temperatures in the cuvette. The temperatures recorded by the digital thermometer were found to be consistently 0.1°C higher than those obtained with the glass/mercury thermometer. Temperatures reported for the digital thermometer have therefore had 0.1°C subtracted from them.

6.1.6 GLASSWARE

Glassware was cleaned using chromic acid, after which it was well rinsed in tap water before being rinsed at least six times in distilled water. Glassware was then dried in an oven after a final rinse with 113/n-hexane (section 6.3.1).

Particulate free glassware for electrophoresis studies was obtained by treating the glassware with steam and Arcton 113 vapour. Stoppers were washed with $0.01\ \mu\text{m}$ membrane filtered distilled water and Arcton 113, and dried using filtered air and stored over P_2O_5 .

When possible silica suspensions were prepared in sample tubes which could be discarded after use, because of the difficulty in cleaning them. When this was not possible e.g. the electrophoresis cuvette, glassware was soaked overnight in approximately 5% Decon 90 solutions; sometimes an ultrasonic bath was also used. The glassware was rinsed of traces of Decon solution by leaving it in flowing tap water for several hours, before finally rinsing with distilled water. Manufacturers' literature for Decon states that such a procedure will remove all traces of the surfactant (184).

Glassware to contain oleic acid or Aerosol OT was aged overnight using an appropriate concentration of surfactant solution, before being rinsed with 113/n-hexane and dried.

When excessive deposition occurred during electrophoresis studies (e.g. section 9.1.2), the inner walls of the cuvette were treated with Glass Treet; the active constituent dimethyldichlorosilane reacts with any active sites on the glass surface. Treatment was as detailed in the manufacturer's literature. The previously cleaned and dried cuvette was filled with Glass Treet and allowed to stand for 5 - 10 minutes. The cuvette was then thoroughly rinsed with dried methanol (dried as in section 6.3.6) and dried overnight at approximately 95°C before being allowed to cool in a desiccator over P₂O₅.

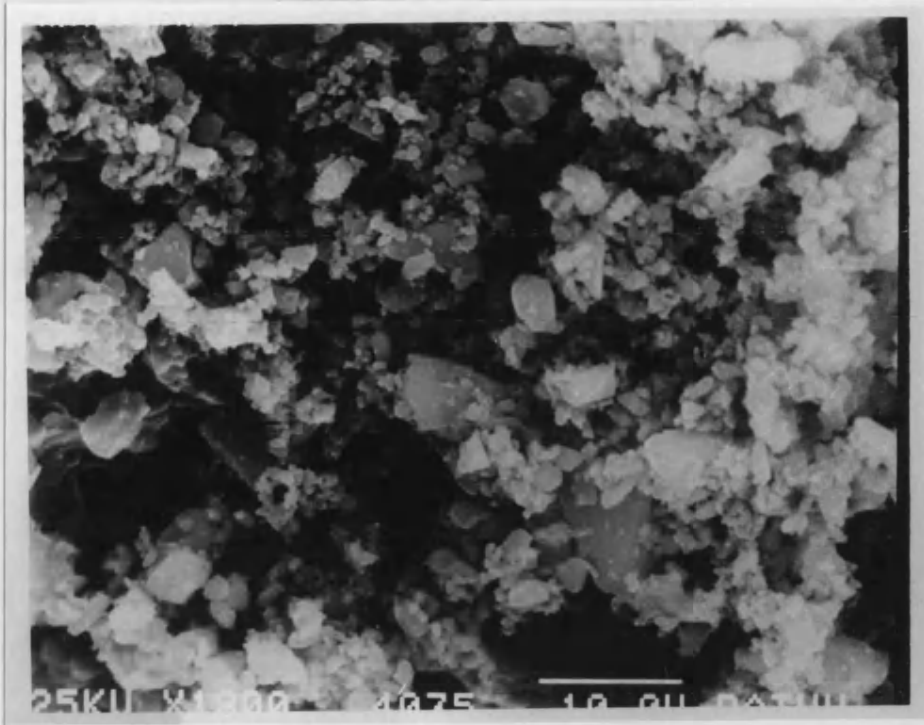
6.1.7 pH MEASUREMENTS

Prior to making any pH measurements the pH meter was calibrated using standard buffers at 25°C ± 0.1°C. The two buffers used were 0.05 M potassium hydrogen phthalate buffer of pH 4.008 and a 0.01 M sodium tetraborate buffer of pH 9.180. All solutions under test were similarly equilibrated at 25°C ± 0.1°C unless indicated otherwise.

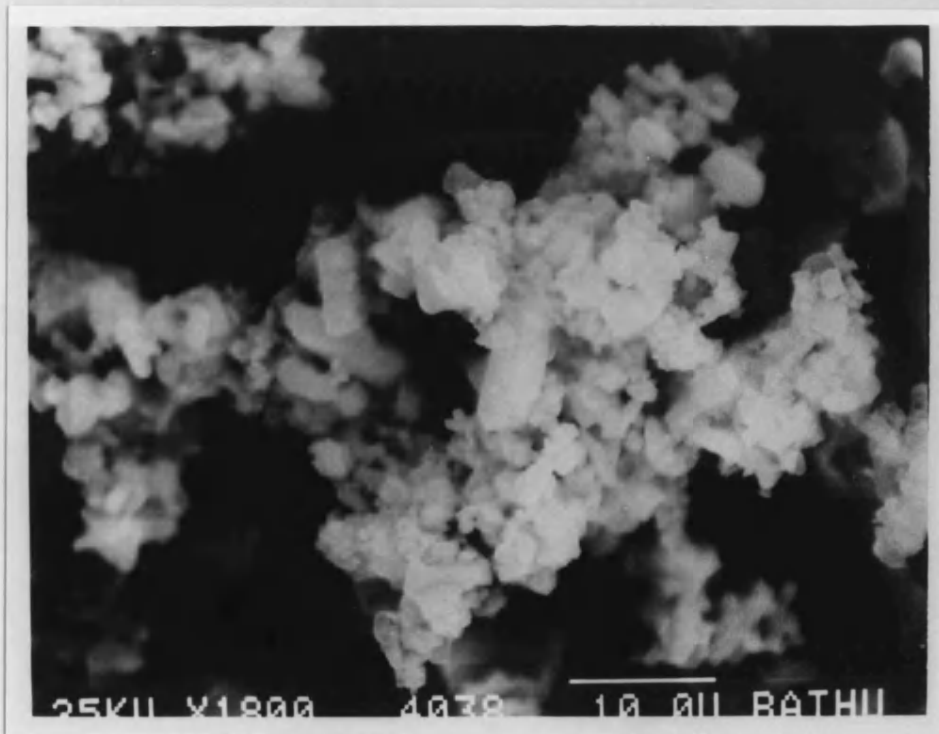
6.2 Characterisation of drug materials

6.2.1 PARTICLE SIZE OF MICRONISED POWDER

The particle size distribution of the micronised drug materials, could not easily be determined from electron micrographs taken using the Jeol JSM-35C scanning electron microscope (Figure 6.4). A Malvern 2200 particle sizer was therefore used. The samples were prepared as dispersions in light liquid paraffin. Prior to examination each dispersion was placed in an ultrasonic bath for 20 minutes. This was to



A. Betamethasone Valerate

10 μ m

B. Salmefamcl

10 μ mFigure 6.4 Scanning Electron Micrographs of Micronised Drug Materials

break up any aggregates which might be present; microscopic examination of a sample confirmed their absence.

The particle sizer presented the results as cumulative percent under-size, fitted to a log-normal distribution (Figure 6.5). The median particle size for the micronised salmefamol was $3.5 \mu\text{m}$ and $2.3 \mu\text{m}$ for the micronised betamethasone valerate. The goodness of fit to the distribution is given by an instrumental 'log error' term; a numerical value of less than 5 is considered to represent a good fit (185). The 'log error' values for salmefamol and betamethasone valerate were 3.96 and 3.79 respectively, indicating a good fit to the model.

The Malvern particle sizer operates using the Fraunhofer diffraction pattern produced by particles in a coherent beam of monochromatic light. Since the size range for this technique is limited to between approximately $1.2 \mu\text{m}$ to $1876 \mu\text{m}$ (186), the results must be considered with caution, as 28% of the betamethasone valerate and 13% of the salmefamol particles are below the theoretical lower limit. What can be concluded is that both micronised powders exhibited a wide size distribution, namely,

micronised betamethasone valerate 28% $< 1.2 \mu\text{m}$, 2% $> 20 \mu\text{m}$,

Micronised salmefamol 13% $< 1.2 \mu\text{m}$, 4.5% $> 20 \mu\text{m}$.

However, since particle sizes are expressed by weight, the actual number of larger particles present in both samples is relatively small. This was confirmed by the electronmicrographs of the powders.

6.2.2 DENSITIES OF DRUG MATERIALS

Densities were determined using the Micromeritics helium/air pycnometer; unmicronised samples of each drug were used as they could be

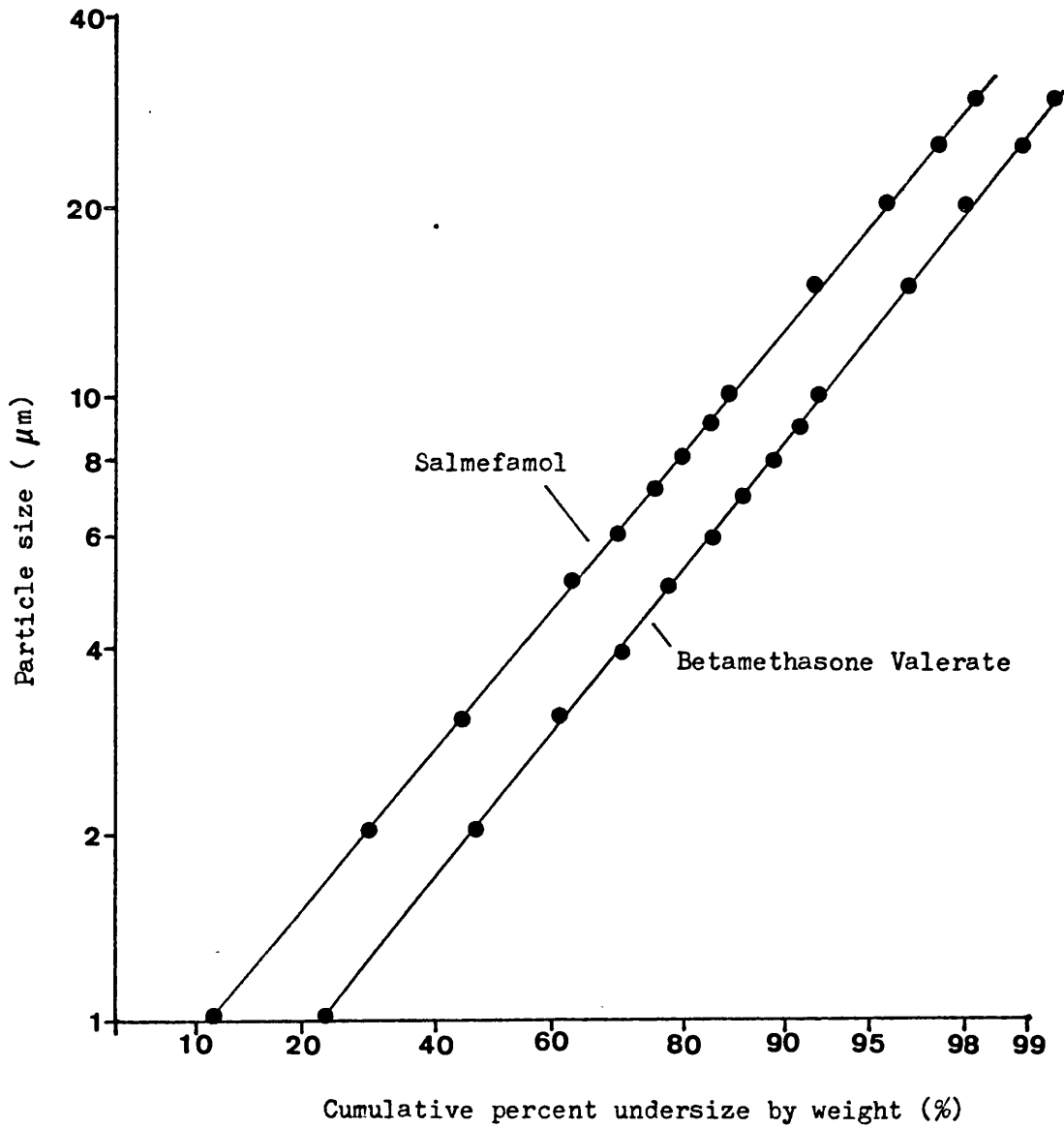


Figure 6.5. Particle Size Distribution of Micronised Salmefamol and Betamethasone Valerate Fitted to a Log-Normal Distribution as Obtained from a Malvern 2200 Particle Sizer

more easily degassed. Unmicronised samples were considered acceptable as there is no evidence that polymorphic changes occur during micronisation. The apparatus was checked using a stainless steel test sphere of known volume (8.55 cm^3). Each powder sample was repeatedly outgassed until reproducible results were obtained. Two separate determinations were carried out on each powder (Table 6.1).

The mean value for betamethasone valerate was taken as $1.31 \times 10^3 \text{ kg m}^{-3}$ approximately 3% larger than the $1.27 \times 10^3 \text{ kg m}^{-3}$ obtained by Glaxo Group Research using the same technique. Some of this difference may be accounted for by limitations in the accuracy of the method used; one estimate of the test volume deviated by 1.4% from the certified volume. The mean volume of the test sphere was 8.50 cm^3 , standard deviation = 0.05, coefficient of variation = 0.6%. Since the discrepancy in betamethasone valerate densities is greater than the maximum error noted with the test sphere, experimental error does not fully explain the difference. The variation in values most likely arises from differences in the degree of outgassing of the samples; insufficient outgassing will lead to an underestimate in the density of the powder.

A mean density of $1.28 \times 10^3 \text{ kg m}^{-3}$ was taken for the salmefamol.

6.2.3 ELECTROSTATIC CHARGES ASSOCIATED WITH MICRONISED DRUG MATERIALS

It was noted that when micronised powders were being weighed out, drug particles would adhere to most surfaces with which they came into contact. This observation was thought to be due to an electrostatic charge on the powder. The charges associated with micronised powders were therefore determined after contact with high density polyethylene.

Sample	Determination Number	Test Value (cm ³)	Powder Weight (g)	Determined Powder Volume (cm ³)	Density (kg m ⁻³ x 10 ⁻³)
Beta-methasone Valerate	1	8.56	11.1706	8.46	1.32
	2	8.51	9.2290	7.06	1.31
Salmefamol	1	8.50	5.9359	4.58	1.30
	2	8.43	5.8412	4.60	1.27

Table 6.1 Densities of Unmicronised Samples of Betamethasone Valerate and Salmefamol as Determined by Helium Pycnometry.

Several grams of the powder to be investigated were placed into a vibrating hopper lined with high density polyethylene, and set to deliver approximately 500 mg min^{-1} into a Faraday Well situated underneath. The Faraday Well, which was connected to an electrometer, was earthed to remove residual electrical charges. Approximately 500 mg was then delivered into the Faraday Well; the exact amount was determined by weighing the Faraday Well before and after delivery. The sign and magnitude of the charge associated with the delivered powder was recorded on the electrometer. Three separate determinations were carried out for each of the two materials studied. The experiment was carried out under normal laboratory conditions of $21 - 22^{\circ}\text{C}$ at a relative humidity of 60%.

The results obtained are summarised in Table 6.2; surface charge densities being calculated using the specific surface areas of the powders (section 6.1.2).

6.3 Physico-chemical properties of the propellant model and other liquids

6.3.1 THE PROPELLANT MODEL

A typical propellant blend of propellants 11 and 12 (boiling points = 23.8°C and -29.8°C respectively (40)) will at 25°C have an absolute vapour pressure of 505kPa (atmospheric pressure is approximately 101kPa) (40, 62). To study dispersions in such mixtures would necessitate the use of pressurised containers or low temperatures. Since this would complicate the development of an electrophoresis technique, a propellant model was used.

The basic requirements of the model were;

1. a boiling point above room temperature,

Material	Sample Number	Weight Delivered (g)	Measured Charge		Charge Density ($C\ m^{-2} \times 10^8$)
			Sign	Magnitude ($C \times 10^8$)	
Beta-methasone Valerate	1	0.610	Negative	3.9	1.3
	2	0.625	Negative	4.1	1.3
	3	0.630	Negative	4.5	1.4
Salmefamol	1	0.497	Positive	0.9	0.7
	2	0.508	Positive	1.0	0.7
	3	0.467	Positive	1.4	1.1

Table 6.2 Surface Charge Densities Observed for Micronised
Betamethasone Valerate and Salmefamol Delivered
from a Hopper Lined with High Density Polyethylene.

2. a relative permittivity similar to conventional propellants (relative permittivities of propellants 11 and 12 at 29°C are 2.28 and 2.13 respectively (63)),
3. that it should not dissolve the suspended particles,
4. a density of similar order as the suspended solid, so as to minimise sedimentation effects during electrophoresis (the density of a typical propellant blend is $1.38 \times 10^3 \text{ kg m}^{-3}$ (40)).

The model used was a mixture of Arcton 113 (trichlorotrifluoroethane, density (30°C) = $1.553 \times 10^3 \text{ kg m}^{-3}$, boiling point = 45.6°C, relative permittivity (30°C) = 2.44 (31)) and n-hexane (density (20°C) = $0.6603 \times 10^3 \text{ kg m}^{-3}$, boiling point = 69°C, relative permittivity (20°C) = 1.89 (180)) mixed in a ratio of 6.9:3.1 by volume. Evaporation of this mixture at 10°C was minimal (section 8.1.2), its density (10°C) was $1.296 \times 10^3 \text{ kg m}^{-3}$ (section 6.3.4) with a relative permittivity (10°C) of 2.251 (section 6.3.8).

6.2.3 PURIFICATION OF AEROSOL OT

Aerosol OT - 100 was further purified using a standard method described by Kunieda and Shinoda (187). Water soluble impurities were removed by shaking 50 ml volumes of approximately 15% w/v solutions of Aerosol OT in benzene with an equal volume of water. Emulsification occurred, so the mixture was left to settle for several hours before the lower water phase was discarded. This extraction was repeated twice more before the benzene solution was evaporated to recover the surfactant.

The Aerosol OT was then dissolved in 25 ml of 25% aqueous-methanol solution and was extracted in a similar manner with petroleum ether

100/120 to remove oil soluble impurities, the upper organic phase being discarded. The solution was then evaporated to recover the Aerosol OT and dried to constant weight over P_2O_5 at $30^\circ C$ under a vacuum of 760 mm Hg.

6.3.3 PURITY OF OLEIC ACID

The 99% pure oleic acid from Larodan Fine Chemicals came supplied with a gas chromatogram showing its purity profile (Figure 6.6). However, it was unclear whether the method used would resolve oleic acid (the cis isomer) from any elaidic acid (the trans isomer) which might be present in the sample. Elaidic acid may be found in significant quantities in commercial grades of oleic acid.

Infra-red spectra were therefore obtained from 1% solutions of the 99% pure oleic acid, elaidic acid (biochemical grade) and Priolene 6952 (commercial grade oleic acid) in carbon disulphide. Examination of the spectra obtained from elaidic acid (Figure 6.7A) revealed a sharp peak at around 970 cm^{-1} . This was interpreted as being due to a trans $CH=CH$ bend in the molecule (188). The same peak, although less intense, was seen in the Priolene 6952 spectra (Figure 6.7B), indicating the presence of elaidic acid in significant quantities. The spectra obtained from 99% pure oleic acid (Figure 6.7C) showed a barely perceptible shoulder at 970 cm^{-1} , indicating the possibility of only small quantities of elaidic acid being present.

6.3.4 DENSITY DETERMINATION OF PROPELLANT MODEL AND ITS SOLUTIONS

Liquid densities were determined using a glass pycnometer. The pycnometer was cleaned in chromic acid, well rinsed in tap water, then distilled water, before finally being dried using a filtered

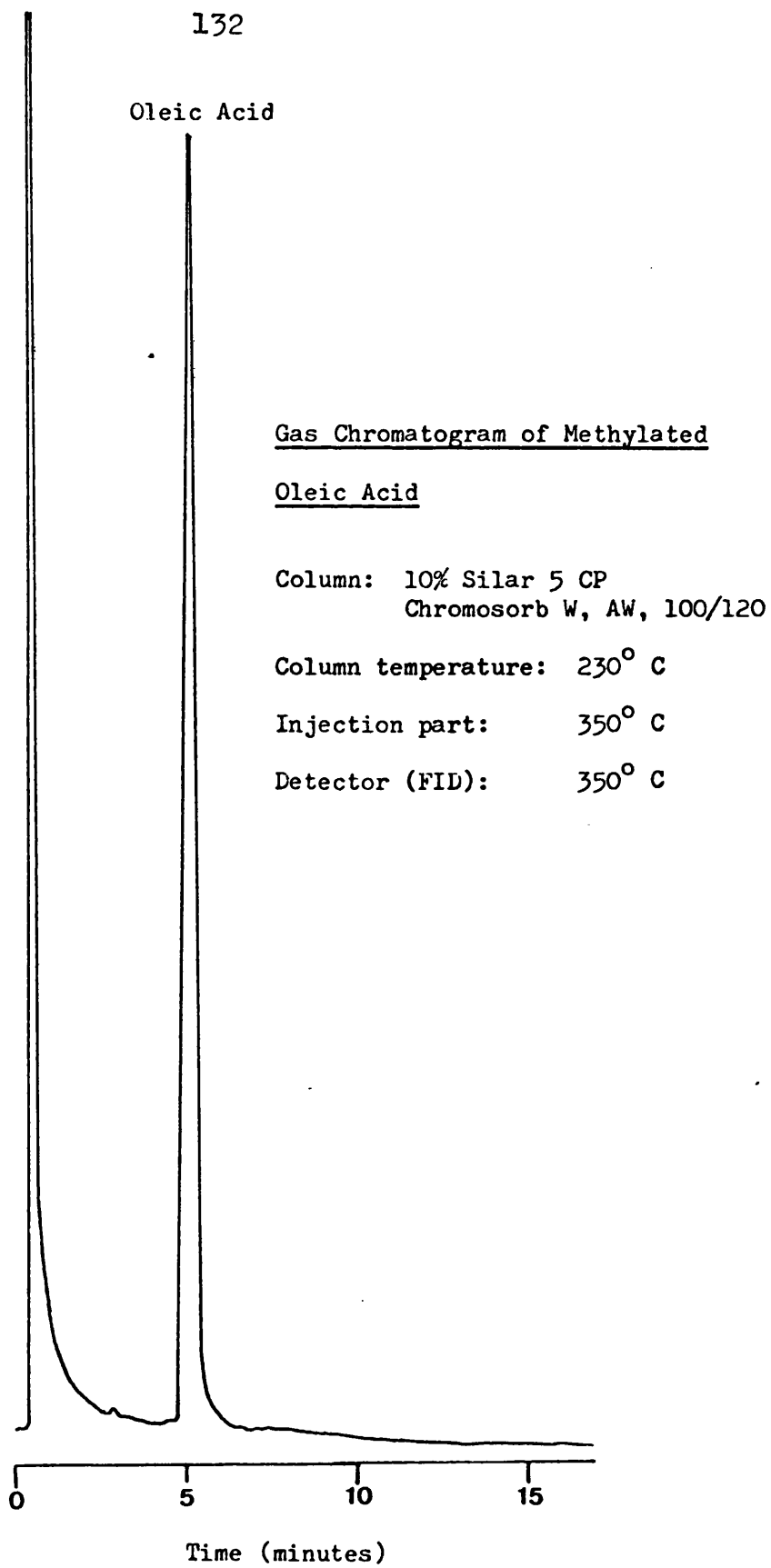


Figure 6.6 Purity Profile of Oleic Acid Batch 3015-2 as
Supplied by Larodan Fine Chemicals

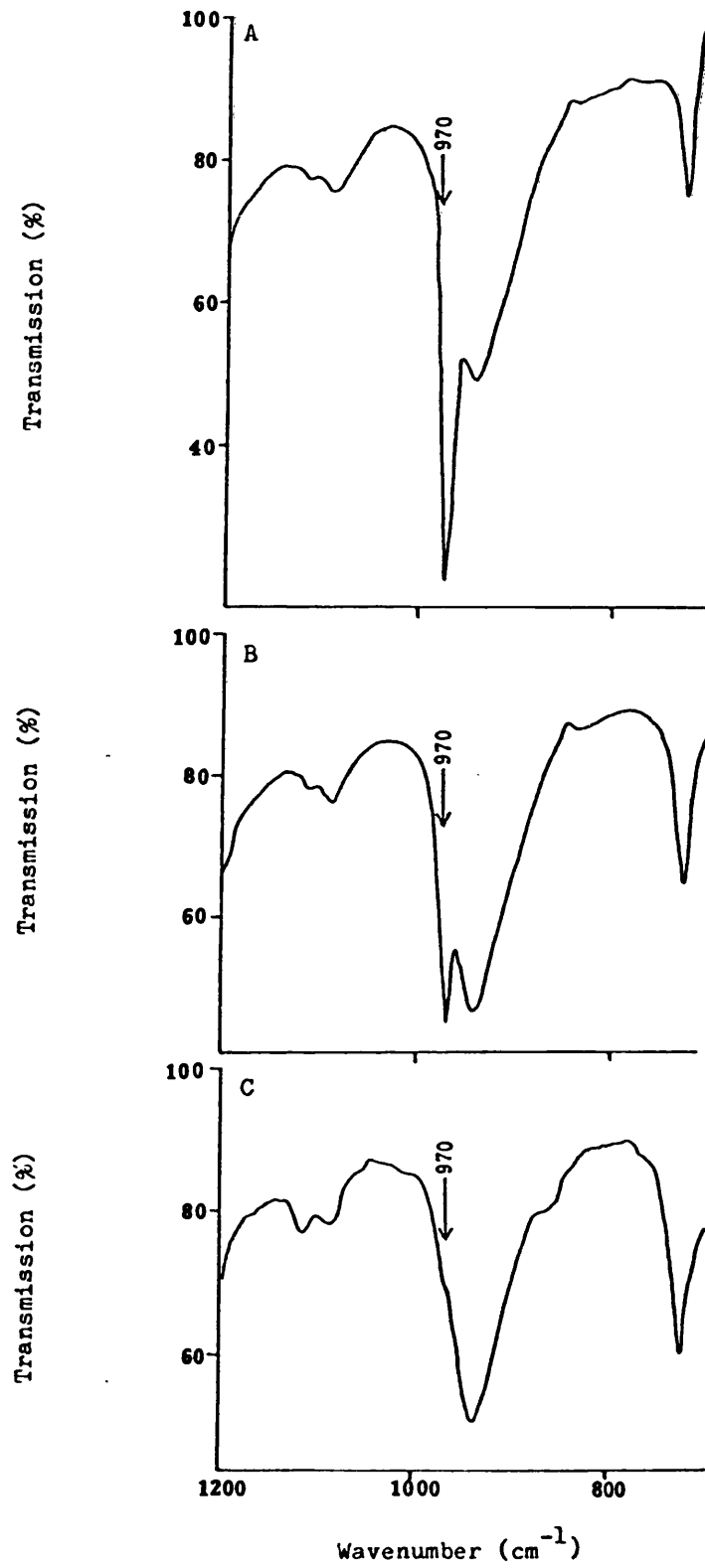


Figure 6.7 Infra-Red Spectra Obtained from
A : Elaidic acid
B : Commercial oleic acid (Priolene 6952)
C : Pure oleic acid used in study
(all 1% solutions in CS_2)

airline. The caps were rinsed in distilled water and similarly dried.

After being weighed, with caps, the pycnometer was filled with distilled water and placed in a thermostatically controlled water bath; only the pycnometer arms protruded above the water. After equilibration for 15 - 20 minutes, the volume of the water was adjusted so as to fill the pycnometer from the tip of one arm to a graduated mark on the other. A further 5 minutes was then allowed for re-equilibration, if the volume was then correct the caps were replaced and the pycnometer removed from the bath. After drying with tissue (great care being taken not to warm the pycnometer with the hands) the pycnometer was reweighed. After being thoroughly cleaned the method was repeated using the 113/n-hexane. The density of the 113/n-hexane was then calculated using equation 6.1 (189),

$$\rho_U = \frac{w_U}{w_{H_2O}} \times \rho_{H_2O} - \frac{0.0012 (w_U - w_{H_2O})}{w_{H_2O}} \quad - 6.1$$

Where ρ_{H_2O} is the density of water w_U and w_{H_2O} the weights of the 113/n-hexane and water respectively. The second part of the equation takes into account the buoyancy of air. Replicate determinations were carried out for each of the temperatures used; values for density of water were taken from Langes Handbook of Chemistry (190).

To check the method the density of n-hexane was determined at 20°C, the results are summarised in Table 6.3. The mean calculated density of 660.7 kg m⁻³ is in close agreement to the literature value of 660.3 kg m⁻³ (180). The density of 113/n-hexane was determined at

Liquid Studied	Temperature (°C)	Sample Number	Weight of Water (g)	Weight of Liquid (g)	Density ($\text{kg m}^{-3} \times 10^{-3}$)	Mean Density ($\text{kg m}^{-3} \times 10^{-3}$)
n-Hexane	20	1	9.8459	6.5141	0.6608	0.6607
		2	9.8471	6.5133	0.6607	
113/n-Hexane	10	1	9.8481	12.7717	1.2961	1.2961
		2	9.8489	12.7731	1.2962	
10 x 10 ⁻³ M Oleic acid in 113/n-Hexane		1	9.8484	12.7719	1.2961	1.2960
		2	9.8479	12.7694	1.2959	
10 x 10 ⁻³ M Aerosol OT in 113/n-Hexane		1	9.8487	12.7730	1.2962	1.2961
		2	9.8481	12.7714	1.2961	

Table 6.3 Density of Liquids as Determined Using a Glass Pycnometer.

10°C and was found to be $1.296 \times 10^3 \text{ kg m}^{-3}$ (Table 6.3). The densities of $10 \times 10^{-3} \text{ M}$ solutions of oleic acid and Aerosol OT were also determined at 10°C and were found not to differ significantly from that of the 113/n-hexane alone (Table 6.3).

6.3.5 DETERMINATION OF LIQUID VISCOSITIES

Viscosities of liquids were determined using a suspended level viscometer, size 1, according to the method given in the British Standard (BS) 188: 1977.

Dynamic viscosities were calculated from the flow times using equation 6.2;

$$\eta = c.t.\rho \quad - 6.2$$

where η is the dynamic viscosity ($\text{kg m}^{-1} \text{ s}^{-1} \times 10^3$), t the mean flow time (s), c the calibration factor of the viscometer used and ρ the density of the liquid ($\text{kg m}^{-3} \times 10^{-3}$). This equation can be used since the flow times recorded, typically 500 - 600 seconds, were of sufficient duration such that a kinetic energy factor was not necessary (191).

Temperature control was $\pm 0.03^\circ\text{C}$ at 10°C and $\pm 0.01^\circ\text{C}$ at 20°C, these being the limits set by BS 188.

The viscometer was cleaned using chromic acid, followed by rinsing thoroughly with copious quantities of tap and then distilled water. Finally the viscometer was rinsed with 113/n-hexane and dried using a filtered airline.

The supplied calibration of 0.0008079 was checked using double distilled water at 20°C and 10°C. Freshly filled viscometers were allowed to equilibrate for 20 minutes prior to use. BS 188: 1977

states that the variation in this factor with temperature is considered negligible. The results are shown in Table 6.4, reproducibility of three consecutive flow times was within the BS 188: 1957 requirement of 0.25%. The calculated experimental values for water are in good agreement with those quoted in the literature.

The dynamic viscosity of 113/n-hexane and a series of surfactant solutions in 113/n-hexane was determined at 10°C. Flow times were measured after equilibration in the viscometer for 20 minutes. A density value of $1.296 \times 10^3 \text{ kg m}^{-3}$ was used to calculate all dynamic viscosities; it was found experimentally that the low surfactant concentrations studied, did not significantly alter this density value (section 6.3.4). Results are summarised in Table 6.5; both oleic acid and Aerosol OT were found to increase the dynamic viscosity of 113/n-hexane.

6.3.6 THE CONTROL AND ASSAY OF MOISTURE

For reliable analysis of small quantities of water, the Karl Fischer titration is the method most widely used. It is based on the chemical reaction outlined in equation 6.3.



The assay is normally performed with all reagents except iodine in excess; iodine being used as the titrant, with a colorimetrically determined endpoint. Automation of the method using the Mitsubishi moisture meter is possible by starting with a reagent mixture in which iodine is present, but predominantly as the iodide ion. Electrolysis results in the production of iodine, which reacts with any water present; current flow is therefore proportional to the amount of

Temperature (°C)		10	20
Flow Times (s)	Determination 1	1622.41	1240.96
	Determination 2	1619.94	1241.47
	Determination 3	1619.87	1241.26
	Mean	1620.74	1241.23
	SD	1.45	0.25
	CV	0.09	0.02
Dynamic Viscosity (kg m ⁻¹ s ⁻¹ x 10 ³)	Calculated	1.309	1.001
	Literature (Reference 180)	1.307	1.002

(SD = Standard Deviation, CV = Coefficient of Variation (%))

Table 6.4 Determined Flow Times and Calculated Viscosities
For Water at 10°C and 20°C.

(Density of water from reference 190, calibration factor = 0.0008079)

Surfactant		Dynamic Viscosity ($\text{kg m}^{-1}\text{s}^{-1} \times 10^3$)
	Concentration ($\text{M} \times 10^3$)	
None	-	0.597
Aerosol OT	0.05	0.597
	0.5	0.597
	1.0	0.598
	2.0	0.598
	3.0	0.599
	4.0	0.599
	6.0	0.601
	8.0	0.604
Oleic Acid	10.0	0.609
	1.0	0.597
	2.0	0.599
	4.0	0.602
	6.0	0.607
	8.0	0.610
	10.0	0.619

Table 6.5 Determined Dynamic Viscosities of Solutions
of Aerosol OT and Oleic Acid in 113/n-Hexane
at 10°C.

iodine formed. Thus determination of current flow allows calculation of the amount of water associated with the reaction.

Samples for assay, usually in sealed 10 ml glass ampoules, were filled into oven dried glass syringes inside a dry nitrogen filled Atmosbag. The syringe, with dried needle attached, was then wrapped in Nescofilm, removed from the Atmosbag and weighed. A portion of the sample was injected into the moisture meter and the syringe reweighed; the weight delivered varied to ensure at least 10 μg of water was present in the sample. Great care was taken to ensure that all Nescofilm wrapping was accounted for in both weighings. The quantity of water present in the sample was displayed on the moisture meter, and was used to calculate the water content in parts per million by weight (ppm) from the injected sample weight.

Since the amount of water was determined from the number of coulombs used in the electrolysis (1 mg water = 10.71 C), no standardisation of reagents was required (192). A solution of methanol labelled as containing between 3.8 and 4.1 mg of water per ml was supplied by the manufacturer to check for satisfactory operation of the apparatus. 50 μl samples were injected into the apparatus, the syringe having been previously twice flushed with the solution. Typical check results are shown in table 6.6; the coefficient of variation on no occasion exceeded 3%.

The water content of liquid materials used in this study was determined on receipt, additionally a sample of Arcton 113 was taken from a 5l container which had been part used. The determined water contents are summarised in Table 6.7.

Determination Number	μg Water in 50 μl Sample	Solution Water Content (mg ml^{-1})
1	208	4.16
2	198	3.96
3	199	3.98
4	201	4.02

Mean Solution Content = 4.03 mg ml^{-1}

Standard Deviation = 0.09 mg ml^{-1}

Coefficient of Variation = 2.2%

Table 6.6 Typical 'Check Solution' Results Obtained
Using the Mitshubishi Moisture Meter CA-02

Determination	Weight of Sample Assayed (g)					Calculated Moisture Content (ppm)							
	1	2	3	4	5	1	2	3	4	5	Mean	SD	CV
Sample													
Arcton 113 Old Batch	1.5204	1.5606	1.5140	1.4998	1.4833	13.8	12.8	13.8	12.7	12.8	13.2	0.55	4.2
Arcton 113 New Batch	3.0681	3.0041	3.0909	2.9699	2.9235	4.6	4.5	4.3	4.4	4.4	4.4	0.10	2.3
N-Hexane	1.4843	1.6772	1.5955	1.6097	1.5413	27.6	26.2	23.6	25.9	24.9	25.6	1.5	5.8
Priolene 6952	0.0488	0.0479	0.0434	0.0640	0.0614	1352	1356	1382	1406	1319	1363	32.8	2.4
Pure Oleic Acid	0.1206	0.1357	0.1522	0.4290	0.1680	365	368	368	370	368	368	1.8	0.5

(SD = Standard Deviation, CV = Coefficient of Variation (%))

Table 6.7 Typical Water Contents of Materials Used in Study as Determined Using the Mitsubishi Moisture Meter

The water content of the n-hexane and Arcton 113 on receipt and the subsequent pick up of moisture from the atmosphere made it necessary to dry these liquids. This was done by passing one litre batches of the 113/n-hexane mixture through a 1 m column packed with previously dried molecular sieve beads (110°C for at least 48 hours). The flow rate through the column was around 1 ml min⁻¹. All glassware used was oven dried and sealed with Nescofilm on removal. When assembled all joints were sealed with Nescofilm and any pressure equilibration required within the apparatus was through tubes packed with CaCl₂.

Samples of all liquids for moisture determination were taken with a dried glass syringe and sealed into 10 ml dried glass ampoules until it was possible to assay them. To validate the use of ampoules, a sample from a freshly dried batch of 113/n-hexane was assayed directly, this was compared with samples from the bulk solution after 24 hours and samples sealed in ampoules and stored. The results are summarised in Table 6.8. Analysis of variance of the results shows there to be no significant difference ($p < 0.05$) in the moisture contents of the fresh bulk, 24 hour bulk and the 24 hour stored in ampoule samples. Similarly the moisture content of the 113/n-hexane after storage for 15 months was in the same range; only two results are available due to accidental breakage of remaining ampoules.

All dried liquids were stored in sealed Duran bottles until required. Surfactant solutions were made up in a nitrogen flushed dry glove box containing P₂O₅ with large pipettes sealed into a hole in the top. These precautions were necessary since dried 113/n-hexane left in an open beaker, unprotected, rapidly picked up water. At a relative humidity of 8% (20°C) such moisture pick up was not observed.

Sample	Assayed Water Content (ppm)						
	1	2	3	4	Mean	SD	CV
Fresh bulk	10.6	9.6	11.0	10.7	10.5	0.60	5.7
24 hour bulk	10.0	9.2	10.0	12.3	10.4	1.35	13.0
24 hour ampoules	10.7	9.2	10.0	10.2	10.0	0.60	6.0
15 month ampoules	10.2	9.1	NR	NR	range 9.1 - 10.2		

(NR = No Result, SD = Standard Deviation, CV = Coefficient of Variation (%))

Table 6.8 Moisture Content of 113/n-Hexane Determined From Bulk and After Packing in Ampoules.

Source	Sum of Squares	Degrees of Freedom	Mean Squares	F ratio	F 0.05
Between Samples	0.447	2	0.223	0.26	4.26
Within Samples	7.642	9	0.849		
Total	8.089	11			

Analysis of Variance (Table 6.8 excluding 15 month result)

Sample	Assayed Water Content (ppm)						
	1	2	3	4	Mean	SD	CV
Initial	10.4	10.8	10.6	11.4	10.8	0.45	4.2
10 Minutes in Unprotected Beaker	15.9	15.0	16.2	14.4	15.4	0.85	5.5
10 Minutes in Open Beaker (RH = 8%)	11.2	10.8	12.0	11.0	11.3	0.55	5.0

(RH = Relative Humidity, SD = Standard Deviation, CV = Coefficient of Variation (%))

Table 6.9 Moisture Content of 113/n-Hexane After Standing Unprotected From the Atmosphere and at a Relative Humidity of 8% (20°C).

Table 6.9 shows the results after 10 minutes exposure, after correction for concentration due to evaporation. A significant ($t = 9.81$, $p = 0.0001$) increase in assayed moisture is observed for the unprotected beaker, whereas no significant difference ($t = 1.32$, $p = 0.23$) is noted for the 8% relative humidity condition, when the results are compared using the t test.

Hypersil ODS used in the preparation of dry dispersions was dried over P_2O_5 in a vacuum oven at $110^\circ C$, under a vacuum of 760 mm Hg for 72 hours; salmefamol was similarly dried at $25^\circ C$. The dried powders were stored in dry sealed containers over P_2O_5 prior to use. No loss in weight on drying was found for the Hypersil ODS but was between 0.5 and 0.6% w/w for salmefamol.

6.3.7 REFRACTIVE INDICES OF SOLUTIONS USED IN STUDY

Refractive index measurements were carried out using an Abbé refractometer, fitted with a pearl light source. Although a white light source is used, values of refractive index read off the refractometer scale are those of the sodium D line (wavelength 589 nm). The He-Ne laser in the velocimeter apparatus operates at 632.8 nm. Whilst refractive index is dependent upon wavelength, values of the sodium D line were considered acceptable, since liquids of low permittivity are known (193) to show little variation in refractive index with wavelength.

Temperature control was effected by circulating water from a water bath/cooler unit through a metal jacket which surrounds the prisms and is an integral part of the refractometer. Calibration of the apparatus was performed in accordance with the manufacturer's instructions using a glass test piece of refractive index 1.5161 and a small drop of monobromonaphthalene. This calibration was carried out at $20^\circ C$ and is valid

over a wide range of temperatures, since the effect of temperature is negligible (about 0.0001 per 15°C) (194).

To determine the refractive index of a liquid a few drops were placed between the prisms with the refractometer slightly tilted back to stop the liquid flowing away. To ensure this method was suitable for volatile solvents the refractive index of Arcton 113 at 25°C was determined. The mean of 5 determinations was 1.3520 (standard deviation = 2.1×10^{-4} , coefficient of variation = 0.01%); this compares well with the literature value of 1.354 (180). The refractive index of all liquids used in the velocimeter were determined at the appropriate temperature, the results are summarised in Table 6.10. The effect of moisture and surfactant concentration upon the refractive index of 113/n-hexane was very small and the mean value of 1.367 has been used in all calculations.

6.3.8 DETERMINATION OF RELATIVE PERMITTIVITIES

For a given permittivity cell the relative permittivity (ϵ_r) of an unknown liquid can be calculated using equation 6.4.

$$\epsilon_r (\text{unknown}) = \frac{\text{measured capacitance of unknown}}{\text{measured capacitance of reference}} \times \epsilon_r (\text{reference}) - 6.4$$

Cyclohexane was selected as the reference with a relative permittivity of 2.039 at 10°C (180).

Prior to any measurements the Wayne Kerr universal bridge was calibrated and trimmed according to the instrument manual. Samples were maintained at $10 \pm 0.1^\circ\text{C}$ using a coil of PVC tubing around the permittivity cell; water being circulated through this coil. Measurements were made inside a dry glove box (relative humidity < 8%) to

Liquid Studied	Surfactant Present	Concentration (M x 10 ³)	Temperature (°C)	Refractive Index n _D
113/n-Hexane (10 ppm moisture)	None	-	10	1.3663
113/n-Hexane (20 ppm moisture)	None	-		1.3665
113/n-Hexane	Aerosol OT	0.05	10	1.3663
		0.50		1.3665
		1.00		1.3668
		2.00		1.3668
		3.00		1.3669
		4.00		1.3665
		6.00		1.3668
		8.00		1.3672
	10.00	1.3669		
	Oleic Acid	1.00	10	1.3664
		2.00		1.3662
		4.00		1.3671
		6.00		1.3665
		8.00		1.3665
10.00		1.3666		
Toluene	None	-	10	1.5004
Sucrose Buffer (see Chapter 7)	None	-	23.5	1.3475

Table 6.10 Summary of Refractive Index Values Obtained For Liquids Used in Study.

avoid problems of condensation. Water was not circulated around the cell whilst the capacitance was being determined; during this period of approximately 30 seconds, no significant change in temperature was noted. A cleaned glass tube was filled with the liquid to be determined and inserted into the permittivity cell, a rubber band on the tube ensuring reproducibility in its positioning. Measurement of the capacitance was made at 1591.5Hz using the autobalance bridge, after equilibration to 10°C. The measured capacitance was corrected by subtracting the capacitance of the empty glass tube. The method was checked by determining the relative permittivity of n-hexane at 10°C, results are summarised in Table 6.11. The mean value of 1.904 is in good agreement with the literature value of 1.905 (180).

The relative permittivity of 113/n-hexane at two different assayed water contents was determined (Table 6.12). Application of the t-test showed there to be no significant ($t = 0.44$, $p = 0.68$) difference in determined relative permittivities for the two water contents.

The influence of Aerosol OT and oleic acid on relative permittivity was studied, the results are also summarised in Table 6.12.

6.3.9 ESTIMATION OF SOLUTION CONDUCTIVITIES

The determination of specific conductivities of the supernatants of non-aqueous dispersions, allows estimation of the diffuse layer thickness associated with the particles dispersed in that solution (section 2.1). Measurement of the specific conductivity of 113/n-hexane and toluene solutions was not possible with the Wayne Kerr autobalance bridge. A more sensitive apparatus incorporating a General Radio capacitance bridge was therefore used in the Department

	Determination Number		
	1	2	3
Capacitance of n-Hexane (pF)	0.359	0.351	0.359
Capacitance of Cyclohexane (pF)	0.384	0.380	0.381
Calculated Relative Permittivity	1.906	1.883	1.921
Mean Relative Permittivity	1.904		
SD	0.019		
CV	1.0		

(SD = Standard Deviation, CV = Coefficient of Variation (%))

Table 6.11 The Relative Permittivity of n-Hexane at 10°C.

Liquid Studied	Surfactant Concentration (M x 10 ³)	Relative Permittivity					
		Determination Number			Mean	SD	CV
		1	2	3			
113/n-Hexane (10 ppm moisture)	-	2.251	2.254	2.248	2.251	0.003	0.1
113/n-Hexane (20 ppm moisture)	-	2.246	2.248	2.269	2.254	0.013	0.6
113/n-Hexane with Aerosol OT	0.05	2.249	2.256	2.252	2.252	0.004	0.2
	0.50	2.254	2.257	2.256	2.256	0.002	0.1
	1.00	2.261	2.258	2.262	2.260	0.002	0.1
	2.00	2.262	2.265	2.263	2.263	0.002	0.1
	3.00	2.269	2.272	2.269	2.270	0.002	0.1
	4.00	2.285	2.281	2.280	2.282	0.003	0.1
	6.00	2.291	2.296	2.293	2.293	0.002	0.1
	8.00	2.310	2.311	2.305	2.309	0.003	0.1
10.00	2.34	2.326	2.329	2.326	0.003	0.1	
113/n-Hexane with oleic acid	1.00	2.249	2.253	2.255	2.252	0.003	0.1
	2.00	2.258	2.262	2.259	2.260	0.002	0.1
	4.00	2.276	2.278	2.279	2.278	0.002	0.1
	6.00	2.294	2.302	2.301	2.299	0.004	0.2
	8.00	2.305	2.303	2.306	2.305	0.002	0.1
	10.00	2.317	2.315	2.310	2.314	0.004	0.2

(SD = Standard Deviation, CV = Coefficient of Variation (%))

Table 6.12 The Influence of Moisture Content and Surfactant Concentration on the Relative Permittivity of 113/n-Hexane at 10°C.

of Physical Chemistry at the University of Bristol. Using this apparatus attempts were made to measure the conductivity of these solutions at 1.59 kHz.

Since the conductance of the solutions was extremely small, it was necessary to tape and clamp all leads. It was important to ensure no moving objects were in the vicinity of the leads or cell. As a result effective temperature control proved not to be viable, measurements were therefore attempted at room temperature.

Limitations in sensitivity of the null point detector and the level of noise made a precise determination of the specific conductivity of toluene or any of the 113/n-hexane solutions used in this study impracticable. Using a conductivity cell of cell constant 0.00342 cm^{-1} the fluctuations in measured conductivity of the empty cell due to noise was around $0.02 \times 10^{-8} \text{ S}$. When the cell was filled with either toluene or 113/n-hexane solutions, no change in the measured conductivity was noted. It was therefore concluded that all solutions used in this study had a specific conductance of the order of $10^{-10} \text{ S m}^{-1}$ or below.

6.3.10 EVIDENCE FOR THE FORMATION OF OLEIC ACID DIMERS IN 113/N-HEXANE/OLEIC ACID SOLUTIONS

It is known that free fatty acids will dimerise to some extent when in organic solvents, owing to hydrogen bonding between the carboxylic acid groups. Infra-red (IR) spectroscopy can be used to identify the presence of such dimers in solution; vibration of the carboxylic acid group of the molecule when dimerised gives rise to an adsorption band at between 1701 and 1724 cm^{-1} , this compares with 1761 cm^{-1} for the free monomer (188).

A solution of 6×10^{-4} M oleic acid in 113/n-hexane was studied to determine whether dimers were present. The concentration was selected since it was the lowest that could be used and still obtain reasonable IR spectra. The adsorption is however weak and is easily masked by adsorption which arises from the opacity of the 113/n-hexane, due to small differences in pathlength between the sample and reference cell. A variable pathlength cell was therefore used, the adsorption of the cell with 113/n-hexane was balanced, the best baseline obtainable is shown in Figure 6.8. The same figure shows the IR spectra from 1650 cm^{-1} to 1800 cm^{-1} obtained from the oleic acid solution.

Marked adsorption can be seen at around 1715 cm^{-1} and 1765 cm^{-1} , the former is taken to represent the presence of dimers, the latter monomers. It was therefore concluded that oleic acid in 113/n-hexane at concentrations above 6×10^{-4} M was present as both monomers and dimers. The relative intensities of the two adsorption bands might suggest predominance of the dimer form.

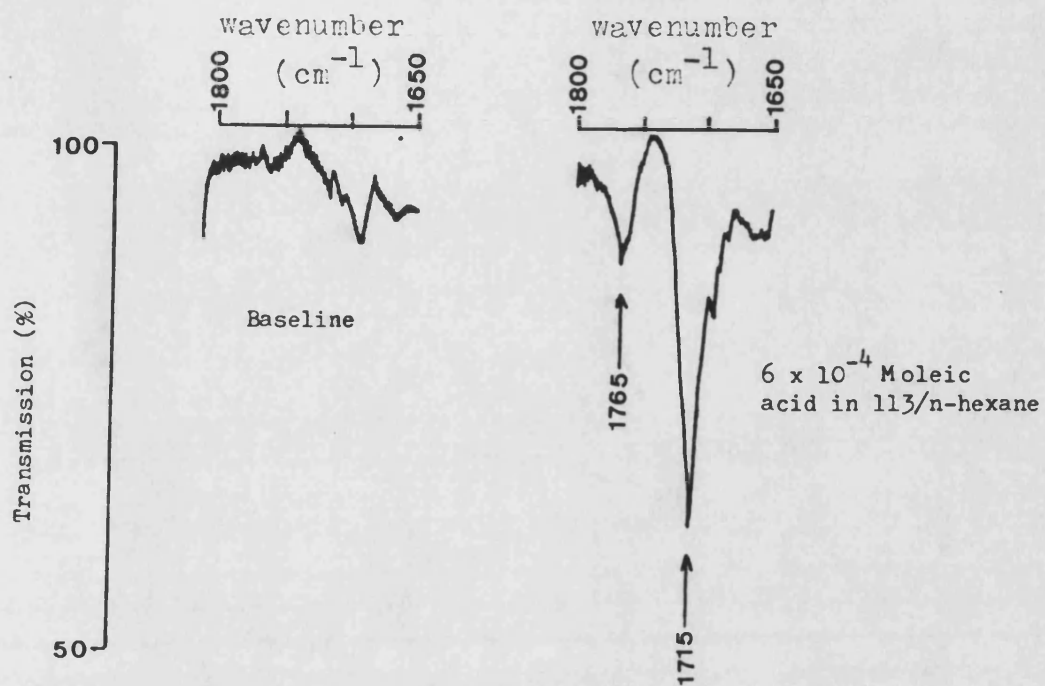


Figure 6.8 Infra-Red Spectra Obtained from a Solution of $6 \times 10^{-4} M$ Oleic Acid in 113/n-hexane

CHAPTER 7VALIDATION OF THE LASER-DOPPLER VELOCIMETER7.1 Introduction

Any apparatus which is to be used for making electrophoretic measurements must first be validated, using a dispersion of known mobility. The results obtained should be in agreement with those available in the literature. Such validation is primarily to ensure that equipment design and experimental technique of the operator is satisfactory.

Novotny (124) points out that no standard non-aqueous dispersions are available, primarily because of the marked effects of trace moisture upon electrophoretic mobility. It was therefore necessary to use an aqueous dispersion to validate the apparatus. Dispersions of healthy human erythrocytes in either phosphate buffer or saline solution give reproducible mobilities, which are independent of race, sex, age or blood group. After the work of Bangham et al (138) the accepted literature value for a dispersion in M/15 phosphate buffer (pH 7.4, 25°C) is $- 1.28 \pm 0.03 \times 10^{-8} \text{ m}^2 \text{ s}^{-1} \text{ V}^{-1}$; other workers report mobilities of $- 1.31$ and $- 1.33 \times 10^{-8} \text{ m}^2 \text{ s}^{-1} \text{ V}^{-1}$ (198, 199). Such dispersions are widely used for validation purposes. Unfortunately these systems are unsuitable for use with the present design of apparatus because of the high current densities which would be experienced.

Platinum black electrodes are unsuitable when used in narrow gap configurations as marked gas evolution is seen with higher ionic strength media. The upper limit of salt concentration for such an

arrangement lies between 0.03 M and 0.05M NaCl (140). To study higher salt concentrations platinised silver chloride or platinised silver electrodes can be used.

The apparatus was therefore validated using dispersions of human erythrocytes in low ionic strength (0.005) media, after the published work of Uzgiris. The reported mobility for human erythrocytes dispersed in a 0.28 M sucrose buffer (pH 7.3, 23.5°C) of ionic strength 0.005 is $-2.84 \times 10^{-8} \text{ m}^2 \text{ s}^{-1} \text{ V}^{-1}$ (200). In a later paper (201) the value for the same system at 25°C is quoted as $-2.90 \pm 0.06 \times 10^{-8} \text{ m}^2 \text{ s}^{-1} \text{ V}^{-1}$. The reproducibility of measurement for any given sample was about $\pm 3\%$ with the absolute accuracy of the mobility determination being estimated to be $\pm 5\%$. Also reported are results obtained in higher ionic strength media, these are in good agreement with those obtained by traditional methods (201).

7.2 Preparation of erythrocyte dispersions

The preparation of the erythrocyte dispersions used was based upon the methods described by Uzgiris (200). The suspending medium consists of an isoosmotic sucrose buffer of ionic strength 0.005, made by diluting Seligman's balanced salt solution with 0.29M sucrose solution.

Seligman's balanced salt solution comprises:

Sodium chloride	7.65 g
Potassium chloride	0.20 g
Sodium acetate	1.50 g
Sodium dihydrogen phosphate (anhydrous)	0.05 g
Potassium dihydrogen phosphate (anhydrous)	0.10 g

Sodium hydrogen carbonate	0.70 g
Glucose	1.00 g
Double distilled water to	1000 ml.

The pH of the solution was adjusted to pH 7.3 at 23.5°C using 0.1M HCl or NaOH as required. To obtain a 0.28 M sucrose buffer of ionic strength 0.005, 1 part Seligman's solution was diluted with 29 parts of a 0.29M sucrose solution, a final pH adjustment to pH 7.3 being made if required.

Fresh whole blood was collected from the thumb using a surgical lance; the volume typically collected was 1ml. Erythrocyte dispersions were prepared by first dispersing the whole blood in Seligman's solution. The cells were then washed by shaking for 5 minutes, followed by centrifugation at 2,500 rpm for 5 minutes and removal of the supernatant. This procedure was repeated three times with Seligman's solution and then twice with isoosmotic sucrose buffer solution.

Prior to the determination of electrophoretic mobility, erythrocytes were diluted in the isoosmotic sucrose buffer to produce a final concentration of $5 - 6 \times 10^6$ cells ml⁻¹. This concentration falls within that predicted and found in practice to be optimum for a differential heterodyne velocimeter (169). Estimation of cell concentration was done using a haemocytometer. All dispersions were freshly prepared, kept at $23.5 \pm 0.1^\circ\text{C}$, and used within 4 hours.

7.3 Preparation of the electrodes

Prior to use the electrodes were cleaned in chromic acid, rinsed well in water and platinised by electrodeposition. As a consequence the

surface area and capacitance of the electrodes was increased, so reducing the tendency of the electrodes to polarise and produce gas.

To produce 'platinum black' electrodes the clean electrodes were immersed in a 1% ^w/v chloroplatinic acid solution and connected to the negative terminal of an adjustable power supply. A small piece of platinum wire, comprising the anode, was also immersed in the solution. A current of between 50 - 200 mA per cm² of electrode surface was allowed to flow for 3 - 5 minutes, until a uniform black film had been deposited. Too large a current led to a non-uniform film which was prone to shedding. The blacked electrodes were then placed in 0.25M H₂SO₄ and a small current passed through them; sufficient to produce vigorous gas production. The electrodes were then reversed at approximately 2 minute intervals for a total duration of approximately 15 minutes.

After rinsing in double distilled water, the electrodes were then placed in a 10% ^w/v solution of bovine serum albumin and left for several minutes, after which they were again rinsed with distilled water. This procedure was developed by Uzgiris (202) to avoid the time dependent decays in the Doppler spectrum which he had observed. It was proposed that the protein coat eliminated a surface reaction between the electrodes and buffer which produced the instability.

The electrodes, when not in use, were stored in double distilled water. The protein coating was repeated when either instability in the spectra or a change in pH of the dispersion was observed. The electrodes were replatinised when visual inspection revealed the appearance of bright platinum through the black film.

7.4 Electrode voltage supply

Studies in aqueous systems require substantially lower field strengths than non-aqueous systems. Therefore a Farnell FM2 sine/square wave oscillator producing a square wave-form of typically 5 - 8V peak to peak was used.

Ideally for aqueous systems a constant current supply should be used, this avoids any distortion in the wave-form due to electrode polarisation; such equipment was not however available. Uzgiris suggests the inclusion of a 100k resistor in series with the electrodes, to maintain a square wave-form when not using constant current devices (140). However, it was found that such a series resistor produced no improvement in the current wave-form, as viewed with an oscilloscope connected across a second 1k series resistor. The 100k series resistor was therefore not used.

The Frequency calibration of the oscillator was checked using the Nicolet spectral analyser; the maximum deviation from marked frequency was 0.25 Hz. The applied voltages were monitored using a multimeter.

7.5 Experimental technique

Electrophoretic mobilities of the erythrocyte dispersion were determined using the apparatus as previously described (chapter 5). Freshly prepared erythrocyte dispersions were equilibrated at $23.5^{\circ}\text{C} \pm 0.1^{\circ}\text{C}$ for at least 15 minutes prior to use. Samples were placed into a clean, dry cuvette and then located into the thermostatic jacket. The electrode assembly was inserted into the cuvette with the protruding screws locating themselves in the grooved

aluminium block. The laser, which had previously been checked for alignment (chapter 5) was switched on, and the positioning of the whole assembly checked to ensure beam intersection occurred in the centre of both cuvette and electrode gap. Adjustments, if necessary, were made by way of the vertical and horizontal adjustable mounts. The intersection angle in air of the beams for all the validation work was 32.0° . The refractive index of the media was determined to be 1.3475 (section 6.3.7), the intersection angle in the media was therefore 23.6° .

A further $2\frac{1}{2}$ minutes was allowed for re-equilibration of the dispersion in the cuvette, after which field strengths of between 2.2 and 3.5 kV m^{-1} were applied. A further minute was allowed prior to collection of the spectra. Averaged power spectra were collected by the Nicolet 100A on the 0 - 200 Hz range setting, each was an average of 64 consecutive collected spectra; the time required for data acquisition being just over 2 minutes. The resolution on this range setting is 0.5 Hz; all mean frequency shifts are however quoted to 0.1 Hz for the purposes of statistical analysis.

A typical averaged spectrum is shown in Figure 7.1; such spectra showed good stability, remaining invariant for periods of over 10 minutes. The frequency shift is the central frequency of the envelope and was determined by eye using the cursor facility on the analyser.

The dispersion temperature after electrophoresis was found not to have varied by more than the $\pm 0.1^\circ\text{C}$ limit in temperature control. The voltages applied to the electrodes never exceeded 4 V. Uzgiris' data shows that under these conditions the associated temperature

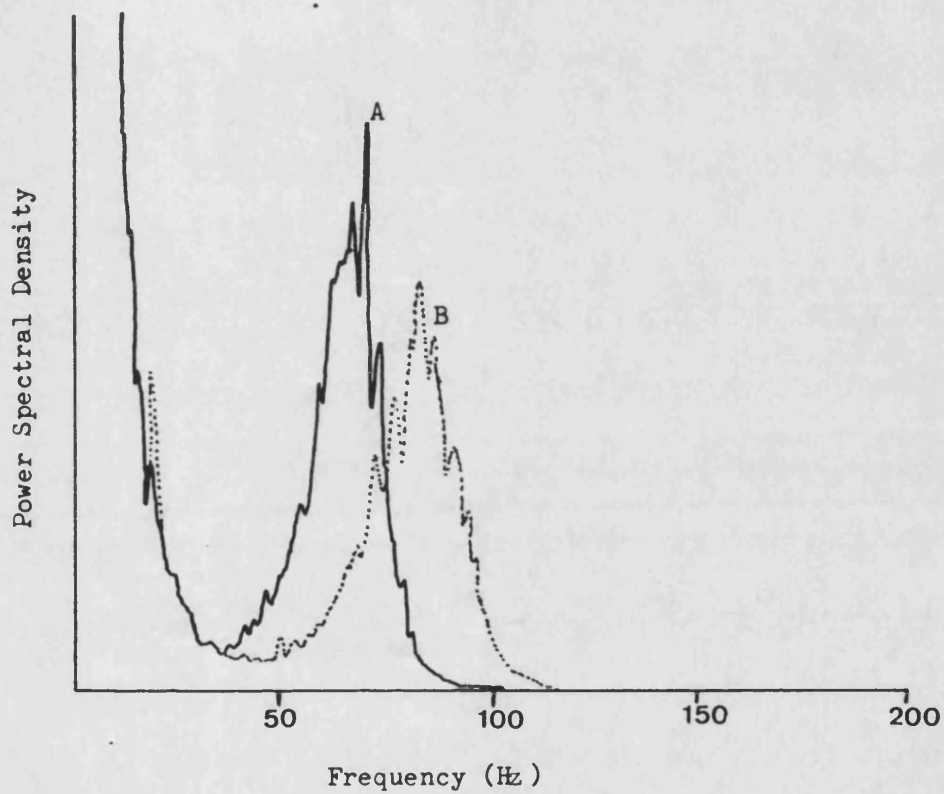


Figure 7.1 Averaged Power Spectrum Collected from Human Erythrocytes in 0.005 Ionic Strength Sucrose Buffer.

(Field reversal rate = 3 Hz, $\theta = 23.6^\circ$,

A = $2.65 \text{ kV} \cdot \text{m}^{-1}$, B = $3.50 \text{ kV} \cdot \text{m}^{-1}$)

rise would be significantly below 1°C (140); the observations made here are in agreement with his findings.

After each experiment the pH of several bulked samples was determined to ensure no change had occurred during electrophoresis.

Where a variation in pH of greater than ± 0.1 was noted the collected spectra were discarded and the electrodes retreated (section 7.3).

7.6 Estimation of operator error in frequency determination

Estimation of frequency shifts by eye is, by definition, a subjective procedure, since it requires the operator to estimate the centre of the frequency envelope. To establish the reproducibility in frequency determination, four consecutive averaged spectra were collected (section 5.7.4) at an applied field of 2.70 kV m^{-1} . As with all the data reported in this chapter, unless otherwise specified, the field reversal rate was 3 Hz and the probe volume was positioned in the centre of the electrode gap $600 \mu\text{m}$ down from the spacer. The averaged spectra were stored in the analyser memory and were presented to the author, by a second person, in such a way that he was not aware of which averaged spectrum was being displayed. Four estimates were made of each averaged spectrum, the order of presentation being random. The results are summarised in Table 7.1.

Analysis of variance shows there to be significant differences between the four averaged spectra, this result was expected because of the exceptional result for the second averaged spectra.

Exclusion of this result still produced a significant ($p > 0.05$) variation in the determined frequency shift between the remaining

Averaged Spectrum Number	Determined Frequency Shift (Hz)						
	Estimation Number				Mean	SD	CV
	1	2	3	4			
1	64.5	65.0	64.0	64.5	64.5	0.40	0.6
2	63.5	63.5	63.5	63.5	63.5	-	-
3	65.5	66.0	65.5	65.5	65.6	0.25	0.4
4	64.5	65.0	66.0	66.0	65.4	0.75	1.1
Mean Frequency Shift (Hz)	64.5	64.9	64.8	64.9	64.8	0.20	0.3
SD (Hz)	0.80	1.05	1.20	1.10	0.95		
CV	1.2	1.6	1.9	1.7	1.5		

(SD - Standard Deviation, CV - Coefficient of Variation (%))

Table 7.1 Variation in Frequency Shift Determined for Four Averaged Spectra Obtained from Human Erythrocytes in 0.005 Ionic Strength Media. ($\theta = 23.6, 2.70 \text{ kV m}^{-1}$, 3 Hz reversal rate).

Source	Sum of Squares	Degrees of Freedom	Mean Square	F ratio	F 0.05
Between Samples	11.125	3	3.708	18.74	3.49
Within Samples	2.375	12	0.198		
Total	13.500	15			

Analysis of Variance

Source	Sum of Squares	Degrees of Freedom	Mean Square	F ratio	F 0.05
Between Samples	2.792	2	1.396	5.29	4.26
Within Samples	2.375	9	0.264		
Total	5.167	11			

Analysis of Variance (excluding averaged spectrum 2)

averaged spectra. This indicates that whilst there was a variation in frequency shift because of the subjective nature of the assessment, the sample studied also produced some variation in the central frequency of the averaged spectra. Frequency estimation produced coefficients of variation of up to 1.1%, corresponding to 95% confidence limits in the mean determined frequency of ± 1.2 Hz. Using equations 3.1 and 4.5 the 95% confidence limits in calculated electrophoretic mobility would be $\pm 0.05 \times 10^{-8} \text{ m}^2 \text{ s}^{-1} \text{ V}^{-1}$. The mean frequency shifts of the four averaged spectra produced a coefficient of variation of 1.5%, which similarly corresponds to 95% confidence limits of ± 1.5 Hz in frequency shift and $\pm 0.06 \times 10^{-8} \text{ m}^2 \text{ s}^{-1} \text{ V}^{-1}$ in calculated electrophoretic mobility.

7.7 Variation in frequency shift with probe volume position

To ascertain that frequency shift was independent of the position of the probe volume within the electrode gap, four averaged spectra were collected from the same sample under the same conditions, but with the probe volume at different positions. The probe volume, whilst positioned in the centre of the electrode gap, was set at varying distances down from the bottom of the Teflon spacer. This was done using the vertically adjustable cell mount, distances being recorded with the fitted micrometer. The order in which vertical positions were studied was random and the experiment was repeated with three further samples.

The results obtained are summarised in Table 7.2. The coefficient of variation obtained from the averaged spectra collected from the four samples at each probe position ranged from 0.4 to 0.6%. Since these values are similar to those recorded for four estimates of a

Distance of Probe Volume from Bottom of Spacer (μm)	Determined Frequency Shift (Hz)						
	Sample Number				Mean	SD	CV
	1	2	3	4			
200	62.0	62.0	62.5	61.5	62.0	0.40	0.6
400	63.0	63.0	63.5	63.5	63.3	0.30	0.5
600	62.5	62.5	62.5	63.0	62.6	0.25	0.4
800	63.5	64.0	63.5	63.5	63.6	0.25	0.4
Mean Frequency Shift (Hz)	62.8	62.9	63.0	62.9	62.9	0.10	0.2
SD (Hz)	0.65	0.85	0.60	0.95	0.70		
CV	1.0	1.4	1.0	1.5	1.1		

(SD - Standard Deviation, CV - Coefficient of Variation (%))

Table 7.2 The Effect of Probe Volume Position on the Frequency Shift Obtained from Human Erythrocytes in 0.005 Ionic Strength Sucrose Buffer
($\theta = 23.6^\circ$, 270 kV m^{-1} , reversal rate = 3Hz)

Source	Sum of Squares	Degrees of Freedom	Mean Square	F ratio	F 0.05
Between Samples	6.125	3	2.0417	21.78	3.49
Within Samples	1.125	12	0.0938		
Total	7.250	15			

Analysis of Variance

single averaged spectra (Table 7.1), it was concluded that there was no appreciable variation between different samples of the same dispersion. Whilst the analysis of variance of the results shows there to be a significant difference in frequency shift with probe volume position. This was not considered to be of importance, since the coefficients of variation of the mean frequency shifts for the differing probe positions was 1.1%; less than that noted in Table 7.1 for consecutive mean averaged spectra collected from a single sample.

7.8 Variation in frequency shift with field reversal rate

The observed frequency shift should be independent of the applied field reversal rate. To check this, averaged spectra were collected from a single sample using an applied field of 2.70 kV m^{-1} at various reversal rates. This experiment was repeated with a further three samples, the results are summarised in Table 7.3.

Analysis of variance shows there to be no significant ($p < 0.05$) difference in frequency shift with reversal rates between 1 Hz and 5 Hz. The coefficient of variation noted for the four samples studied were similar to those noted in Table 7.2.

7.9 Determination of electrophoretic mobility

From the grand mean frequency shifts in Tables 7.1 - 7.3 it was possible, using equations 3.1 and 4.5, to obtain an estimate of the variation in electrophoretic mobility from dispersion to dispersion. The calculated electrophoretic mobilities from Tables 7.1, 7.2 and 7.3 are 2.76 , 2.67 and $2.70 \times 10^{-8} \text{ m}^2 \text{ s}^{-1} \text{ V}^{-1}$ respectively, the mean value being $2.71 \times 10^{-8} \text{ m}^2 \text{ s}^{-1} \text{ V}^{-1}$ (standard deviation = 0.05,

Field Reversal Rate (Hz)	Determined Frequency Shift (Hz)						
	Sample Number				Mean	SD	CV
	1	2	3	4			
1	63.0	63.0	64.0	63.5	63.4	0.50	0.8
3	64.0	63.5	63.5	64.0	63.8	0.30	0.5
5	63.0	63.0	63.5	63.5	63.3	0.30	0.5
Mean Frequency Shift (Hz)	63.3	63.2	63.7	63.7	63.5	0.30	0.5
SD (Hz)	0.60	0.30	0.30	0.30	0.25		
CV	0.9	0.5	0.5	0.5	0.4		

(SD - Standard Deviation, CV - Coefficient of Variation (%))

Table 7.3 The Effect of Field Reversal Rate on the Frequency Shift Obtained from Human Erythrocytes in 0.005 Ionic Strength Sucrose Buffer ($\theta = 23.6^\circ$, 2.70 kV m^{-1}).

Source	Sum of Squares	Degrees of Freedom	Mean Square	F ratio	F 0.05
Between Samples	0.542	2	0.271	2.05	4.26
Within Samples	1.187	9	0.132		
Total	1.729	11			

Analysis of Variance

coefficient of variation = 1.8%). The 95% confidence limits for this mean are $\pm 4.1\%$, slightly larger than the $\pm 3\%$ reproducibility reported elsewhere for this dispersion (20f). This value was obtained at just one field strength (2.70 kV m^{-1}), to ensure true electrophoresis it was necessary to show electrophoretic mobility to be independent of applied field.

Four dispersions were therefore prepared, and for each, averaged spectra were collected at four different field strengths (field reversal rate = 3 Hz, probe volume position = $600 \mu\text{m}$). Increasing the applied field resulted in an increase in frequency shift as shown in Figure 7.1, where increasing the applied field from 2.65 kV m^{-1} (averaged spectra A) to 3.50 kV m^{-1} resulted in averaged spectra B. Electrophoretic mobilities were calculated from the mean frequency shifts obtained at each field strength, using equations 3.1 and 4.5 (a 1 Hz frequency shift corresponds to a particle velocity of $1.148 \times 10^{-6} \text{ ms}^{-1}$). The results are summarised in Table 7.4; the erythrocytes were deduced from visual observations to be negatively charged. The mean calculated electrophoretic mobility was $-2.77 \times 10^{-8} \text{ m}^2 \text{ s}^{-1} \text{ V}^{-1}$ with a coefficient of variation of 2.2%.

Equations 3.1 and 4.5 predict a linear relationship between frequency shift and applied field, which passes through the origin. Linear regression analysis of mean frequency shift against applied field shows a linear relationship (Figure 7.2), with the intercept passing through the origin within ± 2 standard deviations (Table 7.5). The analysis was also performed with the addition of the mean 2.70 kV m^{-1} value derived from Tables 7.1 - 7.3 (63.7 Hz); both regression lines were similar. It was concluded that true

Applied Field (kV m ⁻¹)	2.20	2.65	3.05	3.50	Mean	SD	CV
Mean Frequency Shift from 4 Dispersions (Hz)	54.1	65.0	71.6	83.5			
SD (Hz)	1.20	0.80	0.50	0.50			
CV	2.2	1.2	0.7	0.6			
Calculated Electrophoretic Mobility (-m ² s ⁻¹ v ⁻¹ x 10 ⁸)	2.82	2.82	2.69	2.74	2.77	0.06	2.2

(SD - Standard Deviation, CV - Coefficient of Variation (%))

Table 7.4 Summary of Frequency Shifts and Corresponding
Electrophoretic Mobilities Obtained from Human
Erythrocytes in 0.005 Ionic Strength Sucrose Buffer,
($\theta = 23.6^\circ$, reversal rate = 3 Hz)

	Data in Table 7.4	Data in Table 7.4 Plus Mean 2.70 kV m ⁻¹ Value from Tables 7.1 - 7.3
Slope (x 10 ³)	22.1	22.3
SD (x 10 ³)	1.3	1.3
RSD (%)	5.9	5.8
Intercept	5.60	4.75
SD	3.67	3.73
Correlation Coefficient	0.997	0.995
Probability of Linearity (%)	>99	>99.9
Electrophoretic Mobility from Slope (m ² s ⁻¹ v ⁻¹ x 10 ⁸)	2.54 Mean = 2.55	2.56

Table 7.5 Linear Regression Analysis Results Obtained for the
Relationship Between Frequency Shift and Applied
Field, Obtained from Human Erythrocytes in 0.005
Ionic Strength Media
($\theta = 23.6^\circ$, reversal rate = 3 Hz)

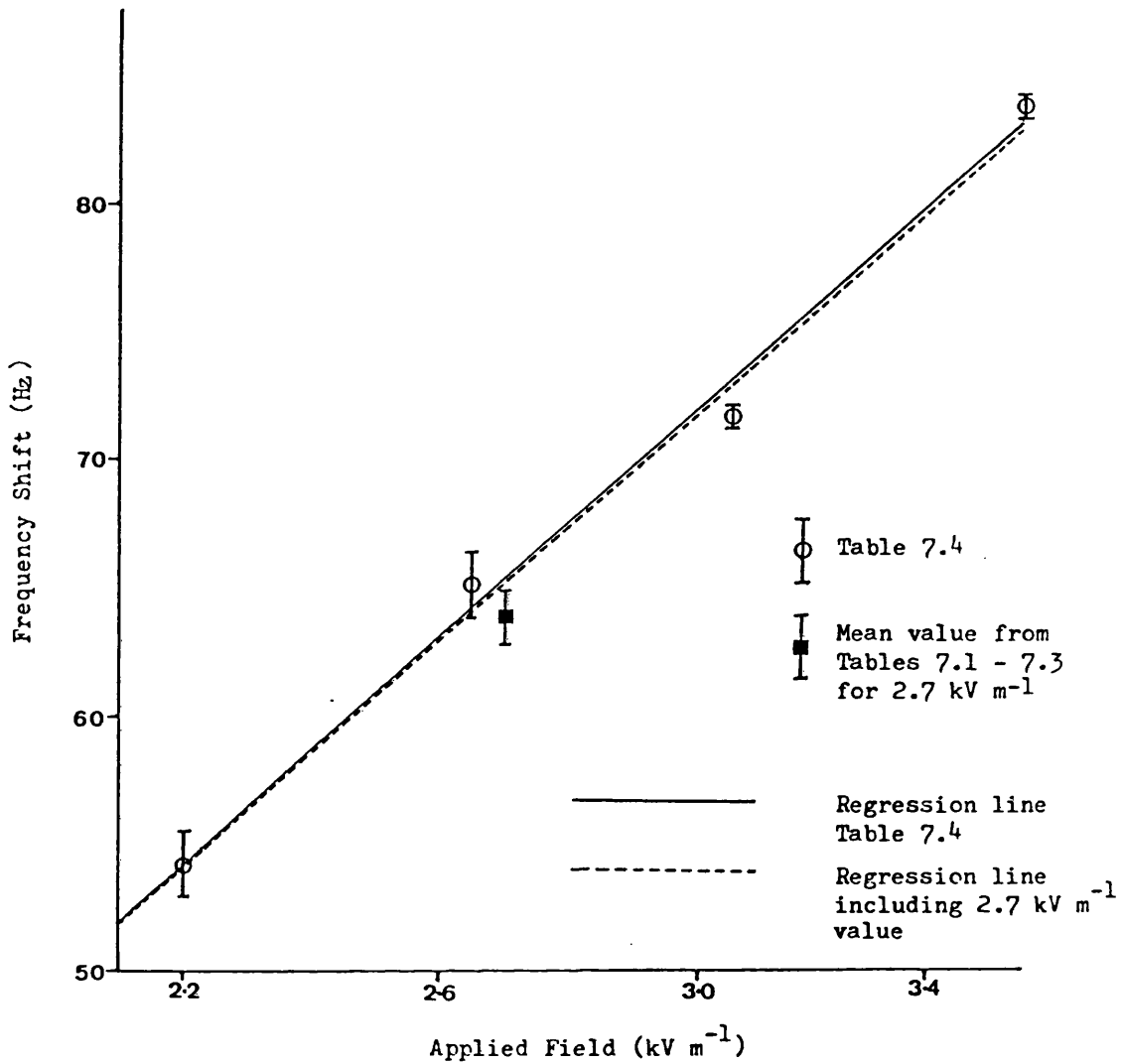


Figure 7.2 Relationship Between Frequency Shift and Applied Field Obtained from Human Erythrocytes Dispersed in 0.005 Ionic Strength Media
 ($\theta = 23.6^\circ$, reversal rate = 3 Hz)

electrophoresis had been observed. An estimate of electrophoretic mobility can be obtained by multiplying the slope of the regression line by the fringe spacing described in the fringe model (equation 4.8). The estimates of electrophoretic mobility from the slope were -2.54 and $-2.56 \times 10^{-8} \text{ m}^2 \text{ s}^{-1} \text{ V}^{-1}$, with coefficients of variation of 5.9 and 5.8% respectively.

The literature value for the system studied was $2.84 \times 10^{-8} \text{ m}^2 \text{ s}^{-1} \text{ V}^{-1}$, a later estimate of absolute accuracy being $\pm 5\%$ ($\pm 0.14 \times 10^{-8} \text{ m}^2 \text{ s}^{-1} \text{ V}^{-1}$). The obtained mean of $2.77 \times 10^{-8} \text{ m}^2 \text{ s}^{-1} \text{ V}^{-1}$ (Table 7.4) was in good agreement with that reported. The mean estimate of electrophoretic mobility derived from linear regression analysis ($2.55 \times 10^{-8} \text{ m}^2 \text{ s}^{-1} \text{ V}^{-1}$) is lower than that obtained in Table 7.4; 95% confidence limits are $\pm 0.19 \times 10^{-8} \text{ m}^2 \text{ s}^{-1} \text{ V}^{-1}$ which produces an upper estimate of electrophoretic mobility of $2.74 \times 10^{-8} \text{ m}^2 \text{ s}^{-1} \text{ V}^{-1}$. This value lies within the $\pm 5\%$ absolute accuracy range of the literature value. Linear regression analysis is not reported as having been used by Uzgiris (140, 149, 154, 161, 175, 200, 201) to calculate electrophoretic mobilities. The coefficients of variation obtained are greater than by the direct calculation method (Table 7.4) which is the traditional method of calculating electrophoretic mobilities.

CHAPTER 8ELECTROPHORESIS IN NON-AQUEOUS SYSTEMS; THE ROLE OF PARTICLE
SIZE8.1 Development of experimental method

8.1.1 VISUAL OBSERVATIONS.

Visual observations were made on dispersions of salmefamol and betamethasone valerate in 113/n-hexane, using extension tubes fitted to the RF313 assembly.

The effect of applying a DC field was investigated; two principle types of behaviour were noted at around 50 kV m^{-1} .

1. Vortices were seen to develop between the electrodes, resulting in particle motion in all directions regardless of the applied field (Figure 8.1). This effect required a finite time to occur.
2. Some particles were seen to touch electrodes and having acquired charge, reverse direction. As a result, particles would oscillate between electrodes touching each in turn.

Reversal of the field using the relay unit was intended to avoid these phenomena in two ways.

- A. Convective turbulence requires a finite time to develop, often being at least that required for conducting ions to cross the electrode gap. Values for the electrophoretic mobility of such ions typically range from $0.4 - 20 \times 10^{-8} \text{ m}^2 \text{ s}^{-1} \text{ V}^{-1}$ (74, 133), representing times of between 0.1 and 5 seconds to cross a 1 mm electrode

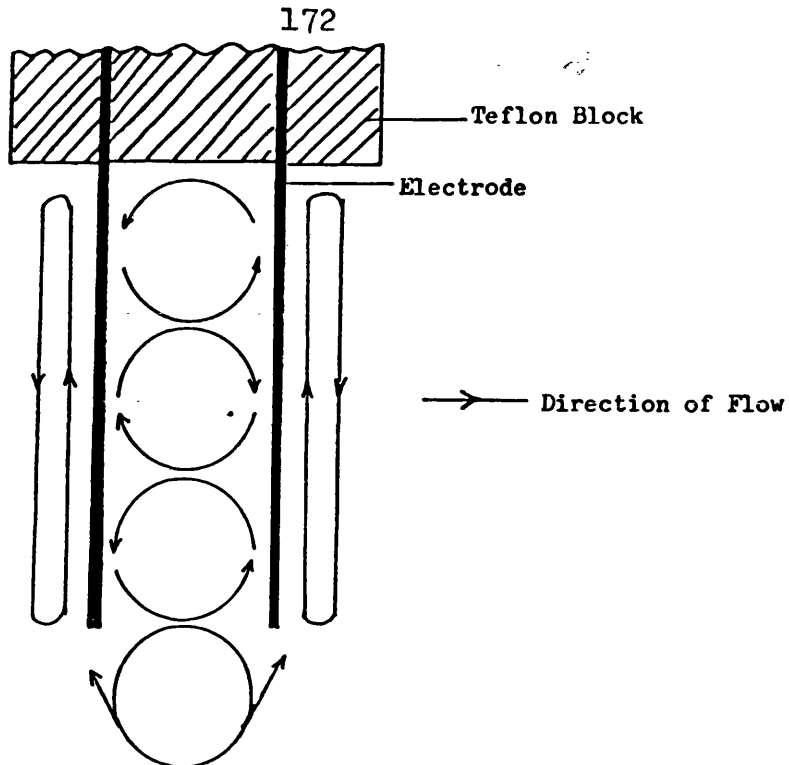


Figure 8.1 Direction of Motion of Salmefamol and Betamethasone Valerate Dispersed in 113/n-Hexane when Subjected to an Applied Field Across the Electrode Gap (deduced from visual observations)

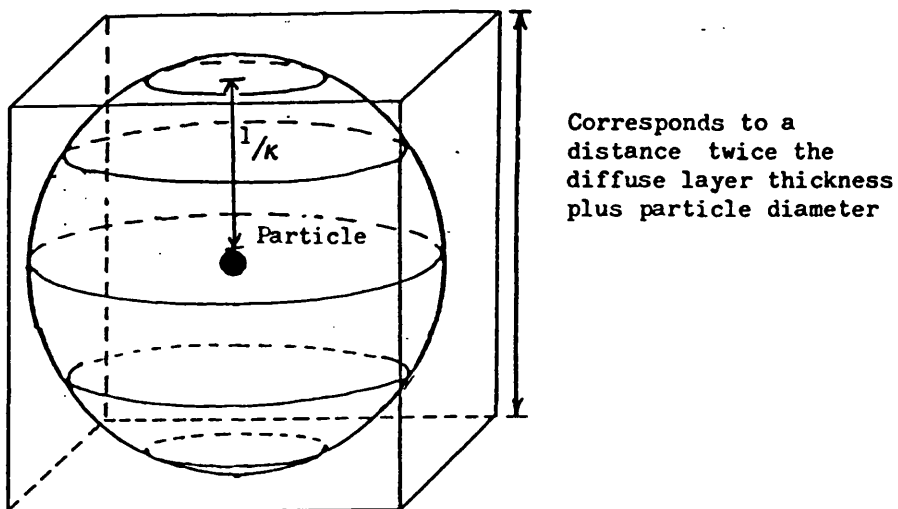


Figure 8.2 Approximating the Particle and its Diffuse Layer to a Cube

gap (applied field = 50 kV m^{-1}). Attempts were therefore made to avoid this effect by reversing the applied field at rates between 1 and 5 Hz.

- B. If the field was reversed at a sufficiently high rate, particles with acquired charge would oscillate close to either electrode surface. Their destructive influence upon the frequency spectrum was then avoided by viewing only the central portion of the electrode gap. This was done with the aid of the reflex viewer and pinhole arrangement of the RF313.

To confirm that these phenomena had been circumvented, it was decided to initially study dispersions of monosize spheres. Their uniformity in shape and size would suggest they all might have similar surface charges and so a reasonably homogeneous electrophoretic mobility, $f(\kappa a)$ (equation 3.7) would therefore not be expected to vary greatly.

8.1.2 EXPERIMENTAL PROCEDURES USED

For optimum operation of a differential heterodyne design of velocimeter the dispersion being studied should contain between 1 and 10×10^6 particles ml^{-1} (169). If the volume occupied by a particle and its diffuse layer, is approximated to a cube of sides equal to the particle diameter plus twice the diffuse layer thickness (Figure 8.2), a dispersion containing 5×10^6 cubes ml^{-1} could have sides of greater than $58 \mu\text{m}$ without overlapping its neighbour. This would suggest that a monodisperse dispersion of $5 \mu\text{m}$ diameter particles could have a diffuse layer thickness of over $25 \mu\text{m}$ before overlapping of adjacent diffuse layers would be expected. The majority

of non-polar dispersions containing surfactant and trace moisture have diffuse layers less than 25 μm (75). 5×10^6 particles ml^{-1} was therefore used as the standard dispersion concentration for all studies.

Attempts to estimate dispersion concentration using a haemocytometer in the manner described by Lewis and Parfitt (103) were unsuccessful, due to the combined effects of evaporation and the slow sedimentation rates of the dispersed particles. An alternative method was used, whereby a known volume of dispersion (typically 45 μl) was measured into a slide well of known dimensions (154 mm^2) using an automatic pipette and allowed, through evaporation to rapidly dry (typically 20 seconds). Using a microscope the number of particles in 5 fields of view was determined, knowledge of the dimensions of the field of view enabled calculation of the dispersion concentration. If the number of particles in one field, typically at least 150, varied from the mean by more than 10% the slide was rejected. The microscopic examination also allowed visual confirmation that dispersions were well dispersed. All dispersions studied contained between 4.5 and 5.5 $\times 10^6$ particles ml^{-1} .

Dispersions of appropriate concentration were made by serial dilution of a 'mother' dispersion. Polymer coated spheres were received as such dispersions in toluene and serially diluted; a typical dilution ratio was 1:800. Materials received as solids e.g. Hypersil ODS, after drying (see section 6.3.6), were dispersed into 113/n-hexane using an ultrasonic field (for a minimum of 30 minutes or until a uniform dispersion had been formed). These dispersions were left for 72 hours to equilibrate, prior to being serially diluted to the

appropriate concentration. In the case of dispersions containing surfactants the 'mother' dispersion was divided equally and half was centrifuged at 2,500 rpm for about 15 minutes. The supernatant was used to serially dilute the remaining dispersion to the appropriate concentration. Dilution with supernatant ensured that any depletion in surfactant concentration, due to adsorption, was taken into account. Dilution effects on the surfactant/particle equilibrium would also be minimised. All such serially diluted dispersions were left to equilibrate for 24 hours prior to being studied.

Where it was important that the moisture content remained constant, dispersions were prepared and diluted under conditions of low relative humidity ($RH < 8\%$) using a glove box containing P_2O_5 . All glassware was oven dried at approximately $120^\circ C$ and allowed to cool inside either a desiccator or glove box containing P_2O_5 . When sufficiently cooled all glassware was sealed with Nescofilm. Dispersions were redispersed ultrasonically for 10 minutes prior to being studied.

To reduce effects due to evaporation, all electrophoretic studies were carried out at $10^\circ C \pm 0.2^\circ C$; no reduction in the weight of a cuvette containing 113/n-hexane solution with the electrode assembly in place was noted for periods in excess of 10 minutes. After placing the dispersion in the cuvette and locating it in the thermostatic jacket, 3 - 4 minutes was allowed for temperature equilibration. Dispersion temperature was monitored using a probe thermometer. The cuvette was positioned so that the beam intersection occurred in the centre of the cell, when viewed from above. The electrode assembly

was inserted and positioned so that the beam intersection was between the electrode gap.

After application of the field a further delay of approximately one minute was allowed before acquisition of signal data; at this point realignment of the photomultiplier was occasionally needed. Field reversal rate was set on the relay unit using an oscilloscope to monitor its output. A digital multimeter was used to check the applied voltage.

Wherever possible the particle charge sign was determined visually, using the RF313 and attached extension tubes. The power supply was manually pulsed and the direction of travel of the particle observed. A knowledge of the polarity of the electrodes enabled deduction of the particle charge sign.

Mean frequency shifts were obtained from averaged (64) spectra collected from several dispersion samples, an averaged spectra being collected for each single sample. Measurement of the dispersion temperature after application of the field showed no variation in temperature outside the control range.

When studying the influence of applied field and reversal rate, the order in which applied fields and reversal rates were studied was randomised. All electrophoretic mobilities were calculated using equations 3.1 and 4.5 from frequency shifts greater than 50 Hz when possible.

8.2 Investigations using dispersions of Polymer B coated silica spheres

8.2.1 VERIFICATION OF ELECTROPHORESIS

Initial studies into whether non-aqueous electrophoresis could be

demonstrated were undertaken using 700 nm B Polymer coated silica dispersions in toluene. The beam intersection angle was 19.0° in toluene (28.7° in air); a 1 Hz frequency shift therefore corresponded to a velocity of $1.277 \times 10^{-6} \text{ ms}^{-1}$.

Application of fields between 35 and 105 kV m^{-1} produced averaged spectra typical of those in Figure 8.3; increasing applied field resulted in an increased frequency shift with a tendency to produce a more flattened frequency envelope.

To ensure that frequency shift was time independent, averaged spectra were collected from a single sample over a time period of 15 minutes. Two additional samples from the same dispersion were also studied; results are summarised in Table 8.1. Analysis of variance shows there to be no significant variation in frequency with time ($p < 0.05$). Inter-sample coefficients of variation of up to 2% were larger than those seen with erythrocyte dispersions (Tables 7.2 and 7.3). This increase in frequency variation was attributed to increased uncertainty in frequency shift determination, as the non-aqueous dispersion produced a less well defined averaged spectra (Figure 8.4).

Reproducibility in frequency determination was assessed in a similar manner to that described in section 7.6. In view of the noted spectral flattening at higher frequencies, five averaged spectra with frequency shifts between approximately 35 and 110 Hz were studied. Coefficients of variation ranged from 0.4 to 1.9% (Table 8.2); larger values being seen at the lower frequency shifts.

Any flattening of the averaged spectra did not produce a decrease in the reproducibility of frequency estimation, as it was offset by a

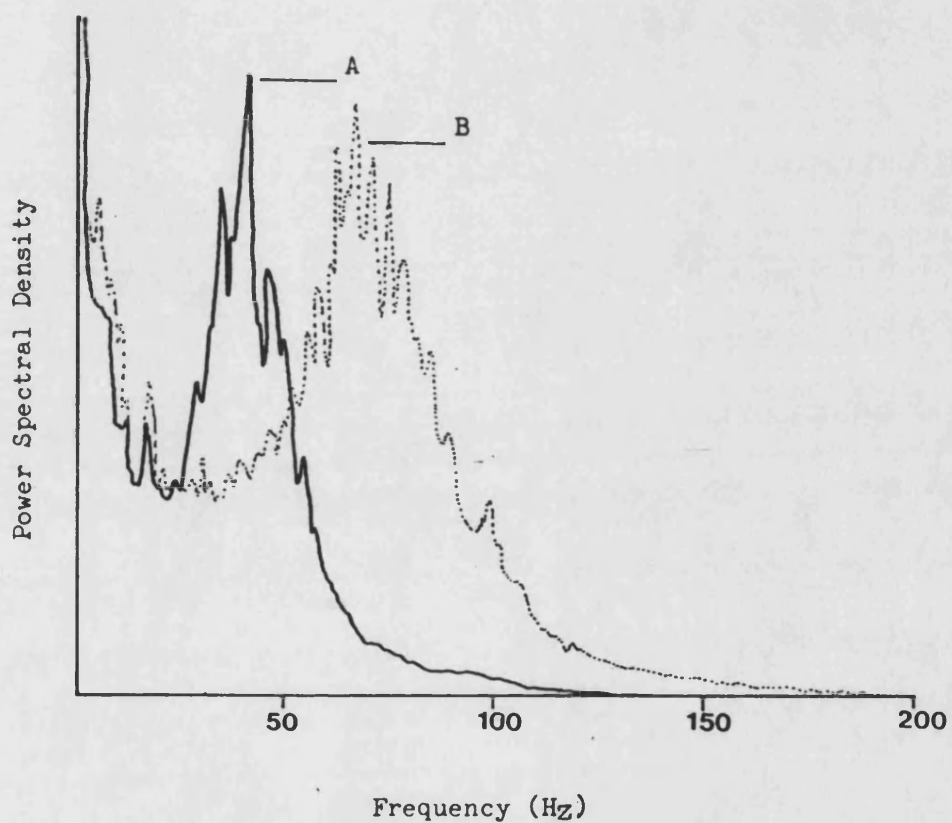


Figure 8.3 Averaged Power Spectra Obtained from 700 nm B Polymer Coated Silica Dispersed in Toluene
(A = 41.2 kV m^{-1} , B = 59.0 kV m^{-1} , $\theta = 19.0^\circ$,
reversal rate = 5 Hz)

Time Elapsed (minutes)	Determined Frequency Shift (Hz)					
	Sample Number			Mean	SD	CV
	1	2	3			
0.5	52.5	53.0	52.0	52.5	0.50	1.0
5.0	52.0	52.5	52.0	52.2	0.30	0.6
10.0	53.5	53.0	51.5	52.7	1.05	2.0
15.0	53.5	52.5	52.0	52.7	0.75	1.4
Mean Frequency Shift (Hz)	52.9	52.8	51.9	52.5	0.55	1.0
SD (Hz)	0.75	0.30	0.25	0.25	(SD = Standard Deviation	
CV	1.4	0.6	0.5	0.5	CV = Coefficient of Variation (%))	

Table 8.1 Variation in the Frequency Shift of Averaged Spectra Obtained from 700 nm B Polymer Coated Silica Dispersed in Toluene

($\theta = 19.0^\circ$, 49.9 kV m^{-1} , reversal rate = 5 Hz;

time elapsed refers to commencement of

collection of averaged spectra)

Analysis of Variance (Table 8.1)

Source	Sum of Squares	Degrees of Freedom	Mean Squares	F	F 0.05
Between Samples	0.500	3	0.167	0.33	4.07
Within Samples	4.000	8	0.500		
Total	4.500	11			

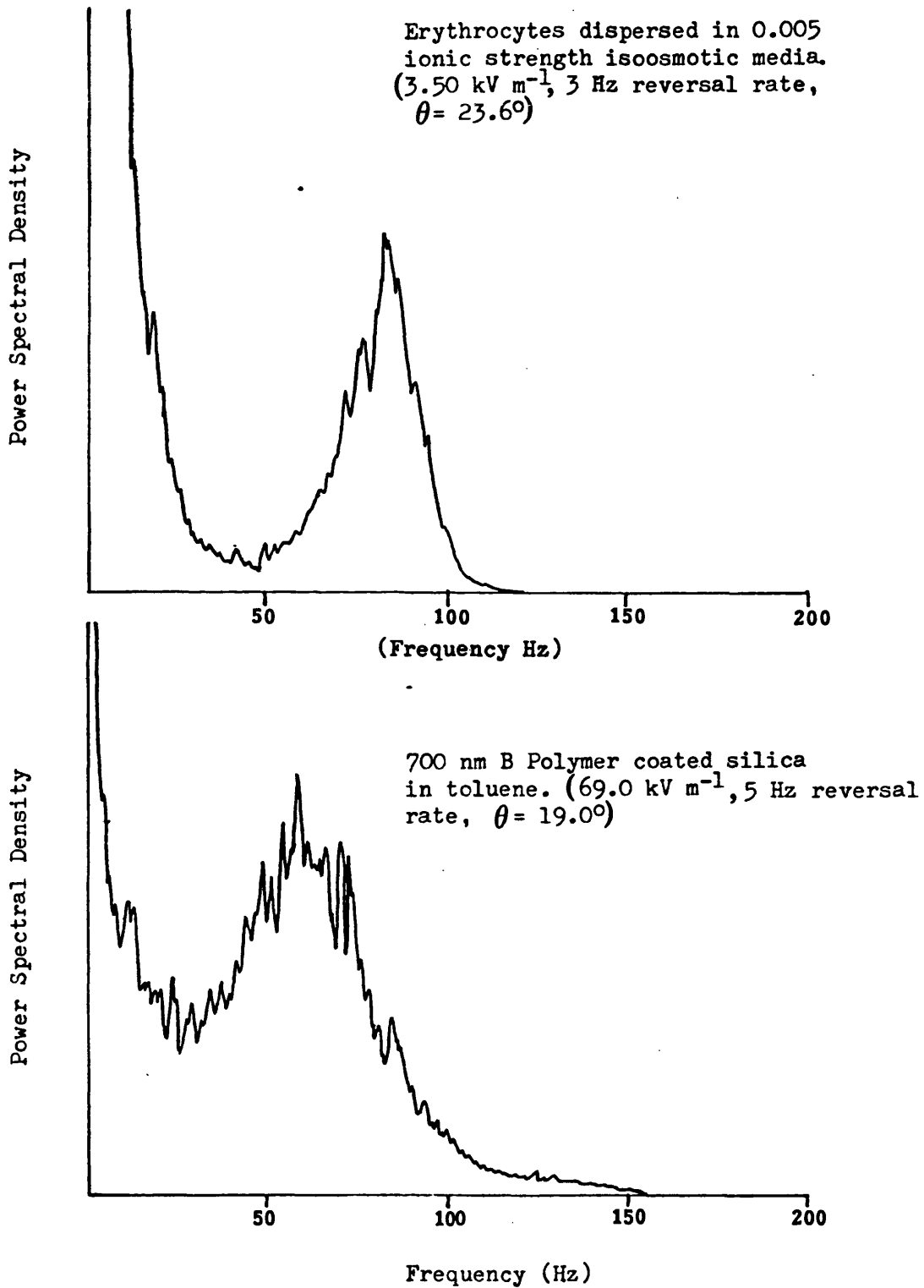


Figure 8.4 Comparison of the Spectral Quality Obtained from an Aqueous and Non-Aqueous Dispersion

Averaged Spectrum Number	Applied Field (kV m^{-1})	Determined Frequency Shift (Hz)						
		Estimation Number				Mean	SD	CV
		1	2	3	4			
1	36.4	37.0	35.5	36.0	36.5	36.3	0.65	1.8
2	50.3	50.0	49.0	48.0	48.0	48.8	0.95	1.9
3	64.7	67.0	65.0	67.0	66.5	66.4	0.95	1.4
4	87.1	87.0	87.0	87.0	88.5	87.4	0.75	0.9
5	105.0	109.0	109.0	109.5	108.5	109.0	0.40	0.4

(SD = Standard Deviation, CV = Coefficient of Variation (%))

Table 8.2 Variation in Frequency Estimation for a Series of Averaged Spectra Obtained from 700 nm B Polymer Coated Silica Dispersed in Toluene
($\theta = 19.0^\circ$, reversal rate = 5Hz)

reduction in the error which arises from the limits in analyser resolution. 95% confidence limits for Table 8.2 range from ± 0.6 to ± 1.5 Hz, the latter being only slightly larger than the value of ± 1.2 Hz found for erythrocyte dispersions (Section 7.6).

An uncertainty of ± 1.5 Hz at an applied field of 50 kV m^{-1} represents an uncertainty in electrophoretic mobility of $\pm 0.04 \times 10^{-9} \text{ m}^2 \text{ s}^{-1} \text{ V}^{-1}$. 95% confidence limits for sample to sample variation (Table 8.1) range from ± 0.7 to ± 2.6 Hz; representing an uncertainty in electrophoretic mobility of up to $\pm 0.7 \times 10^{-9} \text{ m}^2 \text{ s}^{-1} \text{ V}^{-1}$ (applied field = 50 kV m^{-1}).

The data reported in Table 8.2 was collected solely to establish frequency estimation errors, as no moisture assay was made it would be inappropriate to test the results for true electrophoresis.

To ensure the electrode gap was free from electroosmosis and turbulence, a series of averaged spectra were collected consecutively at various positions within the electrode gap. Table 8.3A shows, for a single sample, the results obtained for the probe volume centrally positioned and moved down the length of the electrodes. Table 8.3B shows, for a different sample, the effect of positioning the probe volume at the front and back cuvette walls at the $1000 \mu\text{m}$ vertical position.

Results are also shown for positions of the probe volume towards either of the electrodes; movement from the centre is limited due to clipping of the beam by the electrodes. As the coefficients of variation for the two tables were similar to those for the replicate frequency determinations (Table 8.2), it was concluded that within the limits of frequency estimation, the electrode gap was free from electroosmosis. Application of the t test to the two tables (Tables 8.3A and 8.3B) showed no significant difference between them ($t = 0.37$, $p = 0.72$).

Distance from Top of Electrode Gap (μm)	Determined Frequency Shift (Hz)
200	58.0
400	57.0
600	57.0
800	56.5
1000	58.0
1200	57.5
1400	56.5
Mean	57.2
SD	0.65
CV	1.1

A : Variation in Vertical Position of Probe Volume

(SD = Standard Deviation, CV = Coefficient of Variation (%))

Probe Position at 1000 μm Vertical Position	Determined Frequency Shift (Hz)
Centre	58.0
Front Wall of Cuvette	57.0
Back Wall of Cuvette	56.5
+ 50 μm Towards Left Electrode	56.0
+ 100 μm Towards Left Electrode	58.0
+ 50 μm Towards Right Electrode	57.5
+ 100 μm Towards Right Electrode	56.5
Mean	57.1
SD	0.80
CV	1.4

B : Variation in Horizontal Position of Probe Volume

Table 8.3 The Effect of Probe Volume Position on the Frequency Shift Obtained from 700 nm B Polymer Coated Silica Dispersed in Toluene

($\theta = 19.0^\circ$, 59.0 kV m^{-1} , reversal rate = 5 Hz)

There was a degradation in and eventual loss of the frequency envelope, when the probe volume was close to either of the electrodes. This was ascribed to the destructive influence of light scattered from particles with acquired charge (Section 8.1.1). All subsequent measurements were made at the centre of the 1000 μm vertical position.

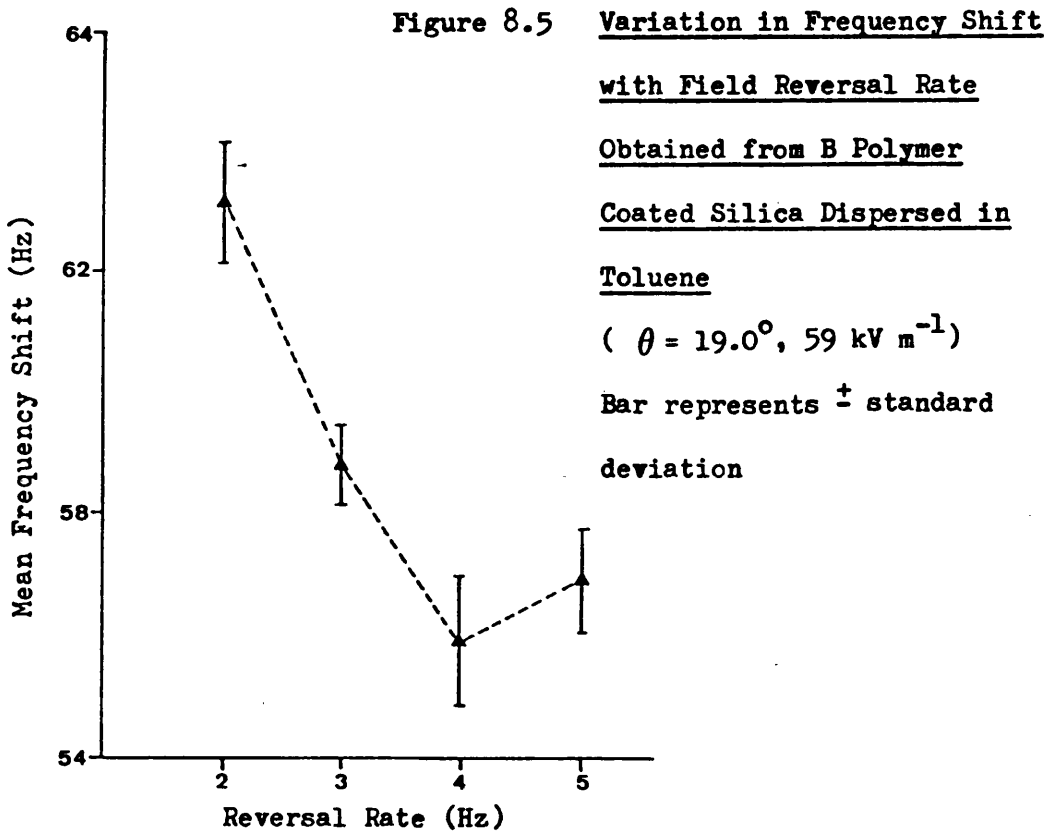
The effect of field reversal rate on frequency shift was examined using four replicate samples; the results are summarised in Table 8.4 and Figure 8.5. The figure shows the frequency shifts initially to decrease with increasing field reversal rate before levelling out; application of the t test shows no significant change ($p = 0.19$) in frequency shift between reversal rates of 4 and 5 Hz. It was observed that at lower reversal rates the averaged spectra became broadened and less well defined; possibly due to the onset of turbulence. This qualitative observation is not reflected by an increased coefficient of variation at lower reversal rates; all rates had values similar to those in Table 8.1. All subsequent measurements were made at a 5 Hz reversal rate.

For true electrophoresis a linear relationship between frequency shift and applied field which passes through the origin is expected. To test for this, two dispersions with an assayed moisture content of 15 ppm, were studied at a series of field strengths between 35 and 60 kV m^{-1} . Four replicate samples were studied from each dispersion, averaged spectra being collected from each at 6 different field strengths. The mean frequency shifts and calculated electrophoretic mobilities are summarised in Table 8.5. Figure 8.6 shows the mean frequency shifts plotted against applied field with the best fitting line as determined by linear regression (Table 8.6).

Field Reversal Rate (Hz)	Determined Frequency Shift (Hz)							Result of t test Against 5 Hz Result (t value, t 0.05 = 2.447)
	Sample Number				Mean	SD	CV	
	1	2	3	4				
5	56.5	56.0	57.0	58.0	56.9	0.85	1.5	-
4	56.5	57.0	55.0	55.0	55.9	1.05	1.9	1.49
3	58.0	59.5	59.0	58.5	58.8	0.65	1.1	3.50
2	63.0	64.0	63.0	62.5	63.1	0.65	1.0	11.79

(SD = Standard Deviation, CU = Coefficient of Variation)

Table 8.4 The Effect of Field Reversal Rate on the Frequency Shift Obtained from 700 nm B Polymer Coated Silica Dispersed in Toluene
($\theta = 19.0^\circ$, 59 kV m^{-1})



Dis- pers-ion A	Applied Field (kV m^{-1})	36.8	41.2	46.0	50.4	55.2	59.5	Mean	SD	CV
	Mean Frequency Shift (Hz)	37.4	47.8	50.3	58.1	59.8	62.5			
	SD (Hz)	0.25	0.65	0.65	0.65	0.60	0.70			
	CV	0.7	1.4	1.3	1.1	1.0	1.1			
	Electro-phoretic Mobility ($\text{m}^2\text{s}^{-1} \times 10^9$)	1.30	1.48	1.40	1.47	1.38	1.34			
Dis- pers-ion B	Applied Field (kV m^{-1})	36.7	41.4	45.6	49.9	55.2	59.8	Mean	SD	CV
	Mean Frequency Shift (Hz)	38.6	45.0	48.5	53.1	59.9	65.6			
	SD (Hz)	0.75	1.85	0.90	1.45	0.85	1.10			
	CV	1.9	4.1	1.9	2.7	1.4	1.7			
	Electro-phoretic Mobility ($\text{m}^2\text{s}^{-1}\text{v}^{-1} \times 10^9$)	1.34	1.39	1.36	1.36	1.39	1.40			

(SD = Standard Deviation, CV = Coefficient of Variation (%))

Table 8.5 Summary of Frequency Shifts and Corresponding Electrophoretic Mobilities for 700 nm B Polymer Coated Silica Dispersed in Toluene
($\theta = 19.0^\circ$, reversal rate = 5Hz, assayed moisture = 15 ppm)

Dispersion	Slope ($\times 10^3$)	Slope SD ($\times 10^3$)	Inter- cept	Inter- cept SD	Correlation Coefficient	Probability of Linearity	Electro- phoretic Mobility from slope ($\text{m}^2\text{s}^{-1}\text{v}^{-1} \times 10^9$)
A	1.06	0.15	1.70	7.10	0.964	>99.0%	1.35
B	1.15	0.03	-3.30	1.66	0.998	>99.9%	1.47

Table 8.6 Linear Regression Analysis Results Obtained for the Relationship Between Frequency Shift and Applied Field From 700 nm Polymer Coated Silica Dispersed in Toluene
($\theta = 19.0^\circ$, reversal rate = 5 Hz, moisture = 15 ppm)

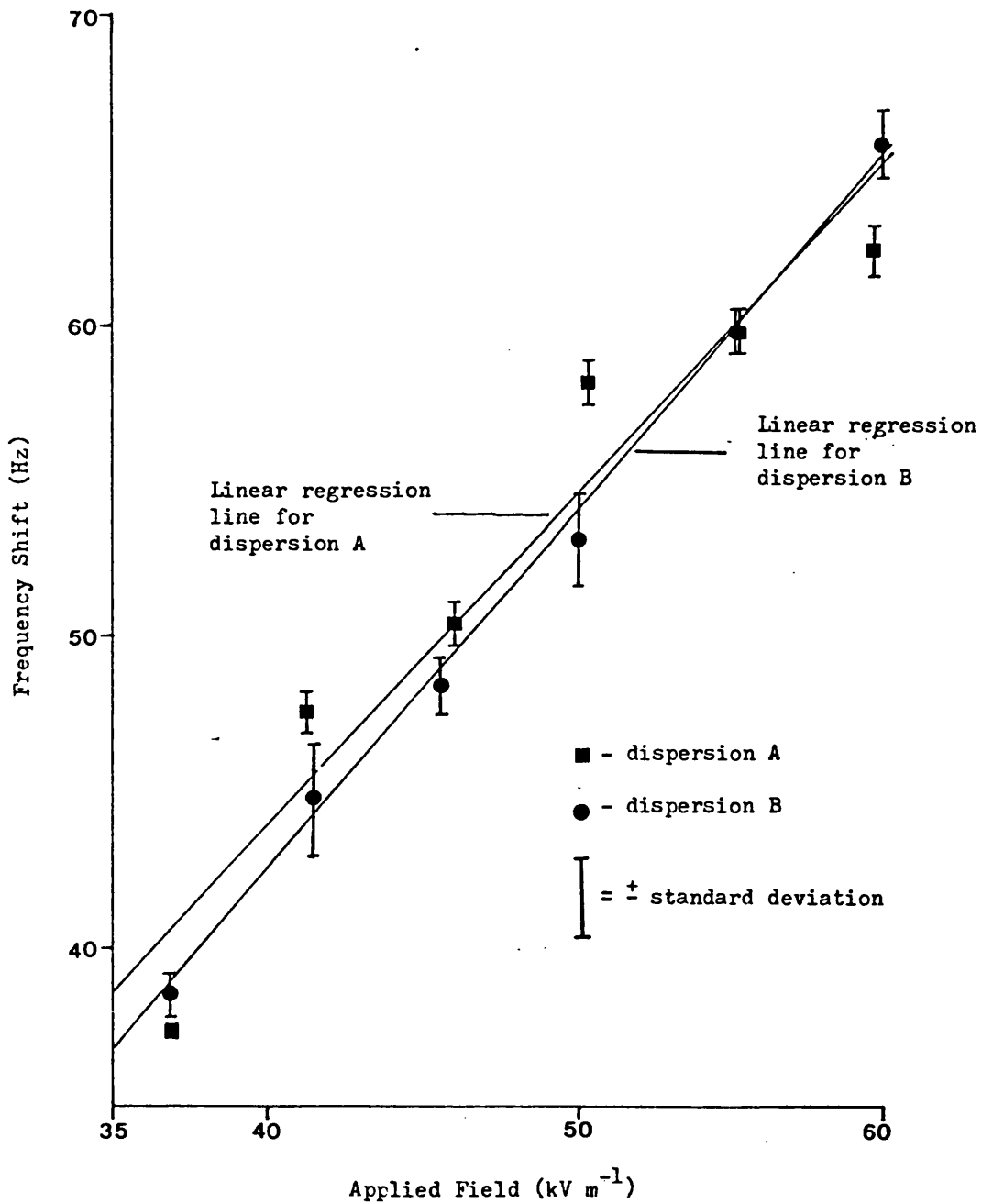


Figure 8.6 Plot of Mean Frequency Shift Against Applied Field Strength, 5 Hz Reversal Rate, for 700 nm B Polymer Coated Silica Dispersed in Toluene

Both dispersions showed a linear dependence between frequency shift and applied field, in the case of dispersion B the fit was the better; both calculated intercepts pass through zero within ± 2 standard deviations. These results demonstrate true electrophoresis, application of the t test to the mean calculated electrophoretic mobilities shows there to be no significant difference ($t = 0.71$, $p = 0.49$) between the two dispersions. Similarly, no statistical difference was found between the slopes of the regression lines when compared using the t test ($t = 0.59$, $p < 0.50$). The electrophoretic mobilities derived from the regression slopes deviated by no more than $0.10 \times 10^{-9} \text{ m}^2 \text{ s}^{-1} \text{ V}^{-1}$ from the mean values in Table 8.5.

The low conductivity of toluene ($< 10^{-10} \text{ S m}^{-1}$, Section 6.3.9), small particle size and absence of surfactant suggests a value of $Ka < 0.1$ (75). Using equation 3.7 ($f(Ka) = 1$) the zeta potentials of the particles studied was about 65 mV ($U_E = 1.4 \times 10^{-9} \text{ m}^2 \text{ s}^{-1} \text{ V}^{-1}$; $\epsilon_r = 2.4$, $\eta = 0.65 \times 10^{-3} \text{ kg m}^{-1} \text{ s}^{-1}$ (180)).

8.2.2 THE INFLUENCE OF PARTICLE SIZE ON ELECTROPHORETIC MOBILITY

An evaluation of the effect of particle size on electrophoretic mobility was made using 700 nm, 300 nm and 82 nm diameter B polymer coated silica dispersions in toluene. The moisture content of the dispersions was kept constant with a mean value of 12 ppm (Table 8.7), by making serial dilutions using the same batch of dried toluene. Analysis of variance shows there to be no significant difference ($p < 0.05$) in the moisture contents of the dispersions studied.

Since the dispersions were found to have lower mobilities than those studied previously, the beam intersection angle was increased to 25.2° in toluene (38.2° in air). A 1 Hz frequency shift corresponded

Dispersion	Sample	Weight of Sample (g)	Assayed Moisture (μg)	Moisture Content (ppm)	Mean Moisture Content (ppm)
700 nm Week 1	1	2.0762	25	12.0	11.3
	2	2.0030	21	10.5	
700 nm Week 2	1	2.4173	25	10.3	11.0
	2	2.3223	27	11.6	
300 nm Week 1	1	1.9872	24	12.1	11.6
	2	2.5321	28	11.1	
300 nm Week 2	1	1.8762	24	12.8	12.4
	2	2.0176	24	11.9	

Table 8.7 Assayed Moisture Contents of B Polymer Coated Silica Dispersions in Toluene Used to Study the Role of Particle Size on Measured Electrophoretic Mobility

Source	Sum of Squares	Degrees of Freedom	Mean Square	F ratio	F 0.05
Between Samples	2.184	3	0.728	1.01	6.59
Within Samples	2.875	4	0.719		
Total	5.059	7			

Analysis of Variance (Table 8.7)

to a velocity of $0.967 \times 10^{-6} \text{ m s}^{-1}$ (equation 4.5). It was not possible to further increase the angle due to clipping of the beam by the electrodes and problems in alignment.

The dispersion containing the 82 nm diameter spheres was found not to produce any detectable signal, no further work was carried out on this dispersion.

Four samples of the remaining 300 nm and 700 nm sized dispersions were studied at 5 field strengths (5 Hz reversal rate), the mean frequency shifts and corresponding electrophoretic mobilities are given in Table 8.8. Additionally a dispersion which comprised a 50:50 mixture of the two dispersions was studied (Table 8.9). The whole experiment was repeated a week later using freshly prepared dispersions, these results also appear in Tables 8.8 and 8.9.

Analysis of variance of the calculated electrophoretic mobilities (Table 8.8) showed there to be a significant ($p > 0.05$) difference between the different dispersions. This can be attributed in part, to a significant week to week variation; comparison of the two 300 nm dispersion results using the t test produces a significant result ($t = 5.18$, $p > 0.001$). This variation is also seen between the 300/700 nm mixed dispersion ($t = 3.18$, $p = 0.013$), but not the 700 nm dispersion ($t = 0.10$, $p = 0.93$). To allow for this variation, analysis of variance was performed using mean electrophoretic mobilities of each dispersion. No significant variation between dispersions was noted ($p < 0.05$), indicating any differences in electrophoretic mobility between different sized dispersions could be attributed to weekly variation.

Table 8.10 gives the linear regression analysis results for a plot of

Dispersion	Applied Field kV m^{-1}	41.2	45.9	50.4	55.0	59.6	Mean	SD	CV
300 nm (Week 1)	Mean Frequency Shift (Hz)	45.9	54.5	60.0	65.8	68.3	1.13	0.03	2.6
	SD (Hz)	0.65	1.25	0.70	0.65	0.85			
	CV	1.4	2.3	1.2	1.0	1.2			
	Electrophoretic Mobility ($\text{m}^2\text{s}^{-1}\text{V}^{-1} \times 10^9$)	1.08	1.15	1.15	1.16	1.11			
300 nm (Week 2)	Mean Frequency Shift (Hz)	41.9	48.9	55.4	57.1	63.9	1.02	0.03	2.9
	SD (Hz)	0.25	1.30	0.95	0.50	1.45			
	CV	0.60	2.70	1.70	0.90	2.30			
	Electrophoretic Mobility ($\text{m}^2\text{s}^{-1}\text{V}^{-1} \times 10^9$)	0.98	1.03	1.06	1.00	1.04			
700 nm (Week 1)	Mean Frequency Shift (Hz)	46.5	51.5	56.0	66.1	68.9	1.10	0.04	3.6
	SD (Hz)	0.70	1.90	1.40	0.85	0.85			
	CV	1.5	3.7	2.5	1.3	1.2			
	Electrophoretic Mobility ($\text{m}^2\text{s}^{-1}\text{V}^{-1} \times 10^9$)	1.09	1.08	1.07	1.16	1.12			
700 nm (Week 2)	Mean Frequency Shift (Hz)	45.8	51.6	57.3	64.8	69.4	1.11	0.03	2.7
	SD (Hz)	0.85	1.25	0.65	0.50	1.50			
	CV	1.90	2.4	1.1	0.8	2.2			
	Electrophoretic Mobility ($\text{m}^2\text{s}^{-1}\text{V}^{-1} \times 10^9$)	1.07	1.09	1.10	1.14	1.13			

(SD = Standard Deviation, CV = Coefficient of Variation (%))

Table 8.8 Summary of Frequency Shifts and Corresponding Electrophoretic Mobilities for 300 nm and 700 nm B Polymer Coated Silica Dispersed in Toluene

($\theta = 25.2^\circ$, reversal rate = 5 Hz, moisture content = 12 ppm)

Dispersion	Applied Field (kV m^{-1})	41.2	45.9	50.4	55.0	59.6	Mean	SD	CV
300 nm and 700 nm (Week 1)	Mean Frequency Shift (Hz)	41.0	46.5	51.4	54.5	58.8	0.97	0.02	2.1
	SD (Hz)	0.40	0.90	0.25	1.30	0.65			
	CV	1.0	1.9	0.5	2.4	1.1			
	Electrophoretic Mobility ($\text{m}^2\text{s}^{-1}\text{V}^{-1} \times 10^9$)	0.96	0.98	0.99	0.96	0.95			
300 nm and 700 nm (Week 2)	Mean Frequency Shift (Hz)	41.6	47.5	52.0	59.4	63.5	1.01	0.02	2.0
	SD (Hz)	0.8	1.0	0.4	1.3	0.7			
	CV	1.9	2.1	0.8	2.2	1.1			
	Electrophoretic Mobility ($\text{m}^2\text{s}^{-1}\text{V}^{-1} \times 10^9$)	0.98	1.00	1.00	1.04	1.03			

(SD = Standard Deviation, CV = Coefficient of Variation (%))

Table 8.9 Summary of Frequency Shifts and Corresponding Electrophoretic Mobilities for 300 nm/700 nm Mixed B Polymer Coated Silica Dispersed in Toluene
($\theta = 25.2^\circ$, reversal rate = 5 Hz, moisture content = 12 ppm)

Source	Sum of Squares	Degrees of Freedom	Mean Square	F ratio	F 0.05
Between Samples	0.1064	5	0.021293	24.57	2.62
Within Samples	0.0208	24	0.000867		
Total	0.1272	29			

Analysis of Variance (Tables 8.8 and 8.9)

Source	Sum of Squares	Degrees of Freedom	Mean Square	F ratio	F 0.05
Between Samples	0.01423	2	0.00712	3.09	9.55
Within Samples	0.00690	3	0.00230		
Total	0.02113	5			

Analysis of Variance (Tables 8.8 and 8.9, mean values only)

Dispersion	Slope ($\times 10^3$)	Slope SD ($\times 10^3$)	Inter- cept	Inter- cept SD	Correlation Coefficient	Probability of Linearity	Electro- phoretic Mobility from slope ($m^2s^{-1}V^{-1}$ $\times 10^9$)
300 nm (Week 1)	1.22	0.13	-2.75	6.56	0.984	> 99.0%	1.18
300 nm (Week 2)	1.14	0.11	-3.92	5.65	0.986	> 99.0%	1.10
700 nm (Week 1)	1.29	0.13	-7.44	6.39	0.986	> 99.0%	1.25
700 nm (Week 2)	1.32	0.05	-8.56	2.46	0.998	> 99.9%	1.28
300 nm and 700 nm (Week 1)	0.95	0.05	2.54	2.68	0.995	> 99.9%	0.92
300 nm and 700 nm (Week 2)	1.21	0.06	-8.39	2.80	0.997	> 99.9%	1.17

Table 8.10 Linear Regression Analysis Results Obtained for the Relationship Between Frequency Shift and Applied Field from B Polymer Coated Silica Dispersed in Toluene

(moisture = 12 ppm)

Source	Sum of Squares	Degrees of Freedom	Mean Square	F ratio	F 0.05
Between Samples	0.0508	2	0.0254	2.04	9.55
Within Samples	0.0374	3	0.0125		
Total	0.0883	5			

Analysis of Variance (Table 8.10)

frequency shift against applied field, in all cases a reasonable linear dependence was obtained. In only two cases did the intercept lie more than ± 2 standard deviations from the origin. Analysis of variance of the regression slopes shows there also to be no significant difference ($p < 0.05$) between the dispersions. It was therefore concluded that electrophoretic mobility was independent of particle size, a conclusion supported by the observation that only one frequency envelope was produced by the mixed size dispersion (Figure 8.7).

A mobility of $1.1 \times 10^{-9} \text{ m}^2 \text{ s}^{-1} \text{ V}^{-1}$ gives a zeta potential of approximately 50 mV (equation 3.7, $f(\kappa a) = 1$), which in turn corresponds to particle charges of $4.7 \times 10^{-18} \text{ C}$ and $2.0 \times 10^{-18} \text{ C}$ for the 700 nm and 300 nm sized particles respectively (equation 2.10). These charges when divided by the surface area of the particle correspond to surface charge densities of $7.1 \times 10^{-6} \text{ C m}^{-2}$ and $3.0 \times 10^{-6} \text{ C m}^{-2}$ for the 300 nm and 700 nm size particles respectively.

The calculated charge density on the smaller sized particle is equivalent to just 13 elementary charges (of $1.6 \times 10^{-19} \text{ C}$), 30 being required for the larger sized particle.

8.2.3 DISPERSIONS IN 113/N-HEXANE

An attempt was made to produce dispersions of B polymer coated silica in 113/n-hexane, so as to demonstrate true electrophoresis in the propellant model prior to investigation of more pharmaceutically relevant systems.

When diluted from the mother dispersion into 113/n-hexane the dispersion was observed to coagulate, forming dense white irreversible agglomerates.

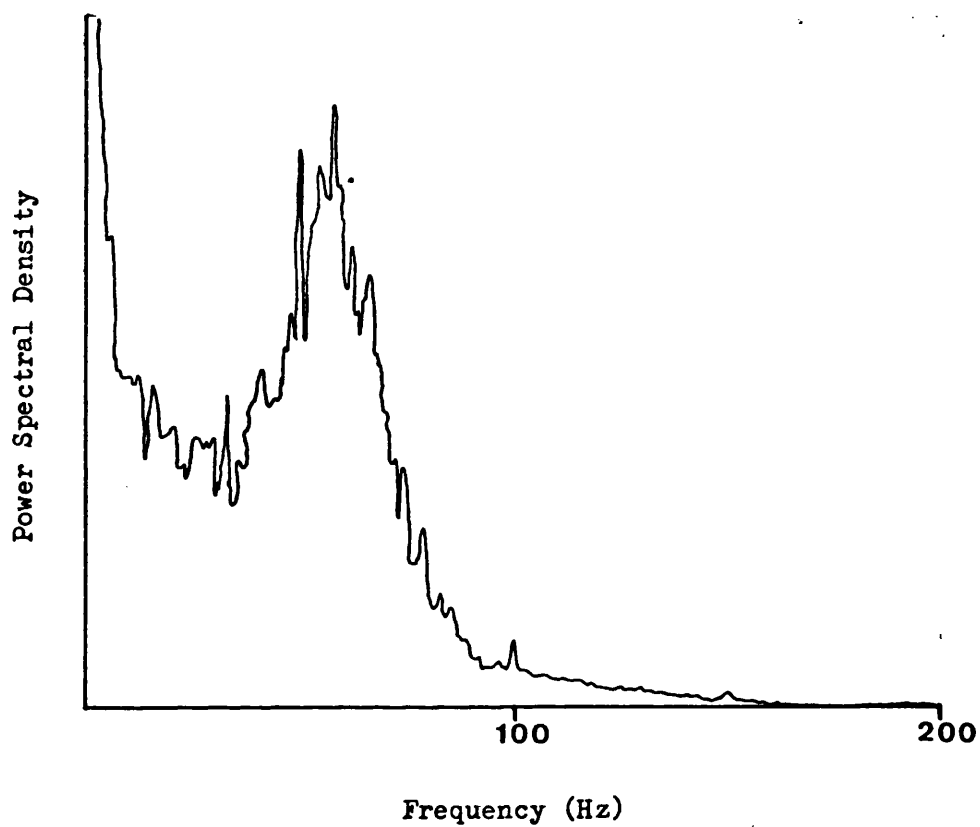


Figure 8.7 Averaged Power Spectrum Obtained from a Mixture of 300 nm and 700 nm B Polymer Coated Silica Dispersed in Toluene
($\theta = 25.2^\circ$, 55.0 kV m^{-1} , reversal rate = 5 Hz)

8.3 Investigations using polymer A coated silica dispersions

Dispersions of 300 nm A polymer coated silica were prepared in toluene for investigation using the same methods as for the B polymer coated silica.

On application of the field, a shift in the signal envelope with increasing time was noted. An example of this behaviour is given in Figure 8.8. This temporal phenomenon was not seen whilst studying the B polymer coated silica dispersions; indicating possibly that this behaviour was associated with the polymer coat itself, or its interaction with the silica surface. It is tentatively suggested that this effect was associated with a stripping off, or distortion of the polymer coat by the applied electric field.

Dispersions of A polymer coated silica in 113/n-hexane did not show coagulation, but were not studied in detail because of uncertainty in the stability of the system.

8.4 Investigations using Hypersil ODS

8.4.1 DISPERSIONS WITHOUT A SURFACTANT

The pharmaceutical dispersion of interest is a coarse dispersion with particles in the range of 1 to 10 μm in diameter. It was therefore important to consider the effect of larger particle sizes on electrophoretic mobility. Since dispersions of larger sized polymer coated spheres were not available, dispersions of spherical Hypersil ODS in 113/n-hexane were studied. Dispersions of nominally 3 μm and 5 μm diameter particles were successfully dispersed in 113/n-hexane. Larger 10 μm diameter particles were also examined but were found to sediment rapidly.

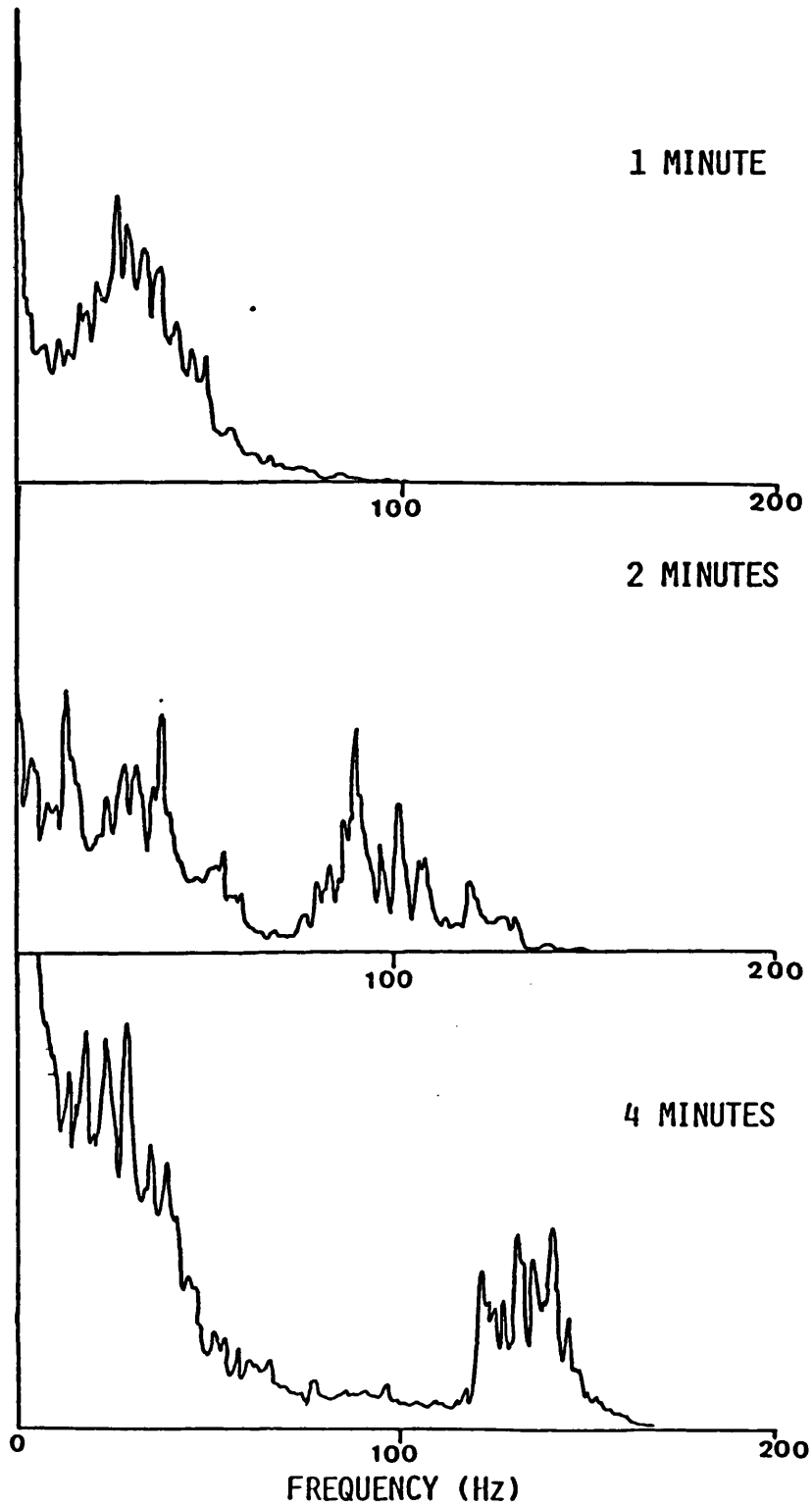


Figure 8.8 Power Spectra Obtained from A Polymer Coated Silica Dispersed in Toluene, Variation of Frequency Envelope with Time
($\theta = 25.2^\circ$, 45.0 kV m^{-1} , reversal rate = 5 Hz)

Samples were then studied to determine whether they showed electrophoretic motion; neither the 5 μm or 3 μm dispersions produced frequency envelopes. Visual examination, using the RF313 assembly and extension tubes, showed there was some movement under the influence of an applied field but this was likely to be attributable to electrohydrodynamic effects.

Providing the particles in the dispersion are reasonably homogeneous in electrophoretic mobility, these observations must suggest that the particles were either uncharged, or possessed small charges which could not be measured. An estimation of the smallest zeta potential which could be seen can be made. The maximum voltage that can be applied to the electrodes is considered to be limited by electrohydrodynamic effects to 110 V for the system studied (equation 3.10); with an electrode gap of 1.1 mm this represents an applied field of 100 kV m^{-1} . The smallest shift that could be clearly resolved from the low frequency noise was taken as 25 Hz. Using equations 4.5 and 3.7 ($f(\kappa a) = 1$) the smallest zeta potential which could have been seen was of the order of 15 mV ($\theta = 20.9^\circ$ in liquid).

It is known from the literature that particles dispersed in non-polar media may not possess any surface charge unless dispersed in the presence of a surfactant or dispersant. Since the silica surface of Hypersil ODS has been specifically treated to remove polar groups, one perhaps would not expect to find any surface charge.

8.4.2 THE INFLUENCE OF MOISTURE AND AEROSOL OT UPON THE DETERMINED ELECTROPHORETIC MOBILITY

In an attempt to produce charged particles, Aerosol OT was added to

the 3 μm and 5 μm Hypersil ODS dispersions. A concentration of $4 \times 10^{-3}\text{M}$ Aerosol OT produced dispersions which showed resolvable Doppler envelopes, similar to those in Figure 8.3; the intersection angle was 20.9° in 113/n-hexane (28.7° in air). The moisture content of the dispersions was 24 ppm with the particles in both dispersions being negatively charged. .

For the 3 μm dispersion, analysis of variance showed there to be no significant variation ($p < 0.05$) in frequency shift with field reversal rate (Table 8.11). In the case of the 5 μm dispersion analysis of variance did produce a ^{statistically} significant variation ($p > 0.05$, $p < 0.01$). For this dispersion the coefficients of variation for each sample (over the range of reversal rates used), were between 0.6 and 1.7%. This is less than the 1.9% noted in Table 8.2 for frequency estimation. The effect of reversal rate was therefore considered not to be practically significant.

Calculated electrophoretic mobilities were however found to be dependent on the applied field, increasing with increasing field strength (Table 8.12). Using linear regression analysis the relationship between frequency shift and applied field was found to show a close linear dependence. Neither regression line passed close to the intercept, over 6 standard deviations away in both cases. Clearly true electrophoresis was not demonstrated.

A possible explanation of these results requires the decoupling of the diffuse layer from its associated particle; once the diffuse layer is fully decoupled, a linear relationship between frequency shift and applied field would be seen (76). From equation 3.8, the relaxation time of the diffuse layer in this system would be around 0.2s. The diffuse layer thickness was estimated, using the approach

Hypersil ODS Size (μm)	Field Reversal Rate (Hz)	Determined Frequency Shift (Hz)					
		Sample Number			Mean	SD	CV
		1	2	3			
3	5	80.5	81.5	80.5	80.8	0.60	0.7
	4	81.0	80.0	79.5	80.2	0.75	0.9
	3	79.5	80.0	80.5	80.0	0.50	0.6
	2	80.0	80.0	81.0	80.3	0.60	0.7
5	5	79.5	79.0	80.0	79.5	0.50	0.6
	4	79.5	77.5	78.5	78.5	1.00	1.3
	3	79.5	80.5	81.0	80.5	0.75	0.9
	2	78.5	78.0	79.0	78.5	0.50	0.6

(SD = Standard Deviation, CV = Coefficient of Variation (%))

Table 8.11 Effect of Field Reversal Rate on Frequency Shift
For Hypersil ODS Dispersions in 113/n-Hexane with
 $4 \times 10^{-3}\text{M}$ Aerosol OT
 ($\theta = 20.9^\circ$, 34.5 kV m^{-1} , moisture content = 24 ppm)

Source	Sum of Squares	Degrees of Freedom	Mean Square	F ratio	F 0.05
Between Samples	1.167	3	0.389	1.04	4.07
Within Samples	3.000	8	0.375		
Total	4.167	11			

Analysis of Variance (3 μm Hypersil ODS)

Source	Sum of Squares	Degrees of Freedom	Mean Square	F ratio	F 0.05
Between Samples	7.062	3	2.354	4.52	4.07
Within Samples	4.167	8	0.521		
Total	11.229	11			

Analysis of Variance (5 μm Hypersil ODS)

Dis- persion	Applied Field (kV m ⁻¹)	27.3	31.8	34.5	36.3	40.1	Result of Linear Regression Analysis of Frequency Shift against Applied Field	
3 μ m	Mean Frequency Shift (Hz)	57.2	70.8	80.0	87.7	103.7	Slope ($\times 10^3$)	3.63
	SD (Hz)	0.30	1.15	2.20	0.75	1.5	SD ($\times 10^3$)	0.19
	CV	0.5	1.6	2.8	0.9	1.4	Intercept	-43.4
	Electro- phoretic Mobility (-m ² s ⁻¹ v ⁻¹ $\times 10^9$)	2.68	2.84	2.96	3.09	3.30	SD	6.5
Correlation Coefficient							0.996	
5 μ m	Mean Frequency Shift (Hz)	52.8	67.0	78.5	87.7	103.2	Slope	3.99
	SD (Hz)	0.30	1.00	1.00	2.25	1.9	SD ($\times 10^3$)	0.19
	CV	0.6	1.5	1.3	2.6	1.8	Intercept	-57.9
	Electro- phoretic Mobility (-m ² s ⁻¹ v ⁻¹ $\times 10^9$)	2.47	2.69	2.91	3.09	3.29	SD	6.6
Correlation Coefficient							0.996	

(SD = Standard Deviation, CV = Coefficient of Variation (%))

Table 8.12 Variation in Frequency Shift and Electrophoretic Mobility of 3 μ m and 5 μ m Hypersil ODS Dispersed in 113/n-Hexane with 4×10^{-3} M Aerosol OT

($\theta = 20.9^\circ$, reversal rate = 2 Hz, moisture content = 24 ppm)

of Kitahara (75), to be around $30 \mu\text{m}$ (equations 2.2, 2.3 and 2.4

Λ_0 Aerosol OT (aqueous) = $120 \text{ S cm}^2 \text{ equiv}^{-1}$ (93). The critical velocity for decoupling (equation 3.9) would therefore be around $150 \mu\text{ms}^{-1}$, representing a frequency shift of the order of 115 Hz (equation 4.5). Whilst shifts approaching this value were obtained (Table 8.12), the phenomenon was noted at velocities of approximately $70 \mu\text{ms}^{-1}$. As the field was only applied for 0.24s, the particle would move about 0.6 of the estimated diffuse layer thickness. Additionally field reversal ensures the particle will oscillate within its own diffuse layer. Decoupling might therefore seem unlikely, however moisture was considered to possibly have a marked effect on the electrophoretic behaviour of the system being studied. It is feasible that if moisture was adsorbed on to the particle surface, a marked reduction in the double layer thickness not predicted by the approach of Kitahara (75) might occur.

Dispersions of dried Hypersil ODS ($3 \mu\text{m}$ and $5 \mu\text{m}$) were prepared in dried 113/n-hexane (section 6.3.6) containing $10 \times 10^{-3} \text{ M}$ Aerosol OT (section 6.3.2). Great care was taken to avoid moisture pick up by the samples; the assayed moisture content of the surfactant solution was taken as 17 ppm (section 9.1.2). Visual observations showed the particles in both dispersions to be negatively charged. Figure 8.9 shows typical signals obtained from such dispersions, their form is similar to that expected theoretically (Figure 4.6).

Both dispersions produced frequency envelopes that were independent of time, for periods of up to 10 minutes. The determined frequency shift was independent of field reversal rate (Table 8.13); analysis of variance shows no significant change ($p < 0.05$) in shift. The coefficients of variation for replicate samples range from 0.5 to

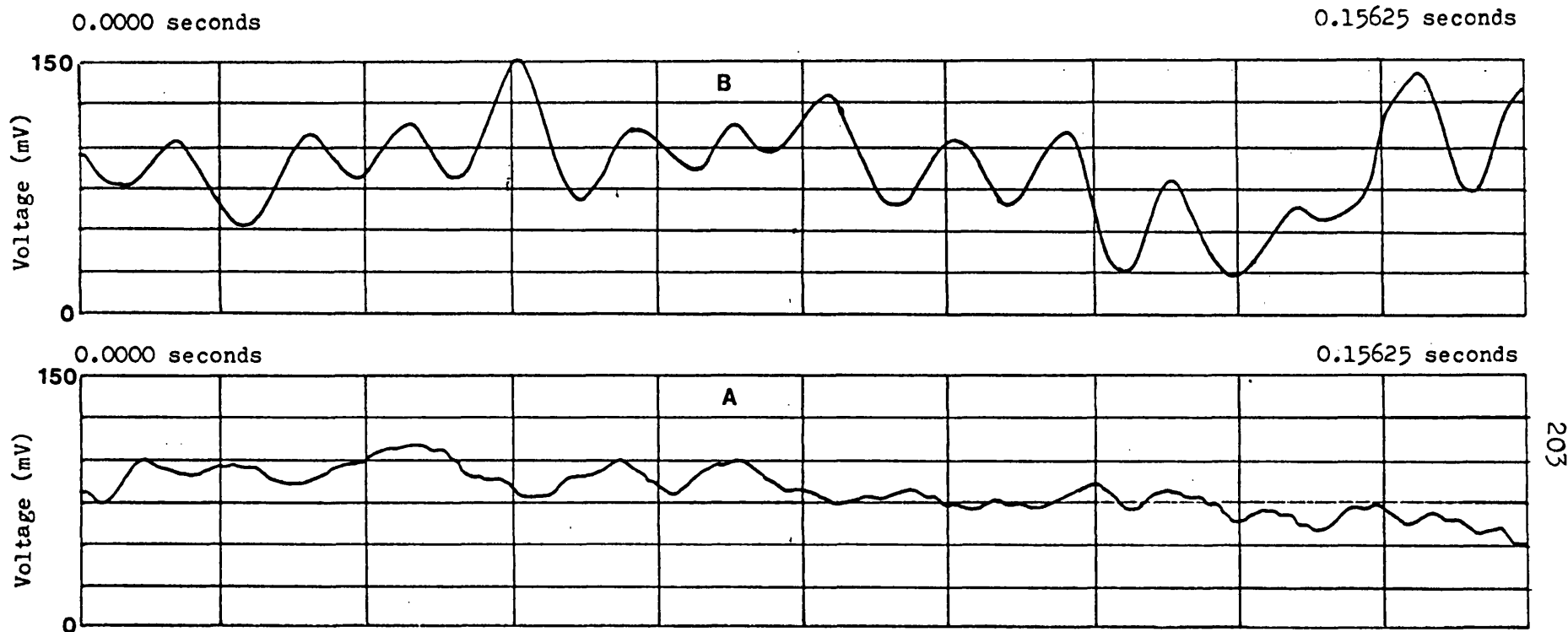


Figure 8.9 Signal Forms Obtained from a Dispersion of 5 μm Hypersil ODS in 113/n-Hexane Containing $10 \times 10^{-3}\text{M}$ Aerosol OT

($\theta = 20.9^\circ$, moisture = 17 ppm)

Trace A, no applied field

Trace B, 32kV m^{-1} , reversal rate = 2 Hz

Hypersil ODS Size (μm)	Field Reversal Rate (Hz)	Determined Frequency Shift (Hz)					
		Sample Number			Mean	SD	CV
		1	2	3			
3	5	62.0	61.0	61.0	61.3	0.60	1.0
	4	63.0	61.5	61.5	62.0	0.85	1.4
	3	61.0	62.5	62.0	61.8	0.75	1.2
	2	60.5	62.0	61.5	61.3	0.75	1.2
5	5	61.0	62.0	61.5	61.5	0.50	0.8
	4	61.0	61.5	62.0	61.5	0.50	0.8
	3	62.0	63.0	62.0	62.3	0.60	1.0
	2	61.5	62.0	61.5	61.7	0.30	0.5

(SD = Standard Deviation, CV = Coefficient of Variation (%))

Table 8.13 Effect of Reversal Rate on Frequency Shift for Hypersil ODS Dispersed in 113/n-Hexane with $10 \times 10^{-3} \text{M}$ Aerosol OT

($\theta = 20.9^\circ$, 34.5 kV m^{-1} , moisture content = 17 ppm)

Source	Sum of Squares	Degrees of Freedom	Mean Square	F ratio	F 0.05
Between Samples	1.062	3	0.354	0.63	4.07
Within Samples	4.500	8	0.563		
Total	5.563	11			

Analysis of Variance (3 μm Hypersil ODS)

Source	Sum of Squares	Degrees of Freedom	Mean Square	F ratio	F 0.05
Between Samples	1.417	3	0.472	2.06	4.07
Within Samples	1.833	8	0.229		
Total	3.250	11			

Analysis of Variance (5 μm Hypersil ODS)

1.4%, no larger than those which arose from estimation errors (Table 8.2). Variation in probe position (method in 8.2.1) revealed no evidence of electroosmosis (Tables 8.14A and B); coefficients of variation also being similar to those due to uncertainty in estimation. Comparison of the two tables using a t test revealed no significant differences ($t = 0.59$, $p = 0.57$). Figure 8.10A shows a typical averaged spectra.

Averaged spectra were collected from 4 replicate samples of the two dispersions at 5 field strengths, the range of field strengths used was smaller than those in Table 8.12. Mean frequency shifts and calculated electrophoretic mobilities are summarised in Table 8.15. Linear regression analysis (Table 8.16) showed a linear relationship between frequency shift and applied field; correlation coefficients were poorer than for the B polymer coated particles (Table 8.10), however both lines passed through the origin within ± 2 standard deviations.

For both the 3 and 5 μm dispersions comparison of the electrophoretic mobilities at 27.3 and 30.9 kV m^{-1} field strengths by the t test shows there to be no significant difference between them (frequency standard deviations are converted to electrophoretic mobility standard deviations; for 3 μm dispersion $t = 2.19$, $p < 0.05$ and for the 5 μm dispersion $t = 2.10$, $p < 0.05$). This contrasts with the results in Table 8.12 ($t = 6.93$, $p > 0.001$ for the 3 μm dispersion and $t = 10.02$, $p > 0.001$ for the 5 μm dispersion) for an increase in the applied field from 27.3 to 31.8 kV m^{-1} . This indicates that an alteration in moisture and surfactant content has permitted true electrophoresis to be observed. Since dispersions

Distance from Top of Electrode Gap (μm)	Determined Frequency Shift (Hz)
200	67.5
400	67.5
600	67.0
800	66.0
1000	65.5
1200	67.5
1400	68.0
Mean	67.0
SD	0.90
CV	1.3

Table A Variation in Vertical Position of Probe Volume

Probe Position at 1000 μm Vertical Position	Determined Frequency Shift (Hz)
Centre	65.5
Front Wall of Cuvette	68.0
Back Wall of Cuvette	67.5
+ 50 μm Towards Left Electrode	67.0
+ 100 μm Towards Left Electrode	67.0
+ 50 μm Towards Right Electrode	68.0
+ 100 μm Towards Right Electrode	68.0
Mean	67.3
SD	0.90
CV	1.3

Table B Variation in Horizontal Position of Probe Volume

Table 8.14 Effect of Probe Volume Position on the Frequency Shift Obtained from 5 μm Hypersil ODS Dispersed in 113/n-Hexane with $10 \times 10^{-3}\text{M}$ Aerosol OT ($\theta = 20.9^\circ$, reversal rate = 2 Hz, moisture content = 17 ppm, 28.9 kV m^{-1})

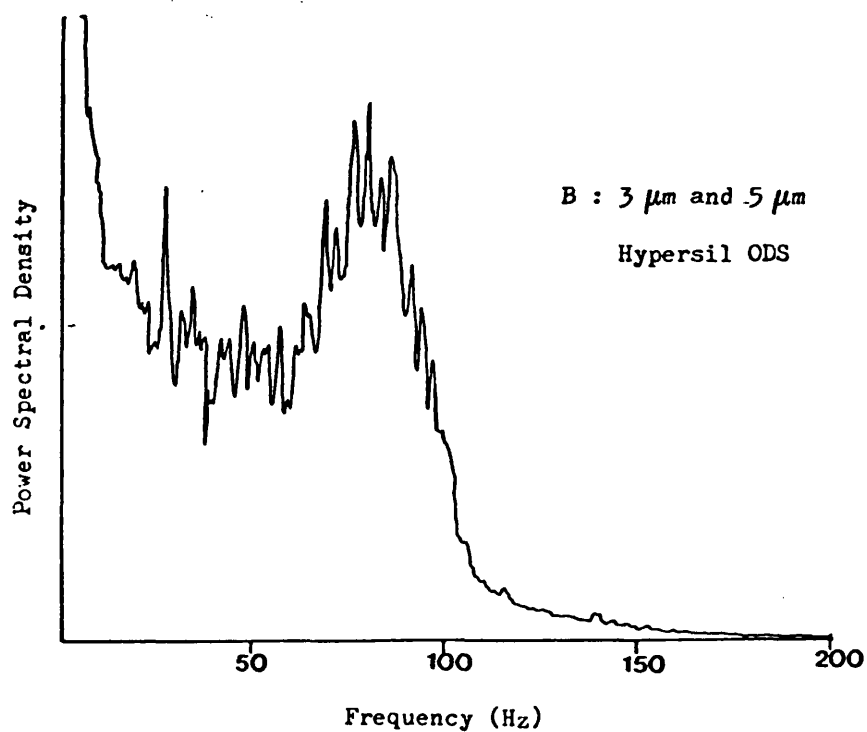
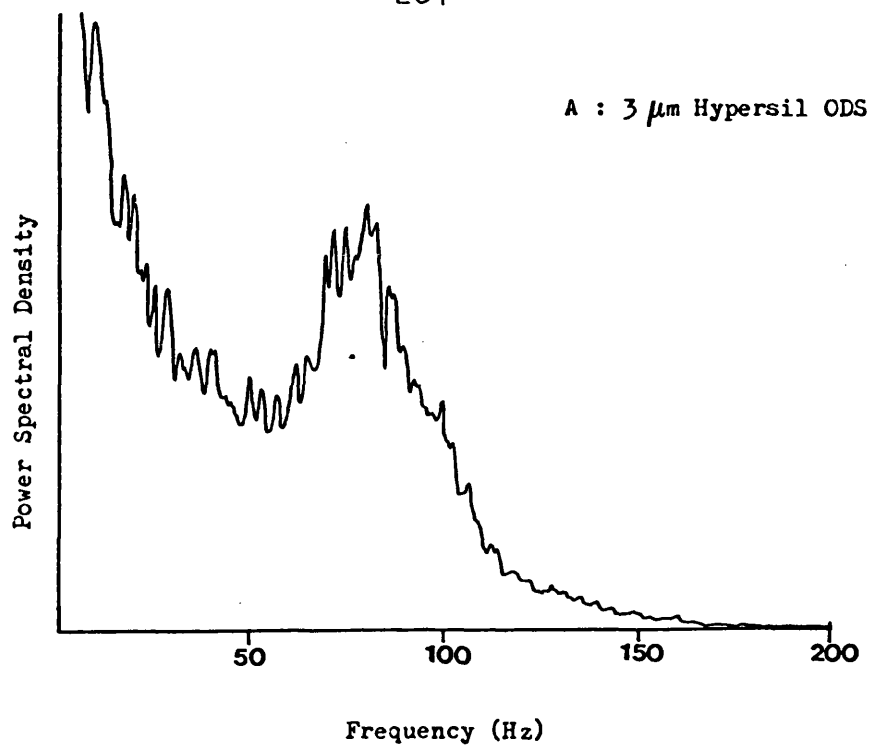


Figure 8.10 Averaged Power Spectra Obtained from Hypersil ODS
Dispersed in 113/n-Hexane Containing 10×10^{-3} M Aerosol OT
($\theta = 20.9^\circ$, 30.9 kV m^{-1} , reversal rate = 2 Hz, moisture
content = 17 ppm)

Dispersion	Applied Field (kV m ⁻¹)	27.3	28.2	29.1	30.0	30.9	Mean	SD	CV
3 μm	Mean Frequency Shift (Hz)	61.6	66.4	67.9	71.0	71.5			
	SD (Hz)	0.75	0.75	0.85	0.80	1.30			
	CV	1.2	1.1	1.3	1.1	1.8			
	Electrophoretic Mobility (m ² s ⁻¹ V ⁻¹ × 10 ⁹)	2.88	3.01	2.98	3.02	2.95	2.97	0.06	2.0
5 μm	Mean Frequency Shift (Hz)	61.8	66.4	67.5	69.5	72.4			
	SD (Hz)	0.60	0.90	0.40	1.10	2.20			
	CV	1.0	1.4	0.6	1.6	3.0			
	Electrophoretic Mobility (m ² s ⁻¹ V ⁻¹ × 10 ⁹)	2.89	3.01	2.96	2.96	2.99	2.96	0.05	1.7

(SD = Standard Deviation, CV = Coefficient of Variation (%))

Table 8.15 Variation in Frequency Shift and Electrophoretic Mobility of 3 μm and 5 μm Hypersil ODS Dispersed in 113/n-Hexane with 10 × 10⁻³M Aerosol OT

Dis- persion	Slope (× 10 ³)	Slope SD (× 10 ³)	Inter- cept	Inter- cept SD	Correlation Coefficient	Probability of Linearity	Electro- phoretic Mobility From Slope (m ² s ⁻¹ V ⁻¹ × 10 ⁹)
3 μm	2.71	0.44	11.21	12.85	0.962	> 99.0%	3.46
5 μm	2.70	0.33	11.05	9.64	0.978	> 99.0%	3.45

Table 8.16 Linear Regression Analysis Results Obtained for the Relationship Between Frequency Shift and Applied Field From 3 μm and 5 μm Hypersil ODS Dispersed in 113/n-Hexane with 10 × 10⁻³M Aerosol OT
(θ = 20.9°, reversal rate = 2Hz, moisture content = 17 ppm)

containing 4×10^{-3} M Aerosol OT were successfully studied at the lower moisture content (section 9.1.1), it would suggest that moisture was responsible for the inability to observe electrophoresis (Table 8.12).

Application of the t test to the mean electrophoretic mobilities obtained in Table 8.15 show no significance ($t = 0.19$ $p = 0.86$) between the two dispersions, similarly no difference is found in their respective regression slopes ($t = 0.02$ $p < 0.9$). It was therefore concluded that variation in particle size of particles of the order of $3 \mu\text{m}$ and $5 \mu\text{m}$ does not influence the observed electrophoretic mobility. This conclusion was supported by the observation that both dispersions produced a single frequency envelope despite showing a degree of size variation. A study of a mixed 3 and $5 \mu\text{m}$ dispersion was undertaken, however the results are not reported because the low humidity environment was found to have been compromised during the experiment. However, the qualitative observation that a single frequency envelope was seen (Figure 8.10) supports the conclusion that electrophoretic mobility was independent of particle size.

An electrophoretic mobility of $-2.95 \times 10^{-9} \text{m}^2 \text{s}^{-1} \text{V}^{-1}$ corresponds to a zeta potential of around -130mV (equation 3.7, $f(\kappa a) = 1$) which results in particle charges of 5.0 and $8.4 \times 10^{-17} \text{C}$ (equation 2.10) on the 3 and $5 \mu\text{m}$ particles respectively. Such charges would arise from approximately 310 and 525 elementary charges on each of the two respective particles; corresponding surface charge densities are 1.77 and $1.07 \times 10^{-6} \text{C m}^{-2}$.

CHAPTER 9THE INFLUENCE OF SURFACTANT CONCENTRATION ON OBSERVED
ELECTROPHORETIC MOBILITY

True electrophoresis has been demonstrated with dispersions of Hypersil ODS in 113/n-hexane in the presence of Aerosol OT (Chapter 8). This chapter reports investigations concerning the influence of surfactant concentration on electrophoretic mobility. The role of two surfactants, Aerosol OT and oleic acid are considered in dispersions of both model and drug particles.

9.1 Studies conducted with Aerosol OT9.1.1 DISPERSIONS OF HYPERSIL ODS IN MODEL PROPELLANT

Before investigating the electrophoretic mobility of a series of dispersions of differing Aerosol OT concentration, it was necessary to establish the time required for equilibration of the dispersion after its preparation.

A dispersion of 5 μm Hypersil ODS, containing $2 \times 10^{-3}\text{M}$ Aerosol OT, was freshly prepared and sealed into dried glass ampoules; the assayed moisture content of the 113/n-hexane solution was 12 ppm. The electrophoretic mobility of the dispersion was determined after 3, 24, 48 and 72 hours using separate ampoules.

After 3 hours the particles were noted to be negatively charged, but no signal envelope could be seen. All other samples were negatively charged and produced signal envelopes; for these averaged spectra were collected from three replicate samples at four field strengths, results are summarised in Table 9.1. Linear regression analysis of

Time (hours)	Applied Field (kV m ⁻¹)	20.7	21.4	22.1	22.7	Mean	SD	CV
24	Mean Frequency Shift (Hz)	84.3	94.8	98.5	103.5			
	SD (Hz)	0.3	0.3	0.5	0.5			
	CV	0.4	0.3	0.5	0.5			
	Electrophoretic Mobility (-m ² s ⁻¹ V ⁻¹ x 10 ⁹)	5.20	5.66	5.69	5.82	5.59	0.27	4.8
48	Applied Field (kV m ⁻¹)	15.9	16.6	17.4	18.0			
	Mean Frequency Shift (Hz)	89.0	92.3	96.3	102.2			
	SD (Hz)	1.0	0.6	0.3	0.3			
	CV	1.1	0.7	0.3	0.3			
	Electrophoretic Mobility (-m ² s ⁻¹ V ⁻¹ x 10 ⁹)	7.15	7.10	7.07	7.25	7.14	0.08	1.1
72	Mean Frequency Shift (Hz)	88.3	91.0	96.8	100.0			
	SD (Hz)	1.5	1.0	1.0	0.5			
	CV	1.7	1.1	1.0	0.5			
	Electrophoretic Mobility (-m ² s ⁻¹ V ⁻¹ x 10 ⁹)	7.09	7.00	7.10	7.09	7.07	0.05	0.7

(SD = Standard Deviation, CV = Coefficient of Variation (%))

Table 9.1 Variation in Frequency Shift and Corresponding Electrophoretic Mobility with Equilibration Time for a 5 μm Hypersil ODS Dispersion in 113/n-Hexane Containing 2 x 10⁻³M Aerosol OT
(θ = 20.9°, reversal rate = 2 Hz, moisture content = 12 ppm)

Time (hours)	Slope (x 10 ³)	Slope SD (x 10 ³)	Intercept	Intercept SD	Correlation Coefficient	Probability of Linearity	Electrophoretic Mobility From Slope (-m ² s ⁻¹ V ⁻¹ x 10 ⁹)
24	9.18	1.44	-104.2	31.3	0.976	95%	11.7
48	6.09	0.77	-8.44	13.2	0.984	99%	7.78
72	5.77	0.46	-4.0	7.8	0.994	99%	7.37

Table 9.2 Linear Regression Analysis Results Obtained for the Relationship Between Frequency Shift and Applied Field for the Equilibration of 5 μm Hypersil ODS in 113/n-Hexane with 2 x 10⁻³M Aerosol OT
(θ = 20.9°, reversal rate = 2 Hz, moisture content = 12 ppm)

mean frequency shift against applied field was performed and the results are given in Table 9.2. Application of the t test to the mean electrophoretic mobilities in Table 9.1 shows a significant difference between the 24 and 48 hour values ($t = 10.99$, $p > 0.001$); no significant difference is found between the 48 and 72 hour results ($t = 1.58$, $p = 0.17$). However 'paired' t tests on the regression slopes produces no significant differences between any of the time points (24 hours vs 48 hours; $t = 1.89$, $p < 0.20$; 24 hours vs 72 hours; $t = 2.26$, $p < 0.05$; 48 hours vs 72 hours; $t = 0.36$, $p < 0.5$). What is noted is a reduction in the coefficient of variation of the slope (from 16 to 8%) and the number of standard deviations required for the intercept to pass through the origin. After 48 hours less than ± 1 standard deviation was required to pass through the origin, 72 hours was the period selected for which dispersions were allowed to equilibrate prior to testing.

In order to determine the effect of Aerosol OT concentration on measured electrophoretic mobility, six dispersions of 5 μm Hypersil ODS with varying Aerosol OT concentration were prepared from the same batch of dried 113/n-hexane. The electrophoretic mobility of the dispersions was then determined at 5 field strengths (2 Hz reversal rate), averaged spectra were collected from three replicate samples of each dispersion. Additionally, 2 samples of each dispersion were used to ensure that frequency shifts were independent of field reversal rate. The order in which the dispersions were studied was random. After a preliminary review of the data two additional Aerosol OT concentrations were studied; $0.05 \times 10^{-3} \text{M}$ and $0.5 \times 10^{-3} \text{M}$. The former proved difficult to study due to adhesion of the Hypersil ODS to the cuvette wall, for this reason only three field strengths and two switching frequencies were studied.

The assayed moisture contents of the solutions used to prepare the dispersions are summarised in Table 9.3; analysis of variance showed there to be no significant difference ($p < 0.05$) in the moisture content of these solutions. The mean moisture content was taken as 17 ppm.

The effect of field reversal rate on frequency shift is summarised in Table 9.4. With the exception of the dispersion containing $4 \times 10^{-3} \text{M}$ Aerosol OT, analysis of variance (Table 9.5) showed there to be no significant difference ($p < 0.05$) in frequency shift at different field reversal rates. The $4 \times 10^{-3} \text{M}$ Aerosol OT dispersion did produce a significant variation at $p = 0.05$, however since sample 2 of this dispersion produced the same frequency shift at both the 2 and 5 Hz reversal rate, any variation was considered to be of little practical significance.

Mean frequency shifts and electrophoretic mobilities are given in Table 9.6, the results of linear regression analysis of mean frequency shifts against applied fields are given in Table 9.7; all particles were negatively charged.

All dispersions exhibited a reasonable linear dependence between frequency shift and applied field; the intercepts in the case of 4 dispersions passed through the origin within ± 2 standard deviations, two of the remaining dispersions required ± 3 standard deviations. One dispersion ($8 \times 10^{-3} \text{M}$) required over ± 3 standard deviations, examination of the electrophoretic mobilities calculated at each field strength for this dispersion does not show a marked increase with increasing field strength.

It is believed that an intercept that does not pass close to the origin (ie ± 3 standard deviations) is indicative of a decoupling

Aerosol OT Concentration, (M x 10 ³)	Sample 1			Sample 2			Mean Water Content (ppm)
	Weight of Sample (g)	Assayed μg of Water	Water Content (ppm)	Weight of Sample (g)	Assayed μg of Water	Water Content	
0.05	1.9188	35	18.2	2.1326	37	17.3	18
0.50	2.1893	37	16.9	1.9447	32	16.5	17
1.00	2.0399	40	19.6	1.7454	28	16.0	18
2.00	1.9799	37	18.7	1.4997	26	17.3	18
4.00	2.1147	33	15.6	1.7652	29	16.4	16.
6.00	1.8419	29	15.7	2.0173	34	16.9	16
8.00	1.3905	26	18.7	1.9326	29	15.0	17
10.00	2.4537	42	17.1	1.5432	22	14.3	16

Table 9.3 Assayed Moisture Contents of Aerosol OT Solutions used to prepare Hypersil ODS and Salmefamol Dispersions

Source	Sum of Squares	Degrees of Freedom	Mean Square	F ratio	F 0.05
Between Samples	10.79	7	1.54	0.62	3.50
Within Samples	19.75	8	2.47		
Total	30.54	15			

Analysis of Variance (Table 9.3)

Initial Aerosol OT Concentration (M x 10 ³)	Applied Field (kV m ⁻¹)	Reversal Rate (Hz)	2	3	4	5	Mean	SD	CV
0.05	23.6	Sample 1	78.0	-	-	70.0	74.0	-	-
		-							
0.50	23.6	Sample 1	75.5	76.5	77.5	75.0	76.0	1.1	1.4
		Sample 2	76.0	76.0	77.5	77.0	76.5	0.8	1.0
1.00	25.5	Sample 1	105.0	103.0	104.0	103.0	104.0	1.0	1.0
		Sample 2	102.0	107.0	105.0	104.0	104.5	2.1	2.0
2.00	29.1	Sample 1	89.0	86.5	87.5	87.0	87.5	1.1	1.3
		Sample 2	87.0	87.5	88.0	88.5	88.0	0.6	0.7
4.00	30.9	Sample 1	86.5	83.0	81.0	84.0	83.5	2.3	2.8
		Sample 2	84.0	84.0	80.0	84.0	83.0	2.0	2.4
6.00	27.3	Sample 1	76.5	76.5	77.0	76.0	76.5	0.4	0.5
		Sample 2	76.0	74.5	75.0	76.5	75.5	0.9	1.2
8.00	29.1	Sample 1	62.5	63.5	62.0	63.0	63.0	0.6	1.0
		Sample 2	63.5	64.5	64.0	62.0	63.5	1.1	1.7
10.00	27.3	Sample 1	61.5	62.0	61.0	61.0	61.5	0.5	0.8
		Sample 2	62.0	63.0	61.5	62.0	62.0	0.6	1.0

(SD = Standard Deviation, CV = Coefficient of Variation (%))

Table 9.4 Variation in Frequency Shift With Field Reversal

Rate For Dispersions of Hypersil ODS in 11 γ /n-Hexane

With Aerosol OT

($\theta = 20.9^\circ$, moisture content = 17 ppm)

Source Initial Aerosol OT Concentration, (M x 10 ³)	Sum of Squares		Degrees of Freedom		Mean Square		F ratio F 0.05 = 6.59
	Between Frequencies	Within Samples	Between Frequencies	Within Samples	Between Frequencies	Within Samples	
0.5	3.62	2.25	3	4	1.21	0.56	2.16
1.0	3.37	13.50	3	4	1.12	3.37	0.33
2.0	1.12	3.75	3	4	0.38	0.94	0.40
4.0	24.34	4.12	3	4	8.11	1.03	7.87
6.0	0.75	4.25	3	4	0.25	1.06	0.24
8.0	2.37	3.50	3	4	0.79	0.88	0.90
10.0	1.75	1.25	3	4	0.58	0.31	1.87

Table 9.5 Summary of Analysis of Variance Results for the Variation of Field Reversal Rate with Dispersions of 5 μ m Hypersil ODS in 113/n-Hexane Containing Aerosol OT

Initial Aerosol OT Concentration, ($M \times 10^3$)	Applied Field ($kV m^{-1}$)	20.0	21.8	23.6	25.5	27.3	Mean	SD	CV
0.05	Mean Frequency Shift (Hz)	54.8	57.5	70.5	-	-	3.56	0.23	6.5
	SD (Hz)	2.5	3.5	9.2	-	-			
	CV	4.6	6.1	13.0	-	-			
	Electrophoretic Mobility ($-m^2 s^{-1} V^{-1} \times 10^9$)	3.50	3.37	3.81					
0.50	Mean Frequency Shift (Hz)	64.3	68.1	76.0	82.1	86.6	4.07	0.05	1.2
	SD (Hz)	0.6	0.6	0.8	0.6	0.8			
	CV	0.9	0.9	1.1	0.7	0.9			
	Electrophoretic Mobility ($-m^2 s^{-1} V^{-1} \times 10^9$)	4.11	3.99	4.11	4.11	4.05			
1.00	Mean Frequency Shift (Hz)	81.6	85.6	95.0	105.8	108.6	5.15	0.11	2.1
	SD (Hz)	4.8	2.3	3.9	2.6	0.5			
	CV	5.9	2.7	4.1	2.5	0.5			
	Electrophoretic Mobility ($-m^2 s^{-1} V^{-1} \times 10^9$)	5.21	5.01	5.14	5.30	5.08			
2.00	Applied Field ($kV m^{-1}$)	27.3	28.2	29.1	30.0	30.9	3.80	0.10	2.6
	Mean Frequency Shift (Hz)	79.0	81.3	88.2	90.7	93.7			
	SD (Hz)	0.5	0.8	1.0	0.6	0.8			
	CV	0.6	1.0	1.1	0.7	0.9			
	Electrophoretic Mobility ($-m^2 s^{-1} V^{-1} \times 10^9$)	3.70	3.68	3.87	3.86	3.87			

(SD = Standard Deviation, CV = Coefficient of Variation (%))

Table 9.6 Mean Frequency Shifts and Corresponding Electrophoretic Mobilities for $5 \mu m$ Hypersil ODS Dispersions in 113/n-Hexane with Aerosol OT
($\theta = 20.9^\circ$, reversal rate = 2 Hz, moisture content = 17 ppm)

Initial Aerosol OT Concentration ($M \times 10^3$)	Applied Field ($kV m^{-1}$)	27.3	28.2	29.1	30.0	30.9	Mean	SD	CV
4.00	Mean Frequency Shift (Hz)	73.5	74.8	78.8	82.6	85.1	3.47	0.06	1.7
	SD (Hz)	0.4	2.2	2.3	2.2	0.6			
	CV	0.5	2.9	2.9	2.7	0.7			
	Electrophoretic Mobility ($-m^2 s^{-1} V^{-1} \times 10^9$)	3.44	3.39	3.46	3.52	3.52			
6.00	Mean Frequency Shift (Hz)	77.5	80.9	81.5	87.3	88.4	3.65	0.05	1.4
	SD (Hz)	1.5	0.5	0.7	2.1	0.5			
	CV	1.9	0.6	0.9	2.4	0.6			
	Electrophoretic Mobility ($-m^2 s^{-1} V^{-1} \times 10^9$)	3.63	3.66	3.58	3.72	3.65			
8.00	Mean Frequency Shift (Hz)	59.4	61.4	63.5	67.0	70.3	2.82	0.06	2.1
	SD (Hz)	1.0	1.1	1.9	1.1	1.3			
	CV	1.7	1.8	3.0	1.6	1.8			
	Electrophoretic Mobility ($-m^2 s^{-1} V^{-1} \times 10^9$)	2.78	2.78	2.79	2.85	2.91			
10.00	Mean Frequency Shift (Hz)	61.8	66.4	67.5	69.5	72.4	2.96	0.05	1.7
	SD (Hz)	0.6	0.9	0.4	1.1	2.2			
	CV	1.0	1.4	0.6	1.6	3.0			
	Electrophoretic Mobility ($-m^2 s^{-1} V^{-1} \times 10^9$)	2.89	3.01	2.96	2.96	2.99			

(SD = Standard Deviation, CV = Coefficient of Variation (%))

Table 9.6 (Continued)

Initial Aerosol OT Concentration	Slope ($\times 10^3$)	Slope SD ($\times 10^3$)	Intercept	Intercept SD	Correlation Coefficient	Probability of Linearity	Electrophoretic Mobility From Slope ($m^2s^{-1}V^{-1} \times 10^9$)	SD	CV
0.05	ONLY 3 DATA POINTS								
0.50	3.20	0.19	0.29	4.53	0.995	>99.9%	4.09	0.24	5.9
1.00	4.06	0.41	-0.63	9.86	0.985	>99.0%	5.18	0.52	10.0
2.00	4.31	0.46	-38.87	13.32	0.984	>99.0%	5.50	0.59	10.7
4.00	3.44	0.29	-21.30	8.34	0.990	>99.0%	4.00	0.37	9.3
6.00	3.13	0.45	-8.06	13.17	0.970	>99.0%	4.00	0.57	14.3
8.00	3.04	0.23	-24.27	6.66	0.992	>99.0%	3.88	0.29	7.5
10.00	2.70	0.33	-11.05	9.64	0.978	>99.0%	3.45	0.42	12.2

(SD = Standard Deviation, CV = Coefficient of Variation (%))

Table 9.7 Linear Regression Analysis Results Obtained for the Relationship Between Frequency Shift and Applied Field from 5 μ m Hypersil OLS in 113/n-Hexane with Aerosol OT

($\theta = 20.9$, reversal rate = 2 Hz, moisture content = 17 ppm)

Initial Aerosol OT Concentration (M x 10 ³)	Initial Aerosol OT Concentration (M x 10 ³)					
	10.00	8.00	6.00	4.00	2.00	1.00
0.50	1.31	0.54	0.14	0.69	2.23	1.90
1.00	2.58	2.17	1.53	1.23	0.41	
2.00	2.84	2.47	1.83	1.60		
4.00	1.68	1.08	0.58			
6.00	0.77	0.18				
8.00	0.85					
					DF = 6	
					t 0.05 = 2.447	

A : Comparison of regression slopes (Table 9.7)

Initial Aerosol OT Concentration (M x 10 ³)	Initial Aerosol OT Concentration (M x 10 ³)					
	10.00	8.00	6.00	4.00	2.00	1.00
0.50	35.34	35.70	12.90	17.61	5.60	19.26
1.00	40.26	40.20	27.17	29.97	20.34	
2.00	17.39	19.33	3.02	6.60		
4.00	15.70	18.07	5.41			
6.00	22.52	24.17				
8.00	4.28					
					DF = 8	
					t 0.05 = 2.306	

B : Comparison of mean electrophoretic mobilities (Table 9.6)

Table 9.8 Summary of t test results for the Influence of Aerosol OT on the Electrophoretic Mobility of Hypersil ODS Dispersions in 113/n-Hexane

of the diffuse layer from the particle (section 8.4.2). Since increasing surfactant concentration would reduce the diffuse layer thickness (75), a progressive movement of the intercept away from the origin with increasing surfactant might be expected. Since this trend was not seen, significant decoupling was not considered to have been induced by the presence of the surfactant.

Analysis of the regression slopes using the t test (Table 9.8A) shows few significant differences. The $10 \times 10^{-3} \text{M}$ slope was significantly different from the $1 \times 10^{-3} \text{M}$ and $2 \times 10^{-3} \text{M}$ slopes, the latter also being significantly different than the $8 \times 10^{-3} \text{M}$ slope.

The variation of mean electrophoretic mobilities (Table 9.6) with surfactant concentration is shown in Figure 9.1. Analysis of these values using the t test show the values at all surfactant concentrations to be significantly different from each other (Table 9.8B). The electrophoretic mobilities show an initial increase in electrophoretic mobility with surfactant concentration, followed by a decline. The peak electrophoretic mobility corresponds to a zeta potential of -231 mV (equation 3.7, $f(\kappa a) = 1$).

9.1.2 DISPERSIONS OF SALMEFAMOL IN MODEL PROPELLANT

Dispersions of salmefamol were found to produce very poor quality spectral envelopes, requiring the averaging of 256 spectra to produce discernible frequency shifts; an example of which is shown in Figure 9.2A. A tendency for the envelope to flatten with time and disappear was noted. Examination of the signal form at all frequency settings revealed no well modulated signals as seen with Hypersil ODS dispersions (Figure 8.9B and 9.2B). Since frequency envelopes were best resolved at low field reversal rates, all observations were made at a 2 Hz field reversal rate, $\theta = 20.9^\circ$.

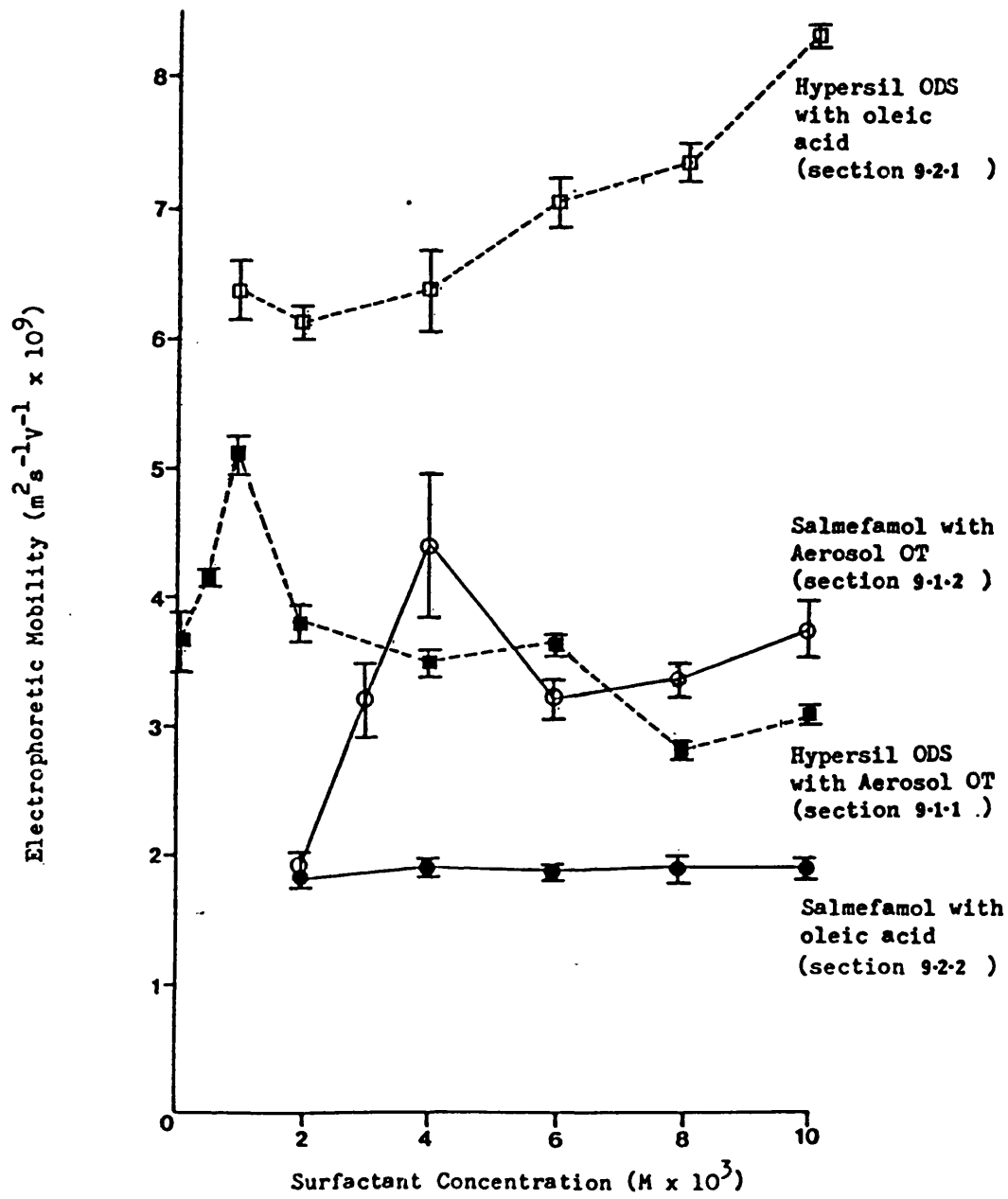


Figure 9.1 The Influence of Surfactant Concentration on the Electrophoretic Mobility of Hypersil ODS and Salmefamol Dispersed in 113/n-Hexane
(Error bar represents \pm one standard deviation)

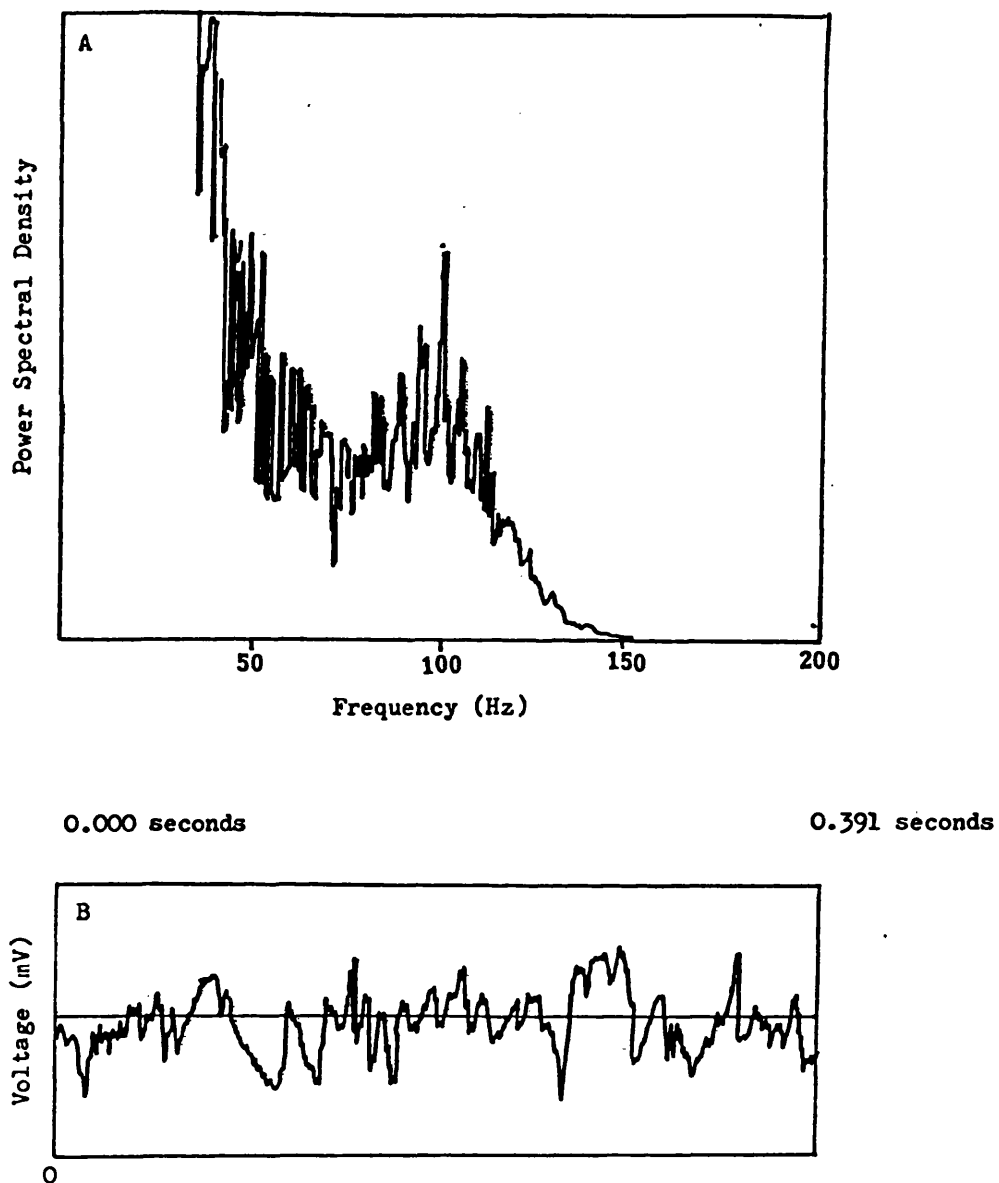


Figure 9.2 Spectra and Signal Forms Obtained from Salmefamol Dispersions.

($\theta = 20.9^\circ$, reversal rate = 2 Hz)

- A. Averaged (256) power spectrum from salmefamol dispersed in 113/n-hexane containing $4 \times 10^{-3}M$ Aerosol OT, 30 kV m^{-1} .
- B. Signal form from salmefamol dispersed in 113/n-hexane containing $2 \times 10^{-3}M$ Aerosol OT, 42 kV m^{-1} .

After preparation of the dispersions an equilibration period of 72 hours was allowed. Because of the problems experienced with salme-famol dispersions, each dispersion was studied at just three field strengths, averaged spectra were collected from three replicate individual samples at each of three field strengths. Six different concentrations of Aerosol OT were studied ranging from $2 - 10 \times 10^{-3}M$, the solutions were of the same batch as those used in section 9.1.1 (mean moisture content = 17 ppm). The $3 \times 10^{-3}M$ Aerosol OT solution was produced by 1 : 1 mixture of the $2 \times 10^{-3}M$ and $4 \times 10^{-3}M$ solutions and was studied after review of the preliminary data. At concentrations below $2 \times 10^{-3}M$ Aerosol OT, adhesion of the drug to the cuvette wall made measurements impossible. Treatment of the cuvette with 'Glass Treet' to remove any polar sites on the surface of the quartz produced no improvement.

All dispersions were found to contain negatively charged particles; frequency shifts and calculated electrophoretic mobilities are given in Table 9.9. The relationship between Aerosol OT concentration and mean electrophoretic mobility is shown in Figure 9.1. An increase in electrophoretic mobility to $4.4 \times 10^{-9} m^2 s^{-1} V^{-1}$ is seen at an initial surfactant concentration of $4 \times 10^{-3}M$ Aerosol OT. Application of the t test showed this electrophoretic mobility to be significantly different ($p > 0.05$) from those observed at all other surfactant concentrations, with the exception of $10 \times 10^{-3}M$ Aerosol OT (Table 9.10). Increasing the initial surfactant concentration from $4 \times 10^{-3}M$ to $6 \times 10^{-3}M$ led to a significant change ($p > 0.05$) in electrophoretic mobility to $3.2 \times 10^{-9} m^2 s^{-1} V^{-1}$; further increases in surfactant concentration produced no significant ($p < 0.05$) differences in electrophoretic mobility when comparing pairs of results using the t test. Using equation 3.7 the peak zeta potential noted was -192 mV.

Initial Aerosol OT Concentration ($K \times 10^3$)	Applied Field ($kV m^{-1}$)	47.2	50.6	53.9	Mean	SD	CV
2.00	Mean Frequency Shift (Hz)	65.8	75.7	81.7	1.88	0.09	4.8
	SD (Hz)	0.75	0.75	1.0			
	CV	1.1	1.0	1.2			
	Electrophoretic Mobility ($-m^2s^{-1}V^{-1} \times 10^9$)	1.78	1.91	1.94			
3.00	Applied Field ($kV m^{-1}$)	24.3	27.8	31.2	3.23	0.24	7.4
	Mean Frequency Shift (Hz)	58.3	76.2	76.5			
	SD (Hz)	1.5	1.8	3.1			
	CV	2.6	2.4	4.1			
	Electrophoretic Mobility ($-m^2s^{-1}V^{-1} \times 10^9$)	3.06	3.50	3.13			
4.00	Applied Field ($kV m^{-1}$)	23.4	26.7	30.1	4.38	0.51	11.6
	Mean Frequency Shift (Hz)	90.3	89.5	92.7			
	SD (Hz)	0.6	3.5	3.5			
	CV	0.7	3.9	3.8			
	Electrophoretic Mobility ($-m^2s^{-1}V^{-1} \times 10^9$)	4.93	4.28	3.93			

(SD = Standard Deviation, CV = Coefficient of Variation (%))

Table 9.9 Mean Frequency Shifts and Corresponding Electrophoretic Mobilities for Salmefamol Dispersions in 113/n-Hexane with Aerosol OT

($\theta = 20.9^\circ$, reversal rate = 2 Hz, moisture content = 17 ppm)

6.00	Initial Aerosol OT Concentration ($M \times 10^3$)	24.3	27.8	31.2	3.21	0.19	5.9
	Applied Field ($kV \ m^{-1}$)						
	Mean Frequency Shift (Hz)	58.5	74.7	76.8			
	SD (Hz)	0.9	1.0	2.4			
8.00	CV	1.5	1.3	3.1	3.36	0.16	4.8
	Electro-phoretic Mobility ($-m^2s^{-1}V^{-1} \times 10^9$)	3.07	3.43	3.14			
	Applied Field ($kV \ m^{-1}$)	27.8	31.2	34.7			
	Mean Frequency Shift (Hz)	71.5	79.5	96.2			
10.00	SD (Hz)	0.90	1.00	0.55	3.72	0.29	7.8
	CV	1.3	1.3	0.6			
	Electro-phoretic Mobility ($-m^2s^{-1}V^{-1} \times 10^9$)	3.28	3.25	3.54			
	Mean Frequency Shift (Hz)	84.7	94.7	91.8			
10.00	SD (Hz)	1.15	0.75	1.55	3.72	0.29	7.8
	CV	1.4	0.8	1.7			
	Electro-phoretic Mobility ($-m^2s^{-1}V^{-1} \times 10^9$)	3.89	3.88	3.38			
	Mean Frequency Shift (Hz)	84.7	94.7	91.8			

(SD = Standard Deviation, CV = Coefficient of Variation (%))

Table 9.9 (Continued)

Initial Aerosol OT Concentration (M x 10 ⁻²)	2.00	3.00	4.00	6.00	8.00
10.00	10.49	2.25	1.96	2.50	1.88
8.00	14.18	0.77	3.33	1.00	
6.00	11.08	0.10	3.73		
4.00	8.43*	3.56			
3.00	9.33				

DF = 4

$t_{0.05} = 2.776$

(except that marked * where DF = 2.1, $t_{0.05} = 4.30$
as variance ratio is $> F_{0.05}$)

Table 9.10 Summary of t test Results for the influence of
Aerosol OT on the Electrophoretic Mobility of
Salmefamol Dispersions in 113/n-Hexane

9.1.3 DISPERSIONS OF BETAMETHASONE VALERATE IN MODEL PROPELLANT

All attempts to show electrophoresis in dispersions of betamethasone valerate in 113/n-hexane failed; even with the addition of Aerosol OT in concentrations up to 10^{-2} M, it was not possible to obtain more than the occasional degraded spectral envelope. When obtained these were invariably unstable and not reproducible (Figure 9.3). Adhesion of the dispersed particles to the cuvette wall was a serious problem, in many cases occurring just adjacent to the edge of the electrodes. Treatment of the cuvette with Glass Treet produced little improvement in the degree of deposition, which was such that diffusion of the laser beams made velocimetry measurements unlikely.

Preliminary studies conducted with drug dispersions which had reduced particle size ranges (e.g. 90% having diameters between 2 and 4 μm), produced no improvement in the spectral envelope. The drug samples for these narrow size range dispersions were obtained by subdivision of the contents of an ^{aerosolised} Bextasol inhaler using an Anderson 2000 Particle Sizing Sampler.

9.2 Studies conducted with oleic acid

This section considers the role of oleic acid in the generation of surface potentials on particles dispersed in 113/n-hexane. Commercial grades of oleic acid contain significant quantities of fatty acids of differing chain length and degree of unsaturation. Typically 26% of Priolene 6952 is composed of fatty acids of chain lengths other than C18 (203). A proportion of the C18 fraction may be the trans isomer (elaidic acid) rather than oleic acid (cis isomer) (section 6.3.3). Such impurities may themselves be capable of charge generation or

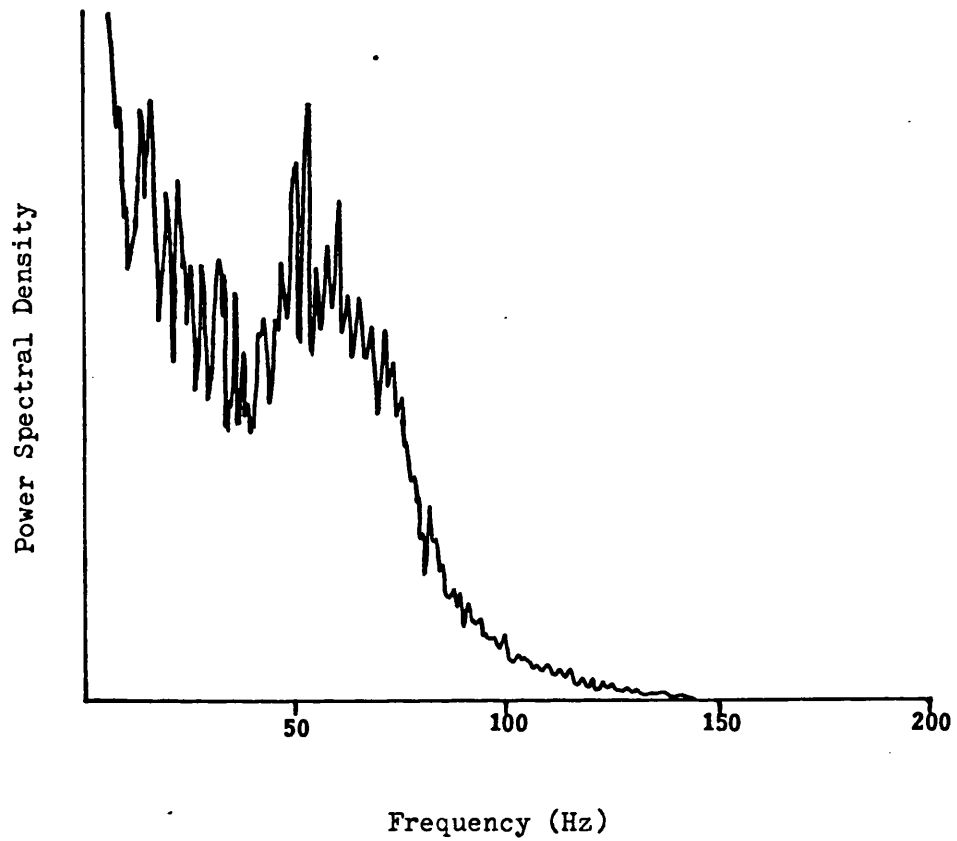


Figure 9.3 An Occasional Spectrum Collected from a Dispersion of Betamethasone Valerate Dispersed in 113/n-Hexane Containing 10×10^{-3} M Aerosol OT
(49 kV m^{-1} , $\theta = 20.9$, 2 Hz reversal rate)

preferential adsorption on to the particle surface and so complicate the system being studied. For this reason high purity oleic acid was used in this study.

9.2.1 DISPERSIONS OF HYPERSIL ODS IN MODEL PROPELLANT

Dispersions of Hypersil ODS containing Aerosol OT were equilibrated for 72 hours (section 9.2.1); this period was considered acceptable for oleic acid containing dispersions as it is nearly five times that determined by Ottewill and Tiffany (204) for dispersions of titanium dioxide in n-heptane. Deposition of Hypersil ODS particles on to the cuvette wall caused difficulties at all concentrations of oleic acid, however below $1 \times 10^{-3} \text{M}$ it was so severe that mobility measurements were not possible. Treatment of the cuvette wall with Glass Treet produced no discernible reduction in this deposition.

The spectral envelopes obtained were poor at all reversal rates; studies were generally conducted at a 2 Hz reversal rate. To ensure decoupling effects were not being seen, three samples of the dispersion containing $10 \times 10^{-3} \text{M}$ oleic acid were studied at various field reversal rates; no variation in frequency was noted (Table 9.11). Since decoupling is not noted at the highest surfactant concentration, where the diffuse layer thickness is the smallest (75), it will not be seen with lower surfactant concentrations.

To ensure that the moisture contents of all dispersions were constant, oleic acid solutions were all prepared from the same batch of dried 113/n-hexane. It was not possible to dry the oleic acid prior to use, because of the risk of oxidation. The assayed moisture content of the oleic acid was 368 ppm. Since the highest oleic acid concentration studied was 10^{-2}M there would be a difference of 0.9 ppm in the

Field Reversal Rate (Hz)	Determined Frequency Shift (Hz)					
	Sample Number			Mean	SD	CV
	1	2	3			
5	89.5	90.0	91.0	90.2	0.75	0.8
4	91.0	89.5	90.0	90.2	0.75	0.8
3	90.5	91.0	89.5	90.3	0.75	0.8
2	89.5	91.0	92.0	90.8	1.25	1.4

(SD = Standard Deviation, CV = Coefficient of Variation (%))

Table 9.11 Effect of Field Reversal Rate on Frequency Shift for Hypersil ODS Dispersions in 113/n-Hexane with 10×10^{-3} M Oleic Acid
($\theta = 20.9, 13.8 \text{ kV m}^{-1}$, moisture content = 20 ppm)

Source	Sum of Squares	Degrees of Freedom	Mean Square	F ratio	F 0.05
Between Samples	0.896	3	0.299	0.36	4.07
Within Samples	6.667	8	0.833		
Total	7.563	11			

Analysis of Variance (Table 9.11)

moisture content of the dispersions, over the range of concentrations studied. This variation was less than that seen between replicate samples in the assay and so was considered to be within the level of moisture control. Table 9.12 summarises the assayed moisture contents of those solutions, with analysis of variance showing no significant difference ($p < 0.05$) in moisture content between the different concentration solutions. The mean moisture content was taken to be 20 ppm.

Because of the possibility of oxidation of the oleic acid, all solutions were protected from light and the headspaces of all containers were flushed with dried nitrogen prior to being sealed.

The electrophoretic mobility of 5 dispersions, containing oleic acid in initial concentrations ranging from 1 to $10 \times 10^{-3} \text{M}$ were studied. In all cases the particles were negatively charged. Averaged spectra were collected from three replicate samples of each dispersion at 4 field strengths, the results are given in Table 9.13. The results of linear regression analysis of frequency shift against applied field are summarised in Table 9.14. The fit to the linear relationship was poorer than for the corresponding Aerosol OT containing dispersions (Table 9.7). In the case of the dispersions initially containing 1 and $6 \times 10^{-3} \text{M}$ oleic acid, it is open to question whether true electrophoresis was noted, as the intercept was over ± 5 standard deviations away from the origin. In the case of the initially $1 \times 10^{-3} \text{M}$ oleic acid containing dispersion, there was no ^{significant} increase in frequency shift with applied field (Table 9.13). 'Paired' t tests of the regression slopes showed there to be no significant difference between the remaining dispersions (Table 9.15A).

Oleic Acid Concentration (M x 10 ³)	Sample 1			Sample 2			Mean Water Content (ppm)
	Weight of Sample (g)	Assayed μ g of Water	Water Content (ppm)	Weight of Sample (g)	Assayed μ g of Water	Water Content (ppm)	
1.0	1.7321	26	15.0	2.4160	47	19.5	17.2
2.0	4.0978	80	19.5	1.2050	31	25.7	22.6
4.0	3.1537	64	20.3	1.0588	22	20.8	20.5
6.0	3.7306	78	20.9	1.3221	24	18.1	19.5
8.0	1.9427	40	20.6	1.0038	21	20.9	20.8
10.0	2.3026	44	19.1	1.6231	33	20.3	19.7

Table 9.12 Assayed Moisture Contents of Oleic Acid Solutions
Used to Prepare Hypersil ODS and Salmefamol Dispersions

Source	Sum of Squares	Degrees of Freedom	Mean Square	F ratio	F 0.05
Between Samples	31.01	5	6.20	1.09	4.39
Within Samples	34.15	6	5.69		
Total	65.17	11			

Analysis of Variance (Table 9.9)

Initial Oleic Acid Concentration (M x 10 ³)	Applied Field (kV m ⁻¹)	15.9	16.6	17.3	17.9	Mean	SD	CV
1.00	Mean Frequency Shift (Hz)	82.9	83.9	85.3	84.9	6.37	0.25	3.9
	SD (Hz)	1.05	2.65	1.50	2.00			
	CV	1.3	3.2	1.8	2.4			
	Electrophoretic Mobility (-m ² s ⁻¹ V ⁻¹ x 10 ⁹)	6.66	6.45	6.29	6.06			
2.00	Applied Field (kV m ⁻¹)	15.9	16.6	17.2	17.9	6.14	0.10	1.6
	Mean Frequency Shift (Hz)	76.1	78.9	84.6	85.4			
	SD (Hz)	4.20	3.20	4.95	2.80			
	CV	5.5	4.1	5.9	3.3			
	Electrophoretic Mobility (-m ² s ⁻¹ V ⁻¹ x 10 ⁹)	6.11	6.07	6.28	6.09			
4.00	Applied Field (kV m ⁻¹)	15.9	17.3	18.6	20.0	6.33	0.30	4.7
	Mean Frequency Shift (Hz)	79.0	80.0	94.3	103.5			
	SD (Hz)	9.60	4.10	8.30	8.15			
	CV	12.2	5.1	8.8	7.9			
	Electrophoretic Mobility (-m ² s ⁻¹ V ⁻¹ x 10 ⁹)	6.34	5.91	6.47	6.61			

(SD = Standard Deviation, CV = Coefficient of Variation (%))

Table 9.13 Mean Frequency Shifts and Corresponding Electrophoretic Mobilities for 5 μ m Hypersil ODS Dispersions in 113/n-Hexane with Oleic Acid ($\theta = 20.9^\circ$, reversal rate = 2 Hz, moisture = 20 ppm)

Initial Oleic Acid Concentration (M x 10 ³)	Applied Field (kV m ⁻¹)	15.9	16.6	17.2	17.9	Mean	SD	CV
6.00	Mean Frequency Shift (Hz)	84.9	89.5	95.5	102.5	7.03	0.22	3.1
	SD (Hz)	5.20	6.10	6.25	8.05			
	CV	6.1	6.8	6.5	7.9			
	Electrophoretic Mobility (-m ² s ⁻¹ V ⁻¹ x 10 ⁹)	6.82	6.89	7.09	7.31			
8.00	Applied Field (kV m ⁻¹)	13.8	15.2	15.9	16.6	7.30	0.20	2.7
	Mean Frequency Shift (Hz)	82.1	85.1	90.0	94.0			
	SD (Hz)	1.65	2.75	1.85	3.65			
	CV	2.0	3.2	2.1	3.9			
	Electrophoretic Mobility (-m ² s ⁻¹ V ⁻¹ x 10 ⁹)	7.60	7.15	7.23	7.23			
10.0	Applied Field (kVm ⁻¹)	13.8	14.5	15.2	15.9	8.28	0.09	1.1
	Mean Frequency Shift (Hz)	90.4	92.5	98.8	103.5			
	SD (Hz)	1.40	1.20	4.00	1.40			
	CV	1.5	1.3	4.0	1.4			
	Electrophoretic Mobility (-m ² s ⁻¹ V ⁻¹ x 10 ⁹)	8.37	8.15	8.30	8.31			

(SD = Standard Deviation, CV = Coefficient of Variation (%))

Table 9.13 (Continued)

Initial Oleic Acid Concentration ₃ (M x 10 ³)	Slope (x 10 ³)	Slope SD (x 10 ³)	Intercept	Intercept SD	Correlation Coefficient	Probability of Linearity	Electrophoretic Mobility from Slope (m ² s ⁻¹ V ⁻¹ x 10 ⁹)		
							Mean	SD	CV
1.00	1.12	0.38	65.2	6.4	0.904	> 90.0%	1.43	0.46	32.2
2.00	5.05	1.06	-4.1	17.9	0.959	> 95.0%	6.45	1.35	20.9
4.00	6.43	1.40	-26.3	25.2	0.956	> 95.0%	8.21	1.79	21.8
6.00	8.90	0.62	-57.3	10.5	0.995	> 99.0%	11.37	0.79	6.9
8.00	4.24	0.82	22.5	12.7	0.964	> 95.0%	5.41	1.05	19.4
10.00	6.51	0.83	-0.44	12.3	0.984	> 98.0%	8.31	1.06	12.8

(SD = Standard Deviation, CV = Coefficient of Variation (%))

Table 9.14 Linear Regression Analysis Results Obtained for the Relationship Between Frequency Shift and Applied Field from 5 μ m Hypersil ODS in 113/n-Hexane with Oleic Acid

(θ = 20.9°, reversal rate = 2 Hz, moisture 20 ppm)

Initial Oleic Acid Concentration (M x 10 ³)	10.00	8.00	6.00	4.00	2.00
1.00	5.90	3.45	10.70	3.66	3.49
2.00	1.08	0.60	3.14	0.79	
4.00	0.05	1.35	1.61		
6.00	2.31	4.53			
8.00	1.95				

DF = 4
t 0.05 = 2.776

A : Comparison of regression slopes (Table 9.14)

Initial Oleic Acid Concentration (M x 10 ³)	10.00	8.00	6.00	4.00	2.00
1.00	14.19	5.78	3.94	0.16	1.68
2.00	31.93	10.41	7.40	1.23*	
4.00	12.32	5.33	3.71		
6.00	10.48	1.84			
8.00	8.81				

* Variance ratio
> F_{0.05} : DF = 3.6
t 0.05 = 3.182
DF = 6
t 0.05 = 2.447

B : Comparison of mean electrophoretic mobilities (Table 9.13)

Table 9.5 Summary of t test Results for the Influence of Oleic acid on the Electrophoretic mobility of Hypersil ODS in 113/n-hexane

Mean electrophoretic mobilities (Table 9.13) for each dispersion were also compared by 'paired' t tests. No significant difference ($p < 0.05$) was noted between the dispersions which initially contained 1 and 4×10^{-3} M oleic acid. However dispersions which initially contained 6×10^{-3} M oleic acid or more, have significantly ($p > 0.05$) greater electrophoretic mobilities than the lower concentrations; with a tendency for increased surfactant concentration to produce an increased electrophoretic mobility. Figure 9.1 shows the relationship between mean electrophoretic mobility and initial oleic acid concentration. Using equation 3.7, $f(\kappa a) = 1$, the peak zeta potential observed was - 375mV.

9.2.2 DISPERSIONS OF SALMEFAMOL IN MODEL PROPELLANT

All salmefamol dispersions containing oleic acid were found to produce poor quality spectral envelopes of the type described in section 9.1.2 and shown in Figure 9.2.

After preparation of the salmefamol dispersions an equilibration period of 72 hours was allowed. As with the salmefamol dispersions containing Aerosol OT (section 9.1.2) it was only possible to assess electrophoretic mobility at three field strengths, with three individual samples being studied at each field strength (2 Hz reversal rate).

Dispersions containing five different oleic acid concentrations were examined, the solutions being of the same batch as used in section 9.2.1 (mean moisture content = 20 ppm). As with the Aerosol OT containing dispersions, at concentrations of less than 2×10^{-3} M, deposition made measurements impossible. Similarly treatment of the cuvette with Glass Treet produced no noticeable improvement.

Dispersions studied therefore initially contained oleic acid in concentrations ranging from $2 \times 10^{-3}M$ to $10 \times 10^{-3}M$.

All dispersions were found to be negatively charged; frequency shifts and calculated electrophoretic mobilities are given in Table 9.16.

No dispersion showed a marked increase in electrophoretic mobility with field strength, so true electrophoresis was considered to have been seen. Figure 9.1 shows the relationship between mean calculated electrophoretic mobility and initial oleic acid concentration.

Analysis of variance showed there to be no significant variation ($p < 0.05$) in mobility with concentration. The dispersions studied possessed zeta potentials of the order of -85 mV (equation 3.7, $f(\kappa a) = 1$).

Initial Oleic Acid Concentration ₃ (M x 10 ²)	Applied Field (kV m ⁻¹)	47.2	50.6	53.9	Mean	SD	CV
2.00	Mean Frequency Shift (Hz)	64.3	74.5	79.7	1.84	0.08	4.3
	SD (Hz)	3.1	1.8	1.5			
	CV	4.8	2.4	1.9			
	Electrophoretic Mobility (-m ² s ⁻¹ v ⁻¹ x 10 ⁹)	1.74	1.88	1.89			
4.00	Mean Frequency Shift (Hz)	70.5	74.5	77.5	1.88	0.04	2.1
	SD (Hz)	5.4	1.3	0.9			
	CV	7.7	1.7	1.2			
	Electrophoretic Mobility (-m ² s ⁻¹ v ⁻¹ x 10 ⁹)	1.91	1.88	1.84			
6.00	Mean Frequency Shift (Hz)	69.4	75.8	75.0	1.86	0.07	3.8
	SD (Hz)	2.1	2.8	1.0			
	CV	3.0	3.7	1.3			
	Electrophoretic Mobility (-m ² s ⁻¹ v ⁻¹ x 10 ⁹)	1.88	1.91	1.78			
8.00	Mean Frequency Shift (Hz)	71.7	75.7	74.0	1.87	0.10	5.3
	SD (Hz)	2.1	2.5	4.0			
	CV	2.9	3.3	5.4			
	Electrophoretic Mobility (-m ² s ⁻¹ v ⁻¹ x 10 ⁹)	1.94	1.91	1.75			
10.00	Mean Frequency Shift (Hz)	72.6	74.5	78.3	1.90	0.05	2.6
	SD (Hz)	4.7	4.5	2.5			
	CV	6.5	6.0	3.2			
	Electrophoretic Mobility (-m ² s ⁻¹ v ⁻¹ x 10 ⁹)	1.96	1.88	1.86			

(SD = Standard Deviation, CV = Coefficient of Variation (%))

Table 9.16 Mean Frequency Shifts and Corresponding Electrophoretic Mobilities for Salmefanol Dispersions in 113/n-Hexane with Oleic Acid

Source	Sum of Squares	Degrees of Freedom	Mean Square	F ratio	F 0.05
Between Samples	0.00663	4	0.00166	0.32	3.48
Within Samples	0.05227	10	0.00523		
Total	0.05889	14			

Analysis of Variance

CHAPTER 10ADSORPTION, SOLUBILITY AND DEPOSITION STUDIES10.1 Analytical techniques

10.1.1 A QUANTITATIVE ASSAY FOR AEROSOL OT

Assays for many anionic surfactants are based on colorimetric methods (205). For improved accuracy and decreased analysis times an HPLC method was developed for the quantitative assay of Aerosol OT.

Conditions used:

Column packing	-	5 μm Hypersil ODS
Mobile phase	-	60 : 40 v/v methanol/water at pH6 (25°C), adjustment made using 0.1N NaOH or HCl
Flow rate	-	1ml min^{-1}
Detection wavelength	-	225 nm, attenuation 0.08.
Column temperature	-	35°C
Chart speed	-	12 cm hr^{-1}

Method:

Injections of Aerosol OT solutions in mobile phase on to the column initially produced no peak. However, after repeated injections a small peak was seen to appear; it was concluded that marked adsorption of the surfactant on to the column was taking place. This was overcome by 'loading' the column with surfactant by recirculating mobile phase containing $5 \times 10^{-3}\text{M}$ Aerosol OT through the column overnight. During the 'loading', and subsequently to maintain column equilibrium, the column was kept at 35°C in a thermostatically controlled water bath. After 'loading', the mobile phase

was reconnected and left until the baseline output from the detector had returned to zero.

A calibration plot was obtained by injecting a series of Aerosol OT solutions in mobile phase, ranging from $0.5 \times 10^{-3} M$ to $2.4 \times 10^{-3} M$ in concentration, on to the column and determining the peak height of the trace obtained. A typical trace is shown in Figure 10.1A, the retention time of the Aerosol OT peak was 350 seconds. Three replicate injections were made for each solution; Table 10.1 summarises the obtained results along with the results of linear regression analysis of peak height versus surfactant concentration. Figure 10.2 gives the obtained calibration plot along with the regression line. The correlation coefficient of 0.999 indicates a good linear relationship, which can be considered to go through the origin, since the intercept passes through the origin within \pm one standard deviation .

The samples of Aerosol OT in 113/n-hexane to be assayed could not be injected directly on to the column, these solutions had therefore to be prepared prior to their assay. 10 ml samples of the solution for assay were evaporated to dryness using a sample concentrator. The residue was then redissolved in 10 ml of mobile phase and diluted, if appropriate, with further mobile phase. To ensure this process did not affect the final assay result, control 113/n-hexane solutions were tested in the same manner. Since no internal standard was used, a standard solution of $1 \times 10^{-3} M$ Aerosol OT in mobile phase was injected on to the column between each assay injection. The determined peak heights of this solution produced a mean recovery of 98.1% with a coefficient of variation of 2%. Two injections of each unknown were made and Aerosol OT concentration was calculated from the mean determined peak height using the regression line obtained from Figure 10.2.

OFF SCALE

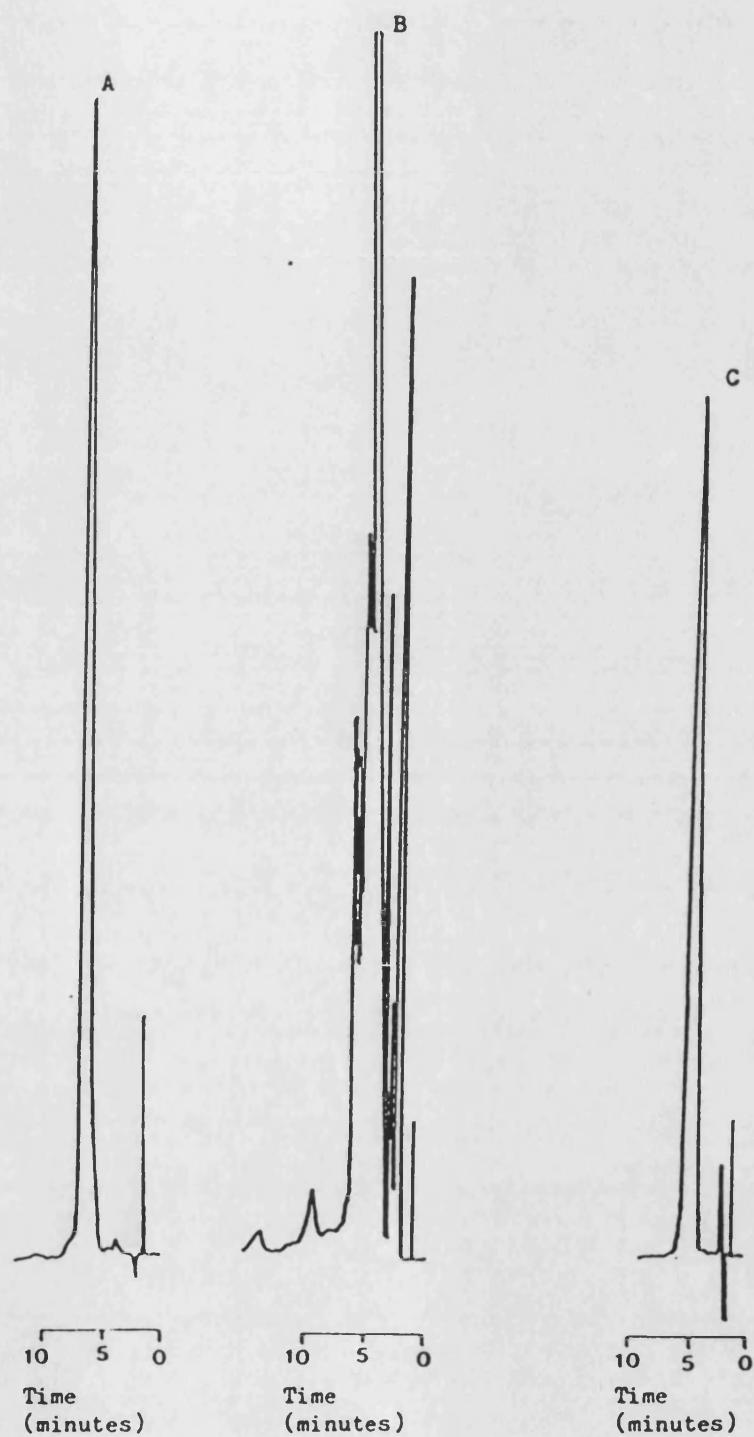


Figure 10.1 HPLC Traces Obtained from the Quantitative Assays of Aerosol OT (Photo reduced)

- A. 2×10^{-3} M Aerosol OT methanol solution using section 10.1.1 assay
- B. 2×10^{-3} M Aerosol OT methanol solution with traces of salmefamol using section 10.1.1 assay
- C. Above solution using section 10.1.2 assay

Aerosol OT Concentration M x 10 ³	Determined Peak Height (mm)					
	Determination Number			Mean	SD	CV
	1	2	3			
0.5	42.0	43.0	42.0	42.3	0.6	1.4
1.0	86.0	87.5	86.5	86.7	0.8	0.9
1.2	110.0	110.0	110.0	110.0	-	-
1.6	143.0	144.0	144.5	143.8	0.8	0.6
2.0	172.0	173.0	173.0	172.7	0.6	0.3
2.4	211.0	211.0	212.0	211.3	0.6	0.3

(SD = Standard Deviation, CV = Coefficient of Variation (%))

Table 10.1 Peak Heights Used for the Construction of the Calibration Plot for the Quantitative Assay of Aerosol OT in the Absence of Salmefamol

Slope (x 10 ⁻³)	87.9
Slope SD (x 10 ⁻³)	2.1
Slope RSD (%)	2.4
Intercept	0.30
Intercept SD	3.37
Correlation Coefficient	0.999

Linear regression analysis of mean peak height against Aerosol OT concentration.

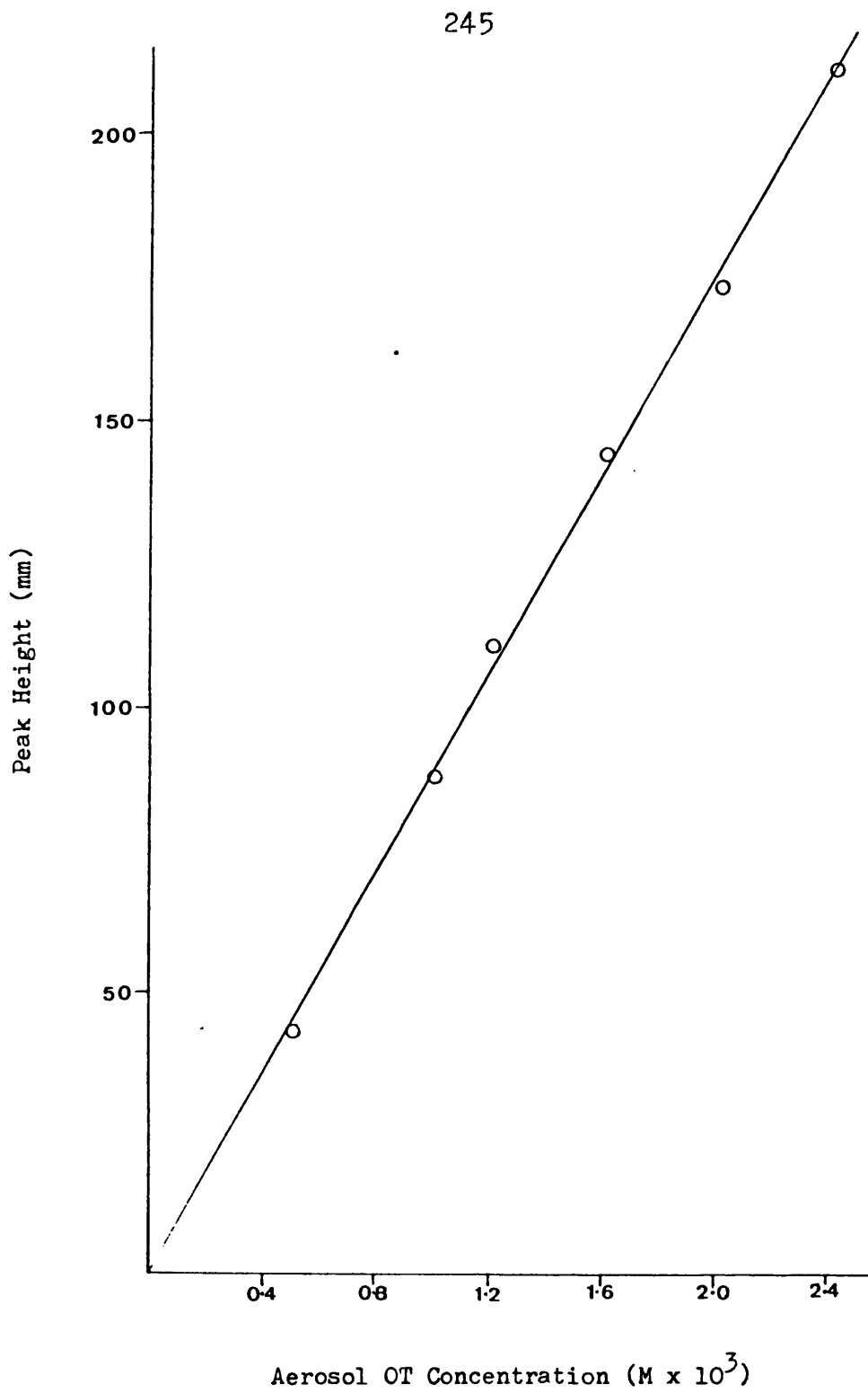


Figure 10.2 Calibration Plot for the HPLC Assay
of Aerosol OT in the Absence of
Salmefamol

10.1.2 A QUANTITATIVE ASSAY FOR AEROSOL OT IN THE PRESENCE OF SALMEFAMOL

The assay described in section 10.1.1 was found unsuitable for the quantitative assay of Aerosol OT in samples which contained traces of salmefamol. Such samples were obtained in the study of adsorption of Aerosol OT on to salmefamol (section 10.2.2) and produced large distorted peaks at the same retention time as the surfactant (Figure 10.1B). This was thought to be due to possible ion pair formation between the salmefamol and surfactant. For such samples an alternative assay was developed.

Conditions used:

Column packing	-	5 μm Hypersil ODS
Mobile phase	-	75 : 25 v/v methanol/water containing $5 \times 10^{-3}\text{M}$ tetra-n-butylammonium hydroxide (TBA) adjusted to $\text{pH}4$ using 0.1N NaOH or HCl
Flow rate	-	2 ml min^{-1}
Detection wavelength	-	215 nm, attenuation 0.08
Column temperature	-	35 $^{\circ}\text{C}$
Chart speed	-	12 cm hr^{-1}

Method:

The column was 'loaded' in the same manner as section 10.1.1. In this assay TBA is being used as an ion pairing agent to pair with the surfactant. Its relatively high concentration in the mobile phase swamps any effect from the drug. The retention time of the surfactant peak was 294 seconds and Figure 10.1C shows a typical trace.

It was necessary to ensure that the presence of salmefamol did not effect the peak height obtained. The peak heights from three replicate injections of $1.005 \times 10^{-3} \text{M}$ Aerosol OT in methanol in the presence, and absence, of 0.1 gml^{-1} salmefamol are recorded in Table 10.2. Application of the t test showed no significant difference in mean peak heights ($t = 0.38$, $p = 0.72$); it was therefore concluded that traces of salmefamol in the assay sample would not alter the assay result. A calibration plot was obtained in the same way as the previous assay, using a concentration range between $0.251 \times 10^{-3} \text{M}$ and $2.010 \times 10^{-3} \text{M}$ Aerosol OT in methanol; these results are also summarised in Table 10.2.

Figure 10.3 shows the calibration plot, which is clearly linear as confirmed by the results of the linear regression analysis given with Table 10.2. Solutions in mobile phase were prepared from the 113/n-hexane sample in the same manner as described in section 10.1.1. Since the calibration plot did not pass through the origin, two standard solutions ($1.005 \times 10^{-3} \text{M}$ and $2.010 \times 10^{-3} \text{M}$) were used. The order of injections on to the column was $S_1 S_1 S_2 S_2 U_1 U_1 U_2 U_2 U_3 U_3 S_1 S_1 S_2 S_2 \dots$ where S_1 and S_2 are standard solutions and $U_1 - U_3$ are three unknown solutions.

The Aerosol OT content of the unknown solutions was calculated from the mean determined peak heights using the regression line given with Table 10.2. The determined peak heights of the standard solutions produced mean recoveries of 101.6% and 98.2% for the $1.005 \times 10^{-3} \text{M}$ and $2.010 \times 10^{-3} \text{M}$ solutions respectively. Both solutions showed a coefficient of variation of below 1.5%.

Aerosol OT Concentration (M x 10 ³)	Determined Peak Height (mm)					
	Determination Number			Mean	SD	CV
	1	2	3			
1.005	70.5	71.0	70.0	70.5	0.5	0.7
1.005 plus 0.1 g ml ⁻¹ Salmefamol	70.0	71.0	71.0	70.7	0.6	0.8
0.251	20.5	21.0	21.0	20.8	0.3	1.4
0.503	38.0	38.0	39.0	38.3	0.6	1.5
0.804	59.0	57.0	57.0	57.7	1.2	2.0
1.206	81.5	82.5	83.0	82.3	0.8	1.0
1.608	108.0	109.0	109.0	108.7	0.6	0.6
2.010	132.0	131.0	129.0	130.7	1.5	1.1

(SD = Standard Deviation, CV = Coefficient of Variation (%))

Table 10.2 Results Used in Validation and Calibration Plot
for the Quantitative Assay of Aerosol OT in the
Presence of Salmefamol

Slope (x 10 ⁻³)	62.6
Slope SD (x 10 ⁻³)	0.9
RSD (%)	1.4
Intercept	6.6
Intercept SD	1.1
Correlation Coefficient	0.999

Linear regression analysis of mean peak height
against Aerosol OT concentration

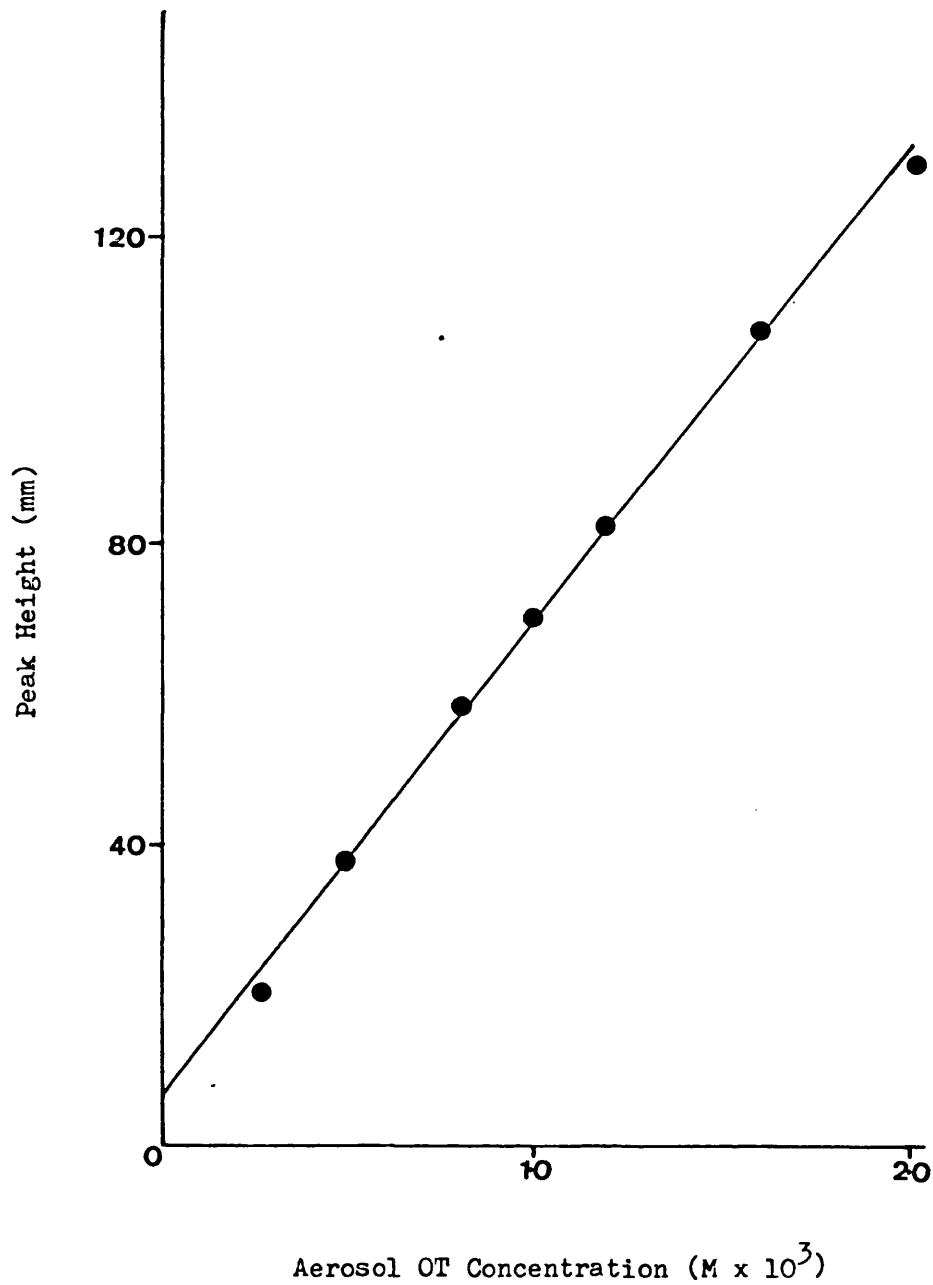


Figure 10.3 Calibration Plot of Peak Height Against Aerosol OT Concentration for the HPLC Assay of Aerosol OT in the Presence of Salmefamol

10.1.3 A QUANTITATIVE ASSAY FOR OLEIC ACID

Long chain fatty acids (greater than C12) are difficult to analyse by conventional gas chromatography (GC) because their peaks show severe tailing. To overcome this problem the acid is often derivatised to its methyl ester, a tedious process. Ottenstein and Supina (206) have reported separation of longer chain free fatty acids using a column packed with DEGS-PS (polydiethylene glycol adipate with H_2PO_4). It was found that whilst separation of the acids was possible by this method the peaks were rather broad and not suitable for a quantitative assay of solutions around $1 \times 10^{-3}M$ in concentration (Figure 10.4).

The capillary GC method described by Korhonen (207) appeared to be more suitable and was used in this study, with slight modifications to the conditions.

Conditions used:

CP Sil 5 - CB, 25 m capillary column

Injection and flame ionisation detector temperature - $275^{\circ}C$

Splitless injection of 1 μl samples

Helium carrier gas pressure - 25 psi

Column temperature, 1 minute at $37^{\circ}C$ subsequently rising at $30^{\circ}C/minute$ to $250^{\circ}C$ for 5 minutes.

Pure myristic acid was selected as a suitable internal standard for the assay with a retention time of 441 seconds; compared with 526 seconds for oleic acid. The internal standard had a concentration of $1.288 \times 10^{-3}M$ throughout. A series of solutions of oleic acid in a concentration range $5 \times 10^{-4}M$ to $2 \times 10^{-3}M$, all containing $1.288 \times 10^{-3}M$

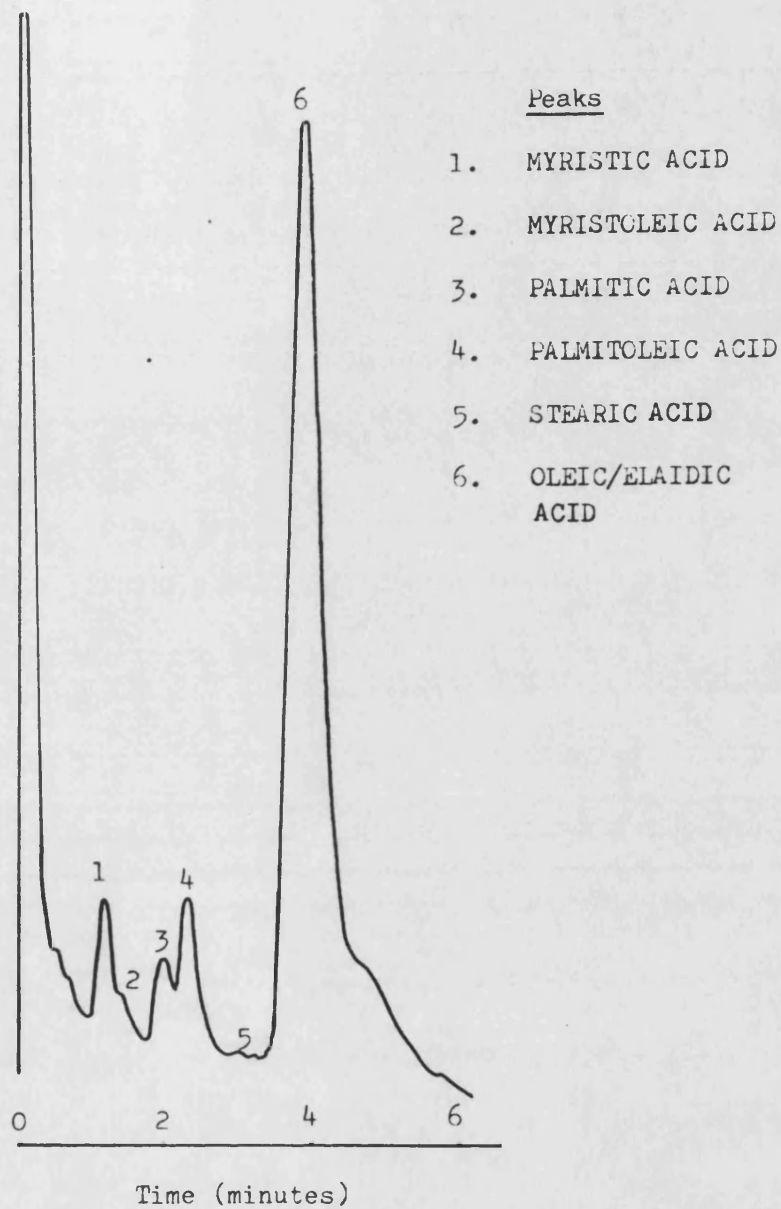


Figure 10.4 Gas Chromatogram of Priolene 6952 after the Method of Ottenstein and Supina (206)
(3 μ l 0.1% Priolene 6952 in n-hexane, 4' x 2 mm coloum packed with 5% DEGA-PS on Supelcoport. Oven = 190°C, N₂ = 25 ml min.⁻¹ injection = 200°C)

myristic acid, were made up in 113/n-hexane. Two 1 μ l injections of each solution were made on to the column and the peak heights of each component measured. A typical trace is shown in Figure 10.5. The ratio of oleic acid peak height to myristic acid peak height was calculated (Table 10.3) and the mean of the two injections was plotted against the oleic acid concentration (Figure 10.6). Linear regression analysis data is given with Table 10.3 and shows a linear dependence. The intercept passed through the origin within less than \pm one standard deviation.

To assay an unknown solution, 1 ml of 6.440×10^{-3} M myristic acid was pipetted into a 5 ml volumetric flask, to which sufficient unknown solution was added that when made to volume with 113/n-hexane, the concentration was between 0.5 and 2×10^{-3} M. After the injection of two samples on to the column, the peak height ratio was calculated. The oleic acid concentration was calculated from the mean peak height ratio using the regression line given with Table 10.3. A standard solution of 1.00×10^{-3} M oleic acid was injected on to the column throughout the assay, it produced a mean recovery of 98.2% with a coefficient of variation of 1.1%.

10.1.4 QUANTITATIVE ASSAY FOR SALMEFAMOL

The assay described here is a colorimetric method which is based upon one used for salbutamol (208).

Immediately before the assay the dimethyl p-phenylenediamine reagent was made up, first by dissolving 100 mg p-nitrosodimethylaniline in 100 ml of hot distilled water, 30 ml of this cooled, filtered solution was then shaken with 0.15 ml of 10% w/v copper sulphate solution and an

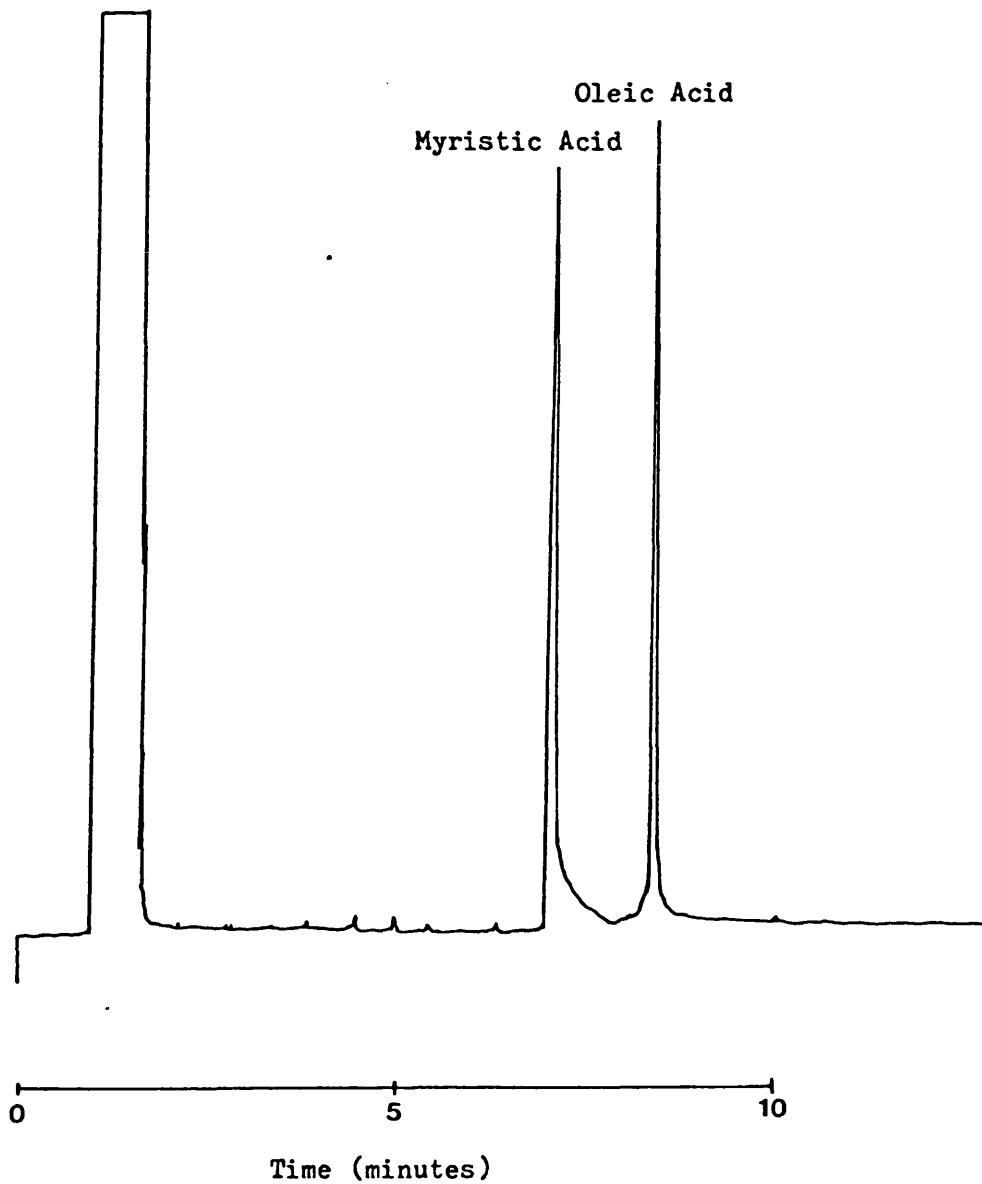


Figure 10.5 Typical Gas Chromatogram Obtained from the
Quantitative Assay of Oleic Acid by Gas
Chromatography, 1 μ l Injection of 1.5×10^{-3} M
Oleic Acid with 1.28×10^{-3} M Myristic Acid
Internal Standard

Oleic Acid Concentration (M x 10 ³)	Peak Height Ratio (oleic/myristic)		
	Determination Number		Mean
	1	2	
0.50	0.333	0.342	0.338
0.80	0.573	0.573	0.573
1.00	0.639	0.644	0.642
1.20	0.798	0.764	0.781
1.50	1.024	1.051	1.038
2.00	1.298	1.340	1.319

Table 10.3 Results Used for the Construction of the Calibration Plot for the Quantitative Assay of Oleic Acid

Slope	657.2
Slope SD	26.6
Slope RSD (%)	4.0
Intercept	0.015
Intercept SD	0.034
Correlation Coefficient	0.997

Linear regression analysis of mean peak height against oleic acid concentration

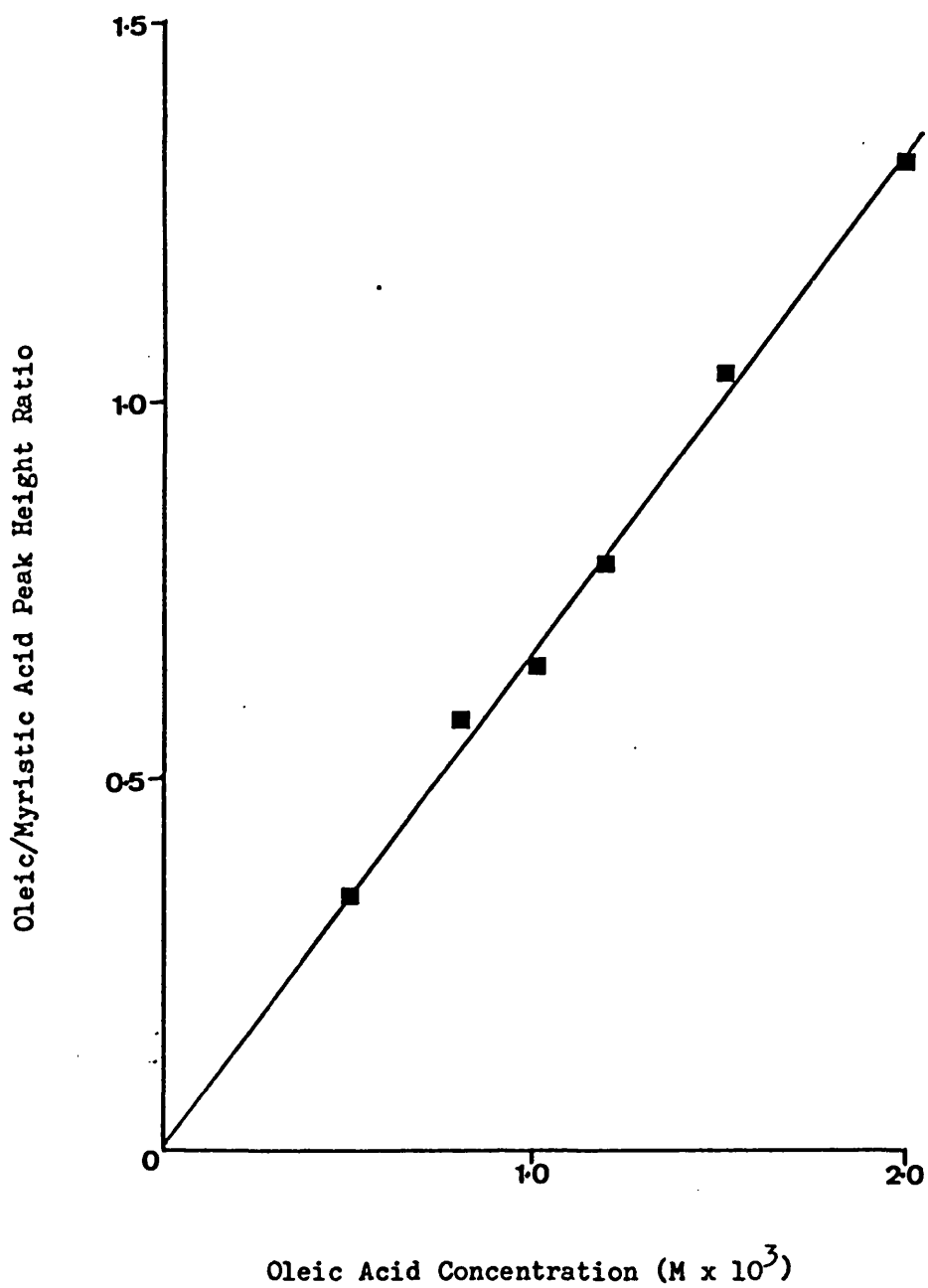


Figure 10.6 Calibration Plot for the Quantitative Assay of Oleic Acid by Gas Chromatography with a Myristic Acid ($1.28 \times 10^{-3}M$) Internal Standard in 113/n-Hexane

excess quantity of powdered zinc was slowly added until the solution was colourless. The solution was filtered before use.

The sample to be assayed, in methanol and of sufficient volume to contain between 5 and 50 μg salmefamol, was placed in a 50 ml separating funnel. If necessary the solution was made up to 20 ml with distilled water. The separating funnel was wrapped in aluminium foil to protect the solution from light. 1 ml of 5% w/v sodium bicarbonate solution, 1 ml of the dimethyl p-phenylenediamine reagent and 1 ml of 8% w/v potassium ferricyanide solution was added and mixed well. After standing for exactly 15 minutes, the solution was extracted using two 4.5 ml volumes of chloroform; the extract being filtered through small plugs of chloroform washed cotton wool. These plugs were then washed with more chloroform, the solution being used to make the extracted solution up to 10 ml.

The absorbance of the solution in a 10 mm cell was then determined at 605 nm, against a blank which consisted of the chloroform extract of a sample of methanol which had been assayed in the manner previously described.

To construct a calibration plot, appropriate volumes of a methanol solution of salmefamol ($1 \mu\text{g ml}^{-1}$) were assayed and the determined adsorbance plotted against salmefamol content (Table 10.4 and Figure 10.7). Linear regression analysis shows the plot to be linear and pass through the origin, since the intercept passes through zero within \pm one standard deviation.

To determine the reproducibility of the assay, standard samples containing 25 μg of salmefamol were regularly assayed throughout the assay period. The mean recovery of these samples was 99.9%

Salmefamol content (μg)	Absorbance of 605 nm					
	Sample Number			Mean	SD	CV
	1	2	3			
5	0.040	0.043	0.040	0.041	0.002	4.9
10	0.082	0.079	0.081	0.081	0.002	2.5
15	0.111	0.124	0.126	0.120	0.008	6.7
20	0.153	0.150	0.159	0.154	0.005	3.2
30	0.235	0.236	0.235	0.235	0.001	0.4
40	0.317	0.316	0.311	0.315	0.003	1.0
50	0.387	0.391	0.391	0.390	0.002	0.5

(SD = Standard Deviation, CV = Coefficient of Variation (%))

Table 10.4 Results Used for Calibration Plot for the
Quantitative Assay of Salmefamol

Slope	7770
Slope SD	50
Slope RSD(%)	0.6
Intercept ($\times 10^3$)	2.15
Intercept SD ($\times 10^3$)	1.43
Correlation Coefficient	0.999

Linear regression analysis of absorbance against
salmefamol concentration

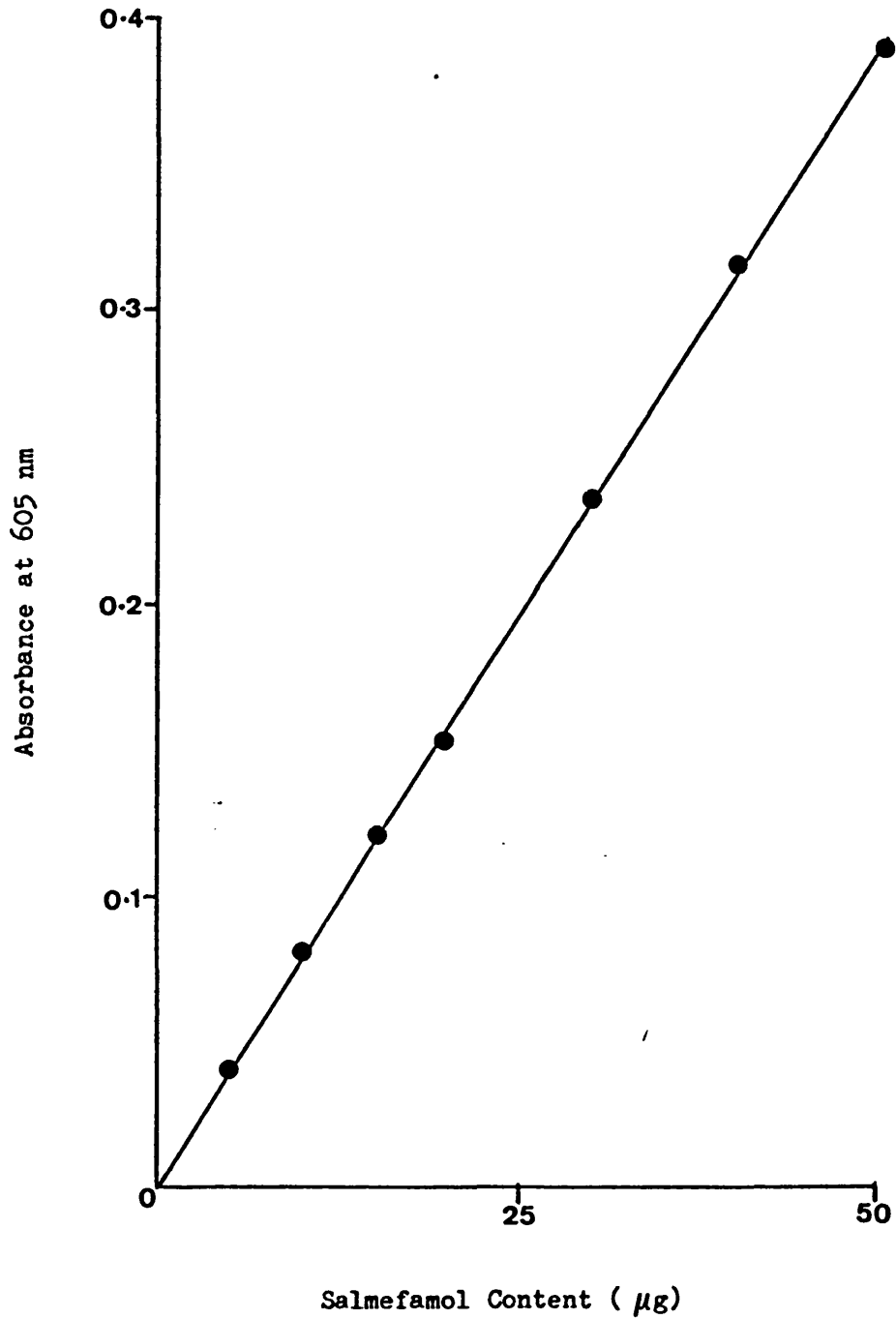


Figure 10.7 Calibration Plot for the Colorimetric Assay of Salmefamol

with a coefficient of variation of less than 0.5%.

10.2 Adsorption studies

In chapter 9 the influence of surfactant concentration on electrophoretic mobility was studied. In order to start to consider the mechanism by which a surfactant might influence the electrophoretic mobility of a dispersed particle, it is necessary to know whether the surfactant is capable of adsorption on to its surface. A series of experiments was therefore conducted to elucidate whether such adsorption was possible.

10.2.1 ADSORPTION OF AEROSOL OT ON TO HYPERSIL ODS FROM 113/N-HEXANE

Approximately 1 g samples, accurately weighed, of dried 5 μm Hypersil ODS were placed into dried 50 ml screw capped centrifuge tubes, and 20 mls of 113/n-hexane solutions of Aerosol OT in concentrations ranging from 1 to $5 \times 10^{-3}\text{M}$ were added. These solutions were made from part of the same batch of dried 113/n-hexane as used in the electrophoresis studies (section 9.1.2). Dispersions were prepared inside a dry glove box and the tubes were sealed with a screw cap; a teflon disc was inserted into each cap to stop solvent 'creep'. The tubes were then wrapped and sealed in several layers of Nescofilm and then polyethylene sheet. The tubes were then placed in an ultrasonic bath for 30 minutes to disperse the Hypersil ODS. The tubes containing the dispersions were then placed in a shaking water bath and left to equilibrate for 72 hours at 20°C . It was found necessary to mount the tubes at approximately 45° to ensure the dispersion did not sediment out. For each dispersion prepared a control tube, containing just the Aerosol OT solution, was treated in exactly the same manner.

After equilibration, the contents of the tubes were transferred to two 10 ml centrifuge tubes and the supernatant was collected after centrifugation at 2,500 rpm for 10 minutes. Temperature control was not possible during centrifugation; as the Hypersil ODS had started to form a plug within the first two of minutes of centrifugation, variation in temperature was not expected to produce a marked effect on the final result. 10 ml volumes of the supernatant were prepared and assayed for Aerosol OT as described in section 10.1.1, two injections being made for each solution.

The results of this experiment are summarised in Table 10.5 and Figure 10.8; the theoretical surface area of the Hypersil ODS is based upon a specific surface area value of $200 \text{ m}^2 \text{ g}^{-1}$ (209). Because of the porous nature of the Hypersil ODS, it was unclear whether the total surface area would be available to the Aerosol OT molecule. The theoretical monolayer coverage quoted assumes all the area is available and the Aerosol OT molecule occupies $60 \times 10^{-20} \text{ m}^2$ at monolayer coverage (95).

The recovery from control solutions ranged from 100.2 to 101.3%, a variation which can be attributed to analytical error (section 10.1.1). Thus it was concluded that adsorption on to the Hypersil ODS had been observed, rather than loss on to the glassware or during sample preparation. This conclusion is supported by the observation that Aerosol OT was probably capable of being adsorbed on to an HPLC column packed with Hypersil ODS (section 10.1.1). Figure 10.8 shows the amount of Aerosol OT adsorbed for the various surfactant concentrations, a steady increase is seen up to an initial concentration of $4 \times 10^{-3} \text{ M}$. The significance of the decline observed between the $4 \times 10^{-3} \text{ M}$ and $5 \times 10^{-3} \text{ M}$ solutions is unclear being most likely attributable to experimental scatter.

		Dispersion Number				
		1	2	3	4	5
Weight of Hypersil ODS (g)		0.9948	0.9521	0.9132	1.0236	1.1158
Aerosol OT Concentration ($M \times 10^3$)	Initial	1.00	2.00	3.00	4.00	5.00
	Assayed Control	1.01	2.02	3.04	4.01	5.01
	Assayed Supernatant	0.00	0.05	0.00	0.36	1.98
Fractional Monolayer Coverage Available		0.036	0.076	0.119	0.141	0.162
Aerosol OT Depleted in Adsorption Experiment ($M \times 10^5$)		2.00	3.90	6.00	7.28	6.04
Adsorption of Aerosol OT per gram of Hypersil ODS ($M g^{-1} \times 10^5$)		2.01	4.10	6.57	7.11	5.41
Theoretical Surface Area occupied by an Aerosol OT molecule ($M^2 \times 10^{17}$)		1.65	0.81	0.51	0.47	0.61

Table 10.5 Summary of Results Obtained for Adsorption of Aerosol OT on to Hypersil ODS from 113/n-hexane

(moisture content = 17 ppm, specific surface area of Hypersil ODS taken as $200 m^2 g^{-1}$, area occupied by Aerosol OT molecule at monolayer coverage = $60 \times 10^{-20} m^2$)

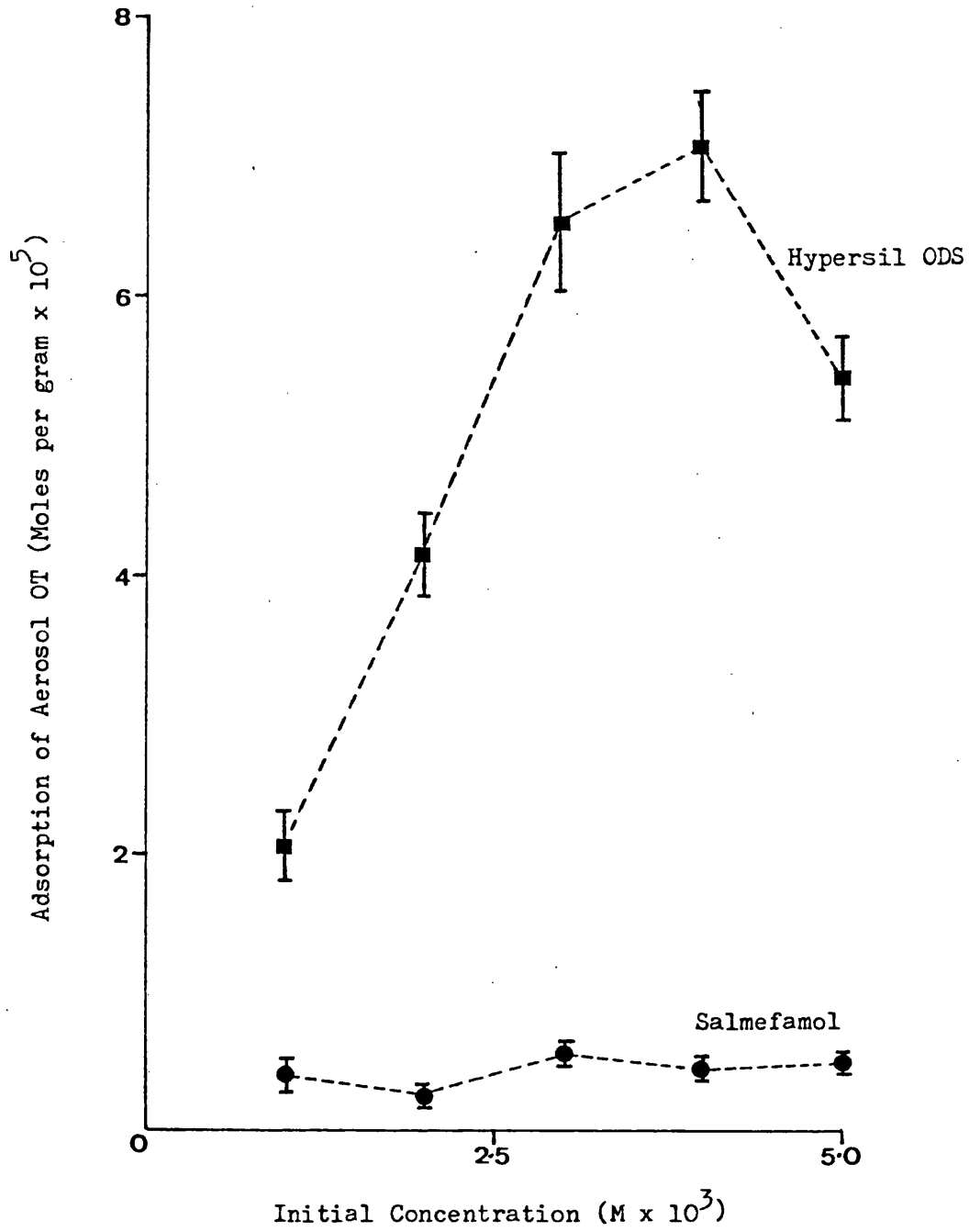


Figure 10.8 Variation in Quantity of Aerosol OT Adsorbed
on to Hypersil ODS and Salmefamol with Varying
Aerosol OT Concentration
(error bar represents \pm one standard deviation)

The smallest area occupied by an Aerosol OT molecule was $4.7 \times 10^{-18} \text{ m}^2$ which is markedly larger than the monolayer coverage value of $60 \times 10^{-20} \text{ m}^2$ quoted in the literature (95). This is however to be expected since monolayer coverage in this experiment was not possible, as insufficient quantities of Aerosol OT were available from solution.

10.2.2 ADSORPTION OF AEROSOL OT ON TO SALMEFAMOL FROM 113/N-HEXANE

To determine whether Aerosol OT was adsorbed on to dried salmefamol from 113/n-hexane an adsorption study was conducted using the method outlined in section 10.2.1. As in that section the mean water content of the solutions used to prepare the dispersions was 17 ppm.

Because of the low specific surface area of the micronised salmefamol ($2.7 \times 10^3 \text{ m}^2 \text{ kg}^{-1}$) when compared with the Hypersil ODS, it was necessary to prepare dispersions containing 3 g of drug in 15 ml of surfactant solution. Separation of the two phases by centrifugation was difficult; instead the tubes were allowed to stand for approximately 8 hours at 20°C , the supernatant then being removed using a pipette. A quantity of salmefamol was still 'carried over', so the supernatant was then passed through a $0.47 \mu\text{m}$ pore size teflon membrane filter. 10 mls of the supernatant was then prepared for assay as in section 10.1.1 and assayed using the method described in section 10.1.2.

The results are summarised in Table 10.6 and Figure 10.8. The recovery from the control solutions ranged from 96.0 to 99.7%, the lower end of this range cannot be accounted for by analytical error (section 10.1.2). This indicates that slight depletion of Aerosol OT had occurred in the control solution. In view of this the depletion of Aerosol OT in the supernatant was calculated taking into account the control tube content. The minimum area occupied by a single

		Dispersion Number				
		1	2	3	4	5
Weight of Salmefamol (g)		2.9924	3.0066	2.9815	3.0128	2.9943
Aerosol OT Concentration ($M \times 10^3$)	Initial	1.00	2.00	3.00	4.00	5.00
	Assayed Control	0.96	1.99	2.92	3.86	4.984
	Assayed Supernatant	0.23	1.45	1.88	3.00	4.03
Fractional Monolayer Coverage Available		0.67	1.34	2.02	2.67	3.35
Aerosol OT Depleted in Adsorption Experiment ($M \times 10^5$)		1.10	0.81	1.56	1.29	1.43
Adsorption of Aerosol OT per gram of Salmefamol ($M g^{-1} \times 10^5$)		0.37	0.27	0.52	0.43	0.48
Theoretical surface Area Occupied by an Aerosol OT molecule ($m^2 \times 10^{19}$)		12.3	16.6	8.6	10.5	9.4

Table 10.6 Summary of Results Obtained for Adsorption of Aerosol OT on to Salmefamol from 113/n-hexane

(moisture content = 17 ppm, specific surface area of salmefamol = $2.7 m^2 g^{-1}$, area occupied by Aerosol OT molecule at monolayer coverage = $60 \times 10^{-20} m^2$)

Aerosol OT molecule was $86 \times 10^{-20} \text{ m}^2$, a figure approaching the $60 \times 10^{-20} \text{ m}^2$ value cited in the literature (95). From Figure 10.8 it can be seen that the general trend was for increased amounts of surfactant to be adsorbed with increasing surfactant concentration, although a degree of experimental scatter was noted.

10.2.3 ADSORPTION OF OLEIC ACID ON TO HYPERSIL ODS FROM 113/N-HEXANE

In order to determine whether oleic acid was adsorbed onto Hypersil ODS from 113/n-hexane an adsorption experiment was conducted. The method used was the same as that in section 10.2.1, with the exception that 0.5 g samples of Hypersil ODS were used and the oleic acid concentration ranged from 0.9 to $4.5 \times 10^{-3} \text{ M}$. Additionally the tubes were protected from light and their headspaces were flushed with dry nitrogen prior to sealing. The dried batch of 113/n-hexane used was the same as that used for the electrophoresis study (section 9.2). The supernatant and control solutions were additionally passed through a $0.47 \mu\text{m}$ pore size teflon membrane filter.

As in section 10.2.1 a control tube, containing just oleic acid solution, was treated in exactly the same manner as the corresponding dispersion. The supernatant and control solutions were assayed for oleic acid as in section 10.1.3.

The results of the experiment are summarised in Table 10.7. The theoretical monolayer coverage assumes the oleic acid molecule to occupy $90.5 \times 10^{-20} \text{ m}^2$, which corresponds to a horizontal orientation of the molecule (204). An orientation with two points of contact (double bond and carboxylic acid group) occupying $48 \times 10^{-20} \text{ m}^2$ might be considered more likely, but might have led to an over-estimate of the amount of oleic acid required to produce a monolayer.

		Dispersion Number				
		1	2	3	4	5
Weight of Hypersil ODS (g)		0.5121	0.5454	0.5047	0.5105	0.5108
Oleic Acid Concentration (M x 10 ³)	Initial	0.90	1.80	2.71	3.61	4.51
	Assayed Control	0.91	1.89	2.71	3.49	4.47
	Assayed Supernatant	0.68	1.69	2.30	3.25	4.28
Fractional Monolayer Coverage Available		0.095	0.180	0.293	0.385	0.481
Oleic Acid Depleted in Adsorption Experiment (M x 10 ⁶)		4.4	2.2	8.2	7.2	4.6
Adsorption of Oleic Acid per gram of Hypersil ODS (M g ⁻¹ x 10 ⁶)		8.6	4.0	16.2	14.1	9.0
Theoretical Surface Area Occupied by an Oleic Acid Molecule (m ² x 10 ¹⁷)		3.86	8.23	2.04	2.35	3.69

Table 10.7 Summary of Results Obtained for Adsorption of Oleic Acid on to Hypersil ODS from 113/n-hexane

(moisture content = 20 ppm, specific surface area of Hypersil ODS = 200 m² g⁻¹, area occupied by oleic acid molecule at monolayer coverage = 90.5 x 10⁻²⁰ m²)

As in section 10.2.1 a value of $200 \text{ m}^2 \text{ g}^{-1}$ was taken for the specific surface area of the $5 \text{ }\mu\text{m}$ Hypersil ODS.

The recovery from the control tubes ranged from 96.7 to 105%.

A small amount of oleic acid was adsorbed onto the Hypersil ODS. This is shown in Figure 10.9, where no general trend in the amount adsorbed with respect to initial surfactant concentration was noted. The relatively large calculated area occupied by the oleic acid molecule indicates either that monolayer coverage was not obtained, or a large percentage of the Hypersil ODS was not accessible to the oleic acid molecule, possibly because of steric restrictions.

10.2.4 ADSORPTION OF OLEIC ACID ON TO SALMEFAMOL FROM 113/N-HEXANE

To determine whether oleic acid was adsorbed on to dried salmefamol, an adsorption study was conducted using oleic acid solutions ranging in concentration from 0.90 to $4.51 \times 10^{-3} \text{ M}$ and the method in section 10.2.2. The supernatant solutions were assayed for oleic acid as described in section 10.1.3.

Table 10.8 summarises the results of the study; theoretical monolayer coverages assume horizontal orientation of the oleic acid molecule and a specific surface area of $2.7 \times 10^3 \text{ m}^2 \text{ kg}^{-1}$. Whilst the recovery from the control solutions ranged from 96.3 to 103.8%, no oleic acid was recovered from any of the supernatant solutions. For this depletion to have been entirely due to adsorption on to the salmefamol would have required multilayer adsorption. Even with the minimum area of $26 \times 10^{-20} \text{ m}^2$ which an oleic acid molecule can occupy (vertical orientation) (204), multilayer adsorption would have occurred in the tube containing $4.5 \times 10^{-3} \text{ M}$ oleic acid.

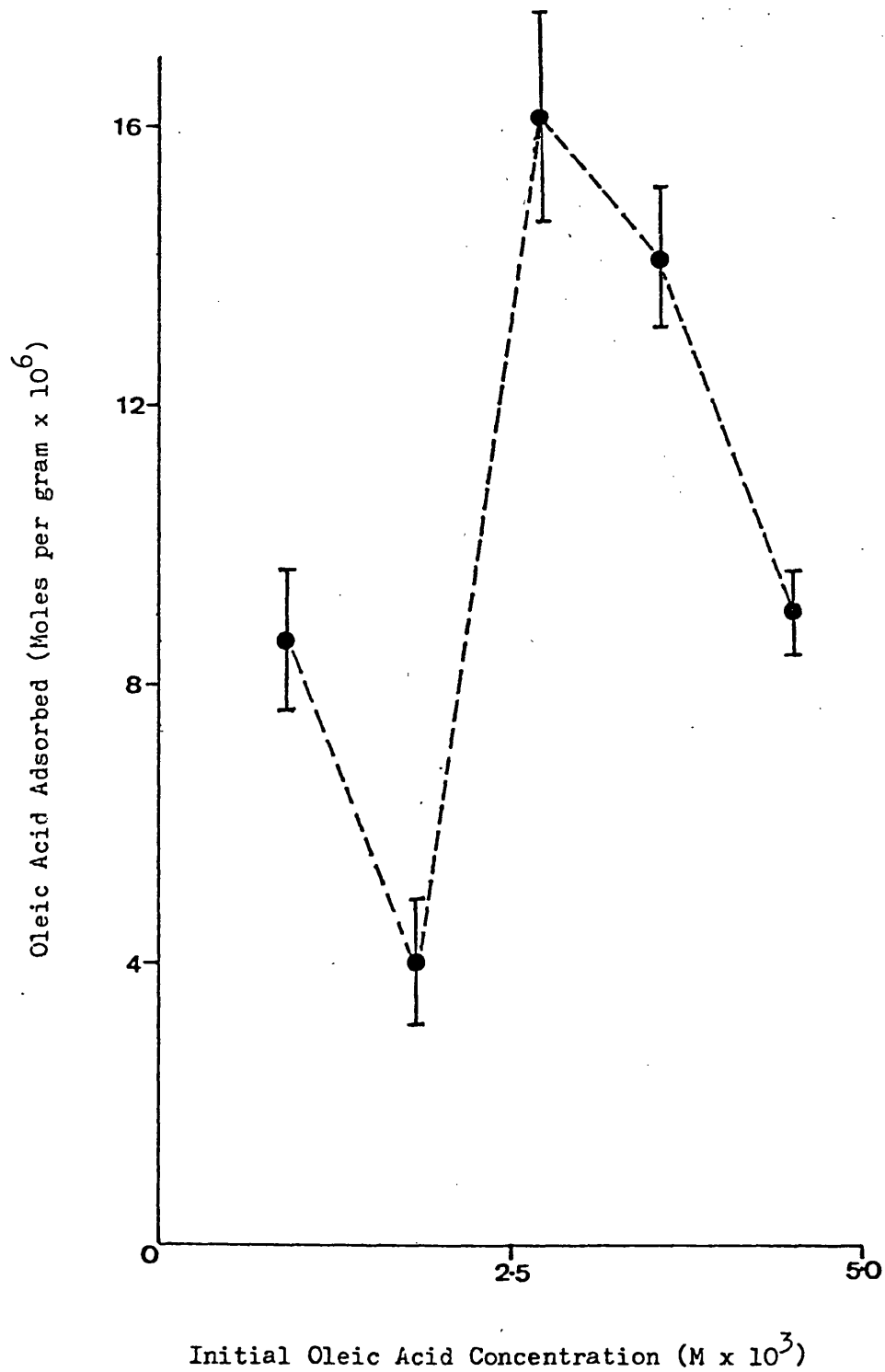


Figure 10.9 Variation in Quantity of Oleic Acid Adsorbed on to Hypersil ODS with Varying Oleic Acid Concentration (error bar represents \pm one standard deviation)

		Dispersion Number				
		1	2	3	4	5
Weight of Salmefamol (g)		3.0379	2.9985	2.9943	3.0083	3.0191
Oleic Acid Concentration (M x 10 ³)	Initial	0.90	1.80	2.71	3.61	4.51
	Assayed Control	0.93	1.87	2.71	3.48	4.55
	Assayed Supernatant	0.00	0.00	0.00	0.00	0.00
Fractional Monolayer Coverage Available		0.90	1.82	2.74	3.63	4.52
Oleic Acid Depleted in Adsorption Experiment (M x 10 ⁵)		1.35	2.70	4.07	5.42	6.77
Adsorption of Oleic Acid per gram of Salmefamol (M g ⁻¹ x 10 ⁶)		4.4	9.0	13.6	18.0	22.4
Theoretical Surface Area Occupied by an Oleic Acid Molecule (m ² x 10 ¹⁹)		10.1	4.98	3.30	2.49	2.00

Table 10.8 Summary of Results Obtained for the Take Up of Oleic Acid on to Salmefamol from 113/n-hexane

(moisture content = 20 ppm, specific surface area of salmefamol = $2.7 \text{ m}^2 \text{ g}^{-1}$, area occupied by oleic acid molecule at monolayer coverage = $90.5 \times 10^{-20} \text{ m}^2$)

Whilst multilayer adsorption of oleic acid on to rutile from n-heptane has been shown to occur (204), it seemed unlikely to have occurred here, as no equilibrium oleic acid was left in solution. This final observation suggests that some chemical reaction between the basic salmefamol and oleic acid might have occurred.

10.3 The solubility of salmefamol in 113/n-hexane

In order to obtain an estimate of the solubility of salmefamol in 113/n-hexane, 2 g of micronised salmefamol was dispersed in 50 ml of 113/n-hexane and left to equilibrate for 72 hours at 20°C using the methods outlined in section 10.2. After equilibration the dispersion was left to stand for approximately 8 hours at 20°C for the two phases to separate. The supernatant was then removed using a pipette. As noted in section 10.2.2 some salmefamol was still 'carried over', to remove this the supernatant was then passed through a 0.01 μm pore size cellulose nitrate membrane filter. Three 10 ml volumes of the collected supernatant were then assayed for salmefamol as described in section 10.1.4.

To assess whether salmefamol was adsorbed on to the filter, 10 ml of a 2 $\mu\text{g ml}^{-1}$ solution of salmefamol in 0.1N HCl was passed through a filter and collected. To assay this solution it was first necessary to neutralise the solution with 0.1 NaOH, and then add 5 ml of methanol, before proceeding as in section 10.1.4.

As an additional control solution 10 ml of the 2 μgml^{-1} salmefamol solution in 0.1N HCl was assayed unfiltered.

The results are summarised in Table 10.9. The additional control solution produced absorbances which were not significantly different

Solution	Sample	1	2	3	Mean	SD	CV
10 ml of 2 μgml^{-1} Salmefamol in 0.1 N HCl con- trol solution	Absorbance at 605 nm	0.149	0.154	0.156	19.4	0.5	2.6
	Salmefamol (μg)	18.9	19.5	19.8			
10 ml of 2 μgml^{-1} Salmefamol in 0.1 HCl (Filtered)	Absorbance at 605 nm	0.157	0.150	0.154	19.5	0.5	2.6
	Salmefamol (μg)	19.9	19.0	19.5			
Supernat- ant of Salmefamol Dispersion in 113/n- hexane	Absorbance at 605 nm	Absorbance was below noise level of spectro- photometer			<5	-	-
	Salmefamol (μg)	<5	<5	<5			

(SD = Standard Deviation, CV = Coefficient of Variation (%))

Table 10.9 Summary of Salmefamol Contents Assayed for the
Determination of The Solubility of Salmefamol
in 113/n-hexane

from that of the 20 μg sample in methanol (Table 10.4, $t = 0.30$, $p = 0.78$). It was therefore concluded that salmefamol presented as a solution in 0.1 N HCl could be assayed in the same manner as methanol solutions.

Since there was no significant difference by t test ($t = 0.23$, $p = 0.83$), between the control solution and that passed through the filter it was concluded that salmefamol was not readily adsorbed on to the filter. The fact that no measurable absorbance was found for the supernatant, indicated that the salmefamol content was less than 5 μg for each sample. Therefore the solubility of the drug in 113/n-hexane was less than $1 : 2 \times 10^6$.

10.4 The deposition of salmefamol on to the electrode surface

A possible explanation for the poor signal quality and flattening of spectra with time, was thought to be due to deposition of salmefamol on to the electrode surface; electrode reactions are known to lead to degraded spectra (202).

To study this the electrodes were cleaned with methanol, rinsed with 113/n-hexane and then oven dried. A similarly clean and dried cuvette was filled with a sample of a salmefamol dispersion containing $2 \times 10^{-3}\text{M}$ Aerosol OT and the electrodes inserted. A field strength of 57 kV m^{-1} at a reversal rate of 2 Hz was applied to the electrodes for 5 minutes. After this the electrodes were removed and gently shaken to remove excess liquid. When all residual 113/n-hexane had evaporated, the electrodes were taken apart and carefully washed with methanol to remove traces of salmefamol; a total of 20 ml being used. This experiment was repeated twice more to produce three replicate

methanol solutions. The experiment was repeated with 57 kV m^{-1} DC and no voltage being applied to the electrodes.

The solutions were assayed for salmefamol content using the assay method described in section 10.1.4. To ensure trace surfactant did not interfere with the assay, washings from electrodes immersed in a solution of $2 \times 10^{-3} \text{ M}$ Aerosol OT was used as the assay blank. No discernible difference in absorbance was noted between this blank and that used in section 10.1.4.

Table 10.10 summarises the results. It can be seen that the amount of drug deposited varied greatly and analysis of variance showed there was no significant ($p < 0.05$) difference in deposition between the different conditions studied.

Applied Voltage to Electrodes	Sample	1	2	3	Mean	SD	CV
No Applied Voltage	Absorbance at 605 nm	0.105	0.067	0.072	10.2	2.7	26
	Salmefamol (μg)	13.2	8.3	9.0			
80 V DC	Absorbance at 605 nm	0.085	0.090	0.045	9.2	3.2	35
	Salmefamol (μg)	10.7	11.3	5.5			
80 V (2Hz)	Absorbance at 605 nm	0.108	0.058	0.110	11.6	3.8	33
	Salmefamol (μg)	13.6	7.2	13.9			

Table 10.10 Summary of Deposition of Salmefamol on to Electrodes from a Dispersion Containing $2 \times 10^{-3}\text{M}$ Aerosol OT

Source	Sum of Squares	Degrees of Freedom	Mean Square	F ratio	F 0.05
Between Samples	8.7	2	4.3	0.41	5.14
Within Samples	63.3	6	10.5		
Total	71.7	8			

Analysis of Variance

CHAPTER 11DISCUSSION AND CONCLUSIONS11.1 Application of Laser-Doppler velocimetry to the study of electrokinetic behaviour in non-polar media

Whilst the physical behaviour of many aqueous pharmaceutical suspensions can be explained in terms of the DLVO theory (section 1.1), its applicability to metered dose inhalation aerosols (MDI), formulated as dispersions of microfine drug in liquified propellant blends is unclear. This lack of understanding arises in part from the problems of determining surface charges associated with particles dispersed in non-polar media; liquified propellant blends being non-polar, possessing relative permittivities of around 2 (section 1.3). The validity of the diffuse layer model to such non-polar dispersions must also be considered (section 2.1). However, the determination of surface charge still remains essential to any test of the DLVO theory.

11.1.1 LASER-DOPPLER VELOCIMETRY

Surface charges are normally derived from experimental methods which are based upon one of the electrokinetic phenomena; electrophoresis, electroosmosis, streaming potential and sedimentation potential. Since dispersions in non-polar media have extended diffuse layers (section 2.1), electrophoresis is the method of choice, since it permits the study of very dilute dispersions where overlap of adjacent diffuse layers can be avoided.

Microelectrophoresis has been used traditionally to study dilute

aqueous dispersions, it has however the principle drawbacks of being slow, tedious and subjective. Laser-Doppler Spectroscopy (LDS), where Laser-Doppler Velocimetry (LDV) is utilised to determine electrophoretic velocities, is now increasingly being used to study aqueous dispersions (section 4.1.3). The technique is rapid and less subjective in nature, with an ability to simultaneously resolve sub-populations of differing electrophoretic mobility in a single sample. Narrow gap electrode assemblies can be used since the geometry of the cell is no longer restricted by the requirement for the sample to be viewed microscopically.

A review of the literature (chapter 3) established that the measurement of surface charge in non-polar media would not be feasible using conventional microelectrophoretic techniques. True electrophoretic motion would not be seen because of space charge, dielectrophoretic, electrohydrodynamic and charge leakage effects (section 3.3 and 3.4). These problems could be avoided by the use of a closely spaced electrode assembly in conjunction with pulsed or alternating applied fields. Decreasing inter-electrode spacing reduces the voltage required to produce a given field to below that critical for the onset of electrohydrodynamics ($\sim 200-300$ V, section 3.3.2). Positioning the electrodes away from the cell walls ensures that charge leakage will not occur. Space charge phenomena and consequent dielectrophoretic motion as well as electrohydrodynamic effects require a finite time to develop, so can be avoided by field reversal within that time interval. The complicating effect of electroosmosis seen with traditional cell designs is also avoided.

In order to measure non-polar electrophoretic velocities, determinations must be rapid; the assessment of an electrophoretic velocity of $50 \mu\text{m s}^{-1}$ having a duration of 0.1 s is a typical requirement (electrophoretic mobility = $10^{-9} \text{m}^2 \text{s}^{-1} \text{V}^{-1}$, applied field = 50kV m^{-1} with a reversal rate of 5 Hz). Laser-Doppler velocimetry rather than flash photography and video techniques (76, 90) was selected to make the electrophoretic velocity determinations in this work. It is more rapid than the two imaging techniques neither of which produces 'real time' results, since the images of the particle track are evaluated after completion of the experiment. Whilst the application of LDV to such measurements has been advocated (124), its reported use is limited to a conference paper containing few details (115).

11.1.2 LASER-DOPPLER VELOCIMETER DESIGN

The development of a Laser-Doppler velocimeter is described in chapter 5, a differential heterodyne design (section 4.2.6) was selected since its optimum operation is with low particle concentrations ($1 - 10 \times 10^6$ per ml) (169). This permits the study of dispersions with diffuse layers in excess of $25 \mu\text{m}$ before packing constraints will result in the overlapping of the double layers (section 8.1.2). The large scattering angles typical of this design also produce increased frequency shifts for any given velocity, when compared with the simpler local oscillator heterodyne designs.

However in order to increase the options available during the study, the optical design was selected so that it could with minor modifications, be used in a local oscillator heterodyne configuration

(section 5.1). A consequence of this flexible approach was that an integrated optical unit could not be used; alignment of the beams was therefore probably found more difficult than it might otherwise have been. The velocimeter was constructed from "off the shelf" optical components (section 5.3).

The electrophoresis cell consisted of an electrode assembly custom built from Teflon and sheet platinum (section 5.4), which was designed to be used with a commercially available quartz cuvette. Whilst this design was satisfactory it could be improved to reduce electrode gap variation.

11.1.3 VALIDATION OF LASER-DOPPLER VELOCIMETER DESIGN

No standard non-aqueous dispersions are available for testing the velocimeter design because of the marked effect of moisture on non-aqueous electrophoretic mobilities (section 2.2.2). The design was therefore validated using a dispersion of erythrocytes in 0.005 ionic strength, isoosmotic buffer whose electrophoretic mobility has been established (chapter 7). These dispersions produced well defined spectral envelopes (figure 7.1), albeit lacking the harmonic structure which might have been expected to result from the use of an alternating electric field (figure 11.1) (140). This absence of finer detail was ascribed to limitations in the spectral analysis equipment used. Fast Fourier Transform (FFT) signal analysis was exclusively used as this was the only apparatus available. It was however the technique of choice as autocorrelation techniques require initial degradation of the signal through digitisation (section 4.3.4).

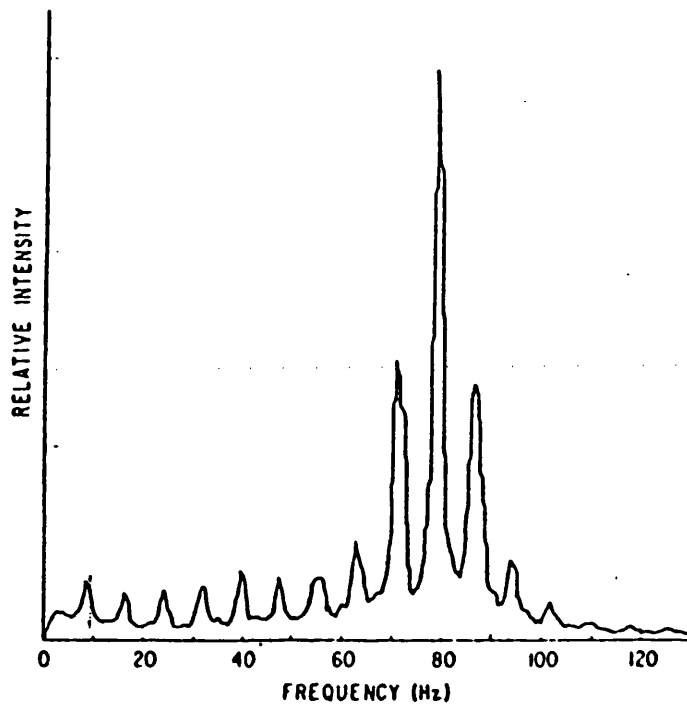


Figure 11.1 Spectrum Obtained from an Aqueous Dispersion of
0.82 μm Polystyrene spheres showing Harmonic
Structure due to Field Reversal, Reproduced
from Reference 175
($\theta = 16.4^\circ$, 3.5 kV m^{-1} , 7.8 Hz reversal rate)

Electrophoretic velocities were calculated using equation 4.5, the intersection angle in liquid having been evaluated using equation 5.3. Although the refractive index was ascertained at the 'D' line of sodium (590 nm), the refractive index of the liquid at the laser wavelength of 632.8 nm might differ by ~one percent from that at the sodium D line (section 6.3.7), this is however of no real consequence as the calculated velocity is independent of refractive index as shown by substitution of equation 5.3 into 4.5. Intersection angles in liquid were only calculated to permit easier visualisation of the beam intersection in the electrode gap.

In aqueous solutions

electroosmotic phenomena were absent from the electrode gap since frequency shift was independent of position within the electrode gap (Table 7.2). The frequency shift was also found to be independent of field reversal rates between 1 and 5 Hz (Table 7.3). Both these observations are as reported in the literature (140). A linear relationship between frequency shift and applied field which was considered to pass through the origin (Tables 7.4 and 7.5) was taken as evidence of true electrophoresis. The mean calculated electrophoretic mobility of $-2.77 \times 10^{-8} \text{ m}^2 \text{ s}^{-1} \text{ V}^{-1}$ for the erythrocytes was in good agreement with that calculated in the same manner and reported in the literature ($-2.84 \times 10^{-8} \text{ m}^2 \text{ s}^{-1} \text{ V}^{-1} \pm 0.14 \times 10^{-8} \text{ m}^2 \text{ s}^{-1} \text{ V}^{-1}$ (200, 201). Estimation of electrophoretic mobility from the regression line of frequency shift against applied field produced a value of $-2.55 \times 10^{-8} \text{ m}^2 \text{ s}^{-1} \text{ V}^{-1}$, with 95% confidence limits of $\pm 0.19 \times 10^{-8} \text{ m}^2 \text{ s}^{-1} \text{ V}^{-1}$. Whilst this method is not traditionally used to calculate electrophoretic mobilities, the upper 95% confidence limit of $-2.74 \times 10^{-8} \text{ m}^2 \text{ s}^{-1} \text{ V}^{-1}$ fell within the literature range.

11.2 The control of non-electrophoretic motion

Visual observation of salmefamol and betamethasone valerate dispersed in 113/n-hexane and experiencing a DC field within the electrode gap, clearly exhibited the turbulence effects associated with electrohydrodynamics (section 8.1.1). The formation of "convective cells" as previously reported by Novotny and Vodvenko (133, 137) was observed, as well as 'charge acquisition', a phenomenon which, whilst known to be a problem has received scant consideration in the literature.

To observe true electrophoresis in non-polar media it is therefore necessary to negate the phenomena of electrohydrodynamics, space charge effects, charge acquisition, charge leakage and electro-osmosis. The use of a narrow gap electrode assembly in conjunction with field reversal rates between 2 and 5 Hz addressed these phenomena in the following manner.

1. Positioning of the electrode assembly away from the cell wall eliminated electroosmosis within the electrode gap and charge leakage through the cell.
2. The narrow electrode gap reduced the voltage required to produce a given field, so reducing the possibility of exceeding the critical voltage associated with electrohydrodynamic effects.
3. Both space charge and electrohydrodynamic effects require a finite time to occur, thus reversing the field within this time interval avoided their occurrence.

4. Field reversal ensured that particles which had acquired charge oscillated close to either electrode. Velocity measurements can be made in the centre of the electrode gap away from their destructive influence.

11.3 Model dispersions

In order to avoid the use of a pressurised cell which would have been required for a standard propellant blend, a model propellant which showed no evaporation from the electrophoresis cell was used (section 8.1.2). This consisted of a mixture of Arcton 113 and n-hexane (6.9 : 3.1 by volume) which had very comparable properties to Propellants 11 and 12 (Table 11.1).

The density of the model propellant was close to that of the two drug materials considered (salmefamol = $1.28 \times 10^3 \text{ kg m}^{-3}$, betamethasone valerate = $1.31 \times 10^3 \text{ kg m}^{-3}$; section 6.2.2). The model propellant's viscosity was similar to that of propellant 11 but a little higher than that of propellant 12. Whilst it is not known how the solution characteristics of the model exactly resemble that of actual propellants, the solubility of salmefamol in model propellant was small, as would be ideal for a suspension aerosol formulation.

The micronised samples of salmefamol and betamethasone valerate were found to be irregular in shape (figure 6.4), possessing a wide particle size range. The salmefamol sample had 13% $< 1.2 \mu\text{m}$ and 4.5% $> 20 \mu\text{m}$, whilst betamethasone valerate gave 28% $< 1.2 \mu\text{m}$ and 2% $> 20 \mu\text{m}$ (section 6.2.1, figure 6.5). When in dispersion a range of κa values would be produced which might result in a range of

Property	Model Propellant	Propellant 11	Propellant 12
Relative Permittivity	2.251 at 10°C (section 6.3.8)	2.28 at 29°C (reference 63)	2.13 at 29°C (reference 63)
Density ($\times 10^{-3} \text{ kg m}^{-3}$)	1.296 at 10°C (section 6.3.4)	1.464 at 30°C (reference 63)	1.292 at 30°C (reference 63)
Viscosity ($\times 10^3 \text{ kg m}^{-1} \text{ s}^{-1}$)	0.597 at 10°C (section 6.3.5)	0.586 at 20°C (reference 210)	0.282 at 20°C (reference 211)
Solubility of Drug in Liquid	Salmefamol solubility at 20°C less than 1 in 2×10^6 (section 10.3)	Should ideally be minimal for a suspension formulated product (section 1.2)	

Table 11.1 Comparison of Propellant Model with Propellants 11 and 12

electrophoretic mobilities from particles with the same zeta potential (equation 3.7). In view of this, initial studies of dispersions in non-polar media were conducted with spherical model particles which possessed a narrow size distribution.

Coated silica spheres were selected as the model particles and sizes in the range of nominally 0.08 to 10.0 μm were considered. Those up to 0.7 μm were coated with methacrylate copolymers (Type A or B, section 6.1.4), whilst those of 3 μm and above possessed a covalently bonded layer of octadecyl chains (Hypersil ODS). Both types of model particle were selected on the basis of availability, neither being the perfect model. Both the polymer coat and the porous nature of the Hypersil ODS were assumed not to alter the hydrodynamic behaviour of the particle markedly from that of a solid sphere. In the case of the Type A polymer it was found that the polymer coat was unstable at high field strengths. It was however an advantage that the polymer coat did improve the physical stability of the dispersions, the influence of the octadecyl chains was however less clear.

The influence of two surfactants on the electrophoretic mobility of dispersions in the propellant model was considered. Aerosol OT was selected since it is known to be capable of charge generation in non-polar dispersions (section 2.2.2). Oleic acid was selected as it is used in MDI formulations. Whilst oleic acid is not traditionally thought of as a surfactant it is known to confer stability to some non-polar dispersions (10⁴, 20⁴).

11.4 Studies with model particles

11.4.1 SPECTRAL QUALITY

Both B polymer coated silica and Hypersil ODS dispersions produced reasonable spectral envelopes, those obtained from the former (Figure 8.3) were however of a better quality than those obtained from the latter (Figure 8.10). This is possibly due to the fact that with the B polymer coated spheres the size/fringe ratio was closer to the optimum value of 0.586 (section 4.2.6); for the angles used in this study (19.0° - 25.2°) the optimum particle size ranges from ~ 570 - 750 nm. This cannot however be the complete explanation since the erythrocyte dispersions produced good spectral envelopes (Figure 7.1) with a size/fringe ratio of 6.5.

A possible contributing factor to spectral degradation is the 10 ms dead time, which was incorporated in to the relay unit providing the necessary field reversal when studying non-polar dispersions (section 5.5). This dead time was required since mercury relays were used to allow the use of voltages up to 300 V. In the event the voltages used did not exceed 100 V, which would permit the use of solid state relays in the design with a consequent elimination of the dead time. Whilst the dead time probably did contribute to spectral degradation, it did create the opportunity for changes in the sample of dispersion within the probe volume, thus increasing sample representation.

Particles of 80 nm nominal diameter were found to scatter insufficient light to be detected by the equipment used (section 8.2.2), thus the lower limit of particle size which could be studied with the system lay between 80 and 300 nm. However an increase in laser power would most likely permit investigation of smaller particles. As to an

upper size limit, it was not possible to obtain spectra from 10 μm Hypersil ODS dispersions because of gross sedimentation (section 8.4.1) although signals were detected. It is therefore likely that had the densities of the two phases been matched for this suspension (density of propellant model (10°C) = $1.296 \times 10^3 \text{ kg m}^{-3}$, silica = $2.2 \times 10^3 \text{ kg m}^{-3}$ (62)) spectral envelopes would have been seen.

11.4.2 DEMONSTRATION OF TRUE ELECTROPHORESIS

In 1952 Van der Minne and Hermanie (86, 87) recognised that care had to be taken to ensure that true electrophoresis was observed when studying non-polar dispersions. In doing so they published criteria for the observation of true electrophoresis, namely:

1. The motion of the particle should be rectilinear between electrodes and uniform.
2. The velocity should be independent of the position of the particle in the electric field.
3. The velocity should be proportional to the field strength and should reverse on reversal of the field.

In this study compliance with these criteria was considered important so as to ensure true electrophoresis was being observed. With one principle exception (3 + 5 μm Hypersil ODS dispersed in 113/n-hexane with $4 \times 10^{-3} \text{ M}$ Aerosol OT and 24 ppm moisture, Table 8.12) which will be discussed later, the dispersions studied were considered to meet these criteria.

The first criterion is the one which is rarely adequately considered. The collection of a single spectral envelope can be taken as good evidence that all particles are in uniform motion, since if this were not the case then no envelope would have been seen. This criterion does assume the electrophoretic mobility of all particles are the same, a reasonable assumption for the spherical monosized model particles. Non-rectilinear motion would arise as a consequence of turbulence, and it is extremely unlikely that this would exactly reverse on field reversal. The laser-Doppler velocimeter measures only the rectilinear component of any particle motion. As a single envelope was collected from an alternating field, particle motion did exactly reverse with field reversal. Thus particle motion was considered to be rectilinear.

Particle velocity was found to be independent of position within the electrode gap, since no variation in frequency shift with position was noted (Tables 8.3, 8.14); compliance with criterion 2 was therefore seen.

The field independence of calculated electrophoretic mobilities together with a linear relationship between frequency shift and applied field which passed through the origin, showed particle velocity to be proportional to applied field (Tables 8.5 - 8.10, 8.15, 8.16, 9.6, 9.7, 9.13, 9.14). This motion reversed exactly with field reversal since a single envelope was obtained with an alternating field, hence fulfilling Van der Minne's third criterion.

On the basis of the studies reported in this thesis, it is proposed that when studying non-polar dispersions a fourth criterion for true electrophoresis needs to be added to those of Van der Minne

and Hermanie; namely that the velocity of the particle should be independent of the duration of the applied field over an appropriate time range. The relevant time ranges will depend in part on the type of electrode assembly used, as excessively long periods may induce electrohydrodynamic and space charge effects. It should ideally exceed the relaxation time of the diffuse layer (section 3.2, equation 3.8). In this thesis application times of up to 0.24s were used with systems which had estimated relaxation times of 0.2s ($\sigma = 10^{-10} \text{S m}^{-1}$, $\epsilon_r = 2.25$). This additional criterion is proposed since it ensures consideration of 'running in' time and onset of decoupling effects (sections 3.2 and 4.3.6).

The frequency shifts obtained from Hypersil ODS dispersions were found to be independent of field reversal rate i.e. duration of the applied field (Tables 8.13, 9.4, 9.11), thus these systems were considered to be free from any 'running in' or decoupling effects. The result also indicated that the continued motion of the particle was relatively insignificant; Novotny (122) has shown experimentally that acceleration and deceleration times for approximately 1 μm titanium dioxide particles in p xylene are less than 10^{-4} s. The characteristic decay time (section 4.3.6) would be around 10^{-5} s for a worst case in the systems studied in this work (10 μm particle). These times are significantly smaller than the 10^{-2} s dead time, thus the conclusion that continued motion is of minimal consequence is a reasonable one.

The situation with the 700 nm B polymer coated silica dispersions was less clear, there being a suggestion of an increase in frequency shift with lower field reversal rates (Table 8.4). Since inertial considerations were found not to be critical for the

larger Hypersil ODS dispersions, it is unlikely they are of any significance with these smaller particles. A more feasible explanation was perhaps that 'running in' phenomena were being experienced. However since photographic techniques have used pulses as short as 7 ms duration to study electrophoresis in dispersions with conductivities of $10^{-11} \text{ S m}^{-1}$, apparently without problems (76), it seems unlikely that 'running in' effects would be significant with the systems studied here, where the field was applied for durations between 90 - 240 ms.

The degradation in spectral quality noted at lower frequencies was surprising, since spectral resolution might have been expected to have improved. A likely explanation is that signal degradation was due to the onset of turbulence due to electrohydrodynamics. Whilst these effects cannot be seen visually at such field reversal rates, electrohydrodynamic effects were noted in 113/n-hexane subjected to a DC applied field (section 8.1.1). Taylor and House (158) employing a laser-Doppler probe to investigate conduction mechanisms in insulating liquids, similarly ascribe spectral broadening to the presence of turbulence. Using equation 3.10 the onset of electrohydrodynamics for the 700 nm B polymer dispersion can be predicted theoretically to occur at around 110 V. It is not necessarily surprising that this phenomenon might develop at lower voltages ($\sim 55 \text{ V}$), as the equations used to predict critical voltages assume a knowledge of the conduction mechanism, equation 3.10 being only valid for unipolar conduction. The conduction mechanism in the systems studied has not been elucidated.

With the Type A polymer coated silica dispersions it was not possible to show true electrophoresis as the spectral envelope was seen to

change with time (Figure 8.8). This temporal instability was thought to be possibly due to an interaction between the applied field and the polymer coat. Such observations do however demonstrate the ability of LDV to follow dynamic changes over relatively short periods.

11.4.3 THE ROLE OF PARTICLE SIZE

The Henry equation (equation 3.7) states that particle size will only influence electrophoretic mobility through the $f(\kappa a)$ term. In coarse aqueous pharmaceutical dispersions κa is generally >100 so $f(\kappa a)$ is taken as equal to 1.5 provided that potentials are low (9). In non-polar media it is generally assumed that $\kappa a < 0.1$ so $f(\kappa a) = 1$ and electrophoretic mobility is independent of particle size. To test whether this was indeed the case, the influence of particle size on electrophoretic mobility was investigated. The electrophoretic mobilities of dispersions of 3 and 5 μm Hypersil ODS in 113/n-hexane with $10 \times 10^{-3}\text{M}$ Aerosol OT were found not to be significantly different (section 8.4.2). A similar result was obtained for two different sized (300 and 700 nm) B polymer coated silica dispersions (section 8.2.2). This result was as predicted by Novotny (123) and demonstrated by Stotz (76) and Vasconcellos (212). As such it was however at variance with the experimental observations of Kuo and Osterle (213) made with larger (50 - 200 μm) glass and indium spheres dispersed in transformer oil. As electrophoretic mobility was found to be independent of particle size and assuming the $f(\kappa a)$ term in equation 3.7 does not alter significantly, zeta potential must be independent of particle size. Consequently the total charge carried by any particle is proportional to its radius (equation 2.10).

11.4.4 DEFINITION OF THE DIFFUSE LAYER

Definition of diffuse layer thicknesses in non-polar media is difficult because of the low ion concentrations present, thus a reasonable estimate of κa could not be made. For the 3 and 5 μm Hypersil ODS particles to have the same electrophoretic mobility (assuming them to have the same surface charge), the diffuse layer thickness must have been at least 25 μm (so that $f(\kappa a) = 1$ for the 5 μm particle). This diffuse layer thickness is similar to that of 30 μm estimated in this thesis from the crude conductivity measurements described in section 8.4.2. Whilst such diffuse layer thicknesses are commonly found in non-polar media (75) they may be an over-estimate, since conductivity measurements of solutions of 10^{-2}M Aerosol OT in cyclohexane with 10 ppm water predict that a particle dispersed in this solution would have a diffuse layer of 5 μm (93). If this is a more realistic estimate of the diffuse layer thickness in the Hypersil ODS dispersions, then inspection of figure 3.1 shows that $f(\kappa a)$ has not markedly changed from 1.0. It is certainly unlikely that the alteration in $f(\kappa a)$ would produce a resolvable difference in electrophoretic mobility, since reproducibility in frequency shift determination produces coefficients of variation of nearly 2% (Table 8.2).

There is indirect evidence from the work in this thesis that in some of the systems studied, the diffuse layer thickness was markedly smaller than the 30 μm estimated from conductivity measurements. The dispersions concerned are the 3 and 5 μm Hypersil ODS dispersions in 113/n-hexane with $4 \times 10^{-3}\text{M}$ Aerosol OT

and a moisture content of 24 ppm. In these dispersions it was concluded that total decoupling of the diffuse layer from the particle had occurred (section 8.4.2). This was evidenced by the fact that although there were linear relationships between frequency shift and applied field, the intercept of the plots were -43.4 Hz ($3 \mu\text{m}$) and -57.9 Hz ($5 \mu\text{m}$) and thus far removed from the origin (Table 8.12). The relaxation time of these dispersions was estimated to be $\sim 0.2\text{s}$ (section 8.4.2). Since decoupling was noted at the lowest velocity of $67 \mu\text{m s}^{-1}$ (frequency shift = 52.8 Hz), the diffuse layer must have been less than $13 \mu\text{m}$. As a frequency shift of $\sim 80 \text{ Hz}$ (Table 8.11) (velocity of $\sim 100 \mu\text{m s}^{-1}$) was independent of field reversal rate, it must be assumed that decoupling was seen at all reversal rates. With the 5 Hz reversal rate (duration of applied field = 0.09s) the particle would have moved less than $9 \mu\text{m}$. This suggests that the diffuse layer thickness was below this value, perhaps substantially if it is accepted that decoupling had to be for a fair proportion of the 0.09s to enable a reasonable signal envelope to be seen.

Since a reduction in water content to 17 ppm (Table 9.6) caused the decoupling phenomenon to disappear, it therefore seems that water is influencing the diffuse layer thickness in a manner which is not predicted by the method of Kitahara (93). The influence of moisture is given further consideration elsewhere (section 11.4.6).

11.4.5 CALCULATION OF ZETA POTENTIAL

The electrophoretic mobility of the non-polar dispersions examined in this thesis fall into the range of 10^{-9} to $10^{-8} \text{ m}^2 \text{ s}^{-1} \text{ V}^{-1}$; these

are of the same order as those reported in the literature for similar dispersions (122, 123, 115, 142, 144).

In order to calculate corresponding zeta potentials it is necessary to set a value for the $f(\kappa a)$ term of the Henry equation (equation 3.7). Throughout this thesis it has been taken that $f(\kappa a) = 1$; this is on the basis that a $5 \mu\text{m}$ particle with a diffuse layer of between 5 and $30 \mu\text{m}$, yields values of κa between 0.08 and 0.5 which from examination of figure 3.1 does not produce a marked deviation from $f(\kappa a) = 1$, assuming the particles behave as non-conducting spheres. The maximum zeta potential calculated for the $5 \mu\text{m}$ Hypersil ODS spheres dispersed in 113/n-hexane with oleic acid was -375 mV (section 9.2.1). This is markedly higher than those obtained from non-aqueous dispersions by traditional microelectrophoresis: rutile, Vulcan R, alumina and copper pthalocyanines dispersed in heptane with Aerosol OT gave zeta potentials between $\pm 35 \text{ mV}$ and $\pm 130 \text{ mV}$ (95); carbon black or barium sulphate dispersed in hexane or cyclohexane with Aerosol OT gave zeta potentials up to $\pm 120 \text{ mV}$ (93).

A zeta potential of $+250 \text{ mV}$ has been reported by Novotny (79) for a dispersion of carbon black dispersed in a mixture of aliphatic hydrocarbons with a metal salt of stearic acid; this value was not derived by microelectrophoresis but by an optical transient technique. The corresponding surface charge density was $4.9 \times 10^{-5} \text{ C m}^{-2}$ which is more than the $1 - 7 \times 10^{-6} \text{ C m}^{-2}$ noted for the silica particles in the work reported in this thesis (section 8.2.2 and 8.4.2).

The situation is further complicated since for values of $\kappa a > 0.1$ and where zeta potentials exceed 25 mV , it is necessary to make

allowances for relaxation effects through the use of the equations of Wiersema (131). To do so requires better characterisation of the system in terms of diffuse layer thickness; this could possibly be effected through the development of a reliable method for the estimation of solution conductivities.

The applicability of the diffuse layer model described in section 2.1 must be seriously questioned with respect to non-polar dispersions. The model requires the surface charge to be spread uniformly over the particle surface; potentials associated with a 300 nm particle were attributed to just 13 elementary charges (section 8.2.2). In view of the small number of charges, is such a requirement met? The personal view of the author is that it is not; it is for that reason only a few zeta potentials as distinct from electrophoretic mobilities are reported in this thesis and then only for comparison with those in the literature. It should be additionally noted that when potentials are calculated they were found to be well in excess of the 25 mV limit for which the Debye-Hückel approximation is valid (section 2.1).

It can also be asserted that the diffuse layer found in a non-polar liquid differs fundamentally from that in the polar aqueous system. In polar media the diffuse layer comprises excess ions of both polarities (i.e. counter and co-ions), which is not the case in non-polar media in that ions of predominantly one polarity (counter ions) are present in solution. For instance where particles have been charged as the result of surfactant adsorption as in the case of Aerosol OT, the low degree of ionisation of the surfactant in the non-polar media results in few co-ions, since the majority would have been adsorbed.

11.4.6 THE INFLUENCE OF MOISTURE CONTENT

The moisture content of both dispersions of model particles was found to influence the electrophoretic behaviour observed. A reduction in the moisture content of a 5 μm Hypersil ODS dispersion in 113/n-hexane containing $4 \times 10^{-3}\text{M}$ Aerosol OT from 24 ppm (Table 8.12) to 17 ppm (Table 9.6) permitted true electrophoresis to be seen. At the higher moisture content decoupling of the diffuse layer from the particle was observed. A further reduction in moisture content from 17 ppm to 12 ppm in a similar dispersion, containing $2 \times 10^{-3}\text{M}$ Aerosol OT, led to an increase in electrophoretic mobility from -3.80 to $-7.07 \times 10^{-9}\text{m}^2\text{s}^{-1}\text{V}^{-1}$. Conversely 700 nm B polymer coated silica dispersed in toluene showed an increase in electrophoretic mobility from -1.1 to $-1.4 \times 10^{-9}\text{m}^2\text{s}^{-1}\text{V}^{-1}$ with a corresponding increase in moisture content from 12 to 15 ppm (tables 8.5, 8.8, 9.1, 9.6)

These two observations are not paradoxical, since review of the literature (section 2.2.2) shows trace water capable of producing both increases and decreases in the electrophoretic mobility of non-polar dispersions.

The increase in electrophoretic mobility noted with the B polymer coated dispersions may indicate that water is playing a key role in the development of surface charge.

The reduction in electrophoretic mobility of the type noted with the Hypersil ODS dispersion may be due to the production of a region of high permittivity adjacent to the particle surface. Such a mechanism ties in with the decoupling phenomena seen in the

24 ppm moisture content dispersion. Such a region of high permittivity would also explain why crude conductivity measurements (section 6.3.9) predict a diffuse layer thickness of $\sim 30 \mu\text{m}$, yet electrokinetic observations (section 8.4.2) indicate a thickness of less than $9 \mu\text{m}$ (as discussed earlier in section 11.4.4). The estimation of diffuse layer thickness from conductivity measurements does not take into account the presence of a region of high permittivity adjacent to the particle surface. If this layer is situated between the particle surface and the plane of shear, as would seem to be the case, it is unclear exactly how the electrophoretically derived zeta potential relates to the surface potential.

11.4.7 THE EFFECT OF AEROSOL OT UPON ELECTROPHORETIC MOBILITY

As indicated above, trace moisture can have a profound effect on the determined electrophoretic mobility of non-polar dispersions. In order to study the effect of Aerosol OT concentration on electrophoretic mobility, it was therefore essential to control moisture content. Preliminary considerations decided that as it would be extremely difficult to work with totally dry systems, the moisture content would be kept constant at 17 ppm. It might be agreed that the presence of trace moisture complicates the system being studied. Alternatively its controlled presence could be considered essential, since in practice non-polar dispersions invariably contain trace moisture.

Under these conditions Hypersil ODS dispersions were found to be negatively charged, with the relationship between electrophoretic mobility and Aerosol OT concentration ($0.05 - 10 \times 10^{-3} \text{M}$) being that described

as Type A by Kitahara (75, 91), when considering zeta potentials (Figure 9.1). A similar initial increase in electrophoretic mobility, followed by a subsequent decline with increasing surfactant concentration has been reported for Aerosol OT with dispersions of carbon black in cyclohexane, n-hexane and benzene (93) as well as copper pthalocyanines in xylene (95). Whilst from the studies undertaken it is not possible to elucidate the precise mechanism of this interaction, it is postulated that the following processes occur.

First it is necessary for the Aerosol OT molecules to ionise to a small degree and for the RSO_3^- anion to be preferentially adsorbed (Figure 11.2) on to the surface of the dispersed particle, producing a nett negative surface charge. Treating the Hypersil ODS particle as a sphere and letting the zeta potential approximate to surface potential, approximately 900 electrons would be required to produce the zeta potential maximum of -231 mV at $1 \times 10^{-3}\text{M}$ Aerosol OT (equation 2.10, surface charge density = $1.8 \times 10^{-6}\text{C m}^{-2}$, section 9.1.1). With a dispersion concentration of 5×10^6 particles per ml (section 8.1.2) and an Aerosol OT concentration of $1 \times 10^{-3}\text{M}$ it would be necessary for approximately 1 in 10^8 molecules to have been ionised and adsorbed. The calculated extent of ionisation is not dissimilar to that reported (1 in 10^7) by Novotny (214), following transient conduction studies of Aerosol OT in n-hexane, xylene and a fluorocarbon.

From section 10.2.1 it was shown that Aerosol OT was capable of adsorption on to Hypersil ODS from 113/n-hexane, although it was not possible to make an estimate of the area occupied by a single

molecule at monolayer coverage because of experimental restrictions. It can however be shown that the adsorption of 900 molecules of Aerosol OT on to a single particle is possible. Examination of Table 10.5 shows with a concentration of 10^{-3} M Aerosol OT it was possible to adsorb 2.01×10^{-5} moles of surfactant per gram of Hypersil ODS. It can be estimated that 1 g of Hypersil ODS contains around 7×10^9 particles (Hypersil ODS is modelled as a $5 \mu\text{m}$ diameter sphere, volume of particle $6.5 \times 10^{-17} \text{m}^3$, density of silica $2.2 \times 10^3 \text{kg m}^{-3}$ (62), mass of sphere $1.4 \times 10^{-13} \text{kg}$), therefore each particle would have adsorbed approximately 1.7×10^9 molecules of Aerosol OT.

The subsequent decline in electrophoretic mobility as the surfactant concentration increases from 2×10^{-3} to 10×10^{-3} M may be explained in several ways. An increasing negative surface charge on the particle causes the positive sodium counter ions in solution to interact electrostatically with the particle surface, and so become adsorbed with a consequent decline in surface potential (Figure 11.2). Alternatively, the surface of the particle will probably have the highest density of ionised molecules producing a region of higher permittivity. This more hydrophilic region will tend to attract water, so forming a layer around the particle. If this layer is within the plane of shear a reduction in zeta potential will be noted. Whilst there is no direct evidence in this study that water forms such a layer at the particle/liquid interface, it has been shown to occur in dispersions of rutile in n-heptane with Aerosol OT (93). The marked influence of water content on the electrophoretic behaviour of Hypersil ODS dispersions discussed in section 11.4.4 might

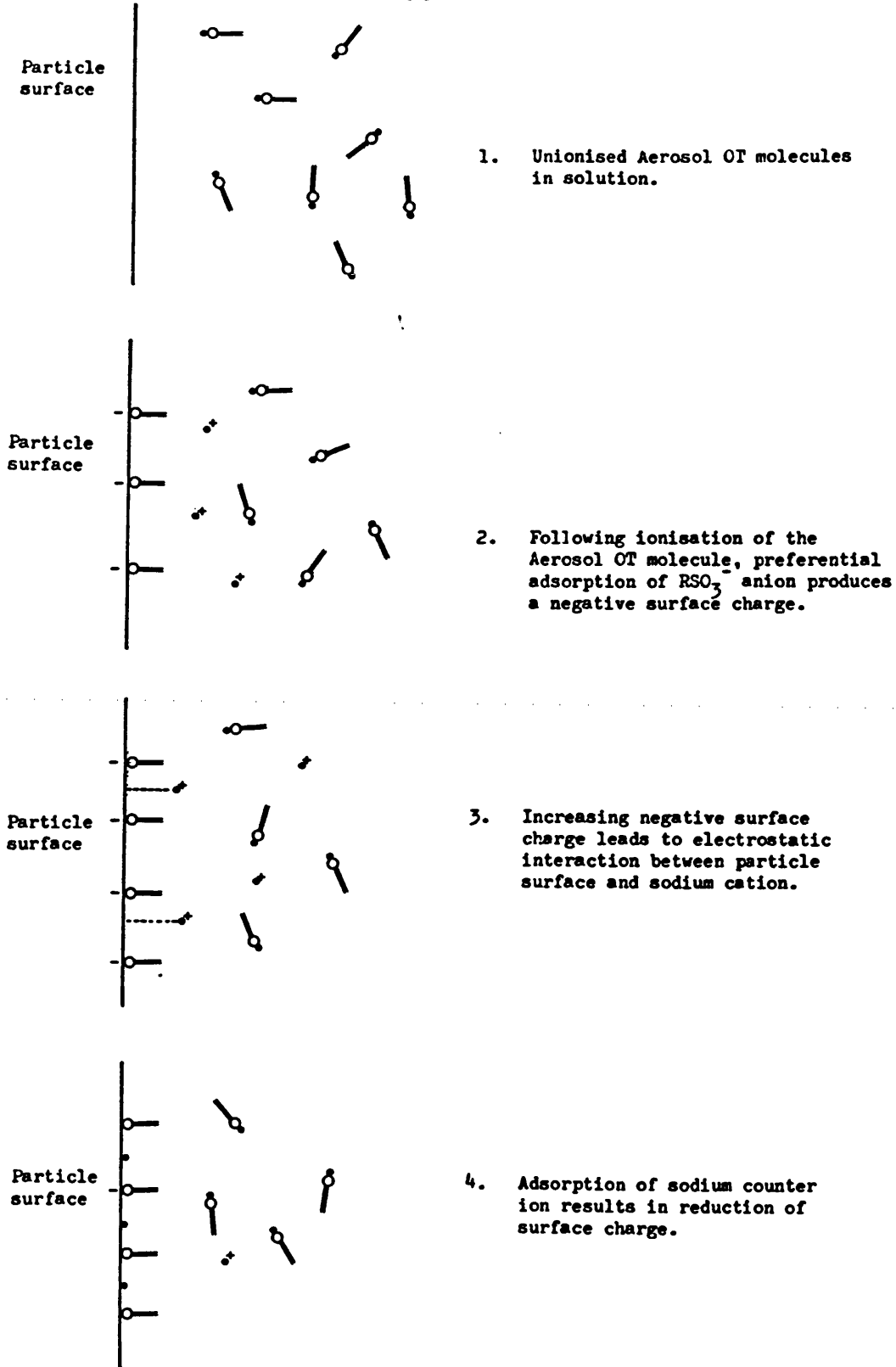


Figure 11.2 Schematic Representation of the Influence of Aerosol OT upon the Surface Charge of a Particle Dispersed in Non-polar Media

(\circ — — Aerosol OT, $\bullet+$ — sodium cation,
 $-\circ$ — — RSO_3^- anion)

indicate the presence of such a water layer. A decline in zeta potential then might arise from adsorption of sodium counter ions into the aqueous layer.

It cannot however be assumed that increasing anion concentration on the particle surface does lead to an increase in the water layer, so accounting for the decline in electrophoretic mobility. Kitahara (93) has shown that increasing Aerosol OT concentration actually reduces the amount of water at the rutile/n-heptane interface. This is because of the formation of inverse 'micelles' in to which the water is solubilised (Figure 11.3). Critical micelle concentrations (CMC) for the inverse 'micelle' range from

$1.35 \times 10^{-3} \text{M}$ in cyclohexane (215) to $4 - 9 \times 10^{-3} \text{M}$ in perchloroethylene (216); about 1.6 moles of water being strongly bound to each mole of surfactant in the latter systems.

It has been shown that secondary water is solubilised by hydration of the sodium ion (217). Kitahara (93) suggests that as the surfactant ionises the mobile sodium ion becomes bound to water in the 'micelle', whilst the RSO_3^- anion is adsorbed on to the particle surface. Thus providing a mechanism for preferential adsorption which gives rise to the initial increase in electrophoretic mobility (Figure 9.1).

11.4.8 THE EFFECT OF OLEIC ACID UPON ELECTROPHORETIC MOBILITY

Dispersions of Hypersil ODS in 113/n-hexane with oleic acid were negatively charged, as reported for dispersions of carbon black in toluene or oil with oleic acid and trace water (88, 97). In this study Hypersil ODS dispersions were found, at constant moisture

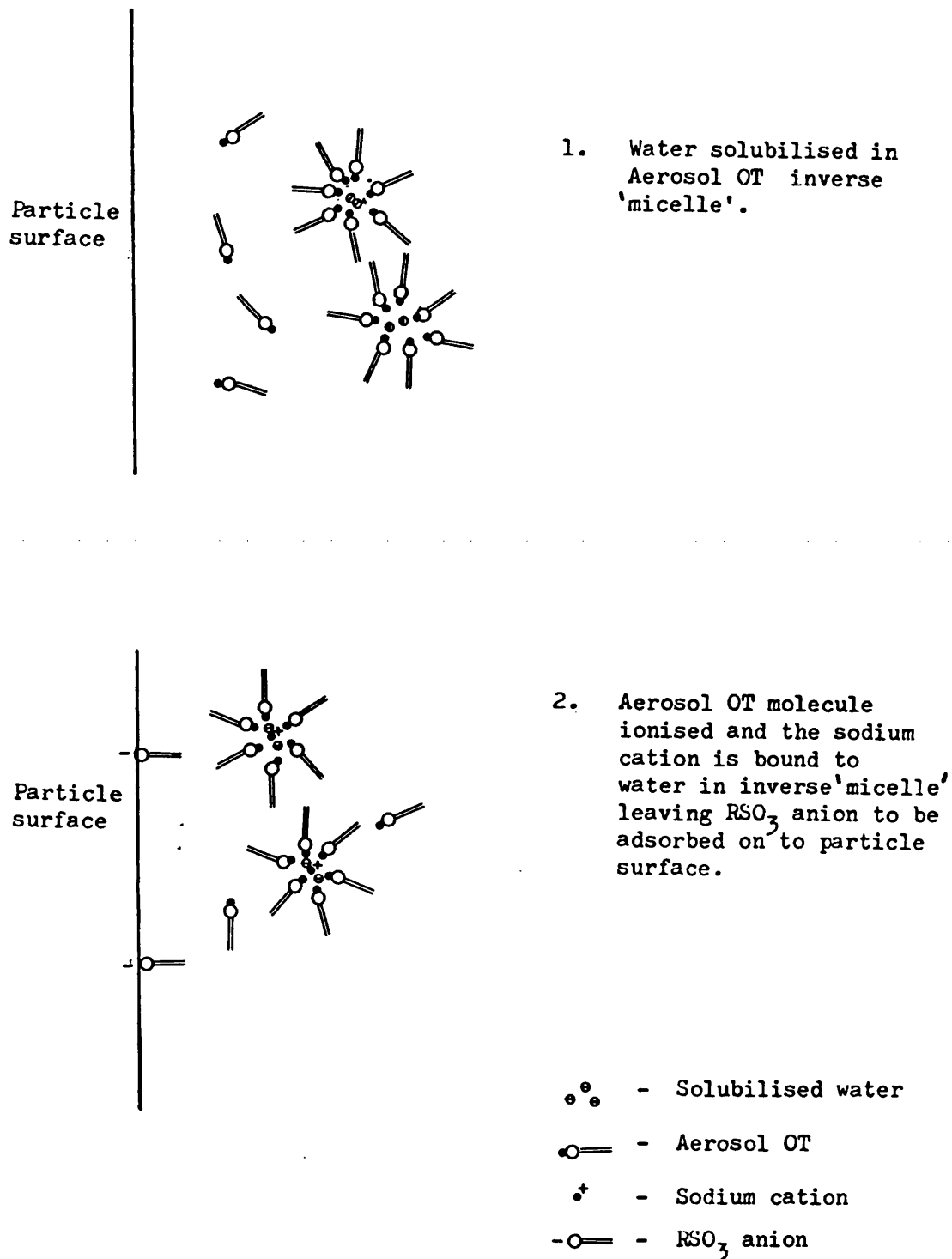


Figure 11.3 A Mechanism for the Development of Surface Charge
On Particles Dispersed in Non-polar Media Containing
Aerosol OT and Trace Water

content (20 ppm), to show a gradual increase in electrophoretic mobility from around 6.3 to $8.3 \times 10^{-9} \text{ m}^2 \text{ s}^{-1} \text{ V}^{-1}$ as oleic acid concentration increased to $10 \times 10^{-3} \text{ M}$ (Table 9.13, Figure 9.1). The high initial electrophoretic mobility ($-6.3 \times 10^{-9} \text{ m}^2 \text{ s}^{-1} \text{ V}^{-1}$) observed in comparison with that of the Aerosol OT dispersion ($3.6 \times 10^{-9} \text{ m}^2 \text{ s}^{-1} \text{ V}^{-1}$, moisture content = 17 ppm, Table 9.6) suggests that the surface charge in the main has been generated by trace water rather than oleic acid.

The gradual increase in electrophoretic mobility with oleic acid concentration might suggest that this is as a consequence of the adsorption of oleic acid. This is not a typical result for a non-ionic surfactant in a non-polar fluid, where no variation (Kitahara Type C behaviour) is expected (section 2.2.2). The change in electrophoretic mobility, with an increase in oleic acid from 2 to $10 \times 10^{-3} \text{ M}$ (6.14 to $8.28 \times 10^{-9} \text{ m}^2 \text{ s}^{-1} \text{ V}^{-1}$) indicates a change in particle charge (equations 2.10 and 3.7, $\zeta = \psi_0$) from $1.73 \times 10^{-16} \text{ C}$ ($\zeta = -275 \text{ mV}$, surface charge density $\approx 2.2 \times 10^{-6} \text{ C m}^{-2}$) to $2.41 \times 10^{-16} \text{ C}$ ($\zeta = -375 \text{ mV}$, surface charge density $\approx 3.1 \times 10^{-6} \text{ C m}^{-2}$). This represents an increase of approximately 425 elementary charges per particle for this to have occurred. Approximately 1 in 3×10^9 molecules would needed to have been ionised.

It has been shown that oleic acid is capable of adsorption on to Hypersil ODS from 113/n-hexane. A reasonable observation since oleic acid is known to be capable of adsorption on to silica from carbon tetrachloride (195) and on to titanium dioxide from hexane (218) and heptane (204). Whilst the area occupied by a molecule

at monolayer coverage could not be determined it was found that up to 1.62×10^{-5} moles of oleic acid could be adsorbed per gram of Hypersil ODS (Table 10.7). Using the approach described in section 11.4.7 it can be estimated that this represents the adsorption of approximately 1.4×10^9 molecules per particle. The adsorption of 425 elementary charges is therefore certainly feasible. Such a mechanism might seem inconceivable, however it must be remembered ion concentrations are low and liquids like n-hexane are considered to be capable of ionisation (74, 75).

An alternative proposal for the mechanism might be that increasing oleic acid concentration reduces the amount of water between the particle surface and the plane of shear, leading to an increase in electrophoretic mobility. Since oleic acid in 113/n-hexane forms dimers through hydrogen bonding (section 6.3.10) it is possible that oleic acid-water hydrogen bonding might also occur, thereby removing water from the particle surface. At present any mechanism by which oleic acid interacts with Hypersil ODS to produce a change in electrophoretic mobility must remain a matter of conjecture.

11.5 Studies with drug dispersions

11.5.1 SALMEFAMOL

True electrophoresis was successfully shown in dispersions of salmefamol (sections 9.1.2, 9.2.2) containing Aerosol OT or oleic acid. The dispersions did however require the presence of at least 2×10^{-3} M surfactant in the 113/n-hexane before any spectra could be collected. The signal forms and spectra were of a poorer quality than those seen for the model particle dispersions,

the former showing also a tendency to flatten and disappear with time (section 9.1.2).

Since spectra, albeit degraded, could be collected it must suggest that the majority of particles in the dispersion were reasonably uniform in motion, so possessing similar electrophoretic mobilities. Degradation in spectral quality possibly arose from a small fraction of particles having a significantly different value of f (κa) (equation 3.7), either through size or shape (this does assume that the zeta potential of all particles were the same).

Drug dispersions were considerably more difficult to handle than the model systems studied, exhibiting gross deposition on to the cuvette wall. If there was significant motion of the particles as they underwent deposition (or possibly aggregation), this would be superimposed on to any electrophoretic mobility, leading to a degradation in spectral quality. This is equally a problem with conventional microelectrophoretic methods. The polymer B coated silica dispersions were physically stable through the interaction of polymer coats on adjacent particles. It might also be the case that the Cl8 groups on the Hypersil ODS surface also provided a small degree of steric stabilisation.

All dispersions of salmefamol in 113/n-hexane were found to be negatively charged in contrast to the dry micronised powder which was electrostatically positively charged (section 6.2.3). This observation must discount one possible source of surface potential in this non-polar dispersion, namely that which might have resulted from the dispersion of charged particles in an insulating medium.

Since reversal of charge was noted with salmefamol it can be reasonably considered that in this system, the surface potential had arisen from being dispersed in 113/n-hexane containing both surfactant and trace moisture.

The degradation of the signal envelope with time observed with salmefamol dispersions, probably resulted from deposition effects or through some interaction between the drug and the electrode surface; gross deposition on to the electrode surface could not be shown (10.4). Narrow gap electrodes are however very prone to problems arising from dispersion/electrode interactions, as evidenced by the need to specially treat the electrodes prior to the aqueous validation study with erythrocytes (section 7.3). The fact that mobility measurements could not be made for dispersions of salmefamol which contained less than $2 \times 10^{-3}M$ surfactant, is probably not due to lack of surface charge, but to the gross deposition which occurred on to the cell wall which resulted in a loss of laser beam coherence.

11.5.2 BETAMETHASONE VALERATE

It proved impossible to make any study of betamethasone valerate dispersions in 113/n-hexane as only occasional degraded spectra could be collected (section 9.1.3). One possible explanation for this could be associated with the heterogeneity of particle shape and size, although microscopically, micronised betamethasone valerate did not appear very different from salmefamol (section 6.2.1, Figure 6.4). Equally it is possible that the dispersed particles did not possess any surface charge although trace moisture was undoubtedly present. A further suggestion is that deposition

effects, in particular along the electrode/quartz junction (a point of high field strength) were responsible. Since this dispersion was only subjected to limited investigation the cause is as yet unresolved.

11.5.3 COMPARISON OF SALMEFAMOL DISPERSIONS WITH MODEL PARTICLE STUDIES

The influence of Aerosol OT concentration upon the electrophoretic mobility of salmefamol was studied (section 9.1.2). As with the Hypersil ODS, an initial increase in electrophoretic mobility with surfactant concentration, followed by a subsequent decline was noted. Figure 9.1 shows that the initial increase in electrophoretic mobility from $1.88 \times 10^{-9} \text{ m}^2 \text{ s}^{-1} \text{ V}^{-1}$ to $4.38 \times 10^{-9} \text{ m}^2 \text{ s}^{-1} \text{ V}^{-1}$ for an increase in surfactant concentration from 2×10^{-3} to $4 \times 10^{-3} \text{ M}$ was more pronounced than that noted with Hypersil ODS ($-3.56 \times 10^{-9} \text{ m}^2 \text{ s}^{-1} \text{ V}^{-1}$ to $-5.15 \times 10^{-9} \text{ m}^2 \text{ s}^{-1} \text{ V}^{-1}$, from 0.05 to $1.00 \times 10^{-3} \text{ M}$ Aerosol OT).

The dispersion was found to be negatively charged which meant that charge reversal had taken place, since the dry powder was electrostatically positively charged. The peak zeta potential noted (-195 mV , surface charge density $\approx 2.2 \times 10^{-6} \text{ C m}^{-2}$, with $4 \times 10^{-3} \text{ M}$ Aerosol OT, section 9.1.2) corresponds to an excess of ~ 550 electrons, taking the salmefamol particle as a $3.5 \mu\text{m}$ diameter sphere (figure 6.5). The charge density on the dry powder of up to $1.1 \times 10^{-8} \text{ C m}^{-2}$ requires only 3 electrons per particle to produce field reversal. Thus taking into account charge reversal ~ 1 in 10^9 molecules of Aerosol OT would have to be ionised and adsorbed to produce the surface potential noted. This value is an

order of magnitude less than that noted for the Hypersil ODS dispersions which was 1 in 10^8 (section 11.4.7).

Adsorption experiments showed that small quantities of Aerosol OT were adsorbed on to salmefamol dispersed in 113/n-hexane (section 10.2.2). 2.7×10^{-6} moles of Aerosol OT per gram of salmefamol were adsorbed with an initial concentration of $2 \times 10^{-3}M$ (Table 10.6). Taking salmefamol to be a sphere of $3.5 \mu m$ diameter (volume of sphere = $2.24 \times 10^{-17} m^3$; density = $1.28 \times 10^3 kg m^{-3}$, section 6.2.2; mass of sphere = $2.87 \times 10^{-11} g$; number of spheres per g = 3.48×10^{10}) each particle adsorbed approximately 4.67×10^7 molecules (area occupied by molecule = $82 \times 10^{-20} m^2$). Thus the ~ 550 required to produce the peak zeta potential could have been feasibly adsorbed. The smallest theoretical area occupied by an Aerosol OT molecule was $86 \times 10^{-20} m^2$, this is slightly larger but not dissimilar to the $60 \times 10^{-20} m^2$ reported in the literature (95).

The variation of electrophoretic behaviour with oleic acid concentration at constant moisture content (20 ppm) was also studied. The particles were found to be negatively charged. However the electrophoretic mobility was lower ($\approx -1.85 \times 10^{-9} m^2 s^{-1} V^{-1}$, section 9.2.2) than that noted in the Hypersil ODS dispersions (up to $8.28 \times 10^{-9} m^2 s^{-1} V^{-1}$, section 9.2.1). In this system it is believed that the oleic acid has reacted chemically with the salmefamol to form the oleate. The adsorption experiment (section 10.2.4) showed complete take up of the oleic acid with no solution equilibrium concentration, despite multilayer adsorption having been predicted. Although there is no direct evidence for this, the formation of salmefamol oleate is a possibility considering the basic nature of the drug.

11.6 Conclusions and further work

This thesis has primarily been concerned with the development of a theoretically and practically sound experimental technique for measuring the electrophoretic mobility of particles, ideally drug particles, dispersed in non-polar media. The technique described has been successful in studying the influence of Aerosol OT and oleic acid upon the electrophoretic mobility of one drug dispersed in a model propellant mixture. There are however serious problems peculiar to drug dispersions which still require to be resolved; namely the temporal degradation of spectra noted with salmefamol and the lack of spectra with betamethasone valerate.

The results reported in this thesis suggest that drugs dispersed in liquefied propellants may well possess appreciable surface potentials, since the model propellant used had a relative permittivity close to that of standard propellants. This has yet to be confirmed by experiment, requiring the development of a pressurised electrophoresis cell to enable studies to be conducted with propellant blends.

Caution is required when applying any of the results reported here to practical aerosol formulations. Water has been found to have a marked influence upon electrophoretic behaviour. Whilst the water content of the dispersions studied was low, their dilute nature makes them, in terms of drug-water ratios, 'wet' in comparison to the commercial product. The water content of a commercial product will be around 2.5% of the drug weight (0.2% w/w dispersion with 50 ppm moisture) whilst the water content of the dispersions studied was nearer 40% (0.005% w/w dispersion with 20 ppm moisture). It would be necessary therefore to conduct experiments with very dry dispersions to obtain more pertinent data.

There are several modifications in velocimeter design which might improve operation of the equipment and increase the amount of information produced. The narrow gap electrode arrangement, whilst successful, did limit the intersection angle of the beams because of 'clipping'. To overcome this a cell could be devised using metal coated glass (e.g. NESA) as the electrodes; the laser beams would then be able to pass through the electrode surfaces, permitting the use of larger scattering angles. The cell might consist of two transparent electrodes (possibly $\sim 5 \text{ cm} \times 5 \text{ cm}$) held apart by a Teflon spacer, making the electrode gap physically more robust and more easily defined. Large electrodes are proposed since this will move the electrode edges away from the probe volume. Electrode edge effects are a likely cause of the problems seen with the drug dispersions.

Improvement in signal analysis equipment would permit Doppler shifts to be obtained directly by computer analysis of power spectral density envelopes, rather than by visual assessment. It is also theoretically possible, in the absence of turbulence, to extract from harmonic structures, size information on the particles from which the light has been scattered (156). Coupling of analysis equipment with field reversal and inclusion of a Bragg cell (for frequency shifting) in one of the two laser beams would enable directional information to be extracted. This can then be used to deduce directly the size of the particle charge. Replacement of the beam splitter and mirror arrangement with an integrated optical unit would also make alignment of the divided laser output simpler.

The question remains unanswered as to whether DLVO theory will be

applicable to the understanding of the physical stability of the suspension aerosol formulation. This will require comparison of physical stability with determined electrophoretic mobilities and comparison of the relationship (if any) to that predicted theoretically.

REFERENCES

- 1 Verwey, E.J.W., Overbeek, J.Th.G. (1948). Theory of the Stability of Lyophobic Colloids. Amsterdam : Elsevier.
- 2 Wilson, R.G., Ecanow, B. (1963). J. Pharm. Sci., 52, 727-762.
- 3 Haines, B.A., Martin, A.N. (1961). J. Pharm. Sci., 50, 228-232.
- 4 Haines, B.A., Martin, A.N. (1961). J. Pharm. Sci., 50, 753-756.
- 5 Haines, B.A., Martin, A.N. (1961). J. Pharm. Sci., 50, 756-759.
- 6 Matthews, B.A., Rhodes, C.T. (1968). J. Pharm. Sci., 57, 569-573.
- 7 Kayes, J.B. (1977). J. Pharm. Pharmacol., 29, 199-204.
- 8 Kellaway, I.W., Najib, N.M. (1981). Int. J. Pharm., 7, 285-292.
- 9 Kayes, J.B. (1977). J. Pharm. Pharmacol., 29, 163-168.
- 10 Kellaway, I.W., Najib, N.M. (1981). Int. J. Pharm., 9, 59-66.
- 11 Matthews, B.A., Rhodes, C.T. (1970). J. Pharm. Sci., 59, 521-525.
- 12 Schneider, W., Stavchansky, S., Martin, A. (1978). Amer. J. Pharm. Educ., 42, 280-289.
- 13 Tempio, J.S., Zatz, J.L. (1980). J. Pharm. Sci., 69, 1209-1214.
- 14 Hiestand, E.N. (1964). J. Pharm. Sci., 53, 1-18.
- 15 Sanders, P.A. (1979). Handbook of Aerosol Technology. New York: Van Nostrand Rheinhold.

- 16 Chemical Specialities Manufacturers Association Guide,
7th edition, 1981.
- 17 Sciarra, J.J., Stoller, L. (1974). The Science and Technology
of Aerosol Packaging. New York: John Wiley.
- 18 Johnsen, M.A. (1982). The Aerosol Handbook. New Jersey:
Wayne Dorland.
- 19 Gorman, W.G., Hall, G.D. (1973). In : Current Concepts in the
Pharmaceutical Sciences: Dosage From Design and Bioavail-
ability (Swarbrick, J., ed), Chp 4, Philadelphia: Lea and
Febiger.
- 20 Clarke, S.W., Pavia, D. (1984). Aerosols and the Lung: Clinical
and Experimental Aspects. London: Butterworths.
- 21 Bell, J.H., Brown, K., Glasby, J. (1973). J. Pharm. Pharmacol.,
25, 32-36P.
- 22 British National Formulary Number 11. (1986). British Medical
Association and the Pharmaceutical Society of Great Britain.
Bath: Bath Press.
- 23 Martindale The Extra Pharmacopoeia, 28th edition. (1982).
London: Pharmaceutical Press.
- 24 Moren, F. (1985). In: Aerosols in Medicine. Principles,
Diagnosis and Therapy (Moren, F., Newhouse, M.T., Dolovich,
M.B. eds.), chp 4, Amsterdam: Elsevier.
- 25 Wiener, M.V. (1958). J. Soc. Cosmet. Chem., 9, 289-297.

- 26 Task Group on Lung Dynamics. (1966). Health Phys., 12, 173-207.
- 27 Heyder, J. (1982). Eur. J. Respir. Dis. Suppl 119 , 63, 29-50.
- 28 Agnew, J.E. (1984). In: Aerosols and the Lung: Clinical and Experimental Aspects (Clarke, S.W., Pavia, D. eds), chp 3, London: Butterworths.
- 29 Pharmacopeial Forum. (1985). Nov-Dec, 934-938.
- 30 Hallworth, G.W., Andrews, U.G. (1976). J. Pharm. Pharmacol., 28, 898-907.
- 31 Nilsson, G., Brunzell, A., Hellberg, H. (1977). Acta Pharm. Suec., 14, 95-104.
- 32 Kim, C.S., Trujillo, D., Sackner, M.A. (1985). Amer. Rev. Resp. Dis., 132, 137-142.
- 33 Kirk, W.F. (1972). J. Pharm. Sci., 61, 262-265.
- 34 Hallworth, G.W., Clough, D., Newnham, T., Andrews, U.G. (1978). J. Pharm, Pharmacol., 30, 39P.
- 35 Moren, F. (1978). Int. J. Pharm, 1, 213-218.
- 36 Polli, G.P., Grim, W.M., Bacher, F.A., Yunker, M.H. (1969). J. Pharm. Sci., 58, 484-486.
- 37 Remingtons Pharmaceutical Sciences, 16. (1980). Pennsylvania: Merk Publishing Co.

- 38 Kanig, J.L., Cohn, R.M. (1962). Proc. Sci. Sect. Toilet Goods Assoc., 37, 19-26.
- 39 Cutie, A.J., Sciarra, J.J. (1980). Aerosol Rep., 19 (12), 401-411.
- 40 Data on Arcton Safety Propellants. Imperical Chemical Industries Ltd.
- 41 Higuchi, T. (1958). J. Amer. Pharm. Ass. Sci. Ed., 47, 657-660.
- 42 Zakrzewski, Z., Pietura, A., Katarzynska, V. (1977). Acta. Pol. Pharm., 34, 203-207 (Translated from Polish)
- 43 Moren, F. (1980). Studies on Pressurised Aerosols for Oral Inhalation. Ph.D. thesis, Uppsala University.
- 44 Thiel, C.G., Porush, I., Law, R.D. (1961). Riker Laboratories. Self-Propelling Powder Dispensing Compositions. U.S. Pat. 3,014,844.
- 45 Brown, K. (1983). Fisons Limited. Composition for Treating Asthma. U.S. Pat. 4,405,598.
- 46 Physicians Desk Reference, 37th edition. (1983). New Jersey: Medical Economics Company.
- 47 Becker, P. (1957). Emulsions: Theory and Practice. A.C.S. monograph series. New York: Reinhold.
- 48 Pietura, A., Zakrzewski, Z., Katarzynska, V. (1978). Acta Pol. Pharm., 35, 477-482, (Translated from Polish).

- 49 Cohn, R.M. (1960). The Effect of Physical Variables upon the Stability of Particulate Solids in an Aerosol System. M.Sc. thesis, Columbia University, College of Pharmacy.
- 50 Lutensol AP Types; Technical Information, BASF, TI/P 2673 e, (821) April 1985 (RB).
- 51 Brown, K. (1982). Fisons Limited. Pressurised Aerosol Formulation. U.K. Pat. GB2001 334B.
- 52 Stafford, P. (1981). Mfg. Chem, Aerosol News, June, 25-27.
- 53 Geary, D.C., West, R.D. (1961), Soap Chem. Specialities, 37, 79-91.
- 54 Pietura, A., Zakrzewski, Z., Katarzynska, V. (1977). Acta. Pol. Pharm., 35, 81-85, (Translated from Polish)
- 55 Newman, S.P., Moren, F., Pavia, D., Little, F., Clarke, S.W. (1981). Amer. Rev. Resp. Dis., 124, 317-320.
- 56 Paterson, I.C., Crompton, G.K. (1976). Brit. Med. J., 1, 76-77.
- 57 Riley, D.J., Weitz, B.W., Edelman, N.H. (1976). Amer. Rev. Resp. Dis., 114, 509-515.
- 58 Hallworth, G.W., Malton, C.A. (1984). Pharm. Int., 5 (3), 61-65.
- 59 Paterson, J.W., Conolly, M.E., Davies, D.S., Dollery, C.T. (1968). Lancet, August, 426-429.
- 60 Clark, T.H.J., Costello, J.F., Soutar, C.A. (1975). Postgrad. Med. J., 51 (4) , 72-75.

- 61 Vincent, B. (1973). *Colloid Sci.*, 1, 238-256.
- 62 Harrison, R.D. (ed). (1972). *Book of Data: Nuffield Advanced Sciences*. Bristol: Penguin.
- 63 *Data on Arcton Refrigerants*. Imperial Chemical Industries Ltd.
- 64 Walton, A.J. (1978). *Paint Mfr.*, June, 15-22.
- 65 Waligora, B., Paluch, M., Szczeglowski, Z., Pajak, J. (1975). *Neftekhimiya*, 15 (6), 928-931.
- 66 Fowkes, F.M., Pugh, R.J. (1984). *ACS Symp. Ser.*, 240, 331-354.
- 67 Vincett, P.S. (1980). *J. Colloid Interface.Sci.*, 76 (1), 83-94.
- 68 Mizuguchi, J., Sumi, K., Muchi, T. (1983). *J. Electrochem. Soc.*, 130 (9), 1819-1825.
- 69 Hunter, R.J. (1981). *Zeta Potential in Colloid Science*. London: Academic Press.
- 70 Helmholtz, H. (1879). *Wied. Ann.*, 7, 337.
- 71 Gouy, G. (1910). *J. Chem. Phys.*, 7, 405.
- 72 Chapman, D.L. (1913). *Phil. Mag.*, 25, 475-481.
- 73 Stern, O. (1924). *Z. Electrochem.*, 30, 508-516.
- 74 Gallagher, T.J. (1975). *Simple Dielectric Liquids, Mobility Conduction and Breakdown*. Oxford: Clarendon Press.

- 75 Kitahara, A. (1984). Nonaqueous Systems. In: Electrical Phenomena at Interfaces (A. Kitahara, A. Watanabe, eds.), pp 119-143. New York: Marcel Dekker.
- 76 Stotz, S. (1978). J. Colloid Interface Sci., 65 (1), 118-130.
- 77 Osmond, D.W.J. (1966): Discuss. Faraday Soc., 42, 247.
- 78 Lyklema, J. (1968). Advan. Colloid Interface Sci., 2, 65-114.
- 79 Novotny, V. (1981). Colloids Surf., 2, 373-385.
- 80 Micale, F.J. (1966). Discuss. Faraday Soc., 42, 238-242.
- 81 Labib, M.E., Williams, R. (1984). J. Colloid Interface. Sci., 97 (2), 356-365.
- 82 Labib, M.E., Williams, R. (1985). Effect of moisture on the donor - acceptor properties of solid surfaces. Proc. 5th Int. Conf. Surf. Coll. Sci. Potsdam, June 1985.
- 83 Labib, M.E., Williams, R. (1985). Relation between zero charge point in aqueous and non-aqueous media - an experimental method to establish a common acidity scale. Proc. 5th int. Conf. Surf. Coll. Sci. Potsdam, June 1985.
- 84 Moskovenko, I.B., Piguleskii, E.O., Semenova, N.G. (1962). Akust. Zh., 8, 479-80.
- 85 Romo, L.A. (1966). Discuss. Faraday Soc., 42, 232-237.
- 86 Van der Minne, J.L., Hermanie, P.H.J. (1952). J. Colloid Sci., 7, 600-615.
- 87 Van der Minne, J.L., Hermanie, P.H.J. (1953). J. Colloid Sci., 8, 38-52.

- 88 Fowkes, F.M., Jinnai, H., Mostafa, M.A., Anderson, F.W.,
Moore, R.J. (1982). ACS Symp. Ser., 200, 307-324.
- 89 Tamaribuchi, K., Smith, M.L. (1966). J. Colloid Interface.
Sci., 22, 404-407.
- 90 Novotny, V.J. (1985). Nonaqueous video electrophoresis. Proc.
5th Int. Conf. Surf. Col. Sci., Potsdam, June 1985.
- 91 Kitahara, A., Amano, M., Kawasaki, S., Kon-no, K. (1977).
Colloid Polym. Sci., 255, 1118-1121.
- 92 Bell, G.M., Levine, S. (1966). Discuss. Faraday Soc., 42, 97.
- 93 Kitahara, A., Karasawa, S., Yamada, H. (1967). J. Colloid
Interface. Sci., 25, 490-495.
- 94 Parreira, H.C. (1970). J. Electroanal. Chem. Interfacial
Electrochem., 25 (1), 69-78.
- 95 McGown, D.N.L., Parfitt, G.D., Willis, E. (1965). J. Colloid
Interface Sci., 20, 650-664.
- 96 Cooper, W.D., Wright, P. (1976). J. Colloid Interface. Sci.,
54(1), 28-33.
- 97 Garner, F.H., Nutt, C.W., Mothadi, M.F. (1952). J. Inst. Petrol.
London, 38, 986-997.
- 98 Sato, T., Ruch, R. (eds). (1980). Stabilization of Colloidal
Dispersion by Polymer Adsorption, pp 37-63. New York: Marcel
Dekker.
- 99 Hoskin, N.E. (1953). Trans Faraday Soc., 49, 1471-1477.

- 100 Hamaker, H.C. (1936). *Rec. Trav. Chim. Pays-Bas.*, 55, 1015-1026.
- 101 Hamaker, H.C. (1937). *Rec. Trav. Chim. Pays-Bas.*, 3, 727-747.
- 102 Schenkel, J.H., Kitchener, J.A. (1960). *Trans. Faraday Soc.*, 56, 161-173.
- 103 Lewis, K.E., Parfitt, G.D. (1966). *J. Oil Colour Chem. Ass.*, 49, 261-274.
- 104 Koelmans, H., Overbeek, J. Th. G. (1954). *Discuss. Faraday Soc.*, 18, 52-63.
- 105 Osmond, D.W.J., Waite, F.W. (1975). In: *Dispersion Polymerization in Organic Media*. (K.E. Barrett ed.) London: Wiley Interscience.
- 106 Pugh, R.J., Matsumaga, T., Fowkes, F.M. (1983). *Colloids. Surf.*, 7, 183-207.
- 107 Albers, W., Overbeek, J. Th. G. (1959). *J. Colloid Sci.*, 14, 510-518.
- 108 Feat, G.R., Levine, S. (1976). *J. Colloid Interface. Sci.*, 54 (1), 34-44.
- 109 Romo, L.A. (1963). *J. Phys. Chem.*, 67, 386-389.
- 110 Sato, T., Ruch, R. (eds). (1980). *Stabilization of Colloidal Dispersions by Polymer Adsorption*, pp 65-119. New York: Marcel Dekker.
- 111 Sato, T., Ruch, R. (eds). (1980). *Stabilization of Colloidal Dispersions by Polymer Adsorption*, New York: Marcel Dekker.

R10

- 112 Goodwin, J.W. ed. (1981). Colloidal Dispersions. Royal Society of Chemistry Specialist Publication No. 43.
- 113 Parfitt, G.D., Rochester, C.H. (1983). Adsorption from Solution at the Solid/Liquid Interface. London: Academic Press.
- 114 Furusawa, K., Matsumoto, M. (1984). Stability measurement of disperse systems. In: Electrical Phenomena at Interfaces (A. Kitahara, A. Wantanabe, eds), pp 225-268, New York: Marcel Dekker.
- 115 Horn, D., Auweter, H., Ditter, W., Eisenlauer, J. (1984). Laser Optical methods for the characterization of disperse systems. Proc. Int. Conf. Organic Coat. Sci. Tech., Athens, July 1984.
- 116 Gregory J. (1985). A sensitive monitor for the control of flocculation processes. Abs. 5th. Int. Conf. Surf. Colloid. Sci., Potsdam, June 1985.
- 117 Briant, J. (1961). Rev. Inst. Fr. Petrole. Ann. Combust. Liquides., 16, 49-75.
- 118 Oyabu, Y., Yashumori, Y. (1972). Talanta, 19, 423-437.
- 119 Kitahara, A., Yamada, H., Kobayashi, Y., Ikeda, H., Koshinuda, Y., (1967). Kogyo Kagaku Zasshi, 70, 2222-2225.
- 120 Kitahara, A., Fujii, T., Katana, S. (1971). Bull. Chem. Soc. Jap., 44, 3242-3245.
- 121 Kondo, A., Yamada, J. (1972). Nippon Kagaku. Kaishi., 716-721.

- 122 Novotny, V.J. (1979). *J. Appl. Phys.*, 50 (1), 324-332.
- 123 Novotny, V.J. (1979). *J. Appl. Phys.*, 50 (4), 2787-2794.
- 124 Novotny, V.J., Hair, M.L. (1980). In: *Polymers Colloids II*,
(R.M. Fitch ed.) p 37, New York: Plenum.
- 125 Novotny, V.J., Harbour, J.R. (1984). *Appl. Phys. Lett.*, 44 (2),
264-266.
- 126 Oja, T., Fairhurst, D., Goetz, P. (1985). An ultrasonic
technique for characterization of concentrated colloidal
dispersions. Abs. 5th Int. Conf. Surf. Colloid Sci.,
Potsdam, June, 1985.
- 127 Smoluchowski, M. Von. (1921). In: *Handbuch der elektrizitat und
des magnetismus*. Vol 2, p 366. Leipzig: Barth.
- 128 Huckel, E. (1924). *Phys. Z.*, 25, 204-217.
- 129 Henry, D.C. (1931). *Proc. Royal Soc. London*, A133, 106-129.
- 130 Overbeek, J. Th. G. (1943). *Kolloid Beih.*, 54, 287-364.
- 131 Wiersema, P.H., Loeb, A.L., Overbeek, J.Th.G. (1966). *J. Colloid
Interface.Sci.*, 22, 78-99.
- 132 Hachisu, S. (1984). *Electrokinetics*. In: *Electrical Phenomena
at Interfaces* (A. Kitahara, A. Watanabe, eds.), pp 99-117.
New York: Marcel Dekker.
- 133 Novotny, V.J. (1982). *ACS Symp. Ser.*, 200, 281-306.
- 134 Parreira, H.C. (1968). *J. Chem. Phys.*, 49 (10), 4711-4712.

- 135 Gemant, A.J. (1939). *J. Phys. Chem.*, 43, 743-758.
- 136 Felici, N.J. (1977/1978). *J. Electrostatics*, 4, 119-129.
- 137 Vodvenko, N.V., Malyarenko, V.V. (1983). *Ukr. Khim. Zh.*,
49 (7), 751-754.
- 138 Bangham, A.D., Flemañs, R., Heard, D.H., Seaman, G.V.F. (1958).
Nature, 182, 642-644.
- 139 Shaw, D.J. (1969). *Electrophoresis*, New York: Academic Press.
- 140 Uzgiris, E.E. (1981). *Prog. Surf. Sci.*, 10, 53-164.
- 141 Shand, E.B. (1958). *Glass Engineering Handbook*. New York:
McGraw Hill.
- 142 Parreira, H.C. (1969). *J. Colloid Interface. Sci.*, 29 (3),
432-438.
- 143 Jackson, P., Parfitt, G.D. (1970). *Kolloid, Z.Z. Polym.*, 239 (1),
611-612.
- 144 Harris, L.B. (1969). *Rev. Sci. Instrumen.*, 40 (7), 905-907.
- 145 Goetz, P. (1985). Obtaining high quality microelectrophoresis
data in nonaqueous media. Abs. 5th. Int. Conf. Surf. Sci.
Colloid Sci., Potsdam, June 1985.
- 146 Yeh, Y., Cummins, H.Z. (1964). *Appl. Phys. Lett.*, 4 (10), 176-178.
- 147 Ware, B.R. (1974). *Advan. Colloid Interface Sci.*, 1-44.
- 148 Ware, B.R. (1971). *Chem. Phys. Lett.*, 12, 81.
- 149 Uzgiris, E.E. (1972). *Opt. Commun.*, 6 (1), 55-57.

- 150 Smith, B.A., Ware, B.R., Weiner, R.S. (1976). Proc. Natl. Acad. Sci., USA, 73, 2388-2391.
- 151 McElroy, M.I., Malihi, F.B., Pulkelnick, T.A., Kondilas, J.T., Jamieson, A.M., (1982). J. Coat. Technol., 54 (694) 37-44.
- 152 Yoshimura, T., Kikkawa, A., Suzuki, N. (1972). Jap. J. Appl. Phys., 11 (12), 1797-1804.
- 153 Goff, J.R., Luner, P. (1984). J. Colloid. Interface. Sci., 99 (2), 468-483.
- 154 Uzgiris, E.E., Costaschuk, F.M. (1973). Nature Phy. Sci., 242, 77-79.
- 155 Jennings, B.R., Fairwood, R.C. (1983). Croatica Chem. Acta, 56 (4), 663-671.
- 156 Goff, J. Luner, P. (1978). Laser Doppler electrophoresis applied to colloidal systems. In: Fibre-Water Interact. in Pap. Making, Trans. Symp. 1977/1978, 163-170.
- 157 Muller, B.W., Muller, R. (1982). Zetapotentialmessungen an hochdispersen Systemen mit Hilfe der Laser-Doppler-Anemotrie, In: Abstracts to Forum Technologicum, 28th Annual Congress, Munich.
- 158 Taylor, R.J., House, H. (1972). Mobility measurement employing a Laser Doppler optical probe to eliminate liquid motion effects. Proc. 4th Int. Conf. Conduction Breakdown in dielectric liquids. Dublin.
- 159 Dickson, L.D. (1970). Appl. Opt., 9 (8), 1854-1861.

- 160 Kogelnik, H. (1965). *Bell Systems Tech. J.*, 44, 455-494.
- 161 Uzgiris, E.E. (1981). *Nato Adv. Ed. Study Inst. Ser B Phys.*, 64, 485-504.
- 162 Durst, F. (1973). *J. Appl. Math. Phys. (Zamp)*, 24, 619-643).
- 163 Wang, C.P., Synder, D. (1974). *Appl. Opt.*, 13 (1), 98-103.
- 164 Drain, L.E. (1980). *The Laser Doppler Technique*. Chichester: John Wiley.
- 165 Kaufmann, R., Steiner, R., Hoffman, W. (1979). *Cell Electrophoresis Clin. Applic. Method: Inserm Symp.*, 11. 435-444.
- 166 Smith, B.A., Ware, B.R. (1978). *Contemp. Top. Anal. Clin. Chem.*, 2, 29-54.
- 167 Rudd, M.J. (1969). *J. Sci. Inst. (J. Phys. E.)*. Ser 2, 2, 55-58.
- 168 Drain, L.E. (1972). *Appl. Phys. (J. Phys. D.)*, 5, 481-495.
- 169 Preece, A.W., Luckman, N.P. (1981). *Phys. Med. Biol.*, 26 (1), 11-18.
- 170 Watrasiewicz, B.M., Rudd, M.J. (1976). *Laser Doppler Measurements*. Butterworths: London.
- 171 Josefowicz, J., Hallett, F.R. (1975). *Appl. Opt.*, 14 (3), 740-742.
- 172 Harvey, J.D., Walls, D.F., Woodford, M.W. (1976). *Opt. Commun.*, 18 (3), 367-370.
- 173 Durst, F., Melling, A., Whitelaw, J.H. (1981). *Principles and Practice of Laser-Doppler Anemometry*. London: Academic Press.

- 174 Durst, F., Whitelaw, J.H. (1973). *Optoelectronics*, 5, 137-151.
- 175 Uzgiris, E.E. (1974). *Rev. Sci. Instrumen.*, 45 (1), 74-80.
- 176 Goff, J.R. (1979). *Laser Doppler Electrophoresis and the mobility of colloidal particles*. Ph.D. thesis, New York University.
- 177 *Spectrum Analysis - Theory, Implementation and Applications*. (1971). Waveland Rockland Inc. TSAHB4 (7/81).
- 178 Yoshimura, T., Kikkawa, A., Suzuki, N. (1975). *Opt. Commun.*, 15 (2), 277-280.
- 179 Spendley, D.G., Jones, D.P., Cooke, E.D. (1983). *ICRS Medical Sciences Biochemistry*, 11, 347-348.
- 180 *CRC Handbook of Chemistry and Physics*. 67th Edition. 1986. Florida: CRC Press.
- 181 Brandrup, J., Immergut, E.H. (eds). (1973). *Polymer Handbook*. Chichester: John Wiley and Sons.
- 182 Brown, P.B., Maxfield, B.W., Moraff, H. (eds). *Electronics for Neurobiologists*. Massachusetts: MIT Press.
- 183 Skuse, D. *Controlled flocculation of non-aqueous dispersions*. Ph.D. thesis. Department of Physical Chemistry, University of Bristol.
- 184 Decon 90, Decon Laboratories Ltd., Technical Information leaflet.
- 185 Malvern 2200 Particle Sizer; Operators Manual, Malvern Instruments.

- 186 Butters, G. Wheatley, A.L. (1981). Experience with the Malvern ST1800 Laser Diffraction Sizer. Reprints of 4th Int. Particle Size Analysis Conf. Loughborough, 1981.
- 187 Kunieda, H., Shinoda, K., (1979). J. Colloid Interface. Sci. 70 (3), 577-583.
- 188 Parker, F.S. (1971). Application of Infra-red Spectroscopy in Biochemistry, Biology and Medicine. London: Adam Hilger.
- 189 Wilson, J.M., Newcombe, R.J., Rickett, R.M.W., Denaro, A.R. (1978). Experiments in Physical Chemistry, 2nd edition. Oxford: Pergamon Press.
- 190 Langes Handbook of Chemistry, 2nd Edition. (1956).
- 191 British Standard 188: 1977.
- 192 Mitsubishi moisture meter: Operators guide; Mitsubishi Corp.
- 193 Born, M., Wolf, E. (1970). Principles of Optics. Electromagnetic theory of propagation, interference and diffraction of light. Oxford: Pergamon Press.
- 194 Abbye refractometer: Users guide; Bellingham and Stanley Ltd.
- 195 Marshall, K., Rochester, C.H. (1975). J. Chem. Soc. Faraday I, 71, 1754-1761.
- 196 Marshall, K., Rochester, C.H. (1975). Discuss. Faraday Soc. 59, 117-132.
- 197 Fuks, G.I., Tikhonov, V.P., Lebedev, R.A. (1982). Kolloid Zh., 44 (1), 77-82. (Translated from Russian).

- 198 Briggs, D.R. (1940). *Ind. Eng. Chem., Anal. ed*, 12, 703-705.
- 199 Abramson, H.A. (1934). *Electrokinetic Phenomena and their Application to Biology and Medicine*. New York: The Chemical Catalog. Inc.
- 200 Uzgiris, E.E., Kaplan, J.H. (1974). *Anal. Biochem.* 60, 455-461.
- 201 Uzgiris, E.E., Kaplan, J.H. (1976). *J. Colloid Interface. Sci.*, 55 (1), 148-155.
- 202 Uzgiris, E.E., Kaplan, J.H. (1974). *Rev. Sci. Instrumen.* 45 (1), 120-121.
- 203 Specification of Priolene 6952, Unichema Chemicals Ltd.
- 204 Ottewill, R.H., Tiffany, J.M. (1967). *J. Oil Colour Chem. Assoc.*, 50, 844-864.
- 205 Waters, J., Taylor, C.G. (1983). The colorimetric estimation of anionic surfactants. In: *Anionic Surfactants Chemical Analysis* (Cross, J. ed.). New York: Marcel Dekker.
- 206 Ottenstein, D.M., Supina, W.R. (1974). *J. Chromatog.* 91, 119-206.
- 207 Korhonen I.C.O. (1983). *Chromatographia*, 17 (2), 70-74.
- 208 Malton, C.A. (1984). *Biopharmaceutical studies of inhalation aerosol*. Ph.D. thesis, Council for National Academic Awards.
- 209 Hypersil ODS, manufacturers literature, Shandon Southern Inst.
- 210 Physical Properties of Arcton 11, GC/4893/1 Ed/13/277, Imperial Chemical Industries Ltd.

- 211 Physical Properties of Arcton 12, GC/4893/1 Ed/13/277,
Imperial Chemical Industries Ltd.
- 212 Vasconcellos, S.R., Kosman, J.J., Rowell, R.L., Medalia, A.I.,
(1983). J. Dispersion Sci. Tech., 4 (4), 409-413.
- 213 Kuo, S., Osterle, F. (1967). J. Colloid Interface. Sci., 25,
421-428.
- 214 Novotny, V., Hopper, M.A. (1979). J. Electrochem. Soc., 126 (6),
925-929.
- 215 Kitahara, A., Kobayashi, T., Tachibana, T. (1962). J. Phys.
Chem., 66, 363-365.
- 216 Wentz, M., Smith, W.H., Martin, A.R. (1969). J. Colloid
Interface. Sci., 29 (1), 36-41.
- 217 Kitahara, A., Tamura, T., Kon-no, K. (1980). Separation Sci.
Tech., 15 (3), 249-261.
- 218 Sheerwood, A.F., Rybicka, S.M. (1966). J. Oil Colour Chem.
Ass., 49, 648-669.
- 219 Davies, C.L., Goldsmith, P.L. (eds). (1980). Statistical
Methods in Research and Production. New York: Longman.
- 220 Bourke, G.J., Daly, L.E., McGilvray, J. (1985). Interpretation
and Uses of Medical Statistics. Oxford: Blackwell.
- 221 Documenta Geigy Scientific Tables, 7th edition (1970).
Basle: J.R. Geigy.
- 222 Fisher, R.A., Yates, F. (1936). Statistical Tables for Biology,
Agriculture and Medical Research, 6th edition. Edinburgh:
Oliver and Boyd.

APPENDIX 1STATISTICAL METHODSA.1.1 Analysis of Variance

For an experiment where k samples have had n analysis performed upon them, analysis of variance was used to compare the means of the samples (219).

For such an experiment an analysis of variance table was set out as below, where the results for the i th sample are denoted by x_{ij} ($j = 1$ to n). The mean of that sample is denoted as \bar{x}_i and the grand mean is denoted as \bar{x} .

Source of Variation	Sum of Squares	Degrees of Freedom	Mean Square	Quantity Estimated by Mean Square
Between Samples	$n \sum_{i=1}^k (\bar{x}_i - \bar{x})^2 = S_1$	$k - 1$	$S_1/k - 1$	$\sigma_0^2 + n\sigma_B^2$
Within Samples	$\sum_{i=1}^k \sum_{j=1}^n (\bar{x}_{ij} - \bar{x})^2 = S_0$	$k(n - 1)$	$S_0/k(n - 1)$	σ_0^2
Total	$\sum_{i=1}^k \sum_{j=1}^n (x_{ij} - \bar{x})^2$	$nk - 1$		

The mean squares provide an estimate of the variance between samples (σ_B^2) and the variance within samples (σ_0^2).

To test whether there was a significant sample to sample variation the null hypothesis was set that $\sigma_B^2 = 0$, i.e. there was no sample/sample variation. If this was the case the analysis of variance

A1-2

table provides two estimates of σ_0^2 , taking their ratio (F ratio) tests whether they are significantly different. A significant value of F discredits the null hypothesis.

A.1.2 t Test

To test whether two sample means were significantly different a t test was employed (220) with values of t being calculated using equation A1

$$t = \frac{\bar{x}_1 - \bar{x}_2}{\sqrt{\frac{s^2}{N_1} + \frac{s^2}{N_2}}} \quad - A1$$

where

$$s = \sqrt{\frac{(N_1 - 1) \sigma_1^2 + (N_2 - 1) \sigma_2^2}{N_1 + N_2 - 2}} \quad - A2$$

\bar{x}_1 and \bar{x}_2 denote the means of samples 1 and 2, σ_1 and σ_2 their corresponding standard deviations and N_1 and N_2 the number of values in each sample.

This equation is valid for small samples where the degrees of freedom ($N_1 + N_2 - 2$) is less than 60 and the variances of the two samples are equal.

To test the equality of the sample the variance ratio was calculated using equation A3.

$$F = \frac{\sigma_1^2}{\sigma_2^2} \quad - A3$$

A1-3

where σ_1^2 is the larger variance. If $F < F_{0.05}$ the equation A1 is valid, otherwise A4 was used (221).

$$t = \frac{x_1 - x_2}{\sqrt{\frac{\sigma_1^2}{N_1} + \frac{\sigma_2^2}{N_2}}} \quad - A4$$

The degrees of freedom n is given by equation A5

$$n = \frac{1}{k^2/(N_1 - 1) + (1 - k)^2/(N_2 - 1)} \quad - A5$$

where

$$k = \frac{N_2 \sigma_1^2}{N_2 \sigma_1^2 + N_1 \sigma_2^2} \quad - A6$$

whichever of the equations was used, the level of probability from tables of the t distribution.

A.1.3. 95% Confidence Interval

95% confidence interval (CL) of a mean value \bar{x} with standard deviation σ was calculated using equation A7

$$95\% \text{ CL} = \frac{\sigma}{\sqrt{N}} \times t_{0.05} \quad - A7$$

$t_{0.05}$ is the value of the t distribution for a probability of 0.05 with $N - 1$ degrees of freedom. N being the number of samples taken to calculate \bar{x} . 95% confidence limits of the mean are equal to $\bar{x} \pm 95\% \text{ CL}$.

A.1.4 Linear Regression Analysis

Data was fitted to the function $y = a + bx$ using a least squares method, the probability of linearity was obtained from appropriate tables, where the degrees of freedom (n) for N points is $n = N - 2$.

The slopes of such regression lines (b) was compared using equation A8 (221).

$$t = \frac{b_1 - b_2}{\sqrt{\sigma_1^2 + \sigma_2^2}}$$

- A8

Where b_1 and b_2 are regression coefficients with standard deviations σ_1 and σ_2 for N_1 and N_2 points. The probability was obtained from t tables where $n = N_1 + N_2 - 4$.

A.1.5 Minitab

Statistical calculations were performed on the raw data using the Minitab statistics package, release 82.1 implemented on Glaxo Prime.

Probabilities when not provided by the statistical package were obtained from Fisher and Yates Statistical Tables (222).